CRCLEME
Cooperative Research Centre for
Landscape Evolution & Mineral Exploration

CSIRO
EXPLORATION
AND MINING

AMIRA
Australian Mineral Industries Research Association Limited ACN 004 448 266

OPEN FILE
REPORT
SERIES

REGOLITH-LANDFORM EVOLUTION AND GEOCHEMICAL DISPERSION FROM THE BODDINGTON GOLD DEPOSIT, WESTERN AUSTRALIA

R.R. Anand

CRC LEME OPEN FILE REPORT 3

November 1998

(CSIRO Division of Exploration and Mining Report E&M24R, 1994.
Second impression, 1998)

CRC LEME is an unincorporated joint venture between The Australian National University, University of Canberra, Australian Geological Survey Organisation and CSIRO Exploration and Mining, established and supported under the Australian Government's Cooperative Research Centres Program.

CRC

RESEARCH ARISING FROM CSIRO/AMIRA REGOLITH GEOCHEMISTRY PROJECTS 1987-1993

In 1987, CSIRO commenced a series of multi-client research projects in regolith geology and geochemistry which were sponsored by companies in the Australian mining industry, through the Australian Mineral Industries Research Association Limited (AMIRA). The initial research program, "Exploration for concealed gold deposits, Yilgarn Block, Western Australia" (1987-1993) had the aim of developing improved geological, geochemical and geophysical methods for mineral exploration that would facilitate the location of blind, buried or deeply weathered gold deposits. The program included the following projects:

P240: Laterite geochemistry for detecting concealed mineral deposits (1987-1991). Leader: Dr R.E. Smith.
Its scope was development of methods for sampling and interpretation of multi-element laterite geochemistry data and application of multi-element techniques to gold and polymetallic mineral exploration in weathered terrain. The project emphasised viewing laterite geochemical dispersion patterns in their regolith-landform context at local and district scales. It was supported by 30 companies.

P241: Gold and associated elements in the regolith - dispersion processes and implications for exploration (1987-1991). Leader: Dr C.R.M. Butt.
The project investigated the distribution of ore and indicator elements in the regolith. It included studies of the mineralogical and geochemical characteristics of weathered ore deposits and wall rocks, and the chemical controls on element dispersion and concentration during regolith evolution. This was to increase the effectiveness of geochemical exploration in weathered terrain through improved understanding of weathering processes. It was supported by 26 companies.

These projects represented "an opportunity for the mineral industry to participate in a multi-disciplinary program of geoscience research aimed at developing new geological, geochemical and geophysical methods for exploration in deeply weathered Archaean terrains". This initiative recognised the unique opportunities, created by exploration and open-cut mining, to conduct detailed studies of the weathered zone, with particular emphasis on the near-surface expression of gold mineralisation. The skills of existing and specially recruited research staff from the Floreat Park and North Ryde laboratories (of the then Divisions of Minerals and Geochemistry, and Mineral Physics and Mineralogy, subsequently Exploration Geoscience and later Exploration and Mining) were integrated to form a task force with expertise in geology, mineralogy, geochemistry and geophysics. Several staff participated in more than one project. Following completion of the original projects, two continuation projects were developed.

P240A: Geochemical exploration in complex lateritic environments of the Yilgarn Craton, Western Australia (1991-1993). Leaders: Drs R.E. Smith and R.R. Anand.
The approach of viewing geochemical dispersion within a well-controlled and well-understood regolith-landform and bedrock framework at detailed and district scales continued. In this extension, focus was particularly on areas of transported cover and on more complex lateritic environments typified by the Kalgoorlie regional study. This was supported by 17 companies.

P241A: Gold and associated elements in the regolith - dispersion processes and implications for exploration. Leader: Dr. C.R.M. Butt.
The significance of gold mobilisation under present-day conditions, particularly the important relationship with pedogenic carbonate, was investigated further. In addition, attention was focussed on the recognition of primary lithologies from their weathered equivalents. This project was supported by 14 companies.

Although the confidentiality periods of the research reports have expired, the last in December 1994, they have not been made public until now. Publishing the reports through the CRC LEME Report Series is seen as an appropriate means of doing this. By making available the results of the research and the authors' interpretations, it is hoped that the reports will provide source data for future research and be useful for teaching. CRC LEME acknowledges the Australian Mineral Industries Research Association and CSIRO Division of Exploration and Mining for authorisation to publish these reports. It is intended that publication of the reports will be a substantial additional factor in transferring technology to aid the Australian Mineral Industry.

This report (CRC LEME Open File Report 3) is a Second impression (second printing) of CSIRO, Division of Exploration and Mining Restricted Report E&M24R, first issued in 1994, which formed part of the CSIRO/AMIRA Projects P240.

Copies of this publication can be obtained from:
The Publication Officer, c/- CRC LEME, CSIRO Exploration and Mining, PMB, Wembley, WA 6014, Australia. Information on other publications in this series may be obtained from the above or from http://leme.anu.edu.au/

Cataloguing-in-Publication:
Anand, R.R.
Regolith-landform evolution and geochemical dispersion from the Boddington Gold Deposit, Western Australia
ISBN 0 642 28256 0
1. Gold - Western Australia 2. Geochemistry 3. Laterites.
I. Title
CRC LEME Open File Report 3.
ISSN 1329-4768

AMIRA
Australian Mineral Industries Research Association Limited ACN 004 448 266

CRCLEME
Cooperative Research Centre for
Landscape Evolution & Mineral Exploration

CSIRO
EXPLORATION
AND MINING

REGOLITH-LANDFORM EVOLUTION AND GEOCHEMICAL DISPERSION FROM THE BODDINGTON GOLD DEPOSIT, WESTERN AUSTRALIA

R.R. Anand

CRC LEME OPEN FILE REPORT 3

November 1998

(CSIRO Division of Exploration and Mining Report E&M24R, 1994
Second impression, 1998)

CRC LEME is an unincorporated joint venture between The Australian National University,
University of Canberra, Australian Geological Survey Organisation and CSIRO Exploration and Mining
Headquarters: CRC LEME c/o CSIRO Exploration and Mining, Private Bag, PO Wembley, Western Australia, 6014

ABSTRACT

Regolith-Landform Relationships

A map of regolith-landform patterns was produced over an 11-km x 11-km area at Boddington. The regolith stratigraphy was established, the regolith units characterized, and a regolith-landform model established for the Boddington district. The model presents relationships in terms of preservation and erosion of the lateritic weathering profile and of local deposition.

The regolith of Boddington, as in other parts of the Yilgarn Craton, has developed over a long period, which is inferred to have taken place under a seasonally-humid climate during the Tertiary. The laterite profile is now undergoing degradation through physical and chemical processes.

A deep lateritic mantle occurs extensively over much of the Boddington district. The profile comprises a gravelly, sandy soil containing loose lateritic pisoliths over a lateritic duricrust (lateritic residuum), thence a bauxite zone, clay zone, saprolite, saprock, and bedrock. The thickness of the horizons varies considerably, depending upon the nature of the parent bedrock. Lateritic residuum forms a continuous blanket over some 30% of the landscape; however, the thickness and facies of lateritic residuum vary within the landscape. Lateritic residuum is either more developed or more preserved on midslopes than on crests or lower slopes. The midslope positions are dominated by pisolitic duricrust which is typically underlain by fragmental duricrust. By contrast, pisolitic duricrust is generally absent on crests and upslope positions where fragmental duricrust is dominant. Lower slope positions are occupied by loosely-packed pisolitic gravels which can reach a thickness of 4 m.

The lateritic duricrust and associated loose lateritic pisoliths and nodules at Boddington are largely residual, but transported nodules and pisoliths are on lower slopes. Several types of nodules and pisoliths occur in the lateritic units and have been classified as lithic, non-lithic, and of mixed origin. Relict textures after andesite are visible through some of the profiles to the level of fragmental duricrust and these correlate with the bedrock relationships which have been established through drilling. Feldspars, in fabrics similar to those of bedrock have been pseudomorphed by gibbsite, showing that at least some of the lateritic duricrust is residual. Relict textures, derived from dolerite, are also present as residual ilmenite in the bauxite zone, as well as in the fragmental and pisolitic duricrusts. The dolerite results in a redder fragmental duricrust and bauxite zone than in those horizons derived from the felsic andesite.

Mineralogy

The saprock consists of smectite, kaolinite, and mixed-layer minerals with relict primary minerals from the bedrock. Kaolinite is the dominant mineral in the clay zone and saprolite. The bauxite zone is characterized by replacement of kaolinite by gibbsite, and the presence of hematite. In the overlying duricrusts and the lateritic pisoliths and nodules, hematite becomes predominant over goethite. Maghemite and amorphous Al-oxide appear in the pisolitic duricrust and become major constituents of the loose lateritic pisoliths and nodules. Hematite and goethite are relatively more abundant in the weathering profiles formed from dolerite than in those derived from andesite. Anatase is an important secondary mineral over dolerite.

Aluminium substitution increases up the profile. In the bauxite and duricrust horizons, Al substitution in goethite ranges from 20-33 mole % whereas in saprolite it is only from 8-18 mole %.

Geochemistry

Chemical analyses of 284 samples of various regolith units, collected systematically from surface and from pit walls, document the multi-element characteristics of the lateritic Au deposits including dispersion during lateritic weathering of the protore and hosting lithologies.

Significantly anomalous concentrations of Au occur close to the surface within the lateritic residuum although the supergene Au ore occurs at greater depth (10 m to 30 m). The concentrations of Au generally decrease into the overlying laterite units, i.e. from the bauxite zone through the lateritic duricrust to loose pisoliths. Gold in pisolitic and nodular lag is variable and is generally much weaker than the underlying pisolitic duricrust.

The protore mineralization is depicted by a multi-element (W, Mo, As, Sn, Cu, Bi) geochemical halo in the lateritic residuum, both in the duricrust and in the lateritic pisoliths and nodules. The element association is As, Bi, Mo, Sn, W, with more erratic Cu and Au. Tungsten, Mo, As, and to some degree, Sn, show a more widespread and homogenous distribution than Cu and Bi.

Variations in the contents of As, W, Sn, Mo, and Au were observed between profiles that reflect variations in the parent rock and bedrock mineralization.

Abstract

The trends in element behaviour in profiles formed from andesite and dolerite are very similar, with minor differences due to the contrasting chemistry and mineralogy of the host rock. The bauxite zone and duricrusts formed from dolerite are richer in Fe_2O_3, TiO_2, Mn, V, and Zn, than the same horizons from felsic andesite. The Ti and Zr contents of the laterite have been used to interpret the origin of the lateritic residuurn, following the method proposed by Hallberg (1984) for saprolite. Most of the samples appear to have been derived from felsic andesite rocks, the remainder from dolerite.

The Mn, Cu, Zn, Ni, and Co are relatively depleted in the upper horizons of the profile, while Fe, Al, Ti, V, Cr, As, Bi, Sn, Ga, W, Zr, Nb, Mo, and Pb are retained or enriched throughout the whole profile.

These elements have accumulated in the lateritic residuum and are either associated with Fe-oxides and gibbsite, or occur as resistant primary minerals such as zircon, cassiterite, and scheelite.

Gold, Cu, and Al are enriched in the non-magnetic pisoliths contrasting with Fe, and As that are relatively more abundant in magnetic pisoliths.

The Boddington Au deposit highlights some of the problems of Au exploration in lateritic terrains which are exemplified by the leaching of Au from surface and near-surface lateritic pisoliths and nodules. A large strong, consistent multi-element anomaly at surface, with or without Au, seems to be the best and most reliable indicator of Au deposits. For Au exploration in the Boddington area, samples of fragmental duricrust instead of loose lateritic pisoliths or pisolitic duricrust, should be collected.

TABLE OF CONTENTS

1.0 PROJECT LEADERS' PREFACE

R.E. Smith and R.R. Anand - 29 March 1994

Fundamental building blocks of the CSIRO-AMIRA *Laterite Geochemistry Project* have been four substantial multidisciplinary geochemical orientation studies: Mt. Gibson, Bottle Creek, Lawlers, and Boddington. In each case the geochemical dispersion arising from concealed Au deposits was studied by establishing an understanding of the regolith, landform, and bedrock relationships, not only of the immediate ore environments, but also of the district within which the deposits lie. In this way a regolith-landform framework of reference was established for each orientation study within which each sample or collection of samples is tightly controlled. Such orientation districts were expanded in the Kalgoorlie region and at Mt. McClure during the project extension, P240A *Yilgarn Lateritic Environments*.

The Boddington research, discussed here, provides an important orientation study of geochemical dispersion in a relatively-high rainfall part of the state. It also allows comparisons and contrasts with orientation studies carried out inland.

2.0 INTRODUCTION

2.1 Previous work

Discovery of the Boddington Au deposit (Davy and El-Ansary, 1986) was particularly significant to Au exploration in WA because it is a large deposit, of a new type, close to Perth, and located within a relatively-small greenstone belt. Despite more than 100 years of prospecting within the state it had remained undetected.

The Au deposits mined to date, which are distributed along 5 km of strike length, are located largely within the saprolitic part of the lateritic mantle and were formed by supergene enrichment during weathering of a Cu-Au porphyry system (Monti, 1987, Symons, *et al.*, 1990). More recently hard rock reserves have been defined and are being mined.

The research at Boddington, discussed here, is an example of geochemical dispersion in a relatively-high rainfall part of the Yilgarn. It also allows comparisons and contrasts with the orientation studies carried out in arid areas, further inland. When the proposal for the CSIRO-AMIRA Laterite Geochemistry Project was being drafted, mining operations were about to commence. It was essential, for future exploration and research, that such a study of geochemical dispersion be carried out before this opportunity was lost, so the sampling of the surface material was an early priority. Through collaboration with Worsley Aluminium, the required systematic sampling, on a close grid over initial areas that were to be disturbed, was completed. Sampling of profiles followed as the pits were developed.

The first significant event for Au and base metals exploration in the region was recognition of the relatively-small greenstone belt by Wilde (1976). A geochemical prospecting programme, seeking Au, Cu, and Zn mineralization in the Saddleback greenstone belt, instituted by the WA Geological Survey followed. This led to the discovery, in 1979, of an area of anomalous Au, As, Cu, Pb, Mo, and Zn (Davy, 1979).

In 1980, Reynolds Australia Mines Pty. Ltd. commenced an exploration programme in the area for commodities other than bauxite (El-Ansary, 1980). Surface laterite sampling, followed by systematic reassaying of bauxite drill samples, led to the discovery of the Boddington Au deposit (60 million tonnes of lateritic ore at 1.6 g/t Au, [Symons *et al.*, 1990]). The mine, commissioned in August 1987, produced 7,166 kg of Au during the first year of operation (Symons *et al.*, 1990).

A study of the mineralogy and geochemistry of four drill holes and geochemical patterns in the lateritic profile at Boddington Au deposit has been carried out by Davy and El-Ansary (1986) while information on primary mineralization is given by Symons *et al.* (1988).

2.2 Objectives of the Boddington district study

The overall objectives of the Boddington study were to provide a well-understood regolith-landform framework over the district and, within this, to carry out multi-element, orientation, geochemical dispersion studies about the concealed Au deposits.

Specific objectives were:

- To establish regolith-landform relationships;
  - to establish regolith stratigraphy;
  - to characterize regolith units; and
  - to generate a model of regolith-landform evolution.
- To elucidate the origin and mode of formation of lateritic pisoliths and nodules;
- To examine the variation in geochemistry, petrology, and mineralogy of regolith units developed on the intermediate to felsic rocks and on the mafic rocks.
- To document the variation in abundances of ore-associated elements including Au and the mineralogy of various laterite morphologies.
- To investigate the element-mineral associations.
- To produce a multi-element orientation geochemistry data base.

2.3 Components of research at Boddington

During this CSIRO-AMIRA project, research at Boddington has been directed at the following components:

- regolith-landform maps;
- classification and characterization of laterite types;
- geochemical dispersion studies;
- siting and bonding of elements of interest; and
- integration of research.

2.4 Location

The Boddington Au deposit occurs within the northern part of the Saddleback greenstone belt, which is centred at 32°50' S and 116°57' E, approximately 100 km south-south-east of Perth (Fig. 1).

2.5 Climate

The climate of the area is Mediterranean with warm, dry summers and mild, wet winters with a mean maximum temperature ranging between 12° and 28° C. Rainfall is estimated at 810 mm per annum and most of the rain falls during the cool winter months from May to September.

2.6 Vegetation

The dominant vegetation is scherophyll forest. Varying proportions of *Eucalyptus marginata* and *Eucalyptus calophylla* form the upper storey on the ridge crest and slopes. The middle and lower storey is dominated by *Banksia grandis, Persoonia longifolia, Xanthorrhoea preisii* and *Macrozomia riedlei. Eucalyptus calophylla* and *Melaleuca preissiana* dominate the upper storey on the valley floor. The lower storey contains *Xanthorrhoea preisii, Kingia australis* and *Hypocalymma angustifolium.*

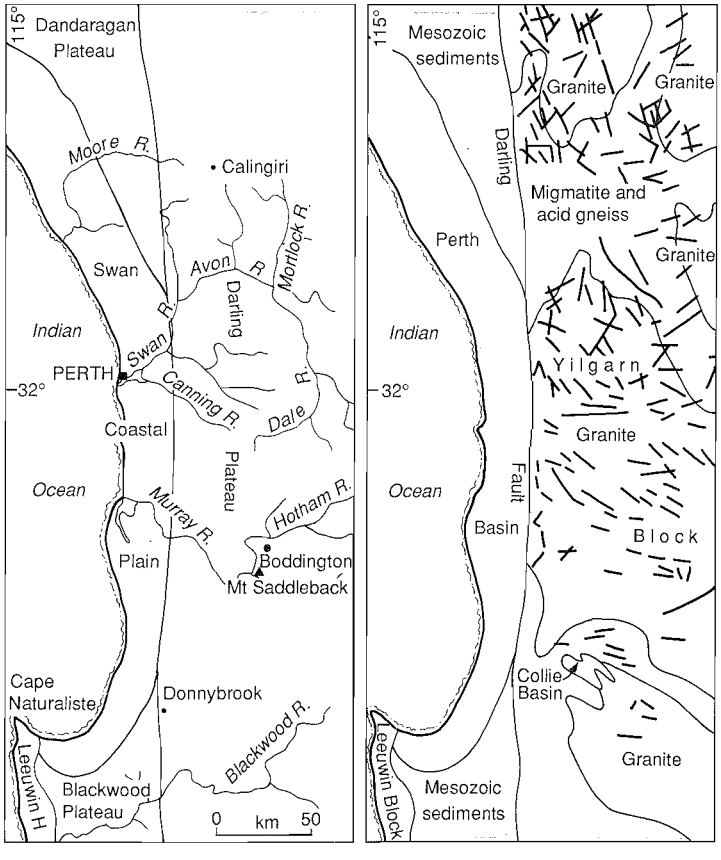

Fig. 1. Location of the study area.

3.0 REGIONAL SETTING OF THE BODDINGTON DISTRICT

3.1 Regional geology

The Saddleback greenstone belt (Wilde, 1976), varies from 5 to 12 km wide and extends 43 km in a north-northwest direction from Mt Saddleback to Mt Wells. It is a steeply-dipping sequence which contains metamorphosed (greenschist to lower amphibolite) sedimentary, felsic, and mafic volcanic and pyroclastic rocks, which have been extensively faulted (Fig. 2). The greenstone sequence, known as the Saddleback Group, is subdivided into the Hotham, Wells, and Marradong Formations. The granite-greenstone contacts are generally considered to be faulted, although intrusive contacts have been established in the southwestern part of the belt (Wilde and Low, 1980) and to the east of the Boddington Au deposit.

Geochronological studies by Wilde and Pidgeon (1986) date the volcanics at 2.65-2.67 Ma indicating a similar age to greenstones from the Eastern Goldfields Province of Western Australia. The entire area has been intruded by post-mineralization doleritic rocks, which are now largely amphibolite, though relict primary textures and minerals occur in places.

Bedrock in the Boddington Au mining area consists of felsic andesite passing to mafic andesite to the east and schist to the west. Mineralization has been found mainly in the andesitic and dacitic rocks; the sequence is traversed by dykes of dolerite, diorite, and occasionally ultramafic mineralogy.

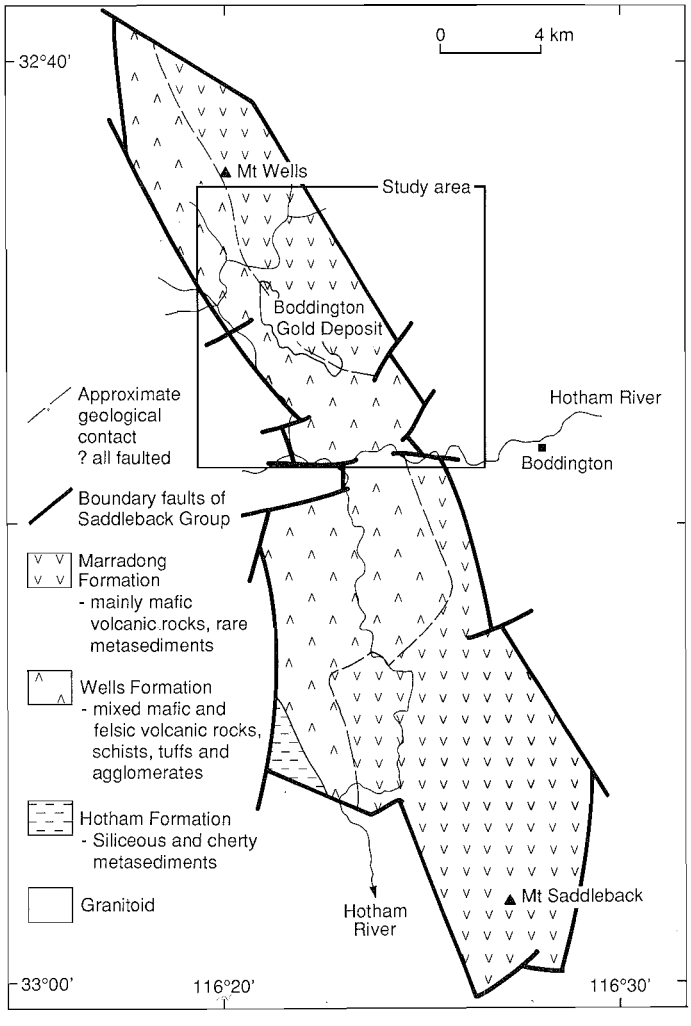

Fig. 2. Generalized bedrock-geological map of the Saddleback greenstone belt (after Wilde and Low, 1980).

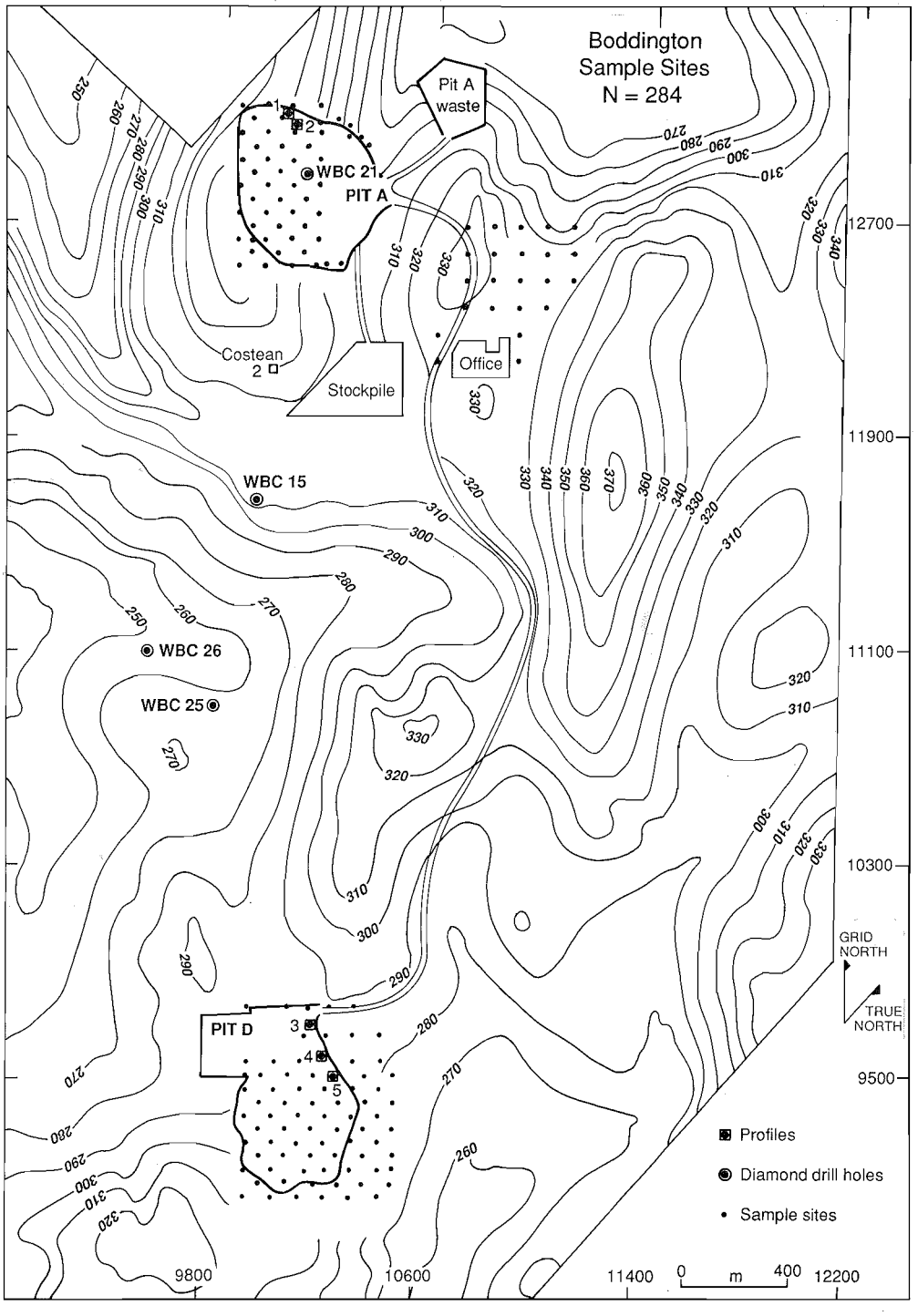

Fig. 3. Map showing the topographic setting of the Boddington gold mining area and the surrounding district (modified after Worsley Alumina Pty Ltd).

3.2 Mineralization

The primary Au mineralization at Boddington is unusual with respect to other Archaean Yilgarn deposits, being an intermediate to felsic volcanic hosted low-sulphide system characterized by intense silicification, potassic and calc-silicate alteration assemblages, and a Au-Cu-Mo-W(Bi) geochemical association (Symons *et al.*, 1988).

Low-grade Au mineralization forms a semi-continuous blanket hosted within the laterite, the bauxite-zone, and the uppermost clay zone portion of the lateritic profile (Symons *et al.*, 1988). This style of Au mineralization constitutes 30% of the total contained Au within the oxidised profile, with the remaining 70% hosted within the lower clay and lower saprolite zones. Gold distribution is relatively homogeneous. Clay-hosted Au mineralization exhibits highly-variable grades and poor lateral continuity. Thin primary quartz veins are commonly well mineralized. Clays adjacent to quartz veins (particularly in footwall locations) are commonly Fe stained and contain anomalously high concentrations of Au. Secondary shallowly-dipping Fe-oxide-rich horizons also contain anomalous but erratic Au concentrations. In addition, kaolinitic clays with little or no quartz or ferruginization can be well mineralized.

3.3 Geomorphology

The Boddington area is situated towards the western edge of the Darling Plateau, a physiographic feature of south western Australia. This area is incised by drainage from the Plateau with the Hotham River forming the major divide. Tributaries of this system grade up to the adjacent undulating plateau surface that forms the principal drainage divide. Thus, the local tributaries may terminate as broadly concave features forming the swales of these undulations. In this location, the plateau has relief of some 50 m, forming a shallow valley floor adjacent to smooth broadly-convex crest (Fig. 3). The latter forms a general skyline at 330 to 360 m above sea level while the floors of the major valley are some 60 m below. More pronounced summits, such as Mt. Wells and Mt. Saddleback emerge above the plateau level at 547 and 575 m respectively above sea level.

4.0 REGOLITH-LANDFORM EVOLUTION IN THE BODDINGTON DISTRICT

4.1 Introduction

In the Yilgarn Craton, the combined effects of prolonged, deep, lateritic weathering under warm, humid conditions followed by differential erosion and chemical modification, particularly under arid or semi-arid conditions, have led to a great variety of materials exposed at the land surface and to an intricate regolith-landform relationship. It is important to understand the regolith-landform relationships in the wide variety of terrain types which have resulted from this complex regolith evolution for two reasons: (i) to design and execute the sampling programme properly; (ii) to present and interpret the data properly. Both of these need to include knowledge of regolith and landscape evolution, weathering, and dispersion processes. This is provided by regolith-landform mapping, establishing the regolith stratigraphy within the mapped units, and synthesizing a regolith-landform model.

This section deals with the regolith-landform evolution. It provides an understanding of the nature, distribution and origin of regolith units of the Boddington over a 11.5 x 11.5 km area. Methodologies include mapping the surface regolith-landform relationships, establishing the regolith stratigraphy, characterizing the regolith units and synthesizing regolith relationships.

4.2 Definitions

The terms used in the description of regolith-landform mapping units and regolith materials are listed below:

Residual regimes, by our definition, are areas characterized by preservation of the lateritic residuum. Soils are generally gravelly. *Erosional regimes* are those where erosion has removed the lateritic residuum to the level where the bauxite zone, saprolite, saprock, or fresh bedrock are either exposed, concealed beneath modern soils, or beneath a veneer of locally-derived sediments. *Depositional regimes* are characterized by sediments, the origin of which may range from local to distal, and the thickness of which can reach tens of metres. Soils in the depositional regimes have developed in both colluvium and alluvium.

Figure 4 shows the typical laterite profile for the Boddington area using terminology standardized between the CSIRO Laterite Geochemistry and Weathering Processes projects (see Anand and Butt, 1988; Anand *et al.*, August 1989; Butt *et al.*, 1991). In the Darling Range bauxitic laterites, an increase in Al_2O_3

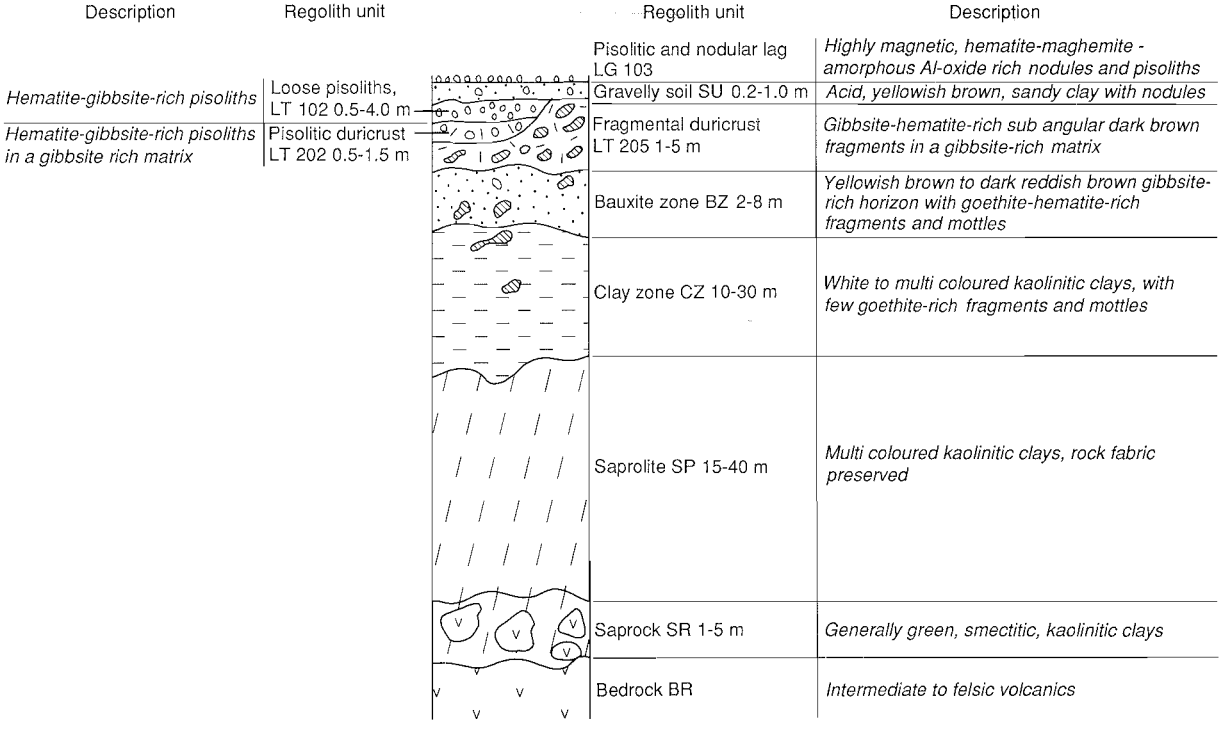

Fig. 4. Typical weathering profile in the Boddington gold mining area.

has taken place in the upper parts of some profiles to the extent that gibbsite occurs in the lateritic residuum, and the mottled zone. The mottled zone is dominant and is referred to as the bauxite zone or B-zone by the local bauxite mining company. Use of the terms upper saprolite, middle saprolite and lower saprolite in the text is only descriptive; they are not formally defined.

The term *fragment* refers to angular to sub-angular variably-ferruginized fragments of saprolite/bedrock. Fragments may contain recognizable pseudomorphs of primary minerals such as feldspars and mica.

4.3 The surface distribution of regolith-landform units

The Boddington area was sub-divided into regolith-landform mapping units following field traverses and inspections, and interpretation of 1:50,000 black and white and 1:20,000 colour air photographs (Kevron, Runs 1 and 2 dated 20.12.89). These units are based on the preservation and truncation of the lateritic residuum. In the weathered terrain, the premise underlying airphoto interpretation is that the landscape was extensively mantled by laterite and the present land surface is the result of long-continued differential stripping of an extensive mantle, and the consequent exposure of variously-weathered and unweathered materials and the moving and sorting of the resultant detritus.

Fig. 5. Map showing the surface distribution of regolith-landform units for the Boddington district.

The degree of erosional modification is often dependent upon slope declivity and available relief, with areas of low gradient providing zones of deposition of detritus. In general the interfluves have been least affected by erosion and are dominated by lateritic materials. Systematic trends in the expression of these features provide a basis for mapping the regolith, and these are well expressed in the Boddington mine area.

Figure 5 shows the distribution of regolith-landform mapping units for the Boddington area. Essentially, the map, originally at a scale of 1:50,000, shows areas dominated by lateritic residuum, separated by various erosional and depositional units. These are described below.

4.3.1 Residual regime

There are areas dominated by lateritic duricrust and a thick mantle of lateritic gravels. They comprise gently-undulating lateritic uplands and associated minor valleys. Duricrust outcrops are covered by a thin veneer of lateritic gravels on the crests and upper slopes. The lateritic gravels become deeper downslope in shallow depressions and the upper parts of these can be cemented.

4.3.2 Erosional regime

As mapped in this study, the erosional regime comprises areas in which there has been extensive removal of the lateritic residuum. Areas of erosional regime range from smooth gentle to moderate (5-12°) slopes. These are mantled by colluvium containing an admixture of lateritic gravels and overlie various saprolitic clays at depth from 0.5 to 1.5 m. On steeper slopes (>12°), there is an increasing effectiveness of stripping of the weathered mantle and exposures of fresh rock. With increasing rock outcrop, the slope becomes increasingly irregular and the regolith relates more closely to the deeper parts of the weathered profile and to fresh rock exposure.

Soils have formed on various deeper parts of the laterite profile as well as on fresh rock. In addition, colluvium derived by erosion from the laterite profile provides an additional type of soil-parent material.

Gravelly red or yellow earths occur on gentle slopes below subdued lateritic scarps. These often extend to valley floors. The soil surface is brown sandy loam changing gradually to red or yellow-brown clay at about 50 cm; much fine gravel occurs throughout the profile.

Red earths occur on steep slopes. The surface horizon consists of dark brown loam and changes gradually to red clay at depth. The deeper subsoil is often yellow clay or saprock.

4.3.3 Depositional regime

The depositional regime comprises valley floors. It has a gradient of about 1:250 and is seldom more than 1 km wide. The lower colluvial slopes grade into the valley floor and it is sometimes difficult to distinguish between these two units. On the valley floor the main soils are yellow earths, the texture of the surface horizon ranges from sand to sandy clay loam.

4.4 Regolith stratigraphy

For the successful geochemical exploration in deeply-weathered terrain, it is important to have an understanding of the regolith stratigraphy. The open pit mining operations have exposed the regolith stratigraphy at Boddington. Pit A, located adjacent to a minor valley, contrasts with Pit D which is part of an undulating lateritic upland surface. Additional opportunities to examine sub-surface regolith relationships were also provided by the spoils from diamond drill holes and costeans. From this information, the stratigraphy was depicted by cross-sections for Pits A and D. The interpretation of these data has provided the basis of understanding the regolith facies relationships. The locations of pits, costeans, and diamond drill holes are shown in Fig. 3.

4.4.1 Regolith stratigraphy - Pit A and Pit D

Pit A and Pit D provide an opportunity to examine the regolith stratigraphy of the residual regime. The general trends in the regolith stratigraphy and morphology of the lateritic residuum from crest to lower slopes is shown in Fig. 6. Yellowish-brown, sandy gravels overlying fragmental duricrust extend down from the ridge crest to the upper slopes. Fragmental duricrust crops out or is overlain by 20-50 cm thick, yellowish-brown, sandy gravels. Sandy gravels increase in thickness to more than 1 m on mid slope and lower slope positions where they overlie various forms of lateritic duricrust including loosely-packed pisolitic duricrust, these in turn overlie the bauxite zone and/or the clay zone. Fragmental duricrust is not generally developed on lower slopes. On lower slopes, a bauxite zone 3-4 m thick underlies the thick mantle of pisoliths which

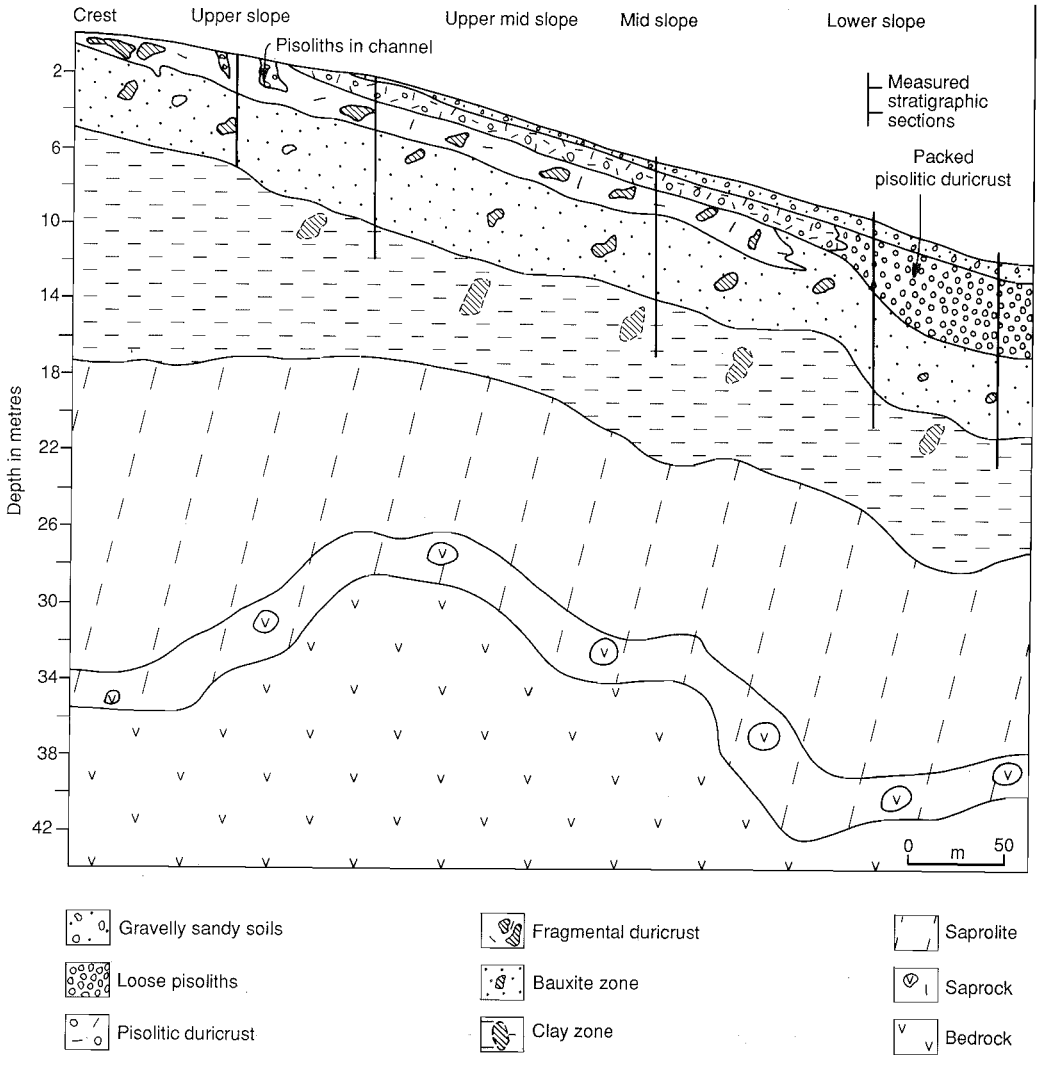

Fig. 6. Cross section for Pit A showing the general trends in the regolith stratigraphy and morphology of the lateritic residuum following a sequence from crest to lower slopes.

can sometimes reach a thickness of 4 m. The bauxite zone is commonly over multicoloured saprolite derived from andesite. The saprolite merges into underlying parent rock through a zone of slightly-weathered rock, the saprock. The depth of weathering is variable, commonly extending to more than 30 m.

Details of the regolith morphology of Pit A, examined at profiles 1 (over andesite) and 2 (over dolerite), are illustrated in Figs 7A and B. In profile 1, fragmental duricrust, 2.2 m thick, overlies the 3.2 m thick, bauxite zone on upper slopes. The boundary between these horizons is gradual (Figs 7A and 8A). Some pisolitic duricrust and even some loose pisoliths, nodules, and compound nodules occur as small vertical channels or pockets within the fragmental duricrust (Figs. 7A, 8B). In upper-mid and mid-slopes (profile 2), the bauxite zone is overlain by a 1.2 m thick fragmental duricrust, with small vermiform voids, itself overlain by a 1.5 m thick pisolitic duricrust (Fig. 7B). The transition from fragmental to pisolitic duricrust is sharp in places and gradual at others. The absence of pisolitic duricrust on the crest and upper slopes suggests that the pisolitic duricrust in the upper slopes and crest has been truncated by erosion. Such a profile could be typical of the upper slopes of the Boddington gold mining area, where the duricrust is known to be thin (Symons *et al.*, 1988).

Pit D occupies mid to lower slope positions. The examples of regolith stratigraphy from Pit D are shown in Figs 7C, D, and E. In mid slopes (profile 3) and mid-lower slopes (profile 4), the bauxite zone is overlain by a 1.7 to 2.0 m thick fragmental duricrust. This horizon is overlain by 0.7 to 1 m of a pisolitic duricrust with small vermiform voids.

On lower slopes, profile 5 shows a fragmental duricrust overlain by 1.2 m of a pisolitic duricrust and loose pisoliths and nodules (Fig. 7E). The loose pisoliths and nodules are overlain by layered loose pisoliths and nodules, which appear to have been transported. Such a profile may be typical of well-drained low areas of the Boddington Au mining area, as the duricrust is known to thin and the loose pisoliths to thicken at topographic lows (Fig. 9A) (Symons *et al.*, 1988).

4.4.2 Regolith stratigraphy - costean 2

Costean 2 is approximately 8 m deep provides an example of the regolith stratigraphy of a dolerite profile located towards the top of a ridge (Fig. 9B). The exposure includes a weathered dolerite dyke, approximately 10 m wide. It consists of a 1-m thick pisolitic duricrust, which is underlain by a 2-m bauxite zone. Although the duricrust over the dolerite is not easily distinguished from the rest of the duricrust, the bauxite zone is

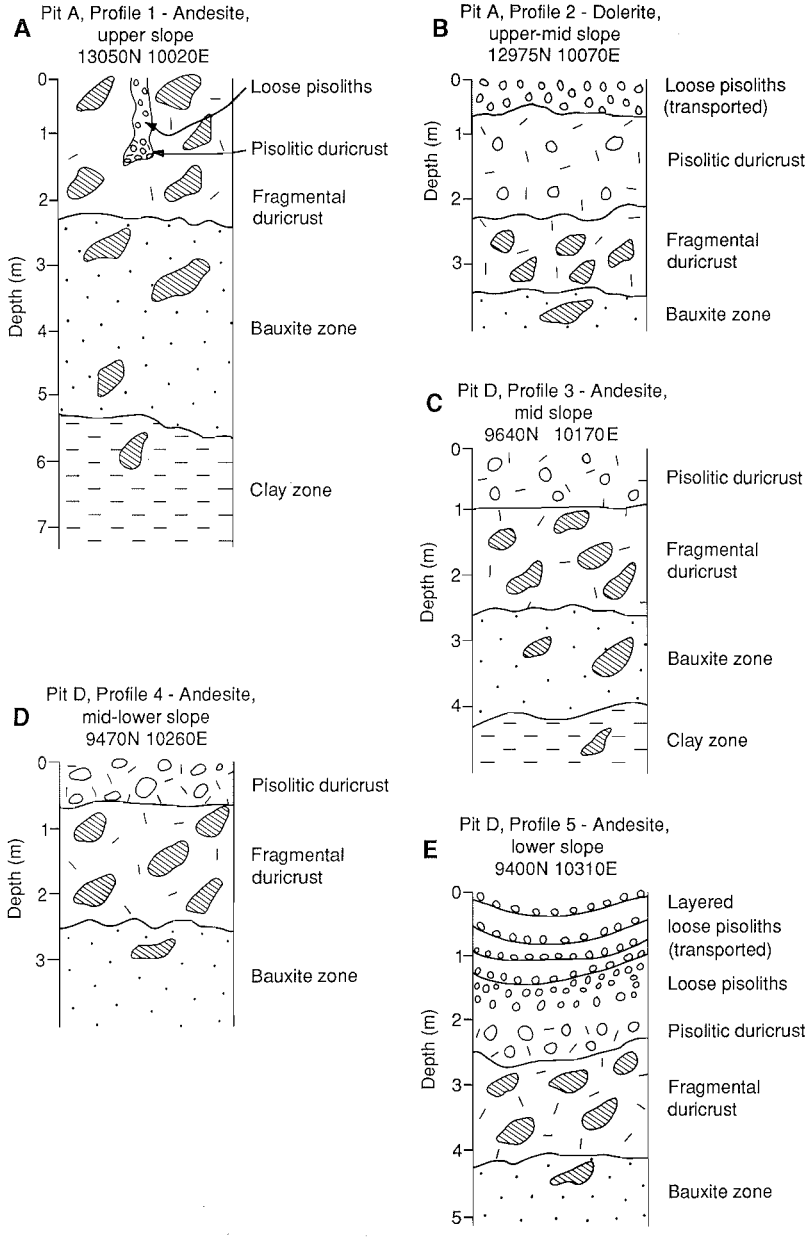

Fig. 7. Profiles from Pits A and D showing the stratigraphy (the geochemistry of these profiles is discussed in Section 5.3.2).

quite different. It is fine grained, redder and more strongly indurated than that over felsic-volcanic rocks, and consists of yellow, brown, and orange clays grading into fresh dolerite only 7 metres below the surface. The doleritic bauxite zone contains many silica- and clay-filled joints and round, weathered, doleritic boulders (up to 25 cm in diameter).

4.4.3 Regolith stratigraphy - costean 3

Costean 3 provides an example of the regolith stratigraphy of a depositional regime. The 17-m deep costean 3 is on a lower slope. Here colluvium, consisting of red to dark brown clay with 20 to 40% lateritic gravels, overlies saprolite. Below the colluvium there is an intensely-leached saprolitic zone comprising light coloured clays with up to 30% ferruginous fragments. The lateritic residuum and bauxite zone are missing.

4.5 Meso and microscopic characteristics of regolith units

4.5.1 Pit A - andesite (profile 1) and dolerite profile (profile 2)

4.5.1.1 Clay zone and saprolite

The saprolite is 25-70 m thick and ranges from pure white to multicoloured kaolinitic clays with mottles, commonly overprinted by liesegang rings. Goethite staining is common around the areas of multicoloured clays and in patches within the white clays. Microscopic examination of thin sections of upper saprolite from profile 1 shows areas that are made up of a mosaic of kaolinite and gibbsite crystals, a few hundred μm to a few μm in size, and passing into goethite-kaolinite-rich areas (Fig. 10A). Tree roots occur in this zone and are commonly surrounded by a cylinder of intensely-bleached clay.

4.5.1.2 Bauxite zone

The bauxite zone is about 4 m thick. It is an earthy, porous, friable to firm, yellowish-brown to dark reddish-brown mass, rich in gibbsite which underlies the lateritic duricrust. It contains fragments, incipient nodules and in places is mottled in appearance. Voids up to 10 cm in diameter are common and are frequently partially filled by coatings of gibbsite. Relict rock fragments and pseudomorphs after feldspars are common in this horizon (Fig. 10B-1). The pseudomorphs are often 1-2 mm in size, with net contours. In the redder parts, they become rarer and their contours are more diffuse, before disappearing completely, leaving only a spongy texture (Fig. 10B-2). These pseudomorphs are micro-crystalline aggregates of gibbsite after feldspar in an isotopic groundmass of Fe-oxides (goethite, hematite) impregnated gibbsite (Fig. 10C) (Kerr, 1977).

4.5.1.3 Lateritic residuum

The lateritic residuum, 2-3 m thick, includes two horizons, an unconsolidated pisolitic horizon and the duricrust, each of which exhibit several morphologies. Two types of morphologies of duricrust are recognized *viz* fragmental and pisolitic. Fragmental duricrust is characterized by subangular to angular, dark brown to red, gibbsite- and hematite-rich fragments of various dimensions ranging from a few mm to more than 3 cm (Fig. 11A). Fragments up to 10 cm in diameter may be present. The fragments are cemented by various amounts of a fine-grained, yellowish-red to strong brown, gibbsitic matrix. In some areas of fragments, the pseudomorphs have mostly disappeared, leaving a spongy mass in which loose quartz grains may occur. The matrix contains numerous pseudomorphs after feldspars, similar to those in the bauxite zone.

The smallest fragments have the same size and shape as the pseudomorphs and thus may have formed from single feldspar crystals (Fig. 11B). Voids, predominantly vermiform and millimetric, are present in the matrix (Fig. 11B). Patches of whitish, soft material, part of which has been removed leaving a centimetric cellular void, are present in both fragments and matrix (Fig. 11A). Voids are dominated by gibbsite with small amounts of quartz, goethite and kaolinite. Spherical white grains, less than 1 mm in size, are present in some areas. Microscopic examination of polished blocks showed that these spherical grains are due to precipitation of a whitish phase in the matrix and around various objects, such as pseudomorphs after feldspars.

In general appearance, the pisolitic-nodular duricrust is darker and less porous than fragmental duricrust and contains black hematite-maghemite rich pisoliths and nodules up to 25 mm in diameter (Figs 11C and D). Samples of pisolitic-nodular duricrust occupying small channels within the fragmental duricrust in profile 1 were examined along with the contact between the two duricrusts. This examination indicated that the pisolitic-nodular duricrust is largely the result of an

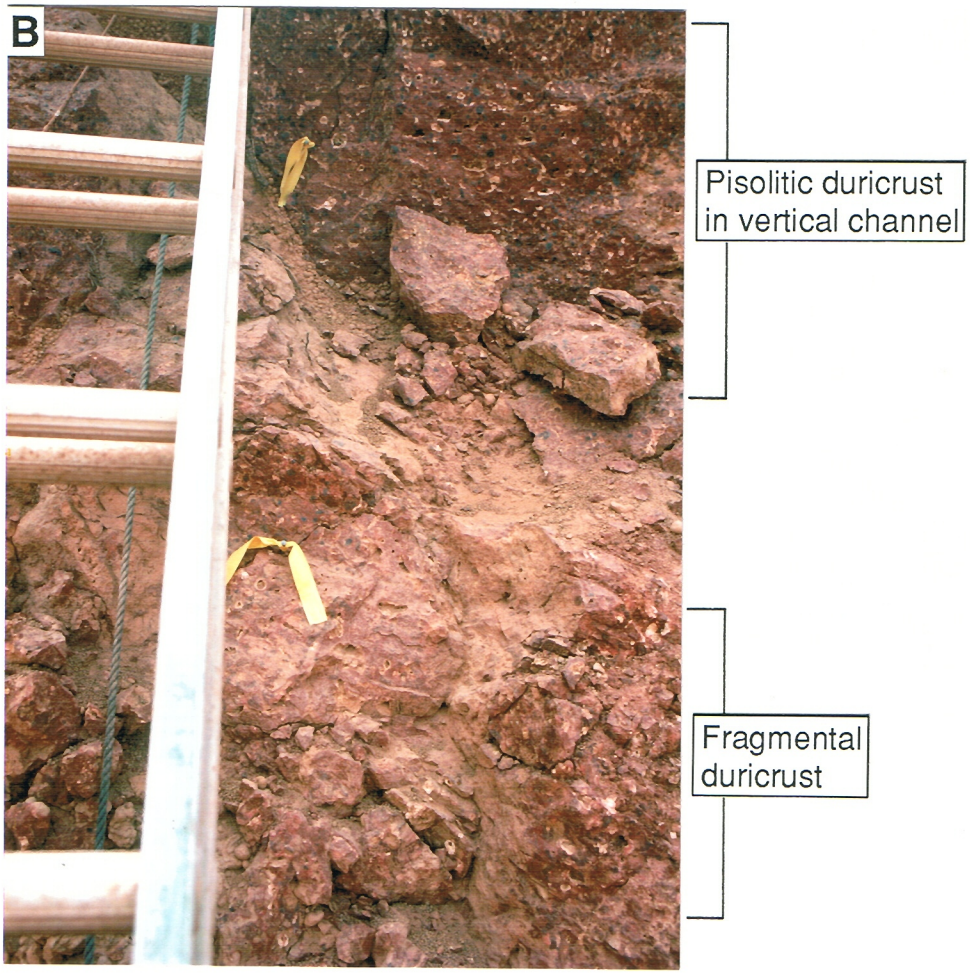

Fig. 8A Vertical profile showing regolith stratigraphy of the profile developed from felsic andesite ; location, upper slope, northern wall of Pit A.
Fig. 8B Vertical profile showing pisolitic duricrust (in vertical channel) overlying fragmental duricrust ; location, upper slope, northern wall of Pit A.

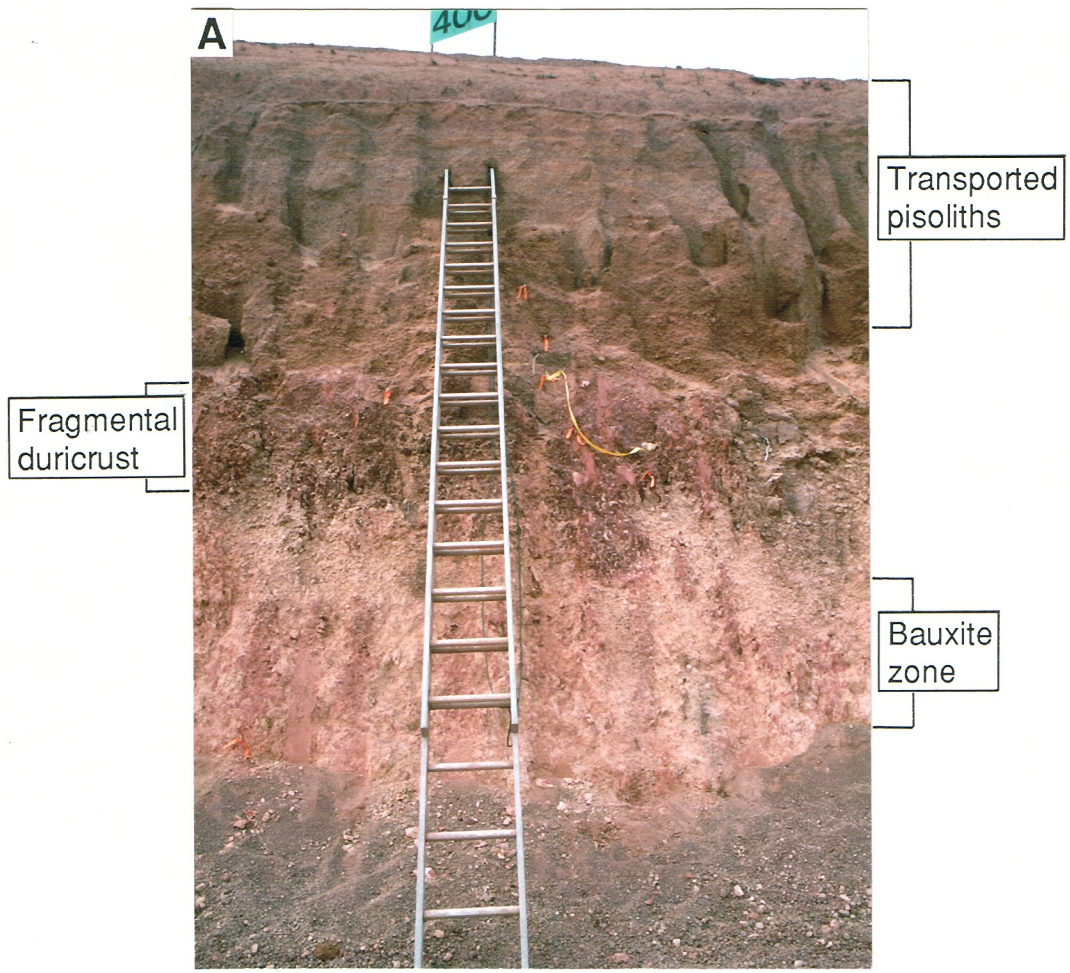

Fig. 9A Vertical profile showing regolith stratigraphy of the profile developed from felsic andesite on the lower slopes: transported pisoliths overlying fragmental duricrust, location northern wall of Pit D.
Fig. 9B Vertical profile showing regolith stratigraphy of the profile developed from dolerite: location costean 2.

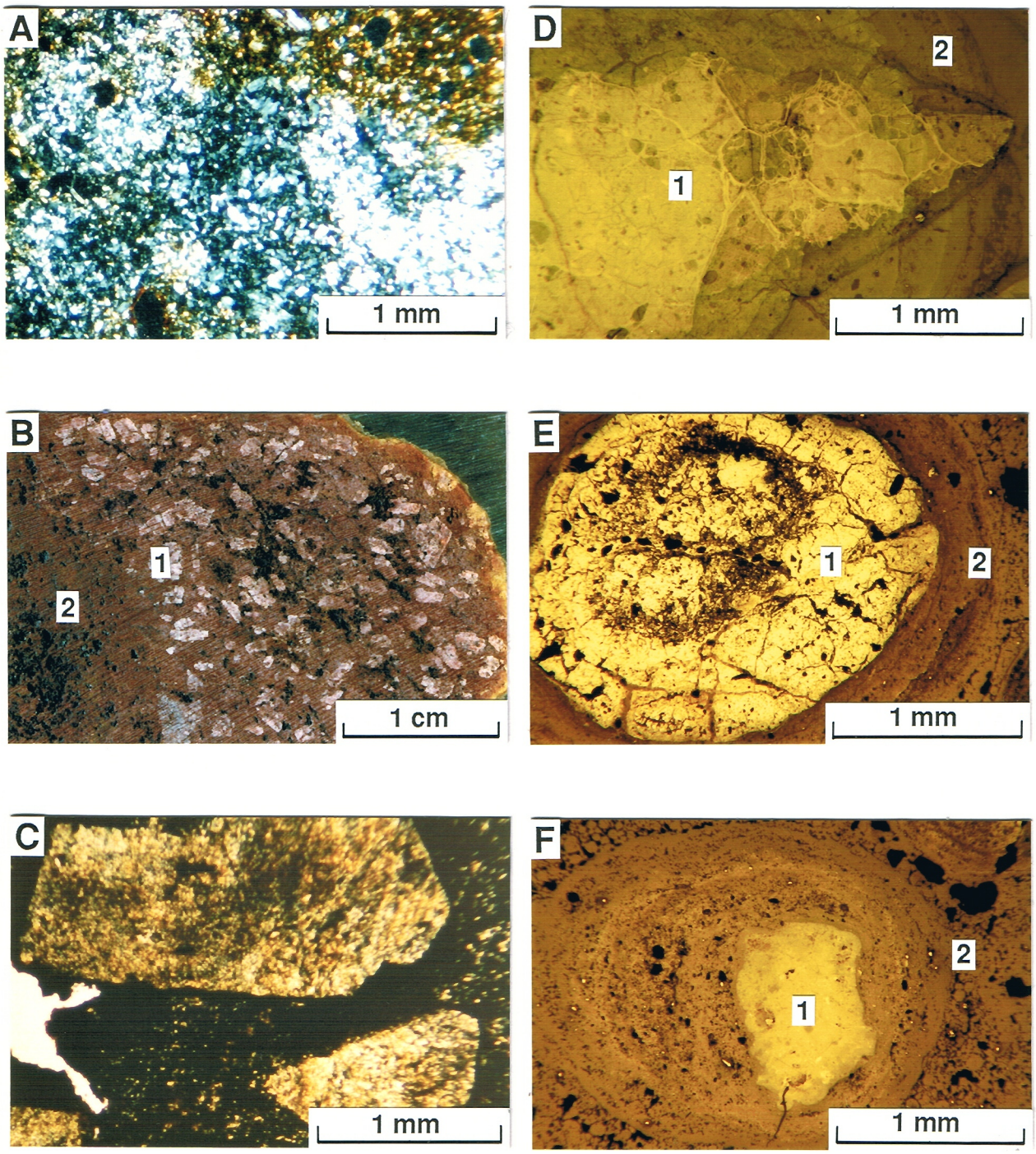

Fig. 10A Photomicrograph of thin section of a clay zone developed from felsic andesite showing mixture of kaolinite and gibbsite. Profile 1, Sample No. 07-1114, Pit A.
Fig. 10B Fragment from a bauxite zone developed from felsic andesite showing gibbsite pseudomorph after feldspar (1) and destroyed relict texture. (2).Profile 1, Sample No. 07-1067, Pit A.
Fig. 10C Photomicrograph of thin section of a fragment showing gibbsite pseudomorphs after feldspars. Profile 1, Sample No. 07-1068, Pit A.
Fig. 10 D,E,F Photomicrographs of polished sections of loose black pisoliths and nodules showing hematite rich core (1) and gibbsite-goethite-rich cutan (2). Profile 1,Sample No. 07-1109, Pit A.

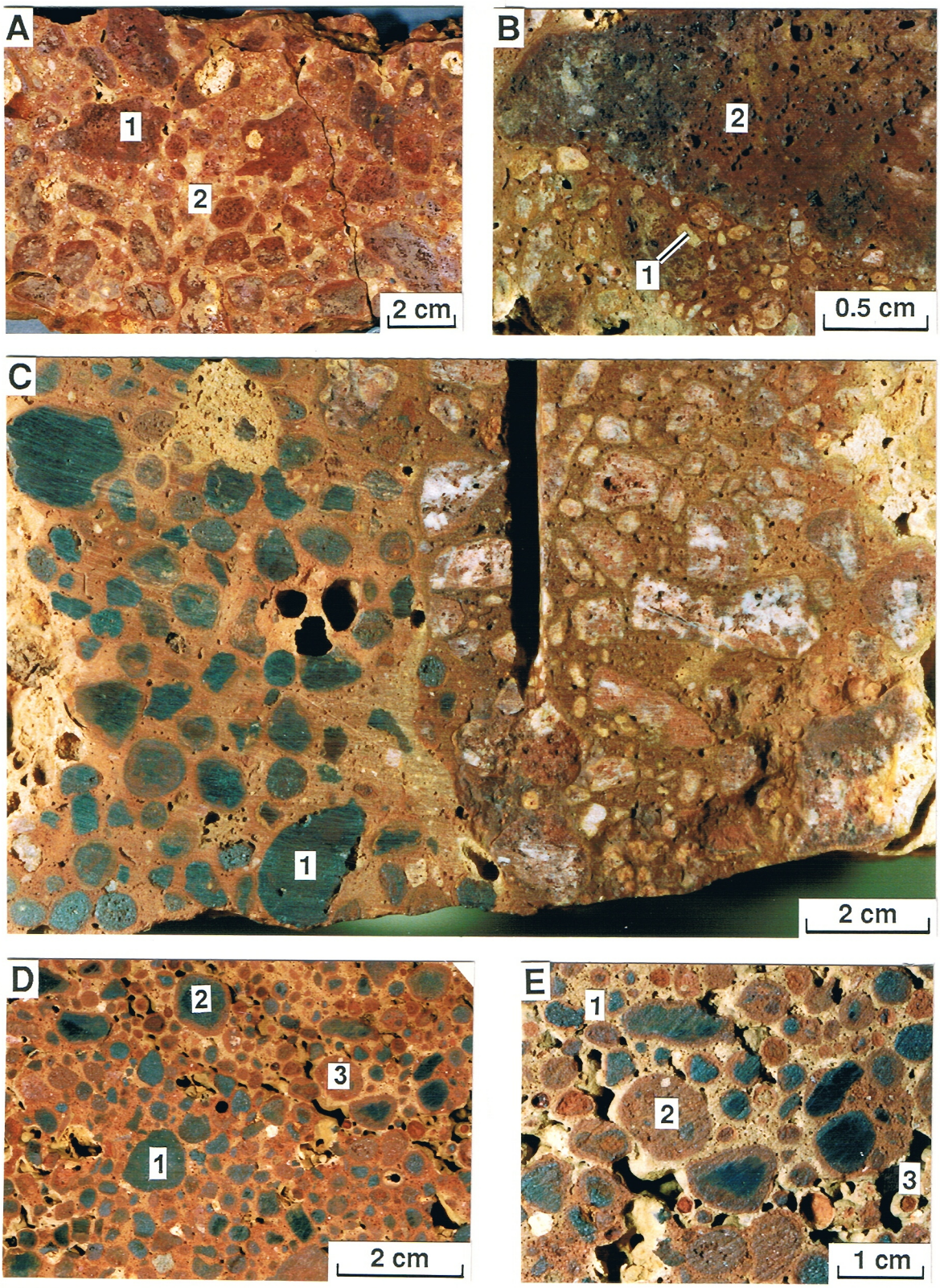

Fig. 11A Slice through a fragmental duricrust showing reddish brown gibbsite-hematite-rich fragments (1) set in a pale gibbsite-rich matrix (2). Profile 1, Sample No. 07-1106, Pit A.
Fig. 11B Slice through a fragmental duricrust showing fragments after single feldspar crystal (1) and spongy texture (2).Profile 1, Sample No. 07-1107, Pit A.
Fig. 11C Slice through a pisolitic and fragmental duricrust showing hematite-rich black nodules (1). Profile 1, Sample No. 07-1106 & 07-1108, Pit A(see text for explanation).
Fig. 11D Slice through a pisolitic-nodular duricrust showing black nodule (1), black nodule with red cutan (2), red pisolith (3) and fragments (4). Sample No. 07-1069, Pit A.
Fig 11E Slice through pisolitic-nodular duricrust showing pale yellow matrix (1), red pisolith (2) and loosening pisolith (3).Sample No.07-1069, Pit A.

in situ evolution. The contact between the two duricrusts is sharp in places and gradual at others. Usually, black nodules (2-10 mm, Figs 11C-1, 11D-1) appear first in a light brown matrix, then followed by black nodules with red cutans (Fig. 11D-2) and red pisoliths (2-8 mm, Fig. 11D-3) in a yellow matrix (Fig. 11D). The black hematite- and maghemite-rich nodules (Fig. 11D-4) are usually massive, magnetic and have similar sizes and shapes to those of the adjacent pseudomorphs. The red gibbsite- and hematite-rich pisoliths and red cutans are due to the further deferruginization of the matrix and concentration of this Fe within the matrix itself and around the nodules, sometimes several at a time. Quartz grains and pseudomorphs after feldspars can also be enveloped in this way. The red pisoliths and red cutans retain the appearance of the matrix (porosity, etc.). Occasionally, gibbsitic pseudomorphs after feldspars persist in the yellow matrix between pisoliths. The yellow matrix shows numerous dissolution cavities, up to the stage where in places only pisoliths and nodules with yellow cutans around them remain in a grain support fabric (Fig. 11E). The loose pisoliths, nodules, and compound nodules associated with the pisolitic and nodular duricrusts in small channels and pockets within the fragmental duricrust in profile 1, thus may have formed *in situ*.

In profile 2 (Fig. 12A), the bauxite zone and fragmental duricrust are much redder than the same horizons from profile 1. No pseudomorphs after feldspars were observed in the bauxite zone and fragmental and pisolitic duricrusts. Instead, microscopic examination revealed numerous ilmenite and spinel crystals (100 μm in size), showing that the parent-rock was dolerite rather than felsic andesite (Fig. 12B) and the redder colour would simply be a consequence of the greater amounts of Fe initially present in dolerite (see Table 3). The overlying horizons, from pisolitic duricrust to loose pisoliths and nodules and compound nodules, show the same phenomena of *in situ* formation and release of nodules and pisoliths as observed for profile 1, thus excluding the possibility of transported materials. The greater thickness of the pisolitic duricrust in this profile could be a consequence of the greater amounts of Fe in dolerite.

4.5.1.4 Soils

The soils forming the upper part of profiles 1 and 2 are a clayey sand. Within a depth of 30-40 cm lateritic gravels often exceed 75% of the total soil mass. Except for a dark surface soil due to the accumulation of organic matter these soils show no pedogenic horizons. The soils range from yellowish-brown to light yellowish-brown and become paler with depth.

4.5.1.5 Pisolitic and nodular lag

The nodules and pisoliths are irregular to rounded, dark-reddish brown to black, highly magnetic, and are normally between 5 and 20 mm in diameter. Pisoliths with multiple cutans are rare. Some nodules may show lithic remnant in their nucleus.

4.5.2 Pit D - andesite profiles (profiles 3, 4 and 5)

Relict textures, similar to the those observed in the bauxite-zone and the fragmental duricrust of profile 1 (Pit A), were also observed in the bauxite zone and duricrust of profiles 3 and 4. Centimetric to millimetric voids and numerous small spherical white grains occur in the matrix (Fig. 12C) which are similar to those in profile 1. Deferruginization has occurred around voids, affecting both matrix and fragments, and leaving a whitish, soft gibbsite-rich material, part of which has been mechanically removed, making the matrix more cellular (Fig. 12C).

No relict textures were observed in profile 5 where secondary structures, such as pisoliths and nodules and the spherical white grains mentioned earlier, are present from the base of the fragmental duricrust.

Examination of loose compound nodules from both profiles 1 and 5 showed that they are mostly remains of pisolitic-nodular duricrust (Fig. 12D). In profile 5, these compound nodules gradually disappear towards the surface, leaving only loose pisoliths and nodules (Fig. 12E).

In profiles 1 and 5, the loose pisoliths and nodules are centimetric to millimetric, they are black and have red cutans and an outer yellow cutan, or are just red with an outer yellow cutan. When black, they are usually not porous, either uniform or containing numerous quartz grains; microscopic examination of polished blocks shows that they can be rather heterogeneous and they are often fissured (Fig. 10D to F). When red, they have retained the characteristics of the matrix from which they formed; that is, they are porous, with quartz crystals, about 100 μm in size, lodged in some of the pores. Millimetric pisoliths of white gibbsitic pseudomorphs after feldspar surrounded by a red cutan are present in profile 1.

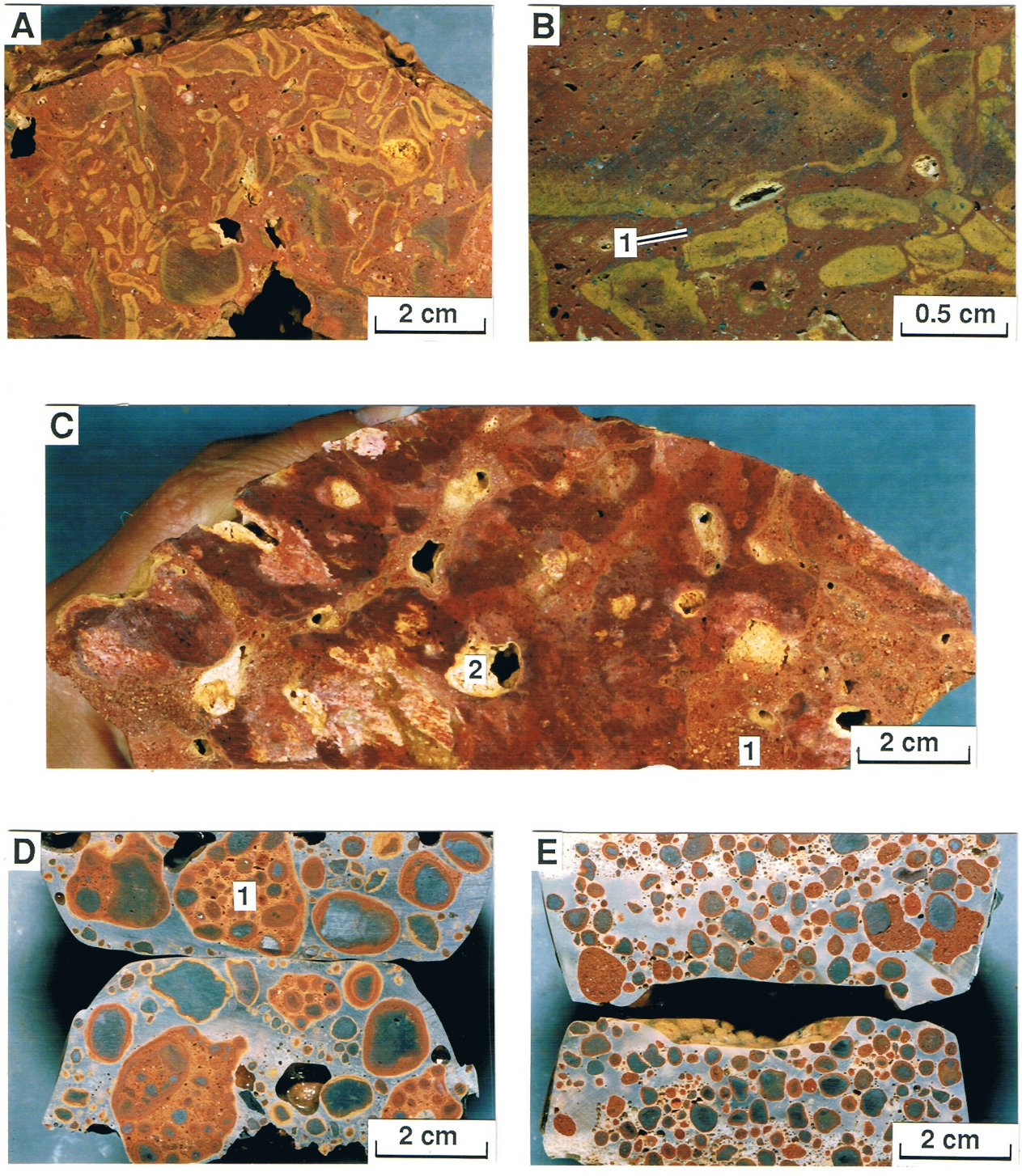

Fig. 12A Slice through a fragmental duricrust developed from dolerite.Profile 2,Sample No.07-1111, Pit A.
Fig. 12B Closeup view showing the ilmenites and spinels (1).
Fig. 12C Slice through a fragmental duricrust showing a matrix with numerous spherical white grains (1) and a void(2).Profile 4,Sample No.07-1100, Pit D.
Fig. 12D Slice through loose pisoliths and nodules showing compound nodules (1). Profile 5,Sample No.07-1095, Pit D.
Fig. 12E Slice through loose pisoliths . Profile 5,Sample No.07-1096, Pit D.

5.0 GEOCHEMICAL AND MINERALOGICAL COMPOSITIONS OF THE REGOLITH

5.1 Introduction

This study is based on the geochemical data for a set of 284 samples. The samples were taken from the surface and vertical sections across the geochemical anomaly. Samples of specific regolith units within vertical profiles generally consisted of a 1.5-kg grab sample. Locations of samples are shown in Fig. 3. The results are presented in three sections:

(a) data from drill holes and costeans (vertical profiles);
(b) data from pit faces (vertical profiles);
(c) geochemical dispersion in pisolitic and nodular lag; and
(d) all samples grouped into six categories of sample type.

5.2 Sampling methods and analytical procedures

5.2.1 Sample preparation

Bulk samples were split into two parts. A small, representative portion of each sample was selected for future reference, slicing and petrographic examination, the remainder was crushed and ground using non-metallic methods described by Smith (1987). Oversize materials, were reduced to minus 8 mm by crushing between zirconia plates in an automated hydraulic press with the undersize then being processed through an epoxy-resin-lined disc grinder with alumina plates and reduced to minus 1 mm. Final milling was done in a motorized agate mill.

5.2.2 Analytical methods

Chemical methods

A combination of chemical analytical methods including inductively coupled plasma spectroscopy (ICP), X-ray fluorescence spectrometry (XRF), and atomic absorption spectrophotometry (AAS) were used to determine a total of 32 elements (Table 1).

Petrography

Samples were prepared for petrographic study under a petrographic microscope. Polished and thin sections of selected samples were prepared and examined using both reflected and transmitted light in order to provide information on mineralogy and internal fabrics.

X-ray diffraction

XRD patterns of pulverized samples were obtained using Cu Kα radiation with a Philips vertical diffractometer and graphite diffracted beam monochromator. The diffraction peaks were recorded over the 2θ range of 3-65° and data collected at 0.02° 2θ intervals. The semi-quantitative abundances of minerals in each sample was estimated using a combination of XRD and chemical analyses of bulk samples. The relative proportions of constituent minerals were estimated from peak intensities of selected characteristic lines on the XRD traces. This approach provides a reconnaissance assessment of relative mineral abundances. The following diffraction lines were used / 111 and 110 lines of goethite, 012 and 202 lines of hematite, 313 and 220 lines of maghemite, 002 of gibbsite, 001 of kaolinite, 101 of anatase, and 101 of quartz.

Aluminium substitution in Fe-oxides

The type, crystallinity, and Al substitution of Fe-oxides are influenced by pedogenic environments (Fitzpatrick and Schwertmann, 1982). Because of its identical valency and its similar size (ionic radius 0.51 Å for Al^{3+} and 0.64 Å for Fe^{3+}), the Al^{3+} ion can replace Fe^{3+} in octahedral positions in Fe (III) oxides. An important characteristic of Al-substituted Fe (III) oxides is their smaller unit cell size (shift in XRD peaks) caused by the slightly smaller size of Al^{3+}. In all samples, the concentrations of goethite and hematite were high enough to be easily detected by XRD without any pre-treatment. For Al-substitution measurements, a NaCl or quartz internal standard was added. Measurement errors in the position of peaks were estimated and the positions of diffraction lines corrected. Aluminium substitution in goethite was determined from the 111 reflection using the relationship of mole % Al = 2086-850.7 d (111) as established by Schulze (1984).

Microprobe analysis

Geochemical analysis of each bulk sample provided the average chemical composition of that sample type. The chemical composition of individual grains, was determined by microprobe analysis which also provided information on the association of elements within particular mineral species. Selected mineral grains in polished sections were thus analysed using a Cameca SX-50 microprobe (specimen current 100 nA beam, accelerating voltage 25 kV). A suite of major and minor elements including Si, Al, Fe, Ti, As, Cu, Zn, As, and W were determined.

5.3 Results and discussion

5.3.1 Andesite and dolerite profiles - drill holes WBC15, 16, 21, 26, and costean 2

This section discusses the geochemistry and mineralogy of the weathering profiles sampled from four diamond drill holes (WBC 15, 16, 21, 26) over felsic andesite and one from the costean over dolerite (see Fig. 3). The purpose of these profiles was to examine the variations in geochemistry (with depth) of the regolith units. This was done in order to establish the weathering behaviour of different elements, to gain knowledge on how the geochemistry and mineralogy of deeply-weathered regolith relate to the underlying bedrock and the utility of various regolith materials as geochemical sampling media.

5.3.1.1 Mineralogical composition and Al substitution

Mineralogical characteristics of the different regolith units of the lateritic profile were established from X-ray diffraction and chemical analyses. The mineralogical compositions for the andesite (WBC21,15) and dolerite profiles (costean 2) related to detailed logging are shown in Figs 13, 14, and 15. The bedrocks in these profiles contain feldspars, quartz, biotite amphiboles, and chlorite. The bedrocks are not entirely fresh because they contain kaolinite and smectite. Minor minerals, not shown in Figs 13, 14, and 15, include ilmenite, and sphene. In andesite profiles, plagioclase feldspars, amphiboles, and biotite have disappeared within 2 m from the bedrock and have altered to a mixture of smectite, kaolinite, and goethite. Primary minerals were not detected in middle and upper saprolite, indicating complete weathering to secondary minerals.

Moving downward through the andesite profiles, the major change from lateritic residuum to saprolite is characterized by the decrease of gibbsite; only small amounts of this mineral present in the saprolite. Gibbsite also decreases appreciably in the top of the lateritic residuum (loose pisoliths) where amorphous Al-oxide becomes the major Al mineral. In the dolerite profile, gibbsite is present almost throughout the profile, but it is relatively-less abundant than in andesite profiles. Gibbsite in the lower horizons of dolerite profile is the result of weathering of plagioclase feldspars directly to gibbsite (Anand and Gilkes, 1984).

Kaolinite, as expected, was most abundant in the middle saprolite, it was much less common at the top and at the bottom of profile.

The bauxite zone is characterized by a replacement of kaolinite by gibbsite, and with the appearance of hematite. Iron-oxides and oxyhydroxides generally increase in abundance upwards. Goethite is present at a greater depth than hematite which is probably due to its formation as an initial alteration product of ferromagnesian minerals. Hematite and goethite are relatively more abundant in the dolerite profile than in andesite profiles. Maghemite, boehmite, and corundum (not shown) occur only in surface or near-surface horizons (loose pisoliths and pisolitic duricrust). These minerals are absent in fragmental duricrust and the underlying horizons.

Quartz decreases in abundance upwards. The relative decrease in the abundance of quartz in the upper horizons may be due to dissolution during weathering or to dilution by introduced Fe and Al minerals from overlying soil horizons. Small amounts of muscovite are present in the bauxite zone, the clay zone, and the upper saprolite. However, muscovite is not present in the bedrocks of WBC15 and 21. Its appearance in significant quantity in the clay zone and bauxite zone may be attributed to dyke-like muscovite-rich rock similar to others seen elsewhere in the Boddington area. Over dolerite and anatase, a weathering product of ilmenite is an important secondary mineral.

In bauxite and duricrust horizons, the Al substitution in goethite ranged from 20-33 mole % Al whereas in saprolite it ranged from 8-18 mole % (Table 2). Aluminium substitution increased up the profile. The high degree of Al-substitution in goethite in upper horizons is possible because goethite has formed in a particularly Al-rich environment as indicated by the presence of abundant

Table 1. Analytical methods and lower limits of detection

Element	Reported as	Method	Detection Limit
SiO_2	wt%	ICP	0.2
Al_2O_3	wt%	ICP	0.04
Fe_2O_3	wt%	ICP	0.03
MgO	wt%	ICP	0.004
CaO	wt%	ICP	0.007
Na_2O	wt%	ICP	0.007
K_2O	wt%	ICP	0.06
TiO_2	wt%	ICP	0.003
Mn	ppm	ICP	15
Cr	ppm	ICP	20
V	ppm	ICP	5
Cu	ppm	AAS	2
Pb	ppm	XRF	2
Zn	ppm	AAS	2
Ni	ppm	AAS	4
Co	ppm	AAS	4
As	ppm	XRF	2
Sb	ppm	XRF	2
Bi	ppm	XRF	2
Mo	ppm	XRF	1
Ag	ppm	AAS	0.1
Sn	ppm	XRF	2
Ge	ppm	XRF	2
Ga	ppm	XRF	4
W	ppm	XRF	4
Ba	ppm	ICP	5
Zr	ppm	ICP	5
Nb	ppm	XRF	2
Se	ppm	XRF	2
Au	ppm	Graphite furnace AAS Aq req.	0.001

ICP = inductively coupled plasma optical spectroscopy, Si, Al, Fe, Ti, Cr, V after an alkali fusion, others after $HCl/HClO_4/HF$ digestion.

XRF = X-ray fluorescence

AAS = Atomic absorption spectrophotometry, after $HCl/HClO_4/HF$ digestion

Table 2. Values of Al (mole %) substitution in goethite for lateritic duricrust, bauxite zone and saprolite

	Lateritic Duricrust		Bauxite Zone	Saprolite
	Fragmental	Pisolitic		
	N = 22	N = 12	N = 13	N = 22
Range	23-31	24-33	20-28	8-18
Mean	25	26	22	12

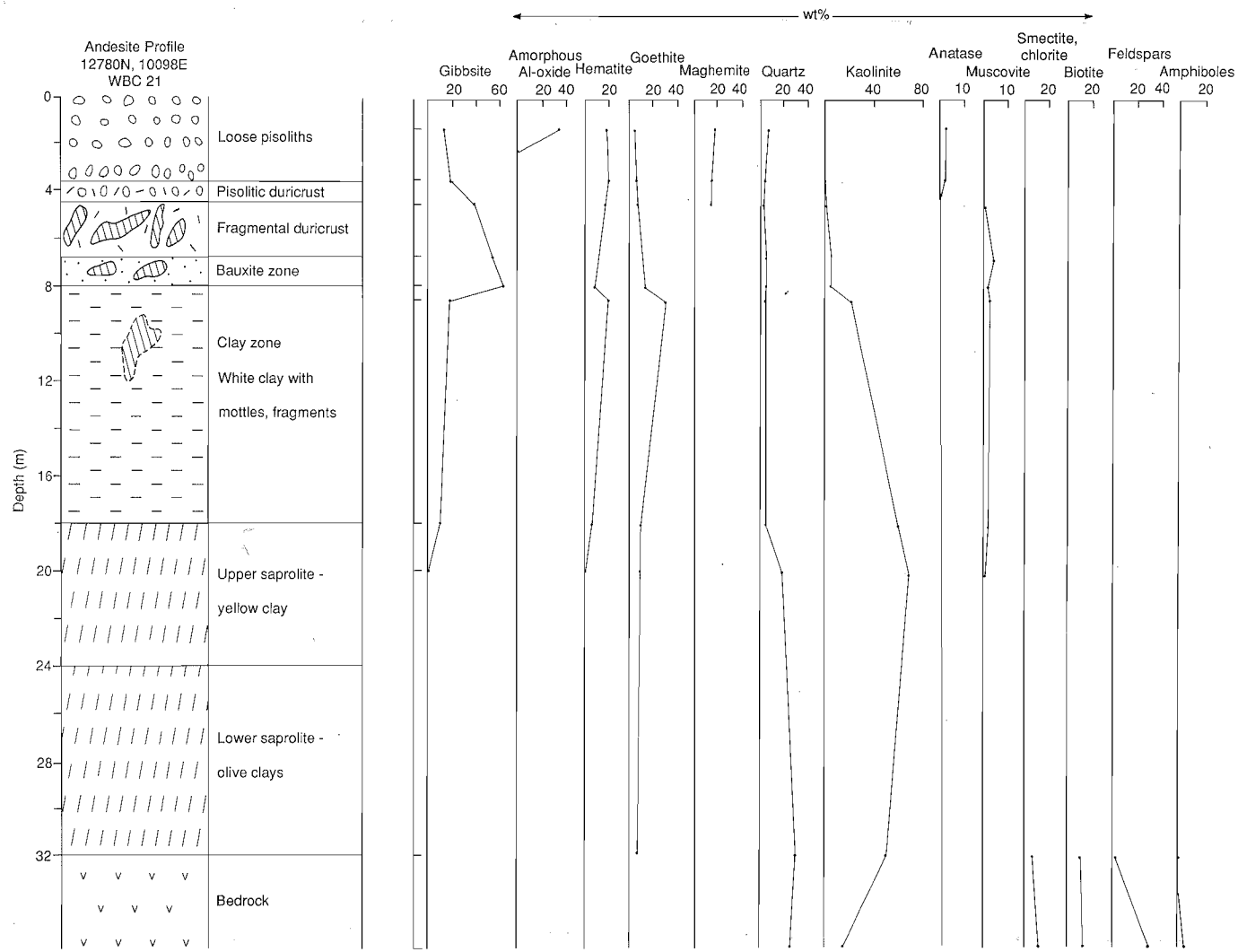

Fig. 13. Regolith stratigraphy and distribution of the dominant minerals in the andesite profile, WBC21.

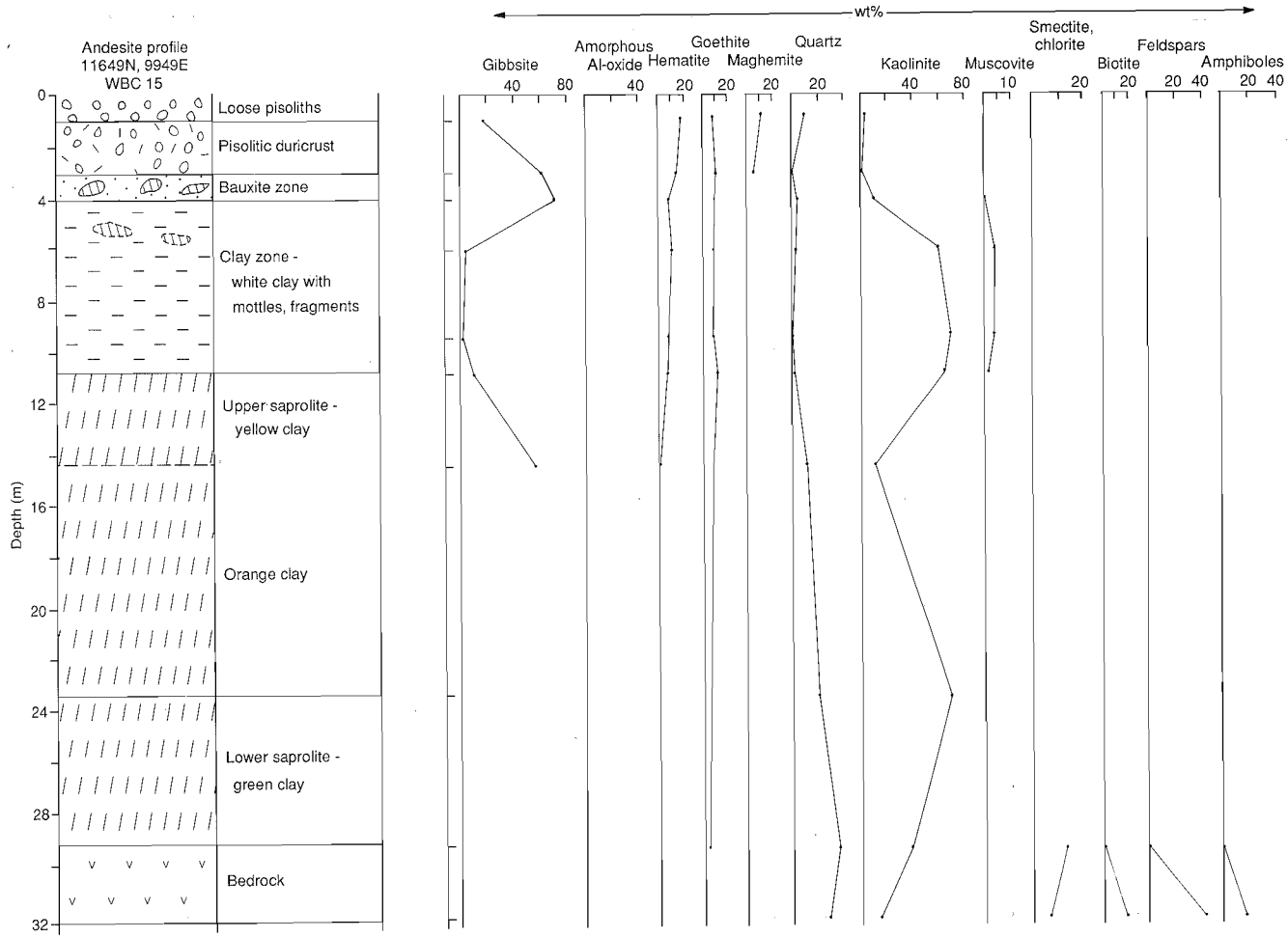

Fig. 14. Regolith stratigraphy and distribution of the dominant minerals in the andesite profile, WBC15.

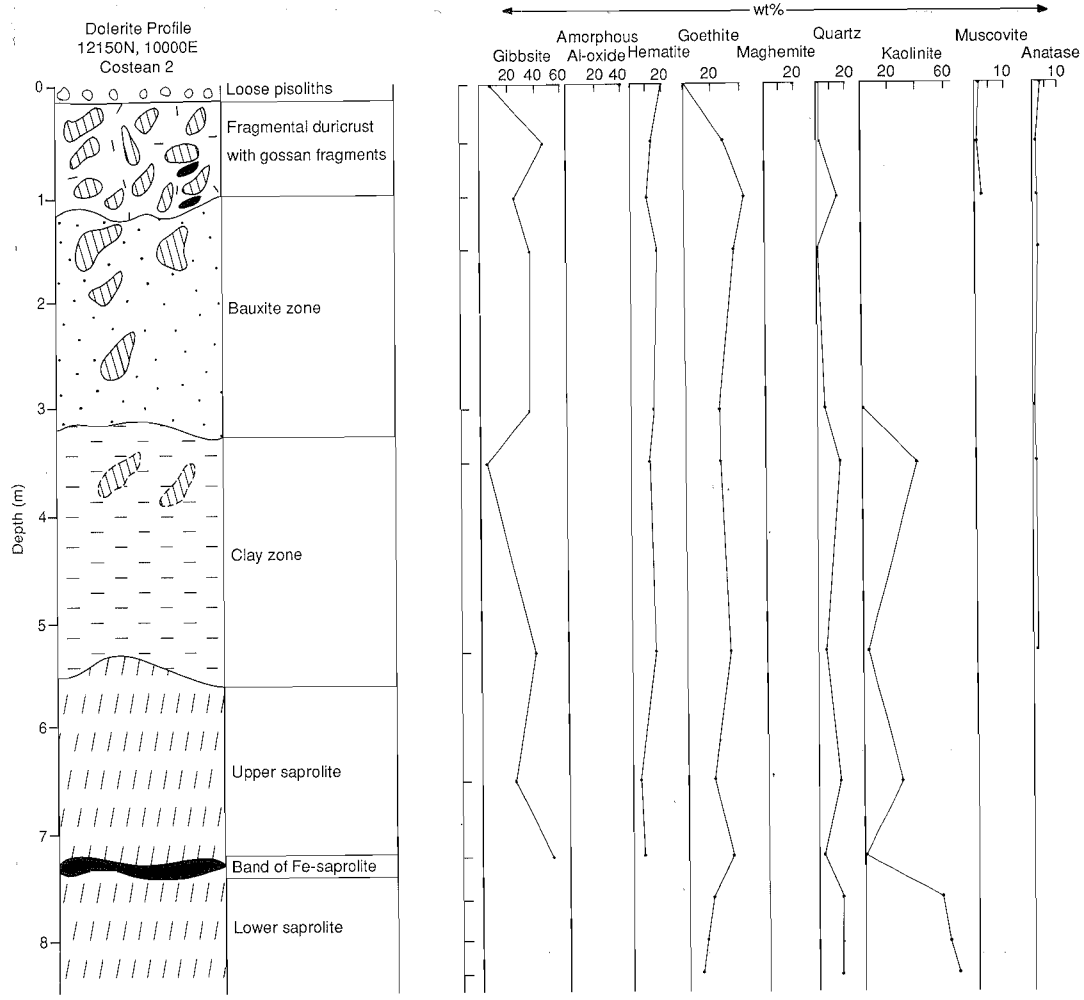

Fig. 15. Regolith stratigraphy and distribution of the dominant minerals in the dolerite profile, costean 2.

gibbsite in these materials (Fitzpatrick and Schwertmann, 1982). The relatively low degree of Al substitution in the goethite from the saprolite is consistent with the low degree of weathering as indicated by the lower amounts of gibbsite and the high amounts of kaolinite.

5.3.1.2 Geochemistry

Major elements

The chemical compositions of bedrock, saprolite (lower, upper), clay zone, bauxite zone, lateritic duricrust and loose pisoliths for andesite and dolerite profiles are given in Table 3, and the distributions of selected elements are compared in Figs. 16 to 21. Chemical data for fresh dolerite are not available and were taken from Monti (1987). Aluminium and Fe_2O_3 are by far the most abundant constituents with values greater than 40% in loose pisoliths and pisolitic duricrust. These are enriched throughout the weathered profile compared to the bedrock. These elements are largely residual products of deep chemical weathering, occurring as goethite, hematite, and maghemite or as gibbsite, amorphous Al-oxide, and kaolinite. Each is strongly enriched in the upper saprolite and overlying horizons, by factors of two or more, due to residual concentration concomitant with the leaching of other elements. The highest concentration of Fe_2O_3 occurs in pisolitic duricrusts and loose pisoliths and is relatively higher in the doleritic profile than in andesitic profiles. The Fe content of dolerite is greater than that for felsic andesite (17.5-21.5% Fe_2O_3 compared with 4.8-8.5% Fe_2O_3). Iron retention or enrichment during lateritization results in laterites derived from dolerite being far more ferruginous than felsic andesite-derived laterite. The concentrations of these elements correspond well with the mineralogical results.

Little Si remains in the bauxite zone and overlying horizons, with only about 1.7% in the loose pisoliths, relative to an initial content of 57.8% in andesite and 12.4% in saprolite. Silica occurs mostly as quartz and kaolinite.

The minor oxides Na_2O, K_2O, CaO, and MgO are strongly depleted in saprolite and overlying horizons. In bedrock, their major elements occur as feldspars (Na, Ca), ferromagnesian minerals (Mg) and mica (K). Of these elements, Ca, Mg, and Na, in particular, are all strongly leached at the onset of weathering and almost totally depleted from the upper saprolite, lateritic duricrust and loose pisoliths. Calcium oxide, MgO, and Na_2O concentrations are low at 0.01-0.06% in the middle and upper saprolite, bauxite zone, and lateritic duricrust.

The K-distribution is controlled by the weathering of micas. However, there is no systematic trend in the distribution of K. Potassium in the bauxite zone and lateritic duricrust occurs as muscovite which is resistant to weathering (Anand and Gilkes, 1987).

Titanium gradually increases upwards through the profiles and is mainly present as anatase and unweathered ilmenite.

Trace elements

The elements Mn, Cu, Zn, Co, and Ni are considered together because they have many similarities in chemical behaviour in the weathering environment. Figures 16 to 21 and Table 3 show that the chemical patterns of these elements are not consistent from profile to profile for andesite profiles. Manganese, Cu, Ni, and Co, for example, are enriched in the lower saprolite of WBC21, but are leached from the lower saprolite of WBC15. However, these elements are strongly leached from the middle saprolite and the overlying horizons in all the profiles. There is a general decrease in Zn and Ni up through the profiles, although there is a near-surface increase in these components. There is also a surface and near-surface increased concentration of Mn and Co.

Vanadium, Cr, As, Bi, Sn, Ga, W, Zr, Nb, and Pb are concentrated up the profiles particularly in the upper saprolite, bauxite zone, and lateritic duricrust. However, the concentrations of W, Sn, and Bi are decreased in the pisolitic duricrust and loose pisoliths relative to the underlying fragmental duricrust and bauxite zone. These elements follow more or less the pattern for Fe_2O_3, which suggests that these elements are associated with Fe-oxides and oxyhydroxides. Some of the elements are retained in primary minerals which are resistant to weathering, such as zircon (Zr, Nb), ilmenite (Cr, V), and sphene (Nb).

There is a gradual increase of Mo up through the profiles. However, in profile 1 there is a slight decrease in the middle part of the profile. Gallium behaves similarly to Al, as its hydroxide. It can substitute for Al in gibbsite and Fe^{3+} in goethite.

TABLE 3. Summary of the Chemical Composition of the Various Regolith Units Over Andesite and Dolerite Bedrocks

	Andesite Profiles							Dolerite Profiles					
	Bedrock	Lower Saprolite	Middle Saprolite	Upper Saprolite	Bauxite Zone	Lateritic Duricrust	Loose Pisoliths	Bedrock*	Lower Saprolite	Upper Saprolite	Bauxite Zone	Lateritic Duricrust	Loose Pisoliths
No. of Samples	4	7	5	9	2	4	3	NA	5	2	3	3	1
Wt %													
SiO_2	57.8-69.7	51.8-72.7	17.5-62.5	12.4-68.0	4.5-8.1	1.7-7.9	1.5-10.9	NA	2.1-50.5	6.2-25.2	1.1-4.7	0.9-3.0	8.3
Al_2O_3	13.37-17.5	15.70-29.09	8.76-47.98	8.05-33.25	47.22-49.30	38.91-50.63	45.34-49.87	10.00-15.10	28.71-38.16	27.20-30.22	30.41-32.49	23.42-42.69	39.10
Fe_2O_3	4.86-8.48	4.70-7.05	1.36-11.41	1.37-43.47	15.01-17.30	16.16-32.03	31.46-36.04	17.50-21.50	9.62-33.60	32.03-40.47	37.75-43.61	27.03-53.77	38.90
MgO	1.38-3.68	0.05-1.16	0.02-0.13	0.03-0.11	0.03-0.04	0.01-0.06	0.02-0.07	1.90-4.00	0.03-0.06	0.01-0.03	0.01	0.01-0.03	0.05
CaO	3.03-6.48	0.02-0.91	0.01-0.04	0.02-0.05	0.02	0.02-0.03	0.04-0.09	2.30-7.30	0.02-0.04	0.01-0.02	0.02	0.02-0.04	0.08
Na_2O	1.81-3.94	0.04-0.43	0.03-0.11	0.03-0.11	0.01-0.03	0.01-0.03	0.03-0.05	1.20-2.80	0.07-0.47	0.01-0.03	0.01-0.05	0.01-0.03	0.03
K_2O	1.42-2.75	0.14-1.45	0.40-0.71	0.10-0.67	0.10-0.18	<0.06-0.4	<0.06-0.12	0.50-1.00	<0.06-0.24	<0.06	<0.06	<0.06-0.19	0.20
TiO_2	0.48-0.72	0.52-0.93	0.25-1.67	0.25-4.09	2.25-2.59	2.37-3.90	2.57-3.32	2.20-2.30	1.22-2.80	2.40-3.00	2.47-2.92	1.68-2.74	3.57
LOI	0.87-2.52	5.03-11.40	6.14-24.10	5.78-13.50	26.10-26.60	18.20-27.10	9.43-10.60	NA	12.10-24.00	13.50-20.70	22.20-22.40	18.30-26.40	9.78
ppm													
Mn	305-865	15-1788	4-50	2-306	5-15	11-99	84-113	775-1675	7-123	127-134	92-103	19-95	137
Cr	16-126	16-182	16-325	16-734	340-490	251-408	354-408	16-25	89-267	127-129	177-217	113-220	424
V	66-91	72-126	89-208	71-744	283-369	361-699	513-699	591-910	163-688	737-806	760-917	169-821	669
Cu	92-4850	191-6740	107-125193	76-3310	36-66	16-308	2-14	117-314	104-222	112-263	98-124	41-279	11
Pb	2-8	<2-14	<2-8	<2-20	<2	<2-14	18-20	<2	<2-6	<2-3	3-6	2-6	23
Zn	52-118	36-119	11-35	13-116	11-13	8-18	32-49	96-198	12-18	13-22	10-13	11-12	14
Ni	35-91	27-139	12-77	15-114	<4	<4	<4-17	25-65	<4-48	<4-27	<4	<4	12
Co	13-28	<4-127	<4-8	<4-15	<4	<4	<4	27-56	<4-9	6	<4	<4-6	6
As	<2-44	<2-62	4-48	9-183	40-109	47-123	35-206	<10	8-58	13-32	51-116	26-76	82
Sb	<2	<2	<2	<2-5	<2	<2-4	<2	<5	<2-3	<2	<2-4	<2-3	<2
Bi	<2-9	<2-10	<2-20	2-26	13-25	8-35	7-12	NA	<2	<2	<2	<2	4
Mo	2-8	2-56	4-39	11-87	14-15	34-88	33-46	<5-5	1-10	<1-4	<1-9	4-11	30
Ag	<0.1-9	<0.1-9	<0.1-233	<0.1	<0.1	<0.1	<0.1	<10	<0.1	<0.1	<0.1	<0.1	<0.1
Sn	15-46	10-26	3-50	14-70	18-72	17-84	7-52	<5	<2-4	<2-4	<2-6	2-4	16
Ge	<2	<2-3	<2-3	<2-5	<2	<2	<2	NA	<2-4	<2	<2	<2	<2
Ga	15-20	17-26	2-42	10-83	59-80	68-93	83-87	NA	22-45	36-44	47-52	42-46	93
W	<4-43	6-61	5-55	14-79	17-43	41-85	7-52	<10-20	<4-21	<4	5-6	<4-6	19
Ba	138-577	56-638	27-624	31-195	30-75	13-109	25-41	83-116	8-92	<5	<5	<5-64	64
Zr	37-109	65-181	65-301	48-689	462-497	420-564	470-700	120-143	106-208	149-174	161-228	241-424	542
Nb	<2-5	<2-10	<2-17	4-24	21-22	17-26	16-28	8-12	6-14	6-7	10-13	11-14	29
Se	<2-26	<2-4	<2-79	<2-15	<2-4	<2-3	<2	NA	2-4	2-4	4-8	3-9	<2
Au	0.29-1.19	0.01-1.53	0.17-5.15	0.54-12	0.56-9.10	0.05-1.01	0.02-0.11	<0.01-0.06	0.02-0.20	0.06	0.42-0.81	0.43-5.02	0.06

* Taken from Monti (1987).

NA = Not available

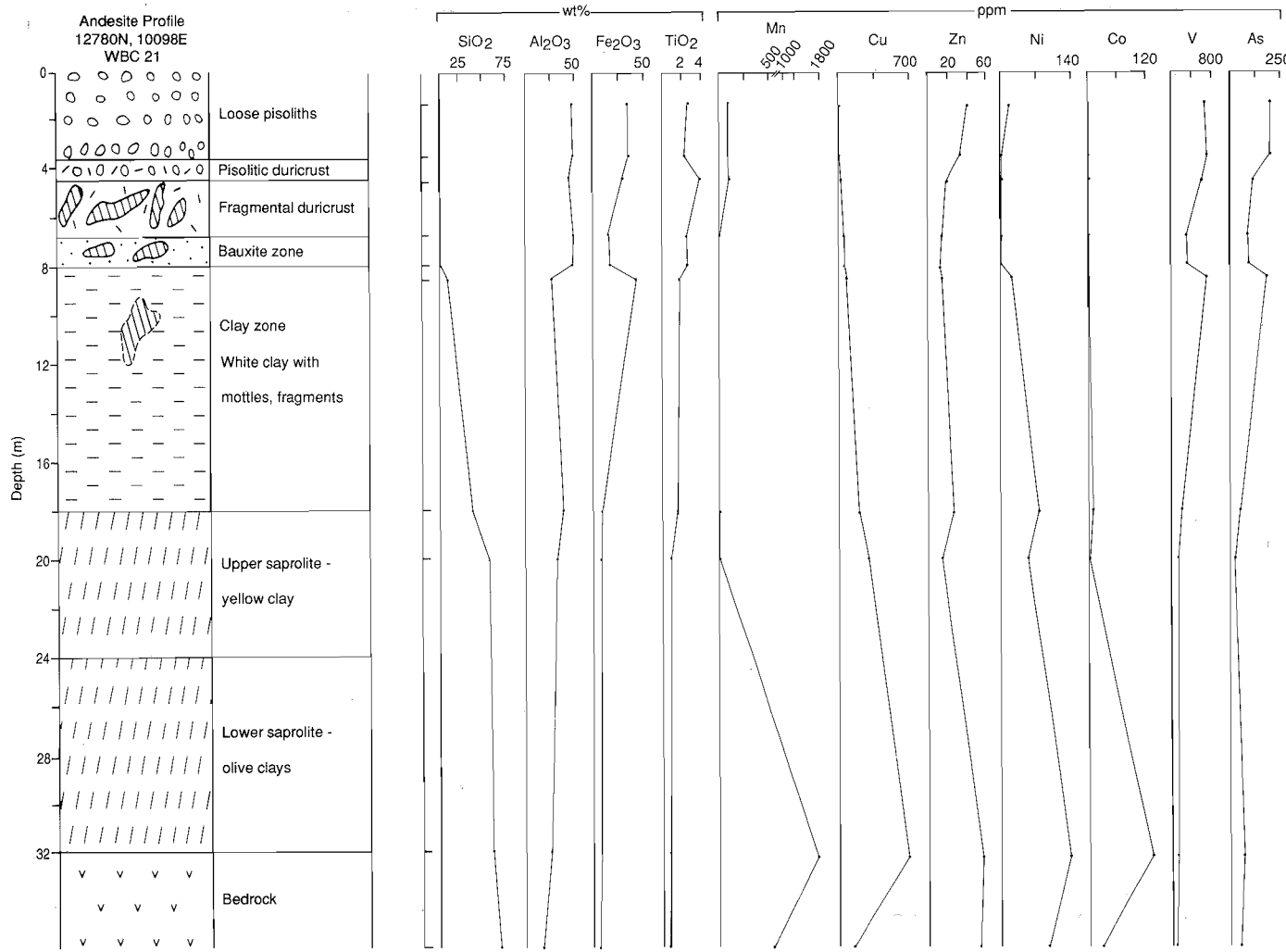

Fig. 16. Vertical distribution of SiO_2, Al_2O_3, Fe_2O_3, TiO_2, Mn, Cu, Zn, Ni, Co, V, and As in the andesite profile, WBC21.

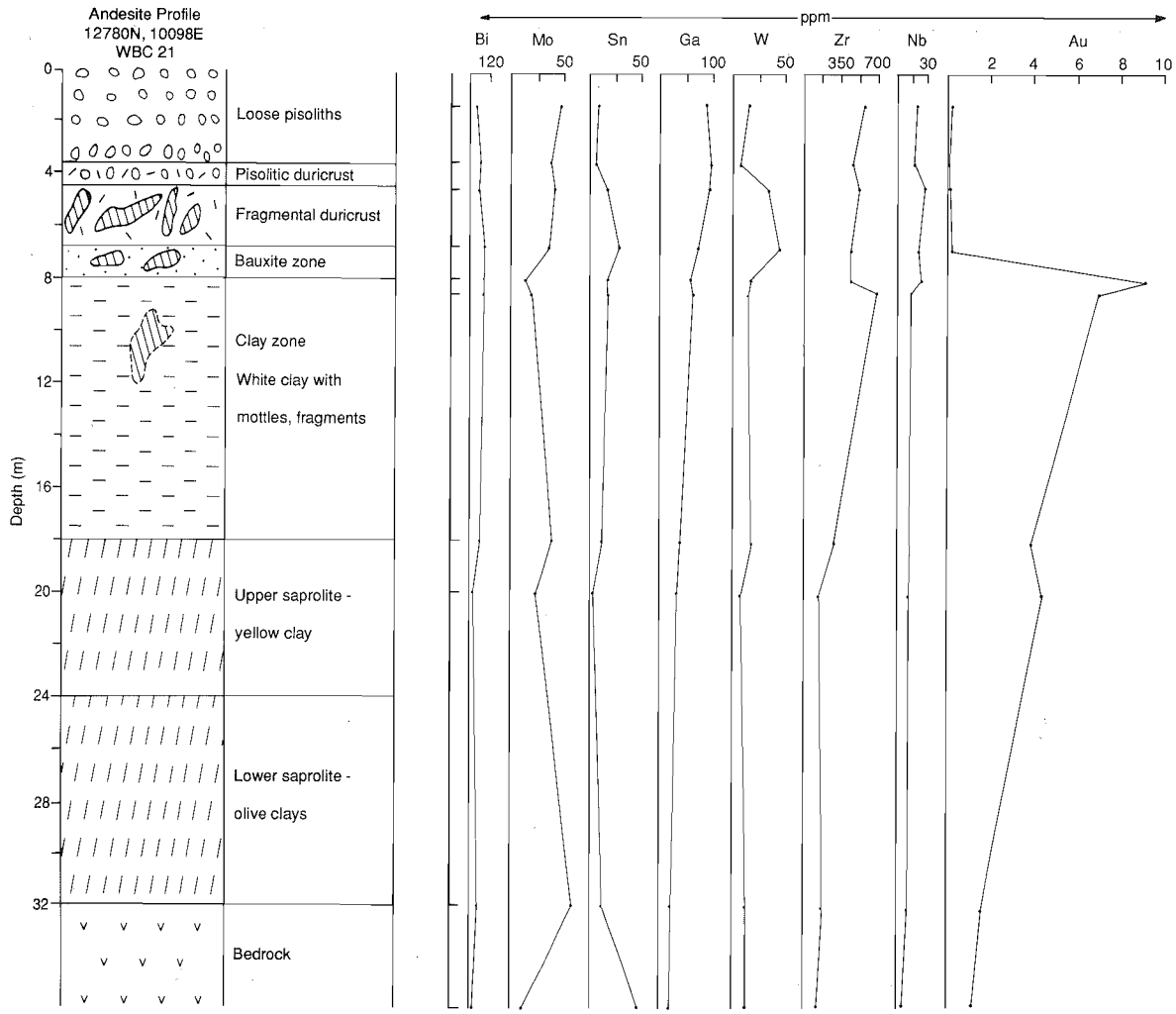

Fig. 17. Vertical distribution of Bi, Mo, Sn, Ga, W, Zr, Nb, and Au in the andesite profile, WBC21.

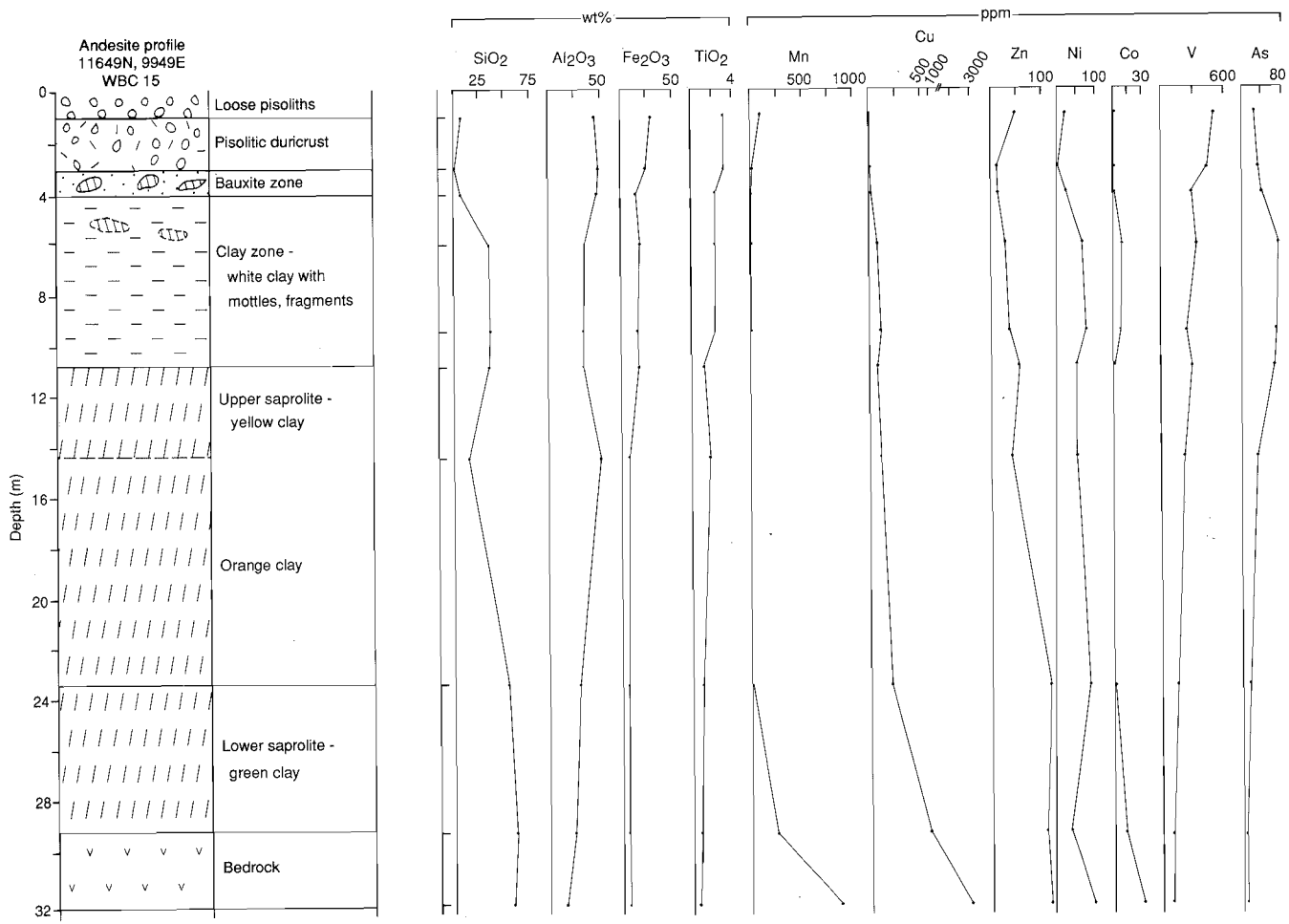

Fig. 18. Vertical distribution of SiO_2, Al_2O_3, Fe_2O_3, TiO_2, Mn, Cu, Zn, Ni, Co, V, and As in the andesite profile, WBC15.

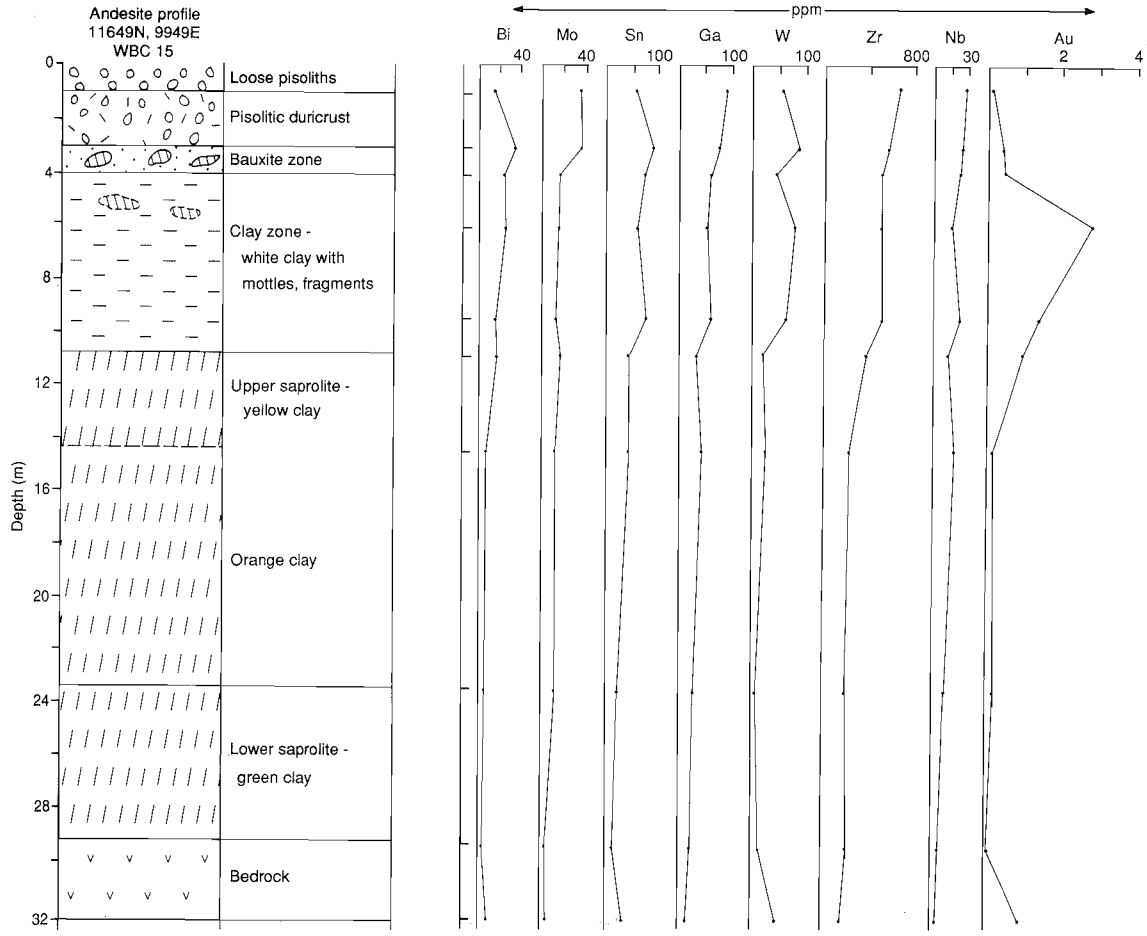

Fig. 19. Vertical distribution of Bi, Mo, Sn, Ga, W, Zr, Nb, and Au in the andesite profile, WBC15.

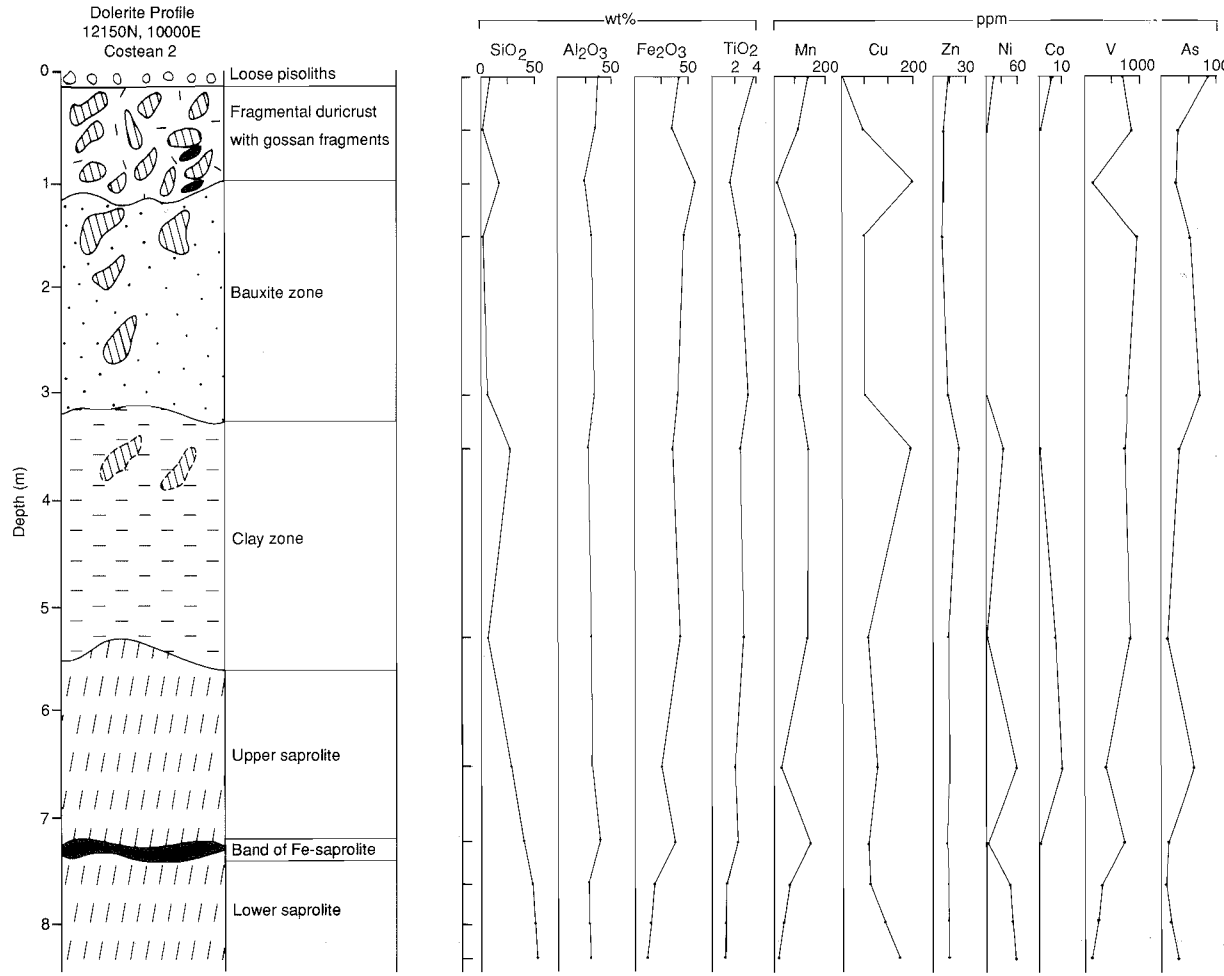

Fig. 20. Vertical distribution of SiO_2, Al_2O_3, Fe_2O_3, TiO_2, Mn, Cu, Zn, Ni, Co, V, and As in the dolerite profile, costean 2.

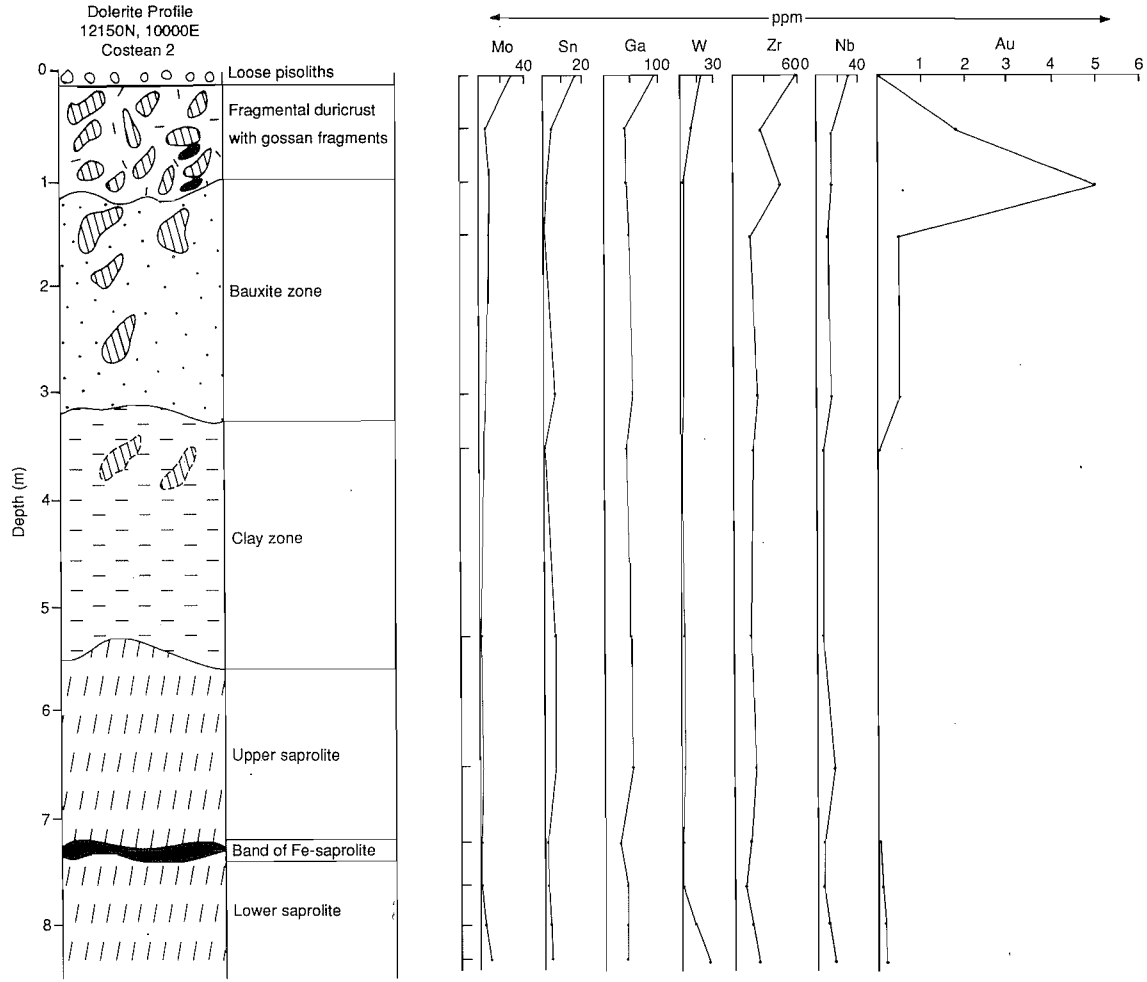

Fig. 21. Vertical distribution of Mo, Sn, Ga, W, Zr, Nb, and Au in the dolerite profile, costean 2. Abundances for Bi in this profile were below detection limits.

The Ba contents are maintained throughout the profiles and Ba is reduced only in lateritic duricrust. The concentrations of Ba are generally slightly enriched in the saprolite compared to the bedrock. High concentrations of Ba are closely related to K concentrations.

Gold is detectable in the pisolitic duricrust and loose pisoliths, but the contents are very low compared to the underlying horizons. Gold is strongly concentrated in the bauxite zone and upper clay zone of all the profiles and it decreases sharply from the bauxite zone to loose pisoliths. Exploration work conducted by Reynolds over the Boddington Au deposit shows that the highest and most continuous Au values in the laterite profile occur over mineralized bedrock. However, it tends to be concentrated at three subhorizontal levels within the profile, namely the lower part of the bauxite zone (Level 1), middle saprolite (Level 2), and lower saprolite (Level 3) (Symons *et al.*, 1988). The three levels are generally separated by barren or weakly-mineralized saprolitic clays. In terms of mineral exploration, Au is showing weak anomalies associated with high As, Mo, Bi, Sn, and W in loose pisoliths and lateritic duricrust.

In the dolerite profile (Table 7), severe leaching of many major and trace elements occurs at the bedrock-saprolite interface. The trends in element behaviour in andesite and dolerite profiles are very similar, with minor differences due to the contrasting chemistry and mineralogy of the host rock. Gold is not enriched in the clay zone and upper saprolite overlying barren dolerite. However, significant amounts of Au are in the bauxite zone and lateritic duricrust which probably have been laterally transported into these.

The presence of W and Sn in all regolith units of the profiles developed from andesite and its absence from the dolerite profile indicates a relative lack of mobility and lateral transport. However, there is a small surface concentration in loose pisoliths, probably because of residual enrichment.

5.3.2 Andesite and dolerite profiles - Pit A and Pit D

This section discusses the geochemistry and mineralogy of five profiles, the locations of which are shown in Fig. 3 and their field relationships in Fig 7A, B, C, D, and E. The purpose of these profiles was to examine in detail the variation in geochemistry and mineralogy of various morphologies of duricrust and lateritic pisoliths while section 5.3.1 described the variation in geochemistry and mineralogy of regolith units in whole profiles.

At the time of the sampling, both Pit A and D, were open at the northern and southern ends of the deposit, exposing the weathered profile from the surface down to the saprolite. Five profiles were selected, two in Pit A and three in Pit D, where samples were taken from the pit faces from the surface down to the bauxite zone or clay zone on a common vertical line wherever possible.

Prior to mining, profiles 1 and 2 from Pit A were located on an upper and upper-mid slope respectively, and profiles 3, 4, and 5 from Pit D were located on a mid to lower slope. According to the geological map of the bedrock (Boddington Gold Mine internal datum), profiles 1, 3, 4, and 5 are on felsic andesite, whereas profile 2 is just above a contact between the felsic andesite and a dolerite dyke; a diorite dyke is immediately adjacent to the felsic andesite at profile 4.

5.3.2.1 Mineralogy

The mineralogical composition of the lateritic units presented here, was established from X-ray diffraction analysis of some 28 samples. The detailed results are given in Table 4.

The clay zone and upper saprolite contain kaolinite and goethite, with lesser amounts of hematite and gibbsite. The bauxite zone is characterized by the disappearance of the clays with replacement by gibbsite which becomes the major constituent and remains so further up. In addition to gibbsite, hematite and goethite are also present in large amounts.

In all the duricrust samples, as well as in the loose pisoliths and nodules, hematite is mostly predominant over goethite. Some maghemite occurs in the pisolitic duricrusts, and it is a major constituent of the loose pisoliths and nodules.

Small amounts (2-4%) of anatase are consistently present throughout the lateritic units in profiles 1, 3, 4, and 5. In contrast, anatase is present in higher amounts (up to 8%) in the dolerite profile. Some quartz is also present throughout the lateritic units, usually in very small amounts.

In addition to all the above minerals, small amounts of ilmenite occur in profile 2, where the parent-rock is a dolerite.

Table 4. Mineralogical Composition (wt%) of Regolith Units from Five Vertical Profiles

Sample No.	Sample Type	Depth Below Surface (m)	Northing (local grid)	Easting (local grid)	Gibbsite	Amorphous Al-oxide	Kaolinite	Hematite	Maghemite	Goethite	Quartz	Anatase
PROFILE 1, PIT A, FELSIC ANDESITE, UPPER SLOPE												
07-1109	Loose pisoliths	1.0	13050	10020	36	15	0	14	14	8	4	3
07-1108	Pisolitic duricrust	1.3	13050	10020	58	0	0	14	10	8	0	4
07-1106	Fragmental duricrust	1.4	13050	10020	70	0	0	15	0	10	0	3
07-1107	Fragmental duricrust	1.6	13050	10020	70	0	0	14	0	12	0	2
07-1114	Clay zone	7.2	13040	10040	10	0	58	4	0	18	5	2
PROFILE 2, PIT A, DOLERITE, MID-SLOPE												
07-1124	Loose pisoliths (transported)	0.4	12975	10070	26	20	0	14	16	8	6	3
07-1115	Loose pisoliths (transported)	0.6	12950	10060	36	14	0	20	12	12	0	3
07-1110	Pisolitic duricrust	0.8	12975	10070	45	12	0	20	10	6	0	6
07-1111	Fragmental duricrust	2.6	12975	10070	50	0	0	25	0	15	0	6
07-1112	Fragmental duricrust	2.8	12975	10070	45	0	0	28	0	20	0	6
07-1113	Bauxite zone	3.6	12975	10070	25	0	0	20	0	4	0	8
PROFILE 3, PIT D, FELSIC ANDESITE, MID-SLOPE												
07-1079	Pisolitic duricrust	0.3	10170	9640	50	0	0	20	10	8	0	2
07-1080	Pisolitic duricrust	0.8	10170	9640	54	0	0	26	0	12	2	2
07-1081	Fragmental duricrust	1.3	10170	9640	58	0	0	20	0	14	0	2
07-1082	Fragmental duricrust	1.6	10170	9640	64	0	0	18	0	12	0	2
07-1083	Fragmental duricrust	1.9	10170	9640	72	0	0	12	0	10	0	2
07-1084	Fragmental duricrust	2.1	10170	9640	72	0	0	12	0	9	0	2
07-1122	Clay zone	4.4	10160	9650	10	0	48	2	0	10	25	0
PROFILE 4, PIT D, FELSIC ANDESITE, MID-LOWER SLOPE												
07-1099	Pisolitic duricrust	0.4	9470	10260	60	0	0	12	5	10	0	3
07-1100	Fragmental duricrust	0.8	9470	10260	64	0	0	18	0	12	3	2
07-1102	Fragmental duricrust	1.8	9470	10260	70	0	0	14	0	10	0	2
07-1103	Bauxite zone	2.8	9470	10260	66	0	0	12	0	10	5	2
PROFILE 5, PIT D, FELSIC ANDESITE, LOWER SLOPE												
07-1096	Loose pisoliths	0.9	9400	10310	44	15	0	14	18	6	0	3
07-1095	Loose pisoliths	1.2	9400	10310	46	15		15	10	10	2	3
07-1094	Pisolitic duricrust	2.2	9400	10310	45	15	0	16	10	8	0	2
07-1093	Fragmental duricrust	2.8	9400	10310	64	0	0	16	0	12	4	2
07-1092	Fragmental duricrust	3.6	9400	10310	62	0	0	18	0	11	3	2
07-1090	Bauxite zone	4.4	9400	10310	64	0	0	14	0	10	8	2

5.3.2.2 Geochemistry

The chemical compositions of the laterite units from profiles 1 to 5 are in Table 5. This data show that the bauxite zone and fragmental duricrust from profile 2 are richer in Fe_2O_3, TiO_2, Mn, V, Zn, and Nb than the same horizons from the other profiles. This can be explained by the doleritic nature of the parent-rock and by the presence, in particular, of the ilmenite. For example, electron-microprobe analysis of ilmenite grains showed them to contain up to 5% Mn. In the overlying loose pisoliths and pisolitic duricrust however, the concentration of Fe_2O_3 is not as high, probably because the loose pisoliths are transported and were formed from the weathering of felsic andesite. Field relationships suggest that the upper layer of loose pisoliths is locally transported, whereas the lower part of the profile appears to be residual (see Fig. 7).

Profiles 1 and 2 from Pit A, and more particularly profile 1 over felsic andesite, are rich in As and Sb, whereas profiles 3, 4, and 5 from Pit D are rich in W and Sn. These are probably primary features, as these elements are moderately mobile to immobile (Andrew-Jones, 1968, Davy and El-Ansary, 1986). They may reflect the arsenopyrite and stibnite mineralization of the bedrock around the Pit A area, and scheelite or wolframite and cassiterite in the bedrock of the Pit D area.

Gold decreases in abundance from the base of bauxite zone to the loose pisoliths except in profile 2 where the loose pisoliths are transported.

Profile 4 is richer in Au and Mo than the other profiles. This could be due to the particular topographic position of this profile, which forms a small crest downslope, or to the diorite dyke immediately adjacent, which could both have acted as a barrier to percolating solutions. However, Symons *et al.* (1988) noted the presence of Au-bearing quartz-veins in diorite dykes. This suggests that the higher abundances of Au in profile 4 are more likely due to mineralization in the adjacent diorite dyke.

There are significant concentrations of Au in the bauxite zone and in the fragmental duricrust, developed from dolerite (profile 2) these suggest lateral transportation of Au. These results are consistent with those already discussed for drill hole dolerite profiles.

In the five profiles, the duricrusts are lower in SiO_2, MgO, K_2O, Na_2O, Au, Ba, Cu, and Ni than the underlying bauxite and clay zones and higher in Fe_2O_3, Al_2O_3, TiO_2, Cr, Ga, Sn, V, Mo, W, As, and Zr. Molybdenum, however, is higher and as a very mobile element might have been transported into the duricrust. The pisolitic duricrusts are lower in Al_2O_3, Au, Cu, and Zr, and higher in most other elements, relative to the fragmental duricrusts.

5.3.3 Geochemical dispersion in pisolitic and nodular lag

The geochemical patterns are based on 146 sample sites of loose nodules and pisoliths. The sampling pattern may be broken into two parts, namely, that over the Pit A and its surroundings and, that from Pit D (Figs. 22 and 23). Bedrock relationships for the corresponding areas are shown in Figs 24 and 25. Surface samples were collected at 100 m intervals and a radius of 5 to 10 m at each site. The lateritic pisoliths and nodules were generally in the size range of 5 to 15 mm and have a 1-2 mm thick goethite gibbsite-rich cutan around dark reddish-brown to black cores. These lag gravels are highly magnetic and are dominated by hematite, maghemite, amorphous Al-oxides with small amounts of goethite, gibbsite, corundum, and boehmite.

The lag gravels are dominated by Al_2O_3 (44% mean) and Fe_2O_3 (40% mean) with lesser amounts of SiO_2 (5% mean). There are no obvious patterns related to bedrock and the high values of Al_2O_3 reflect the bauxitic nature of the area. The CaO, MgO, and Na_2O concentrations are very low, a common feature of lateritic materials. The mean abundances of K_2O are 0.07% with a range commonly from 0.02 to 0.41%. The mean concentrations of TiO_2 are 2% with values ranging from 1.4 to 3.8%.

Some of the analytical data related to Au mineralization for pisolitic and nodular lag from Pit A and Pit D areas are shown in Figs. 26 to 39, that show both the analytical values and manually delineated contours. Analytical data on individual samples are given in Appendix 1.

Au

The geochemical pattern for Au (Figs. 26 and 27) shows small and erratic distribution over the Pit A and Pit D areas with the exception of some higher concentrations (to 1150 ppb) at the southern end of Pit A. Gold abundances, particularly in southeast of Pit A are very small. A threshold of 30 ppb would be appropriate in reconnaissance exploration for such an anomaly, based upon experience from elsewhere in the Yilgarn Craton. Gold distribution shows that, in general, there is a limited surface expression of the bedrock abundances. However, as discussed earlier in Section 5.3.2.2, Au is relatively more abundant in the

Table 5. Chemical Composition of Regolith Units From Five Vertical Profiles

Sample No.	Sample Type	Sample Code	Depth Below Surface (m)	Northing (local grid)	Easting (local grid)	SiO_2 %	Al_2O_3 %	Fe_2O_3 %	MgO %	CaO %	Na_2O %	K_2O %	TiO_2 %	LOI %	Total
PROFILE 1, PIT A, FELSIC ANDESITE, UPPER SLOPE															
07-1109	Loose pisoliths	LT102	1.0	13050	10020	7.3	41.10	32.70	0.070	0.080	0.020	0.12	3.15	15.40	99.92
07-1108	Pisolitic duricrust	LT202	1.3	13050	10020	1.4	42.30	28.30	0.020	0.040	0.010	0.02	3.07	24.90	100.02
07-1106	Fragmental duricrust	LT205	1.4	13050	10020	1.5	47.20	20.58	0.020	0.030	<0.007	<0.06	2.85	27.80	99.98
07-1107	Fragmental duricrust	LT205	1.6	13050	10020	0.9	46.69	21.69	0.020	0.020	<0.007	<0.06	2.19	27.90	99.37
07-1114	Clay zone	cz	7.2	13040	10040	35.5	38.10	17.50	0.300	0.040	0.240	1.01	1.95	9.90	104.54
PROFILE 2, PIT A, DOLERITE, UPPER-MID-SLOPE															
07-1124	Loose pisoliths (transported)	LT102	0.4	12975	10070	7.9	40.60	35.80	0.070	0.090	0.020	0.08	3.47	11.80	99.81
07-1115	Loose pisoliths (transported)	LT102	0.6	12950	10060	0.7	41.90	38.41	0.020	0.030	0.040	<0.06	3.05	15.40	99.57
07-1110	Pisolitic duricrust	LT202	0.8	12975	10070	0.8	43.66	30.59	0.030	0.040	0.010	<0.06	5.20	19.20	99.50
07-1111	Fragmental duricrust	LT205	2.6	12975	10070	1.1	41.50	34.89	0.040	0.050	0.010	<0.06	5.48	16.50	99.61
07-1112	Fragmental duricrust	LT205	2.8	12975	10070	0.4	30.60	41.59	0.020	0.030	<0.007	<0.06	5.47	21.50	99.61
07-1113	Bauxite zone	bz	3.6	12975	10070	1.3	19.10	55.00	0.050	0.050	0.010	<0.06	8.47	15.70	99.66
PROFILE 3, PIT D, FELSIC ANDESITE, MID-SLOPE															
07-1079	Pisolitic duricrust	LT202	0.3	9640	10170	1.2	40.10	35.40	0.030	0.050	0.020	<0.06	2.50	20.60	99.90
07-1080	Pisolitic duricrust	LT205	0.8	9640	10170	1.8	39.40	34.06	0.020	0.040	0.010	<0.06	1.94	22.70	100.00
07-1081	Fragmental duricrust	LT205	1.3	9640	10170	1.8	41.10	29.90	0.020	0.040	0.010	<0.06	1.79	25.30	100.04
07-1082	Fragmental duricrust	LT205	1.6	9640	10170	0.9	44.20	25.32	0.010	0.020	0.010	<0.06	1.65	27.60	99.73
07-1083	Fragmental duricrust	LT205	1.9	9640	10170	0.7	49.40	18.61	0.010	0.030	<0.007	<0.06	1.67	29.00	99.39
07-1084	Fragmental duricrust	LT205	2.1	9640	10170	1.3	49.40	17.91	0.030	0.030	<0.007	0.09	1.97	29.10	99.82
07-1122	Clay zone	cz	4.4	9650	10160	47.4	33.10	9.80	0.040	0.020	0.030	0.09	1.07	8.50	99.75
PROFILE 4, PIT D, FELSIC ANDESITE, MID-LOWER SLOPE															
07-1099	Pisolitic duricrust	LT202	0.4	9470	10260	1.6	45.50	27.75	0.020	0.040	<0.007	<0.06	2.59	24.40	99.90
07-1100	Fragmental duricrust	LT205	0.8	9470	10260	2.6	43.30	25.41	0.020	0.030	<0.007	<0.06	1.97	26.60	99.90
07-1102	Fragmental duricrust	LT205	1.8	9470	10260	1.3	47.10	22.50	0.030	0.020	<0.007	0.09	1.59	27.30	99.94
07-1103	Bauxite zone	bz	2.8	9470	10260	7.3	45.80	18.38	0.170	0.040	0.040	0.19	1.59	26.40	99.92
PROFILE 5, PIT D, FELSIC ANDESITE, LOWER SLOPE															
07-1096	Loose pisoliths	LT102	0.9	9400	10310	2.6	43.20	33.70	0.010	0.040	0.010	<0.06	2.95	17.10	99.56
07-1095	Loose pisoliths	LT102	1.2	9400	10310	2.6	46.70	30.52	0.020	0.040	<0.007	<0.06	2.62	17.30	99.74
07-1094	Pisolitic duricrust	LT202	2.2	9400	10310	2.9	44.40	31.88	0.020	0.050	0.020	<0.06	2.50	18.10	99.89
07-1093	Fragmental duricrust	LT205	2.8	9400	10310	3.7	43.70	25.90	0.020	0.030	<0.007	<0.06	2.30	24.20	99.87
07-1092	Fragmental duricrust	LT205	3.6	9400	10310	3.1	44.71	24.90	0.010	0.030	<0.007	<0.06	2.15	24.80	99.65
07-1090	Bauxite zone	bz	4.4	9400	10310	9.2	43.00	19.85	0.030	0.040	0.020	<0.06	2.24	25.50	99.92

Table 5. Chemical Composition of Regolith Units From Five Vertical Profiles (cont'd)

Sample No.	Mn ppm	Cr ppm	V ppm	Cu ppm	Pb ppm	Zn ppm	Ni ppm	Co ppm	As ppm	Sb ppm	Bi ppm	Mo ppm	Ag ppm	Sn ppm	Ge ppm	Ga ppm	W ppm	Ba ppm	Zr ppm	Nb ppm	Se ppm	Au ppm
PROFILE 1																						
07-1109	112	444	688	5	14	13	18	<4	320	10	5	40	<0.1	14	<2	94	22	42	369	24	3	0.080
07-1108	62	407	648	10	<2	3	14	<4	410	7	3	64	<0.1	13	<2	74	30	15	397	22	3	0.080
07-1106	54	393	426	28	<2	5	10	<4	340	8	2	32	0.20	15	<2	76	18	13	392	20	2	0.110
07-1107	37	404	430	12	<2	6	12	<4	370	4	4	42	0.20	11	<2	56	16	20	468	14	6	0.260
07-1114	86	389	258	150	4	14	50	4	350	6	2	9	<0.1	5	<2	38	42	731	235	7	2	0.250
PROFILE 2																						
07-1124	198	437	684	3	13	12	24	<4	160	6	2	36	<0.1	11	<2	92	16	37	320	28	6	0.200
07-1115	176	538	765	12	6	9	24	<4	150	6	5	60	<0.1	12	<2	145	16	30	477	20	5	0.270
07-1110	536	468	584	3	10	11	14	<4	250	5	<2	30	0.10	12	<2	105	18	27	454	30	<2	0.070
07-1111	561	500	683	2	6	34	18	<4	250	4	<2	36	<0.1	12	<2	110	24	28	385	30	4	0.040
07-1112	1017	435	791	46	17	24	20	<4	280	3	<2	26	0.50	7	<2	70	8	32	478	24	<2	0.530
07-1113	2085	403	997	48	32	40	18	6	72	6	6	4	<0.1	3	4	60	4	64	240	34	11	0.650
PROFILE 3																						
07-1079	56	570	590	14	4	9	18	<4	26	4	4	50	<0.1	54	<2	100	175	20	359	15	<2	0.020
07-1080	75	463	535	22	4	5	16	<4	20	4	7	58	0.40	46	<2	76	190	20	468	12	<2	0.080
07-1081	55	392	488	26	7	15	20	<4	24	3	5	56	<0.1	46	<2	80	175	21	444	13	2	0.110
07-1082	32	327	447	40	<2	9	16	<4	17	2	6	54	<0.1	46	<2	76	155	5	666	11	3	0.310
07-1083	20	304	322	30	5	8	14	<4	12	<2	<2	34	<0.1	56	<2	70	160	26	605	13	<2	0.410
07-1084	42	297	279	24	7	7	14	<4	13	3	7	28	<0.1	52	<2	78	120	45	436	14	<2	0.500
07-1122	20	99	152	230	10	12	34	<4	<2	4	<2	9	<0.1	44	<2	58	74	22	402	11	<2	0.740
PROFILE 4																						
07-1099	43	359	405	18	2	6	14	<4	17	2	4	74	<0.1	38	<2	76	125	10	279	19	<2	0.090
07-1100	28	384	424	34	8	13	16	<4	20	6	7	130	<0.1	38	<2	68	120	24	494	13	<2	1.450
07-1102	21	316	343	48	6	8	10	<4	18	<2	4	58	<0.1	42	<2	70	150	53	390	11	2	2.310
07-1103	49	523	261	64	<2	7	8	<4	28	2	6	56	<0.1	20	<2	58	98	53	267	14	<2	2.110
PROFILE 5																						
07-1096	64	496	515	11	5	9	18	<4	15	2	8	46	<0.1	56	<2	105	185	16	275	20	<2	0.380
07-1095	55	457	469	12	8	10	22	<4	16	<2	4	40	<0.1	54	<2	110	195	11	244	22	<2	0.080
07-1094	56	471	498	13	9	6	20	<4	20	2	2	40	<0.1	54	<2	100	230	9	279	18	<2	0.150
07-1093	35	400	438	20	5	7	12	<4	14	3	5	44	<0.1	48	<2	78	195	2	270	17	<2	0.170
07-1092	36	379	383	26	5	4	16	<4	13	2	3	38	<0.1	48	<2	84	190	5	256	16	<2	0.140
07-1090	36	350	276	74	4	6	26	<4	5	<2	24	11	<0.1	46	<2	80	185	39	299	13	<2	0.050

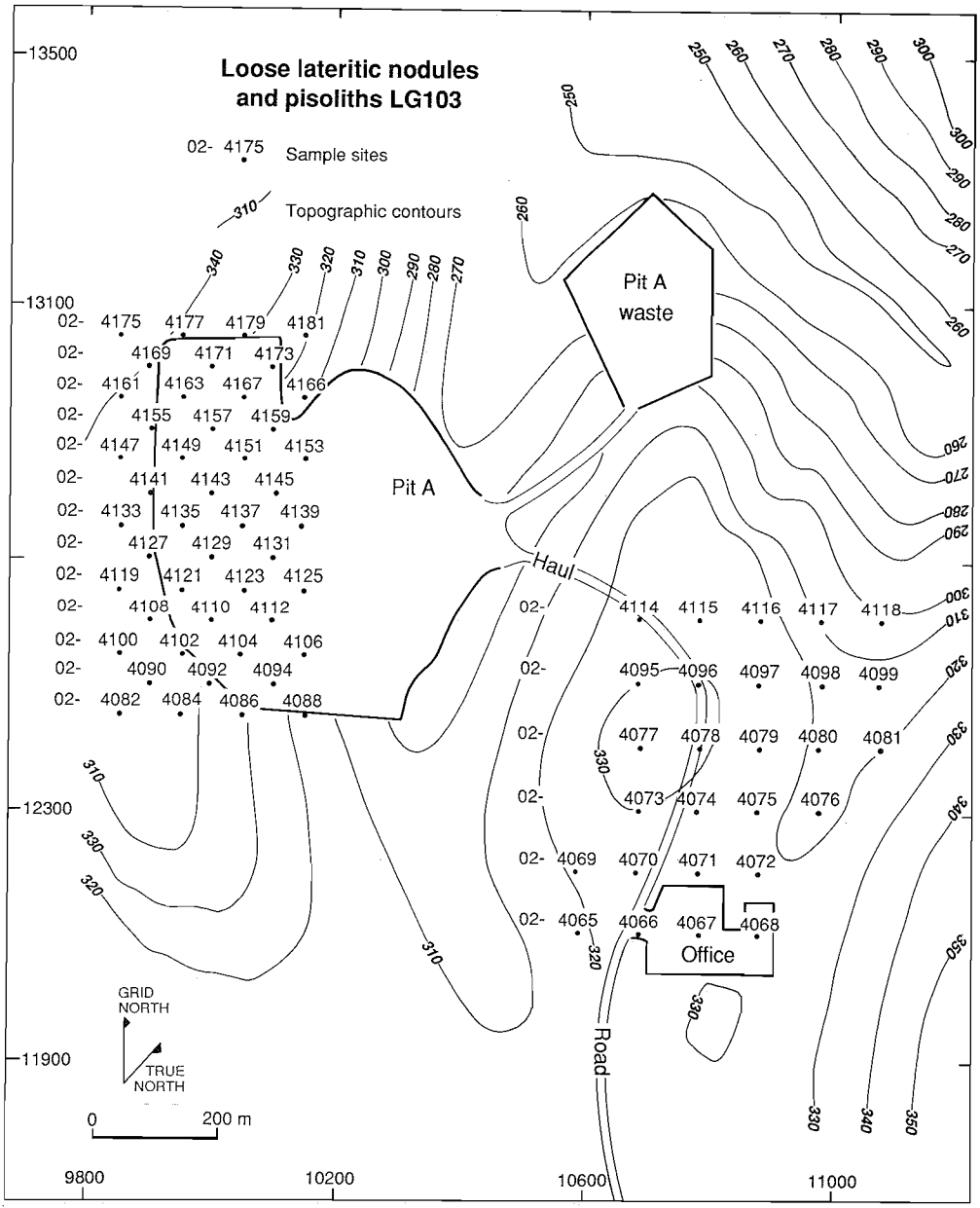

Fig. 22. Map showing the distribution of samples of lateritic nodules and pisoliths from Pit A.

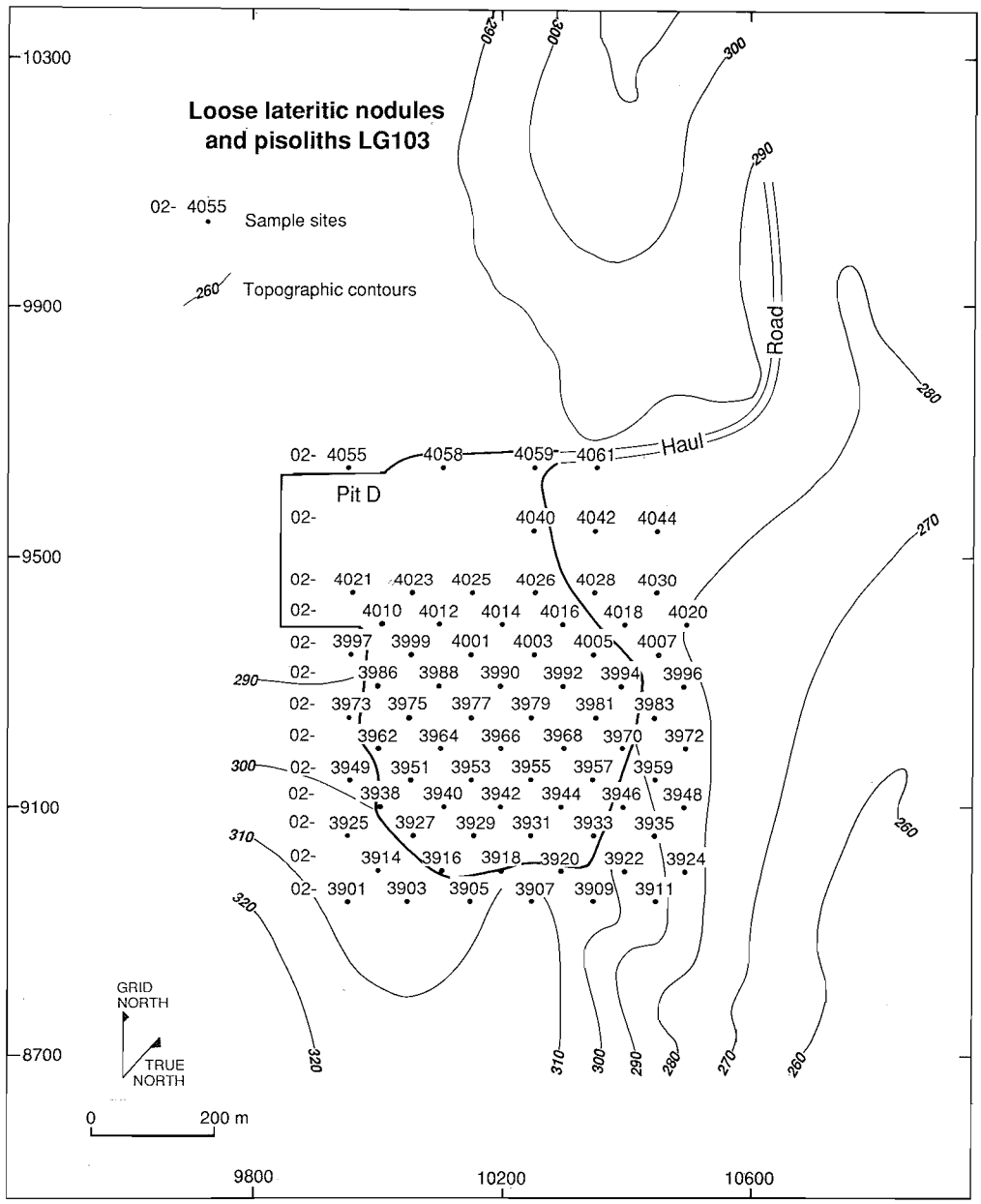

Fig. 23. Map showing the distribution of samples of lateritic nodules and pisoliths from Pit D.

Fig. 24. Bedrock geology map of Pit A and its surroundings (modified after Symons et al., 1990).

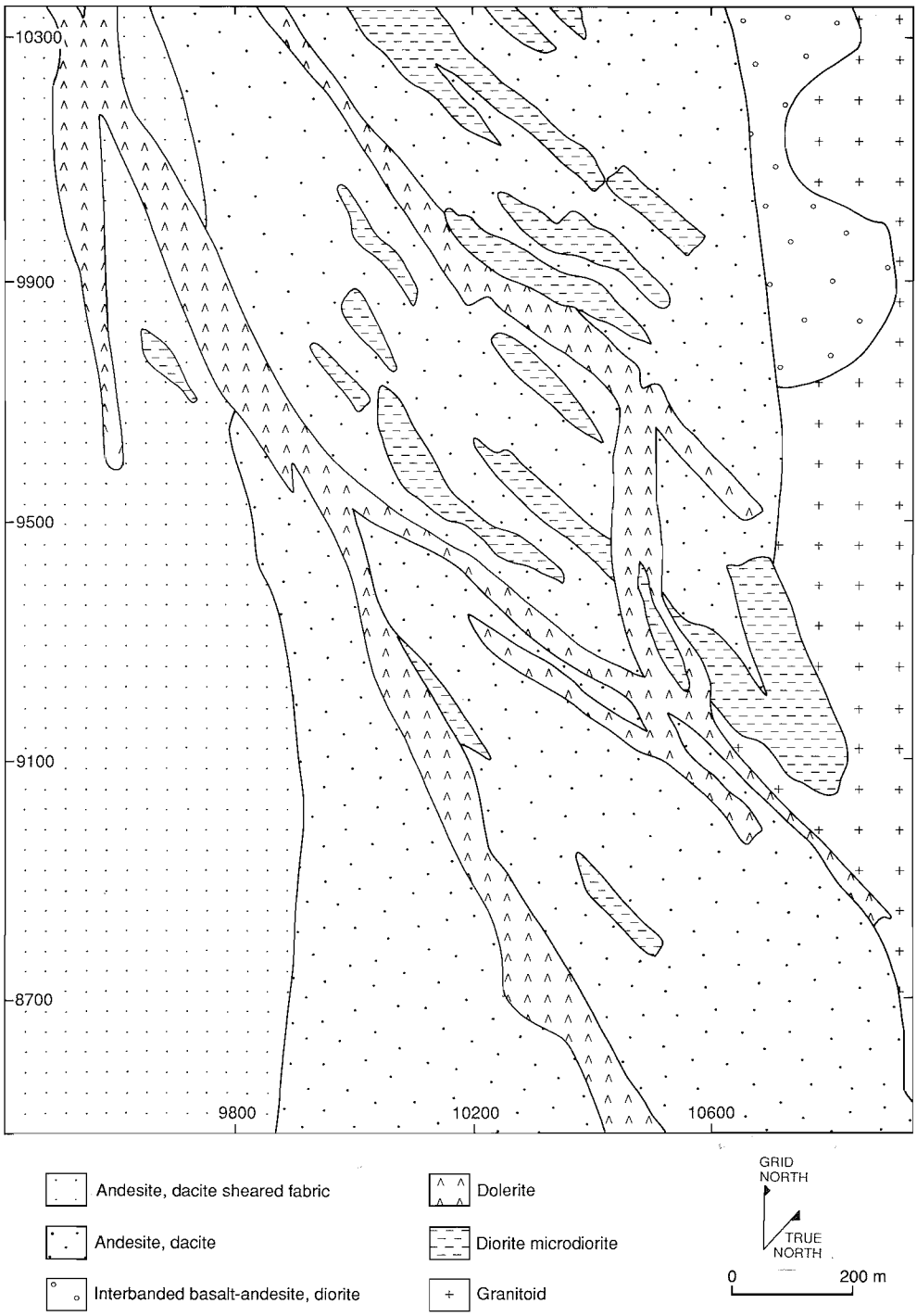

Fig. 25. Bedrock geology map of Pit D and its surroundings (modified after Symons et al., 1990).

underlying fragmental duricrusts and the bauxite zone. The highest and most continuous Au abundances in the laterite profile are over mineralized bedrock (Symons *et al.*, 1988, 1990). In contrast, Davy and El-Ansary (1986) suggest that Au may have dispersed more than 500 m from the point sources.

Arsenic

The As pattern is strong and extensive over Pit A (reaching 350 ppm) but is relatively weaker (to 58 ppm) over Pit D (Figs 28 and 29). It measures some 400 m long and 300 m wide over Pit A and shows a more consistent and widespread distribution than Au. The most marked feature of the As pattern is that it is very strong (reaching 350 ppm) at the north-western end of Pit A. There are also local highs in south-east of Pit A which may be related to the nature of the bedrock mineralization. High concentrations of As in Pit A reflect the arsenopyrite mineralization of the bedrock. These results are consistent with the profile data (see Section 5.3.1.2).

W

Tungsten shows a more consistent and widespread distribution, being most strong and widespread in the south-east of Pit A and in Pit D (Figs. 30 and 31). Tungsten is low in abundance in Pit A (reaching 34 ppm). The W pattern measures some 500 m wide and 400 m long and shows a close relationship to the bedrock. The maximum concentrations of W in lateritic nodules and pisoliths are 130 ppm.

Sn

The Sn distribution is similar to W in the strike continuity and breadth of its dispersion patterns, although the anomalies are rather subdued with peak maximum at 48 ppm (Figs 32 and 33). Tin is relatively more abundant in Pit D and is related to scheelite in bedrock.

Cu, Zn

Copper and Zn are depleted in loose nodules and pisoliths (Figs. 34 and 35). Their patterns are weak and do not appear to be particularly useful in defining patterns related to mineralization. However, local highs (to 120 ppm) of Cu at the southern end of Pit D may be attributed to bedrock mineralization.

Mo

The surface patterns of Mo are anomalous both over Pit A and Pit D reaching a maximum value of 125 ppm (Figs. 36 and 37). However, it is low in abundance in the south-east of Pit A.

Bi

Bismuth is not uniformly distributed within the overall multi-element anomaly, being most strong and widespread in the south-western corner of Pit A (Figs. 38 and 39). Bismuth reaches a maximum concentration of 52 ppm; the high concentrations are related to bedrock mineralization.

Other elements

The pattern for Sb (not shown) in loose nodules and pisoliths is weak with values ranging from 2 to 10 ppm.

Silver was detected in all the samples with values ranging from 0.3 to 0.8 ppm.

Lead, Ni, and Co have generally flat surface patterns which do not reflect the bedrock. Cobalt shows a particularly restricted pattern with most analyses below the detection limit of 4 ppm.

5.3.4 Distribution of minerals and elements – all samples

Two hundred and eighty four samples were grouped according to the nature of the regolith type. These include pisolitic and nodular lag, loose pisoliths (sub-surface), pisolitic duricrust, fragmental duricrust, bauxite zone, clay zone, and saprolite. Figure 40 shows the number of samples analysed for the various units of the profile. Analytical data on sample groups are given in Appendix 1 to 7.

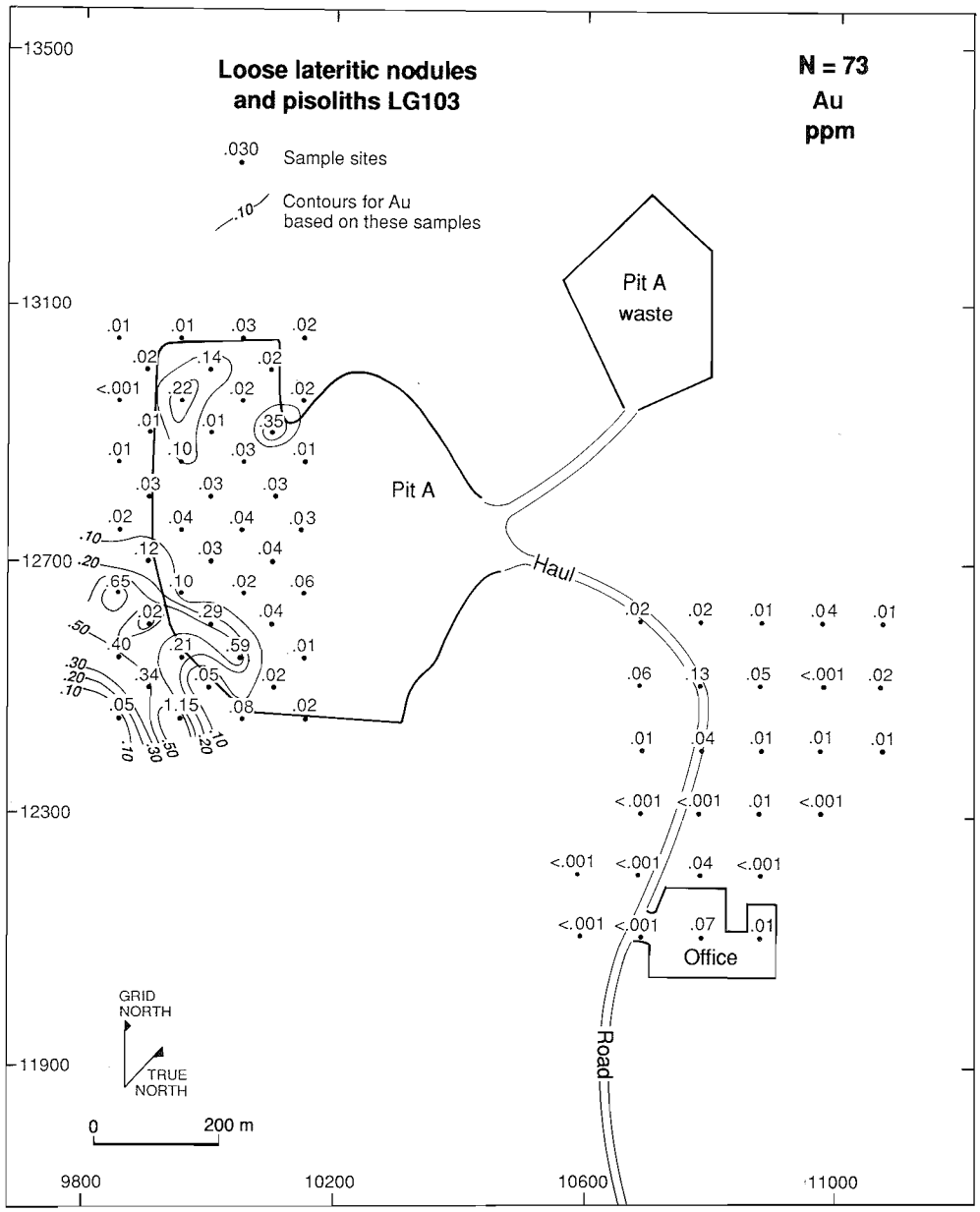

Fig. 26. Map showing the distribution of Au in lateritic nodules and pisoliths from Pit A.

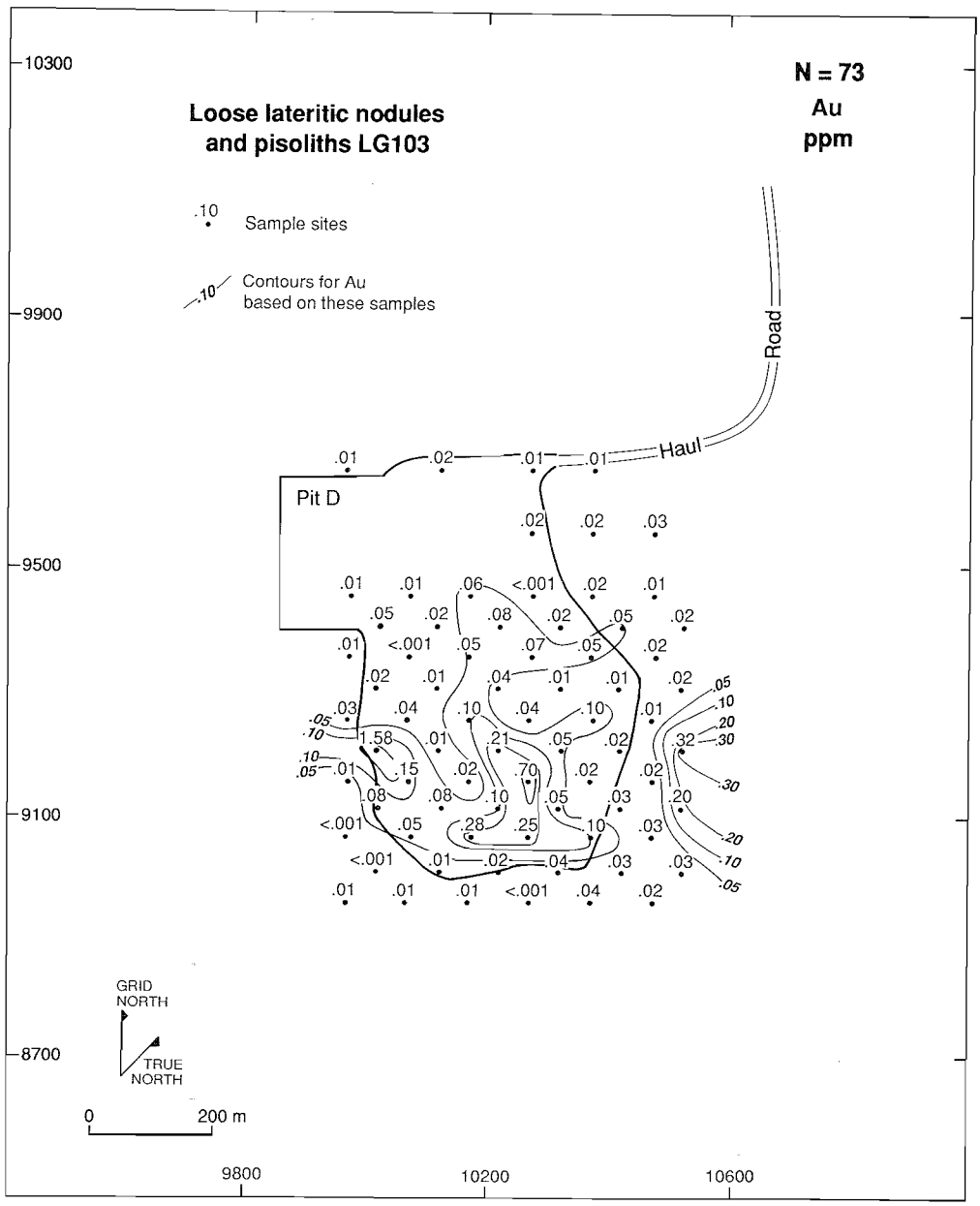

Fig. 27. Map showing the distribution of Au in lateritic nodules and pisoliths from Pit D.

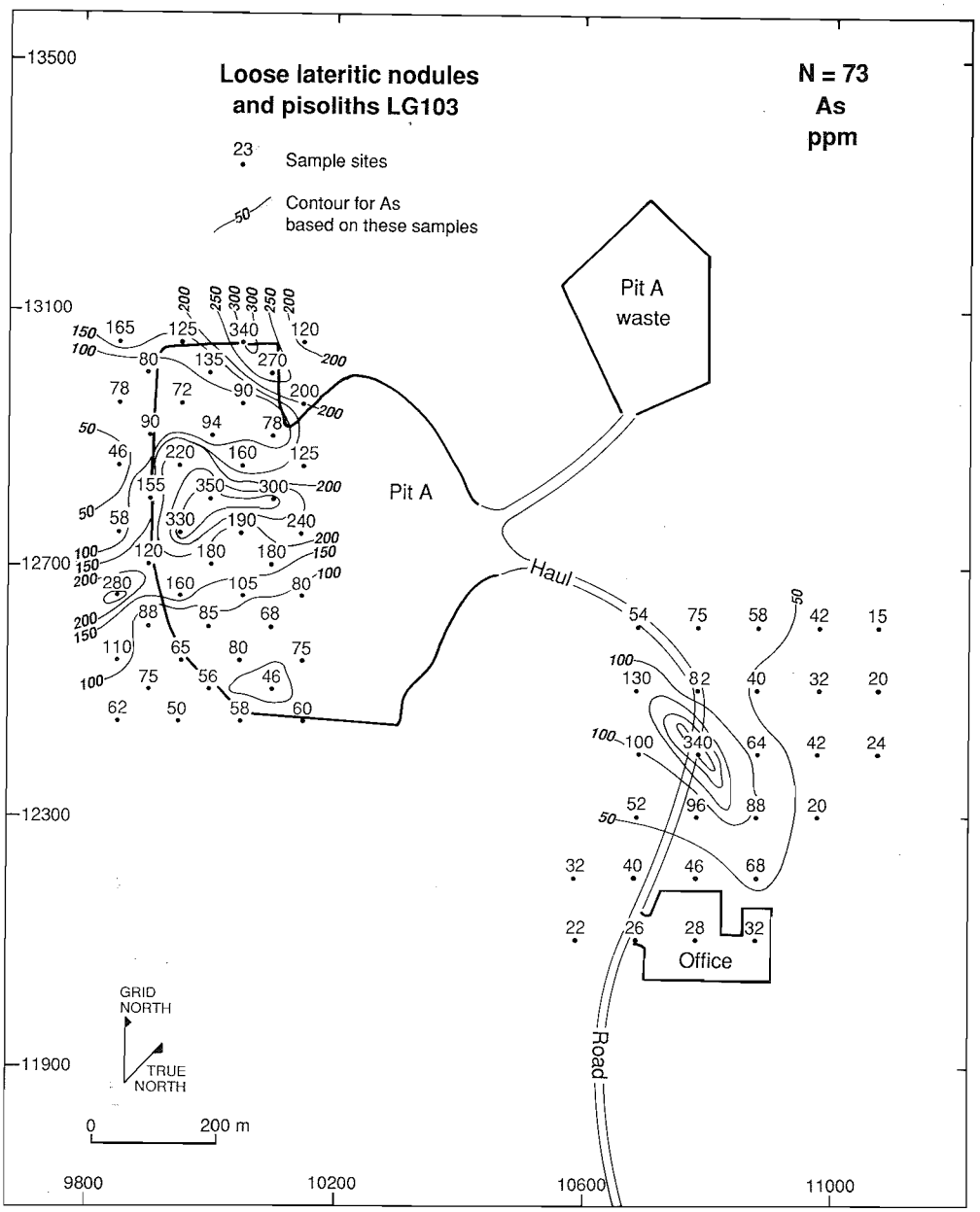

Fig. 28. Map showing the distribution of As in lateritic nodules and pisoliths from Pit A.

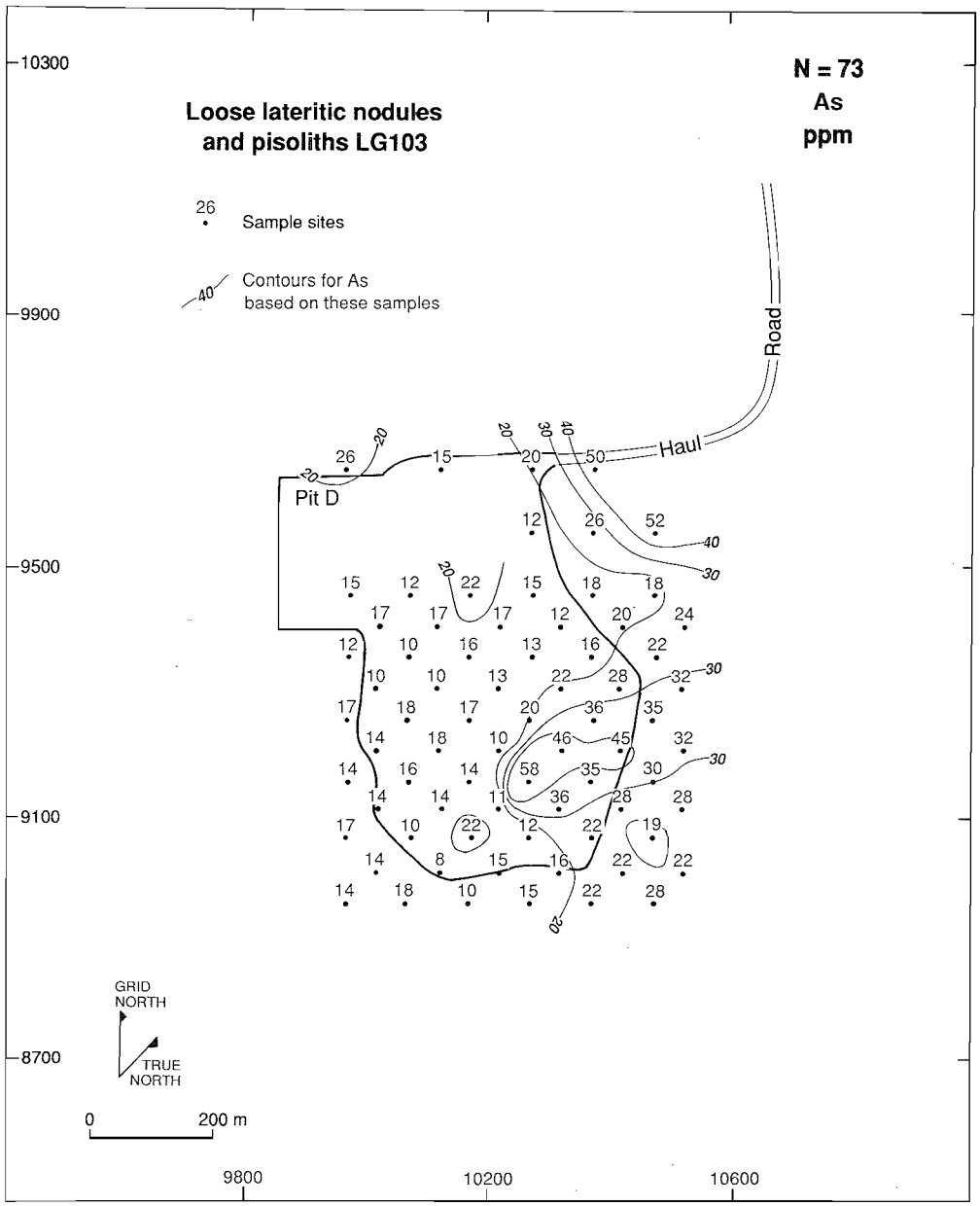

Fig. 29. Map showing the distribution of As in lateritic nodules and pisoliths from Pit D.

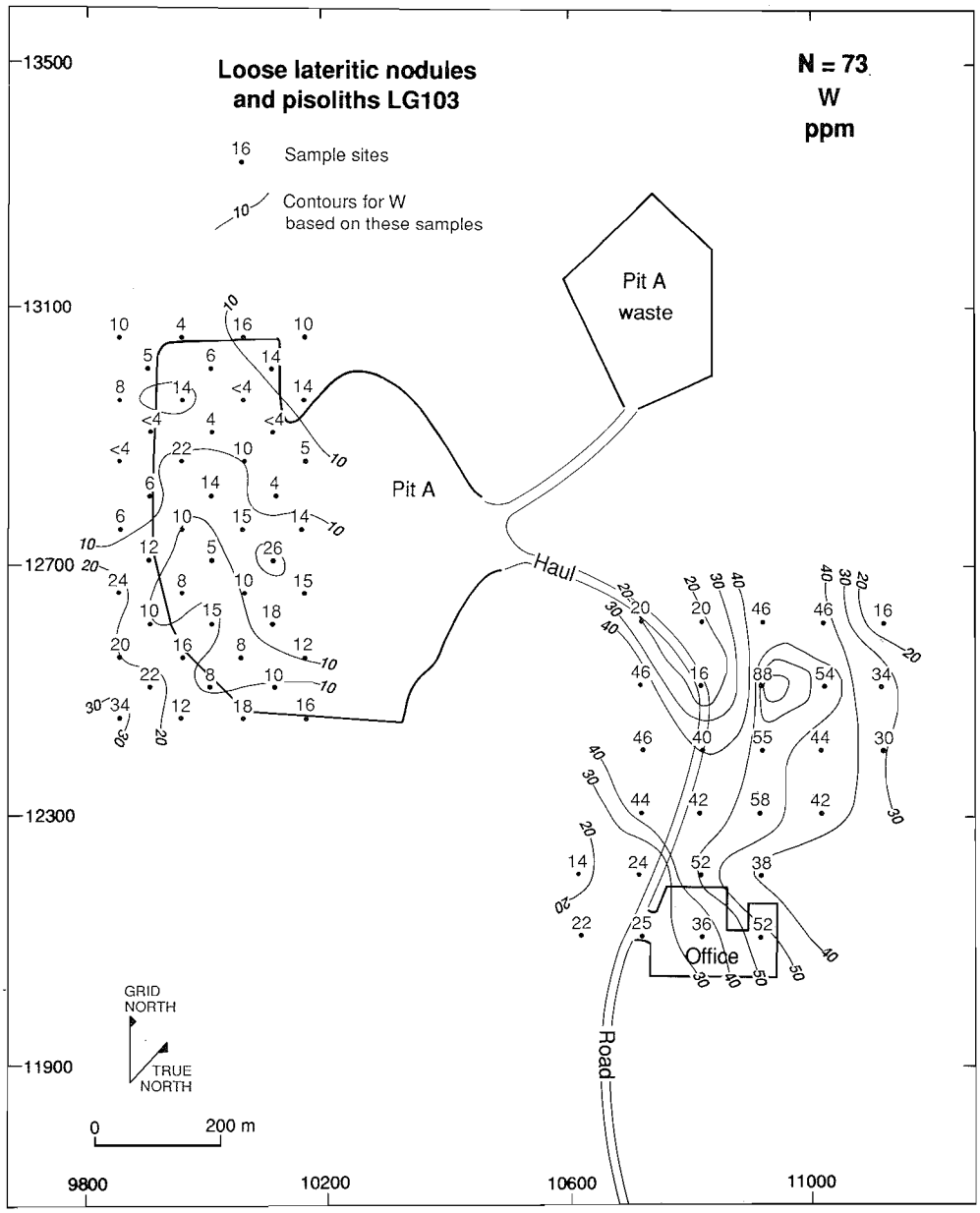

Fig. 30. Map showing the distribution of W in lateritic nodules and pisoliths from Pit A.

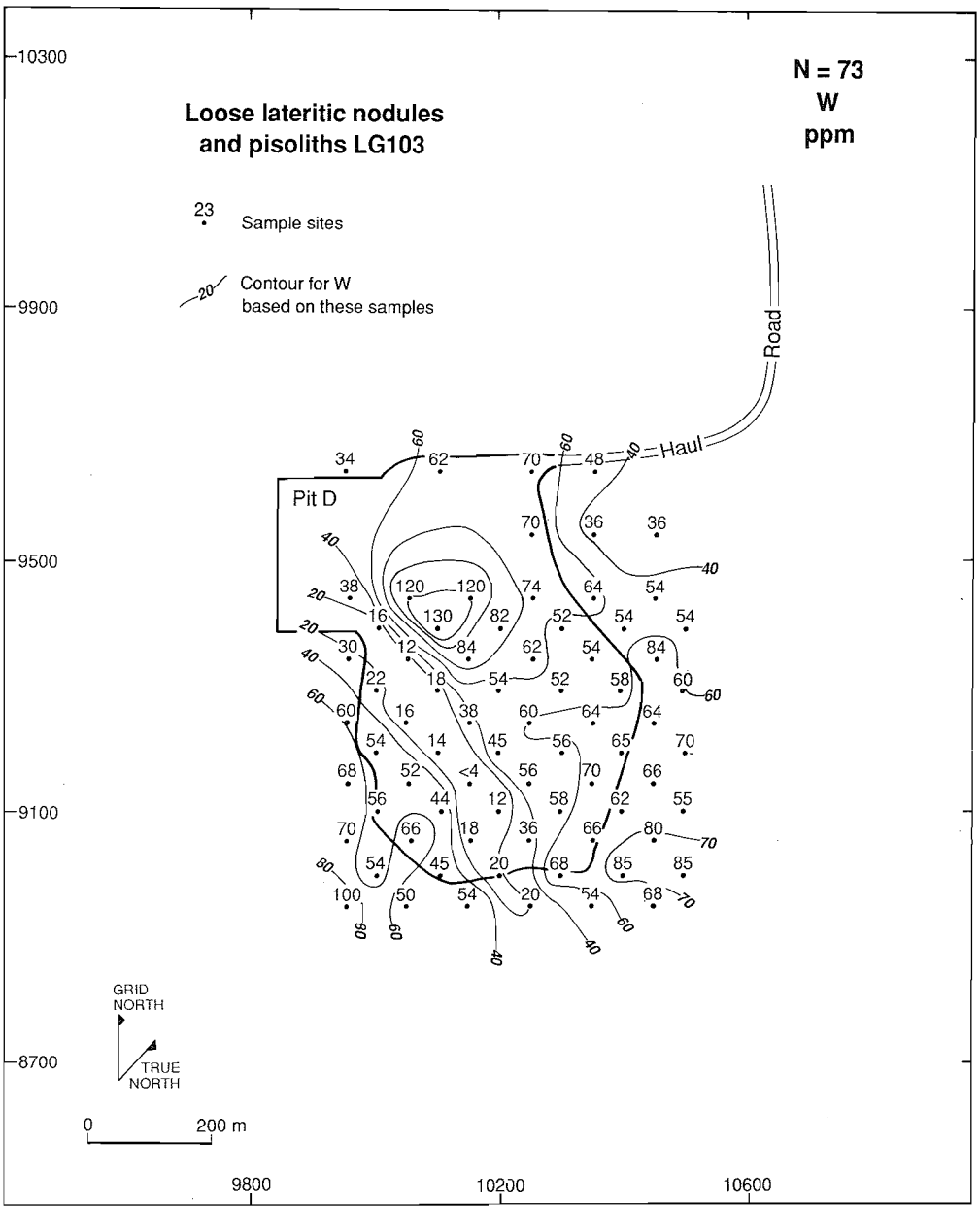

Fig. 31. Map showing the distribution of W in lateritic nodules and pisoliths from Pit D.

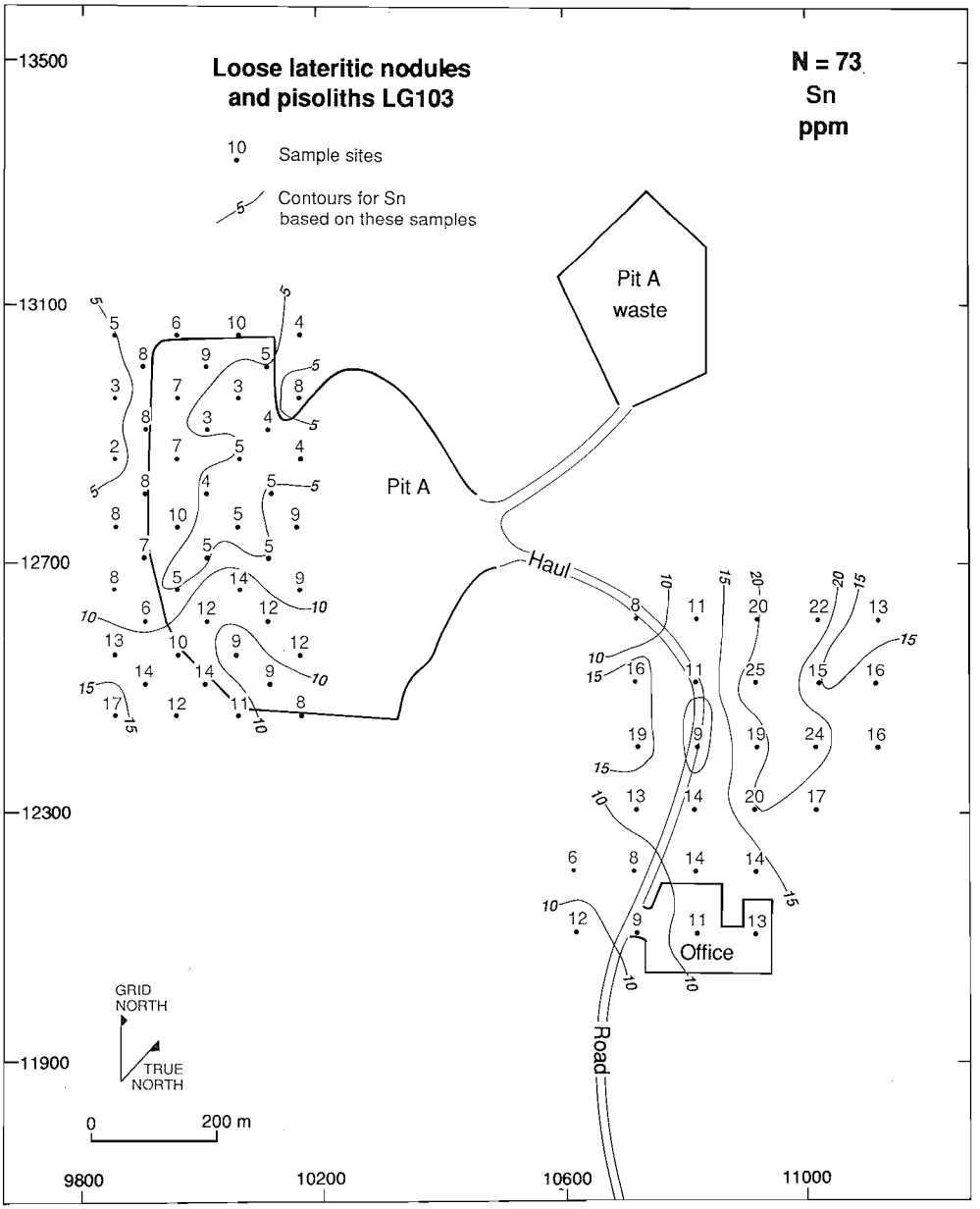

Fig. 32. Map showing the distribution of Sn in lateritic nodules and pisoliths from Pit A.

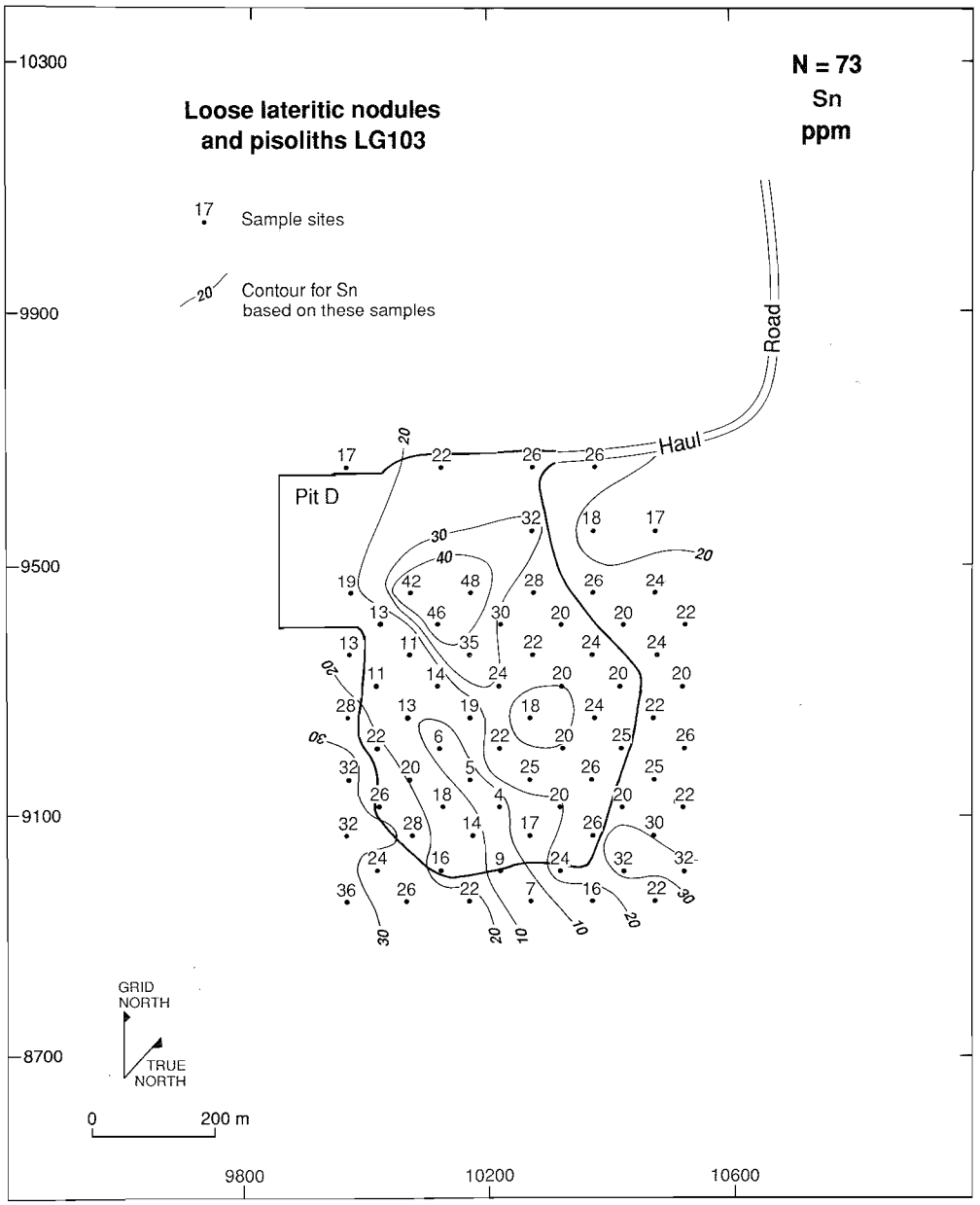

Fig. 33. Map showing the distribution of Sn in lateritic nodules and pisoliths from Pit D.

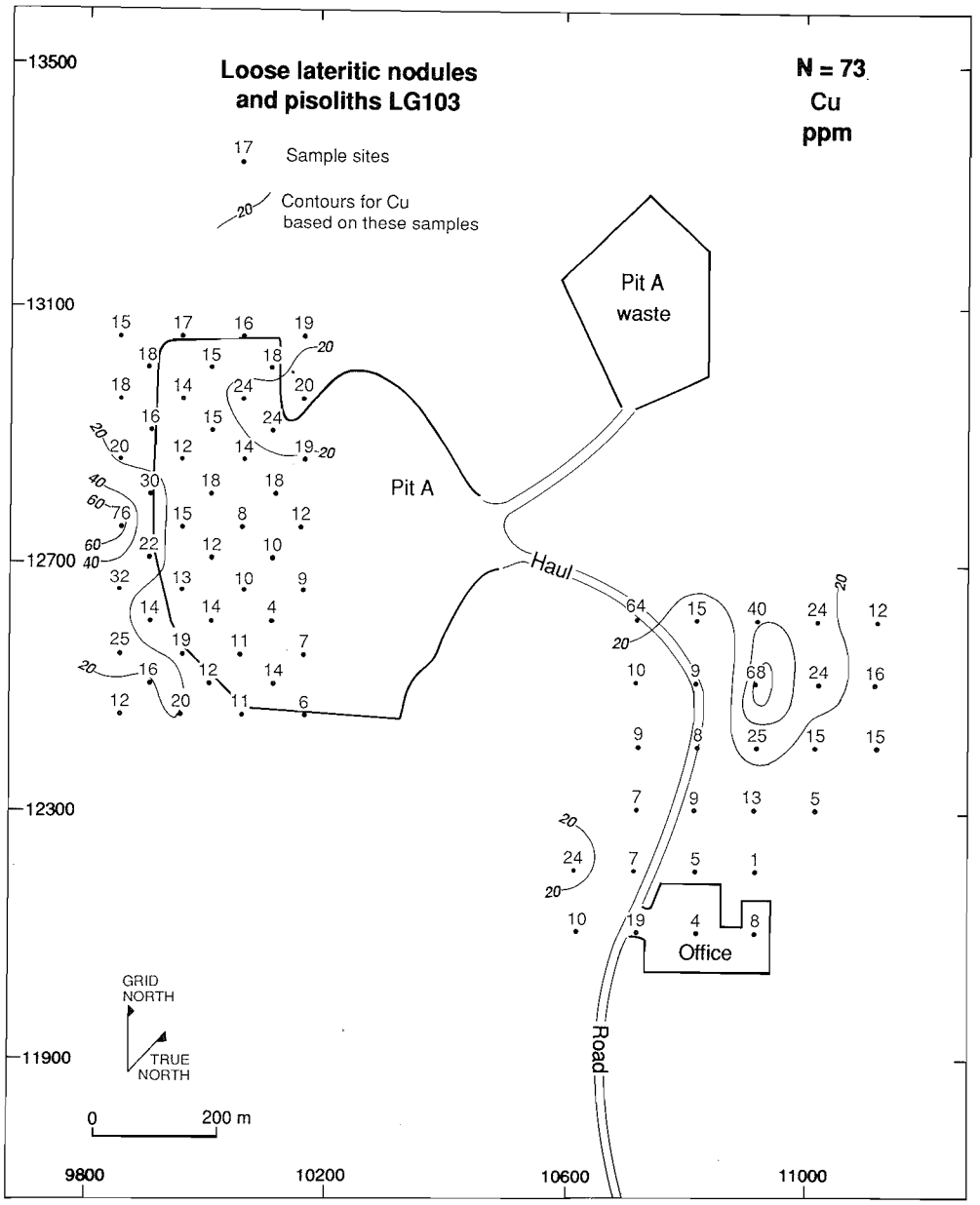

Fig. 34. Map showing the distribution of Cu in lateritic nodules and pisoliths from Pit A.

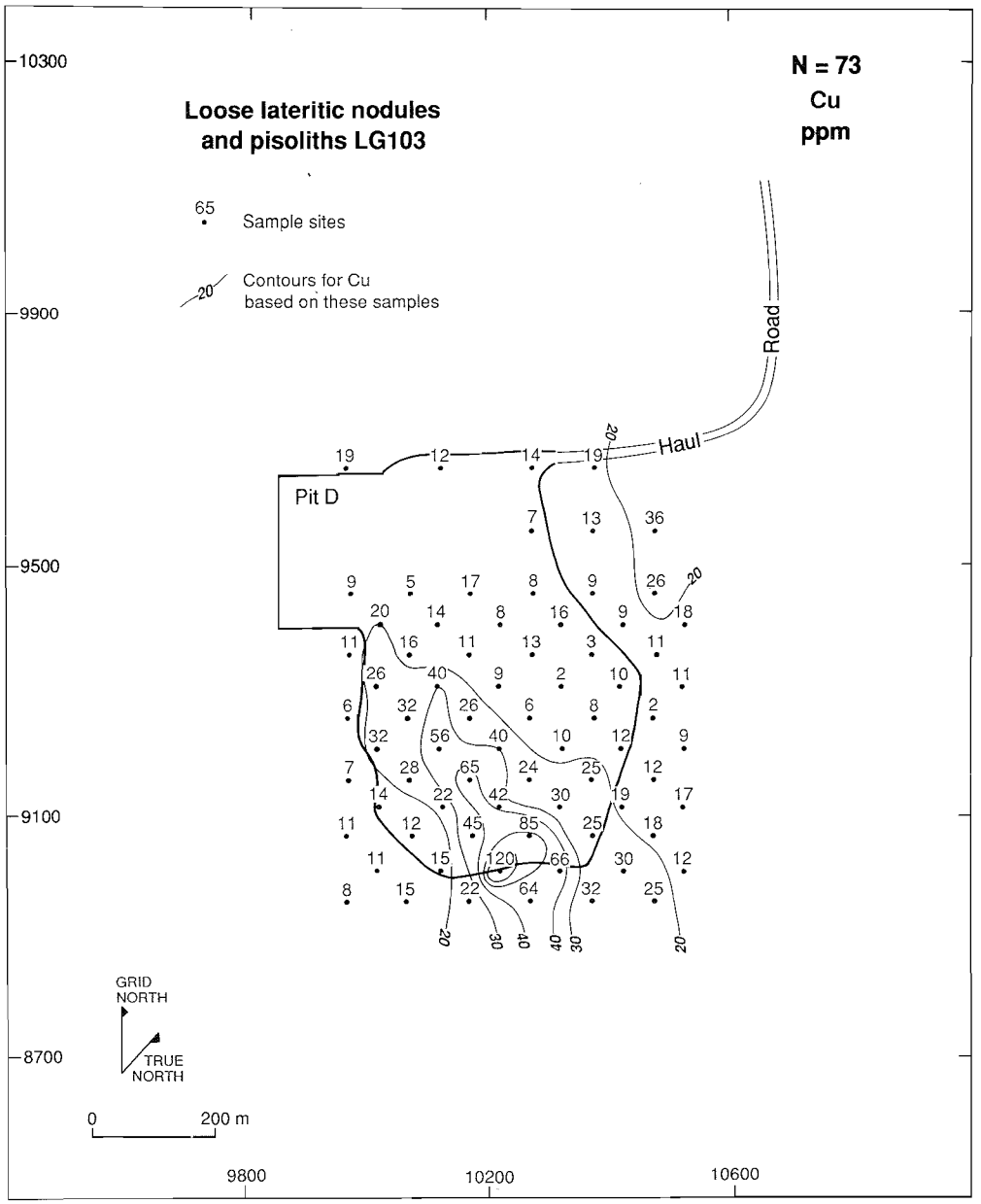

Fig. 35. Map showing the distribution of Cu in lateritic nodules and pisoliths from Pit D.

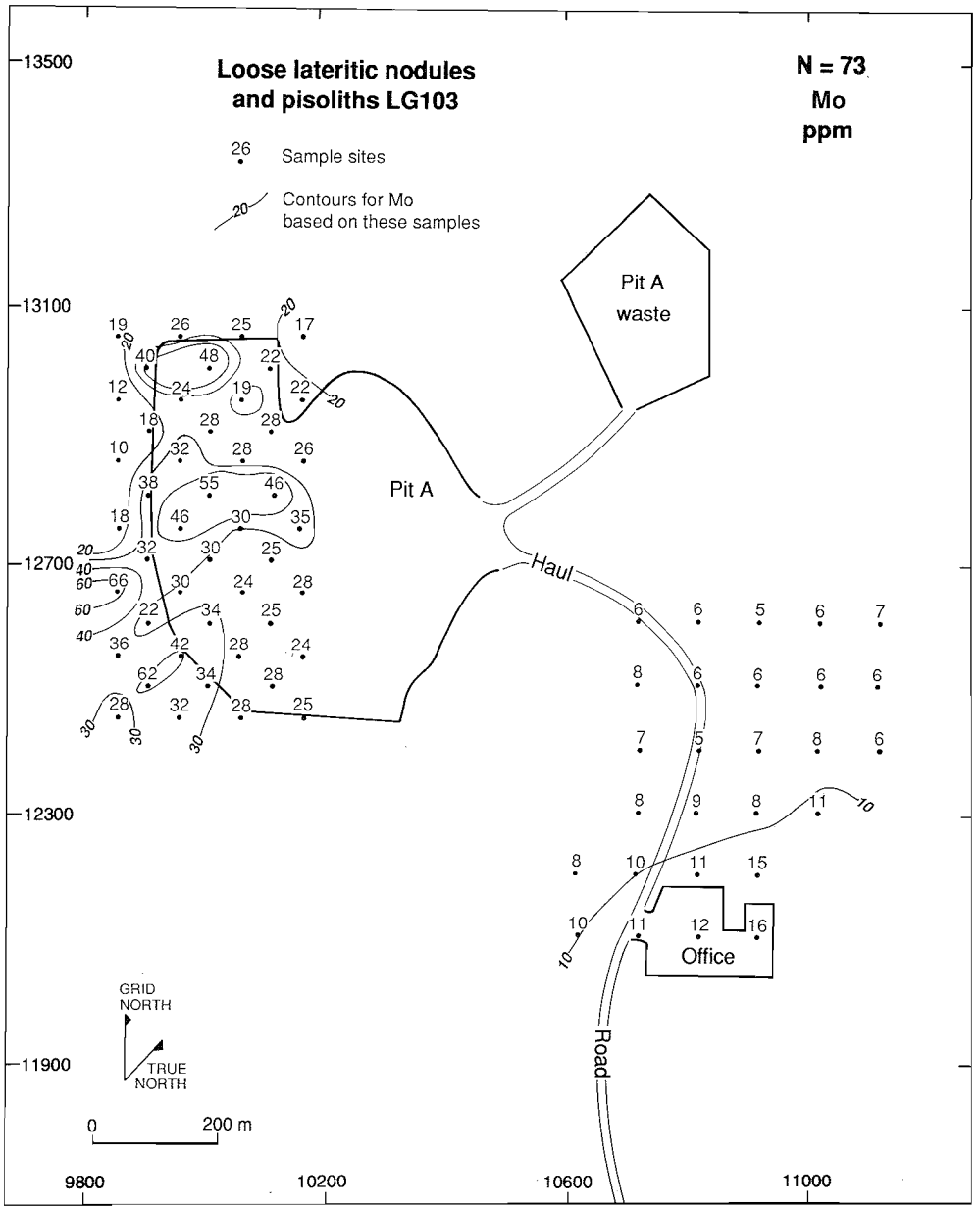

Fig. 36. Map showing the distribution of Mo in lateritic nodules and pisoliths from Pit A.

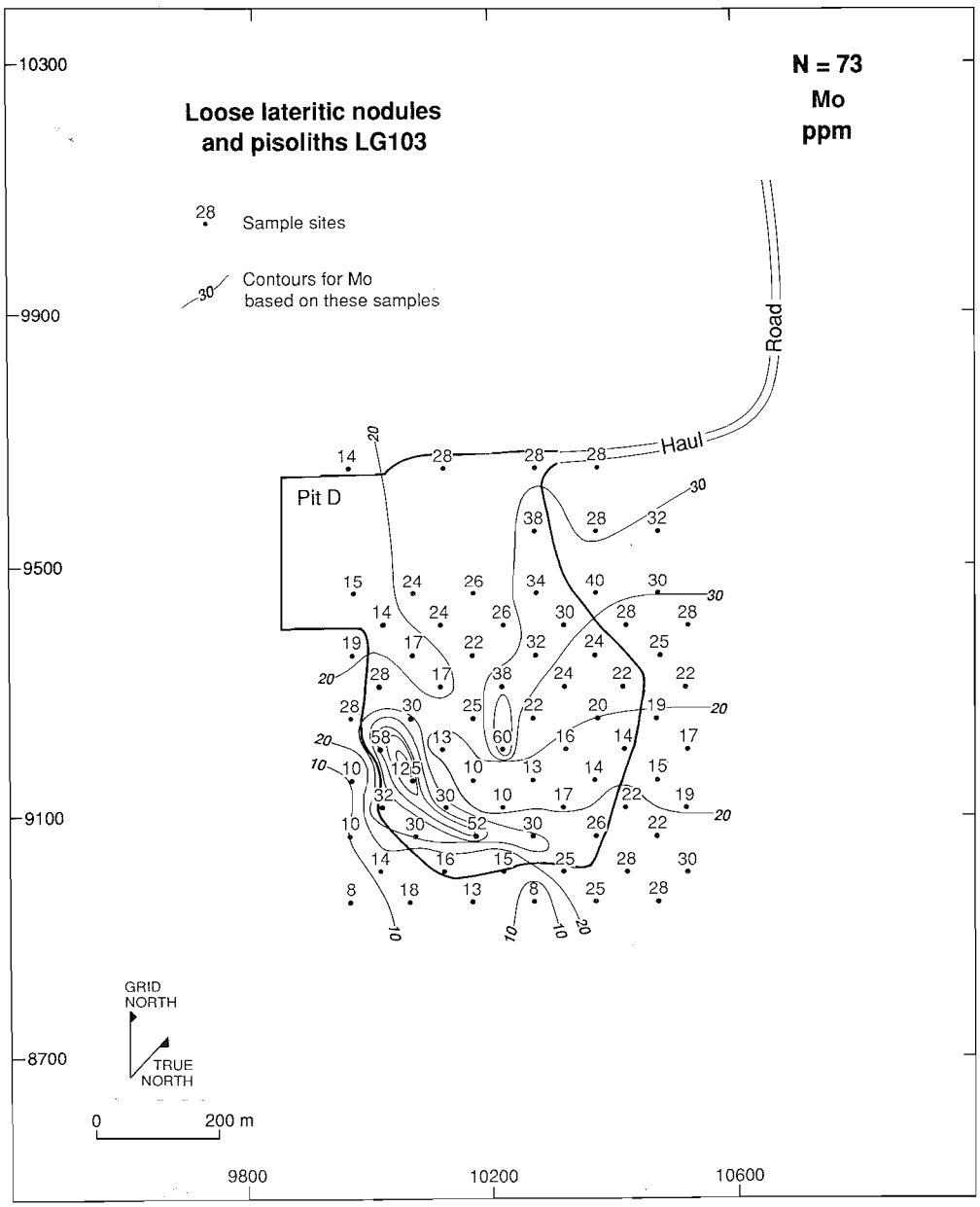

Fig. 37. Map showing the distribution of Mo in lateritic nodules and pisoliths from Pit D.

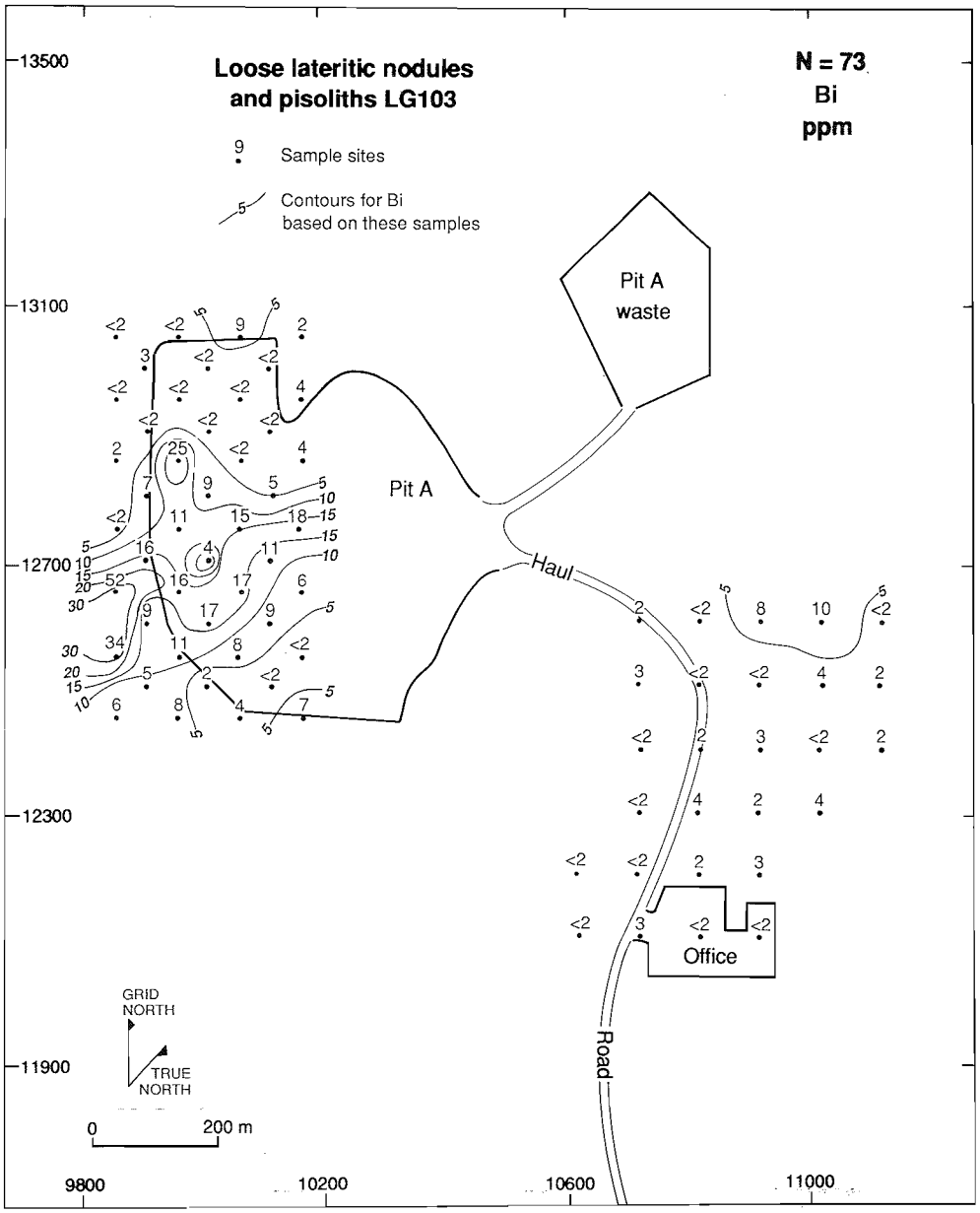

Fig. 38. Map showing the distribution of Bi in lateritic nodules and pisoliths from Pit A.

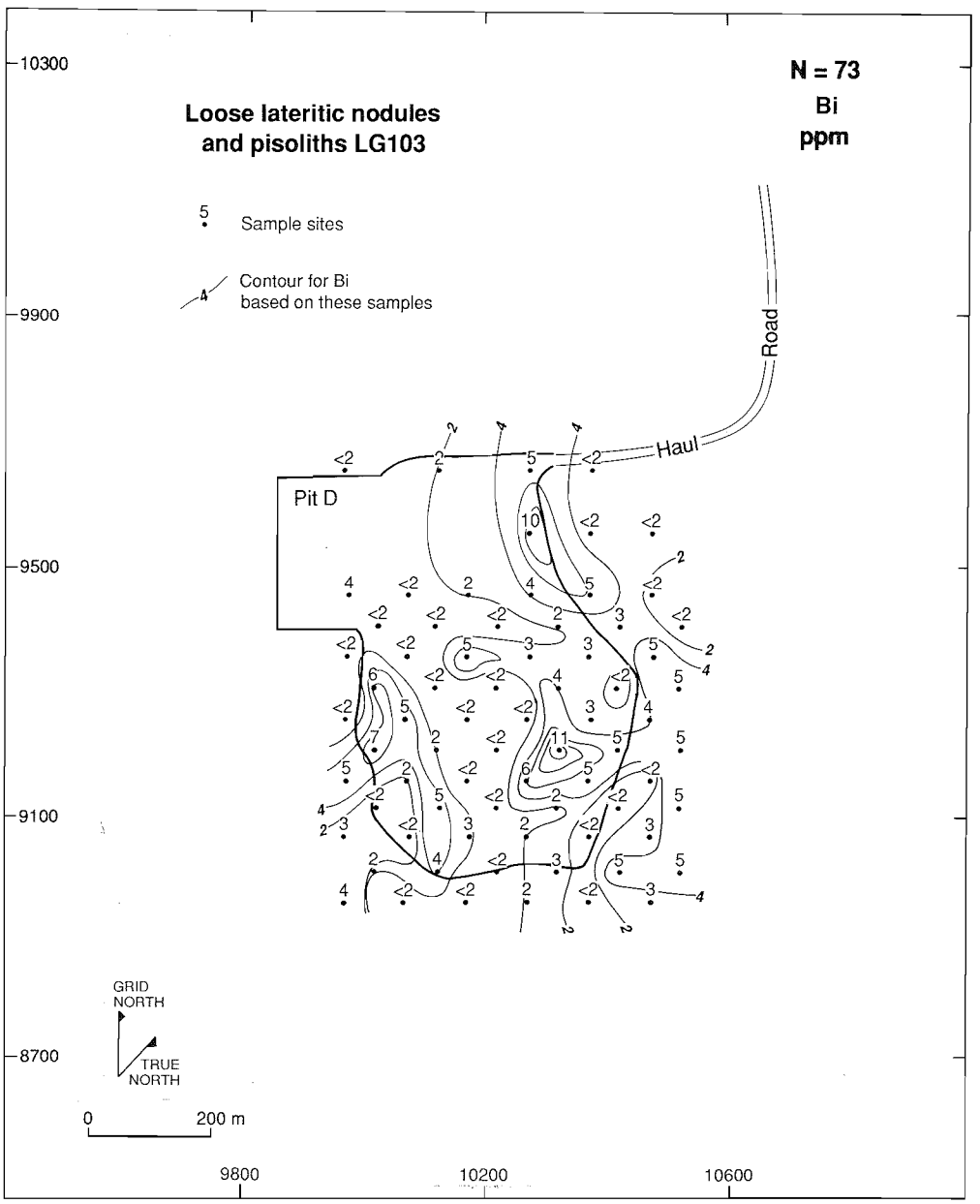

Fig. 39. Map showing the distribution of Bi in lateritic nodules and pisoliths from Pit D.

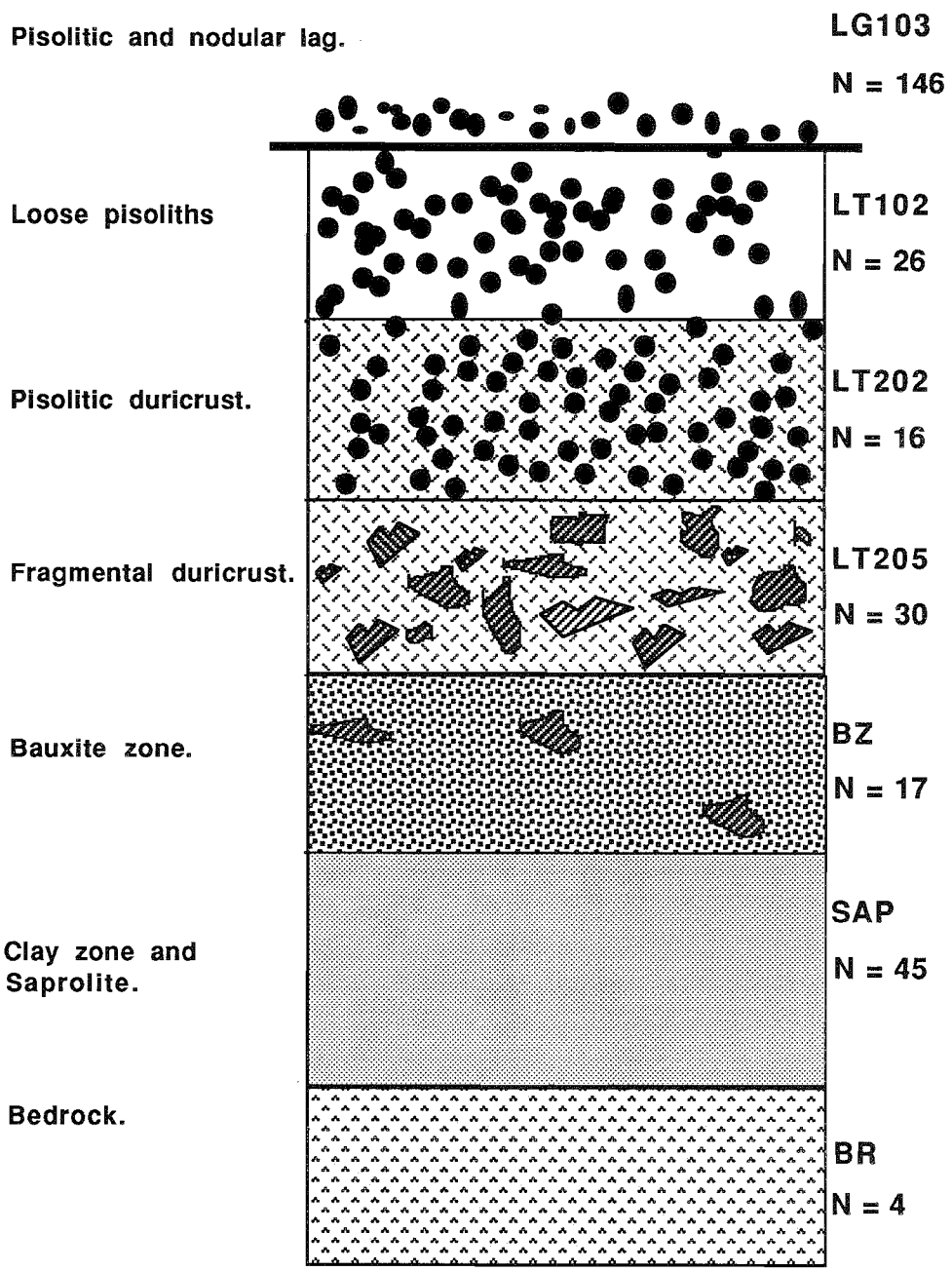

Fig.40 Number of samples analysed from the different regolith units of the profile.

5.3.4.1 Ternary diagrams

Aluminium, Fe_2O_3 and SiO_2 are the major components of the samples analysed. A ternary diagram for oxides is useful in discriminating the various sample groups, as shown in Fig. 41A. The figure also has subsidiary diagrams for each of the main sample types (Figs. 41B, C, D, E, F, and G). Bedrock samples are included for comparison.

As expected, SiO_2 is present in higher amounts in the clay zone and saprolite, whereas Fe_2O_3 and Al_2O_3 dominate in the various categories of laterite (loose pisoliths, pisolitic duricrust, fragmental duricrust) and the bauxite zone. However, there is a wide range of SiO_2 and Al_2O_3 values in the clay zone and saprolite reflecting variable contents of kaolinite and quartz. The duricrusts and loose pisoliths are characterized by higher amounts of Fe_2O_3 and Al_2O_3 and low contents of SiO_2. Iron in duricrust, pisoliths and the bauxite zone occurs as hematite, goethite, and maghemite, Al_2O_3 as gibbsite and amorphous Al-oxide, with some Al in goethite and hematite, and SiO_2 as quartz. In saprolite, Fe_2O_3 occurs as goethite, Al_2O_3 mainly as kaolinite, and SiO_2 as kaolinite and quartz.

The chemical composition also allows distinctions to be made between the various types of duricrust. Figure 41A shows the overlap in the chemical composition of the various duricrust types and pisolitic and nodular lag. Fragmental duricrusts have a wide compositional range (Al_2O_3, Fe_2O_3) evidently reflecting variations in the chemical composition of both the constituent fragments and matrix. By contrast, pisolitic duricrust have a relatively-restricted chemical range. Pisolitic duricrusts have, on average, higher concentrations of Fe_2O_3 compared with the fragmental duricrusts. Aluminium concentrations are similar. Therefore, these two types of duricrusts have been distinguished and processed separately in this study.

As can be seen on the bivariate diagram for Fe_2O_3 and Al_2O_3 (Fig. 42), there are three distinct populations, two with a -ve correlation and one with a +ve correlation. Saprolite samples show that there is a general increase in Al with increase in Fe. An opposite trend exists for other sample types. Figure 43 (Al_2O_3 vs LOI) also shows two distinct populations for Al_2O_3 and LOI, one with a +ve correlation and one with a -ve correlation. For the same level of Al_2O_3, the duricrust and bauxite samples show much higher LOIs than the pisolitic and nodular lag. This suggests that most Al in the pisolitic and nodular lag is not present as gibbsite, but occurs as amorphous Al-oxide. The LOI is essentially an indirect indication of kaolinite and gibbsite contents.

5.3.4.2 Lithological discrimination

The identification of bedrocks from their weathering products using geochemistry largely depends upon the presence of diagnostic immobile elements or elements immobilized in resistant minerals. Ratios and plots of Ti and Zr contents have been reported to be commonly effective in discriminating between the major lithological groups, whether fresh or moderately weathered, but have been found to be less reliable for the lateritic residuum and mottled zone. In the present study, Ti/Zr ratios, originally proposed by Hallberg (1984), were found to be a reliable discriminator of rock type for highly-weathered materials (lateritic duricrust and loose pisoliths), Fig. 44A. Samples of lateritic duricrust and loose pisoliths of known lithologies (andesite and dolerite) can be related to particular rock lithologies (Fig. 44C). Only one sample of loose pisoliths derived from a known dolerite lithology lies in the andesitic field, the remainder are in the doleritic (basaltic) field. The results are not surprising because the fabric of the rock is easily recognizable in the majority of samples suggesting *in situ* formation with little modification. The majority of samples studied occupy the andesitic field which is consistent with the geology of the mine area.

5.3.4.3 Mineralogy

The mineralogical data for selected samples of various types of laterite, including pisolitic and nodular lag, loose pisoliths, pisolitic duricrust, and fragmental duricrust are given in Figs. 45 and 46. The mineralogical trends are very similar to those observed for profile samples from drill holes and pit faces. It is interesting to note that black, highly magnetic pisolitic and nodular lag contain large amounts of amorphous Al-oxide associated with maghemite. Small amounts of boehmite and corundum (not shown) also occur in black lag. Gibbsite is present only in small amounts in pisolitic lag. This suggests that most of the Al in these materials occurs as amorphous Al-oxide and not gibbsite. This is in contrast to the underlying fragmental and pisolitic duricrusts which contain large amounts of gibbsite. Hematite, maghemite, and quartz increase in abundance towards the surface, whereas the trend is opposite for goethite.

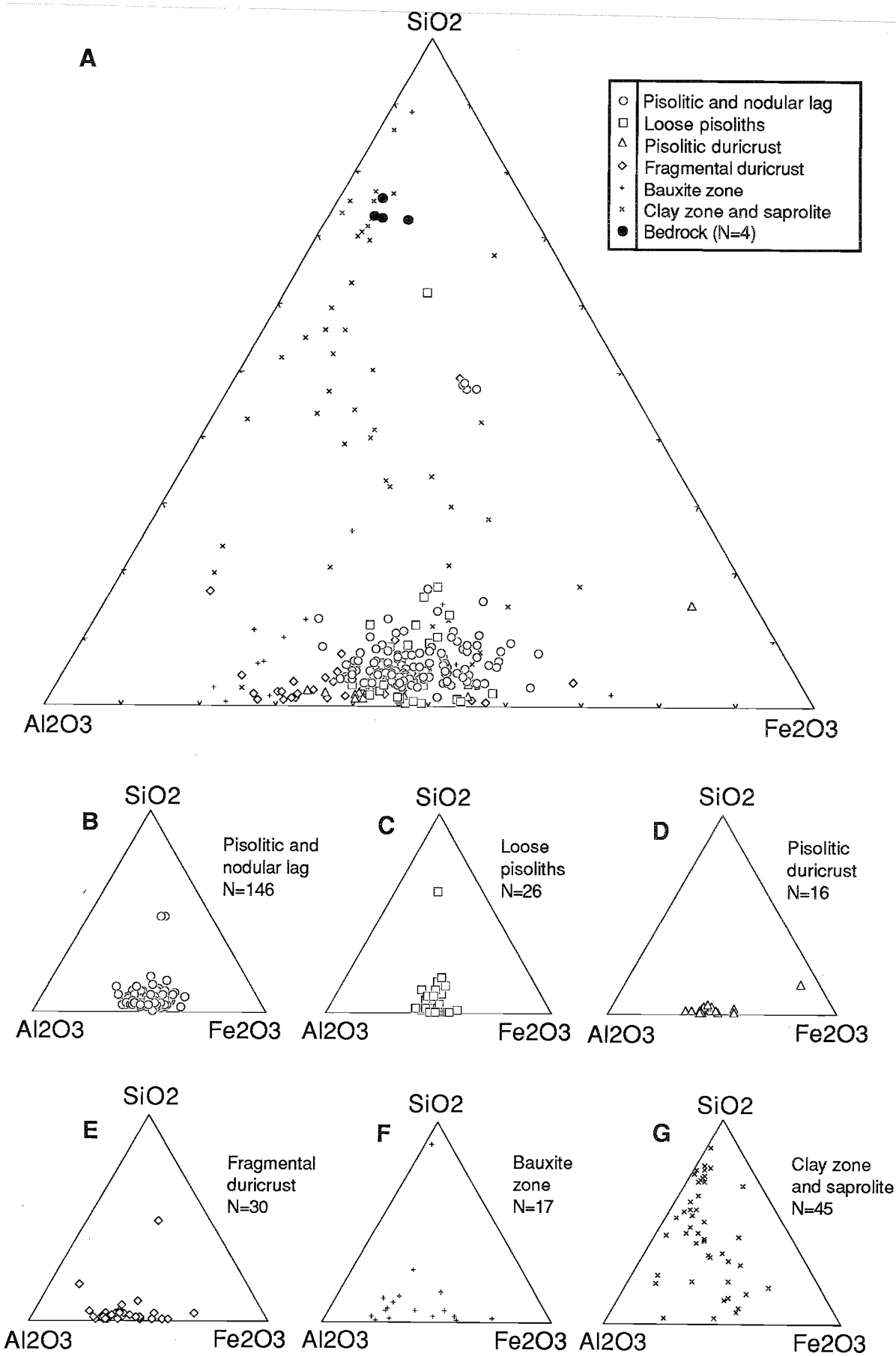

Fig. 41 Ternary diagrams of the major oxides of the regolith units of the laterite profile. Bedrock samples are included for comparison.

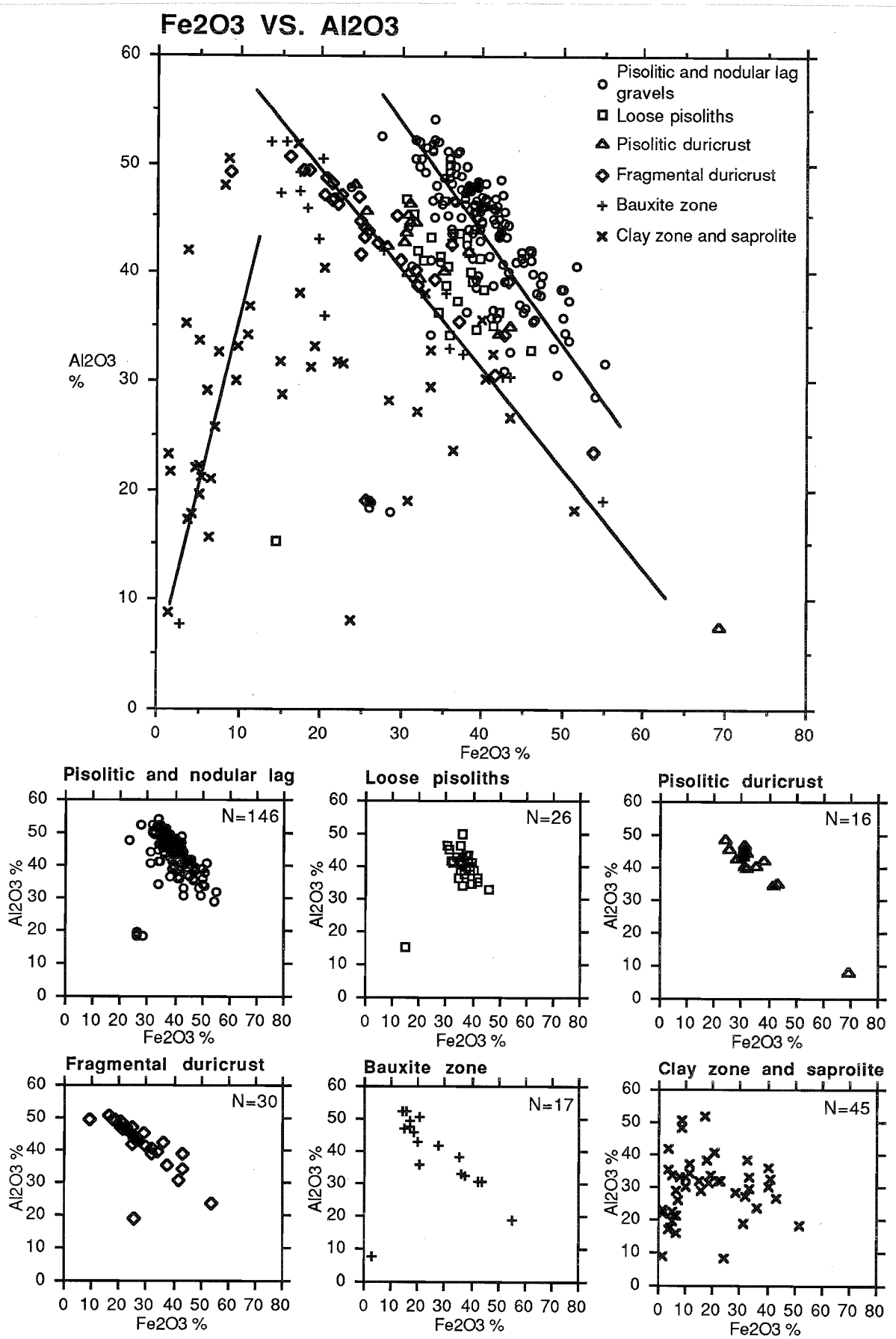

Fig. 42 Correlation diagrams between Fe2O3 and Al2O3 illustrating three distinct populations in regolith units of the lateritic profile.

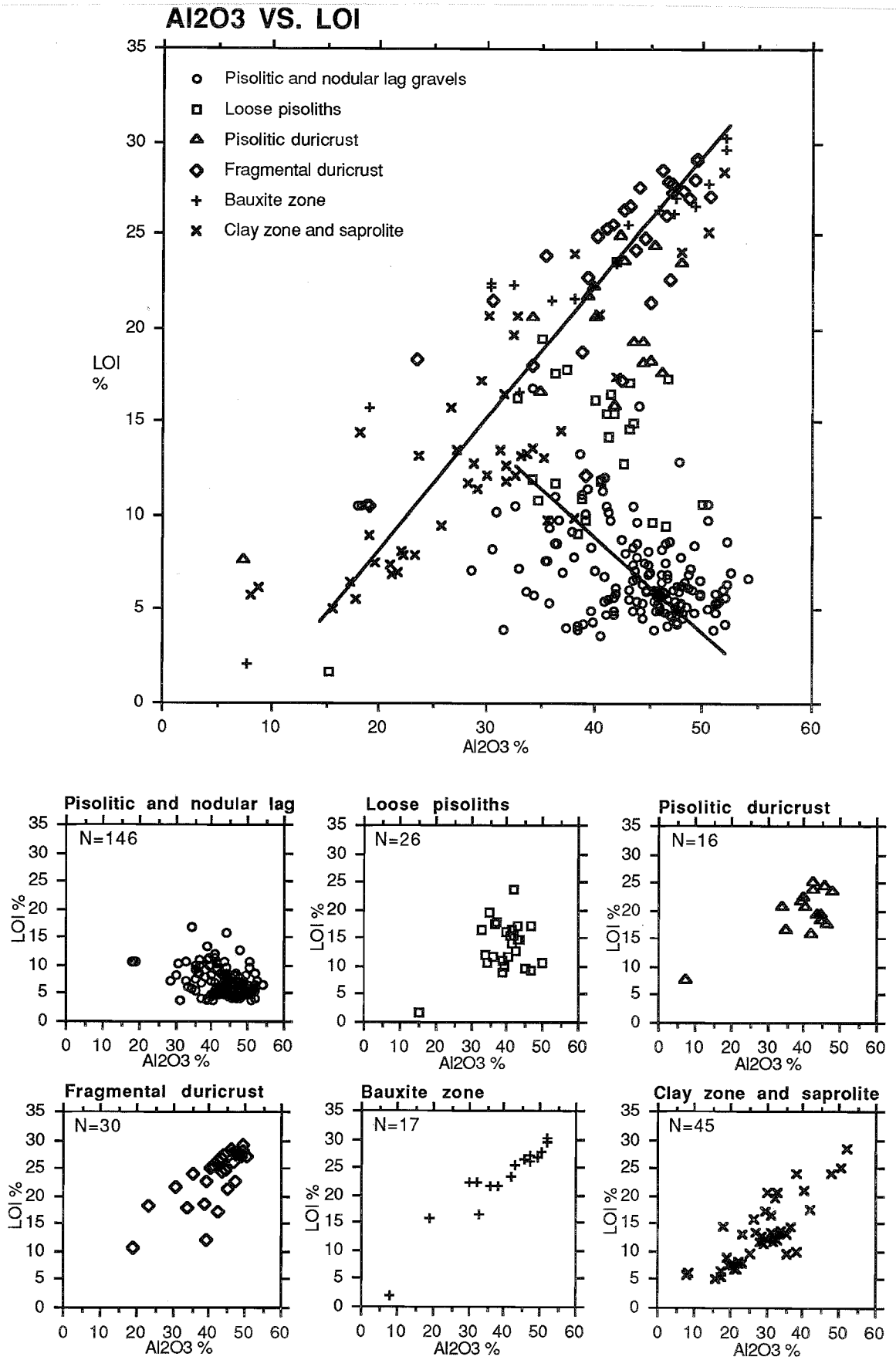

Fig. 43 Correlation diagrams between Al2O3 and LOI illustrating two distinct populations in regolith units of the lateritic profile.

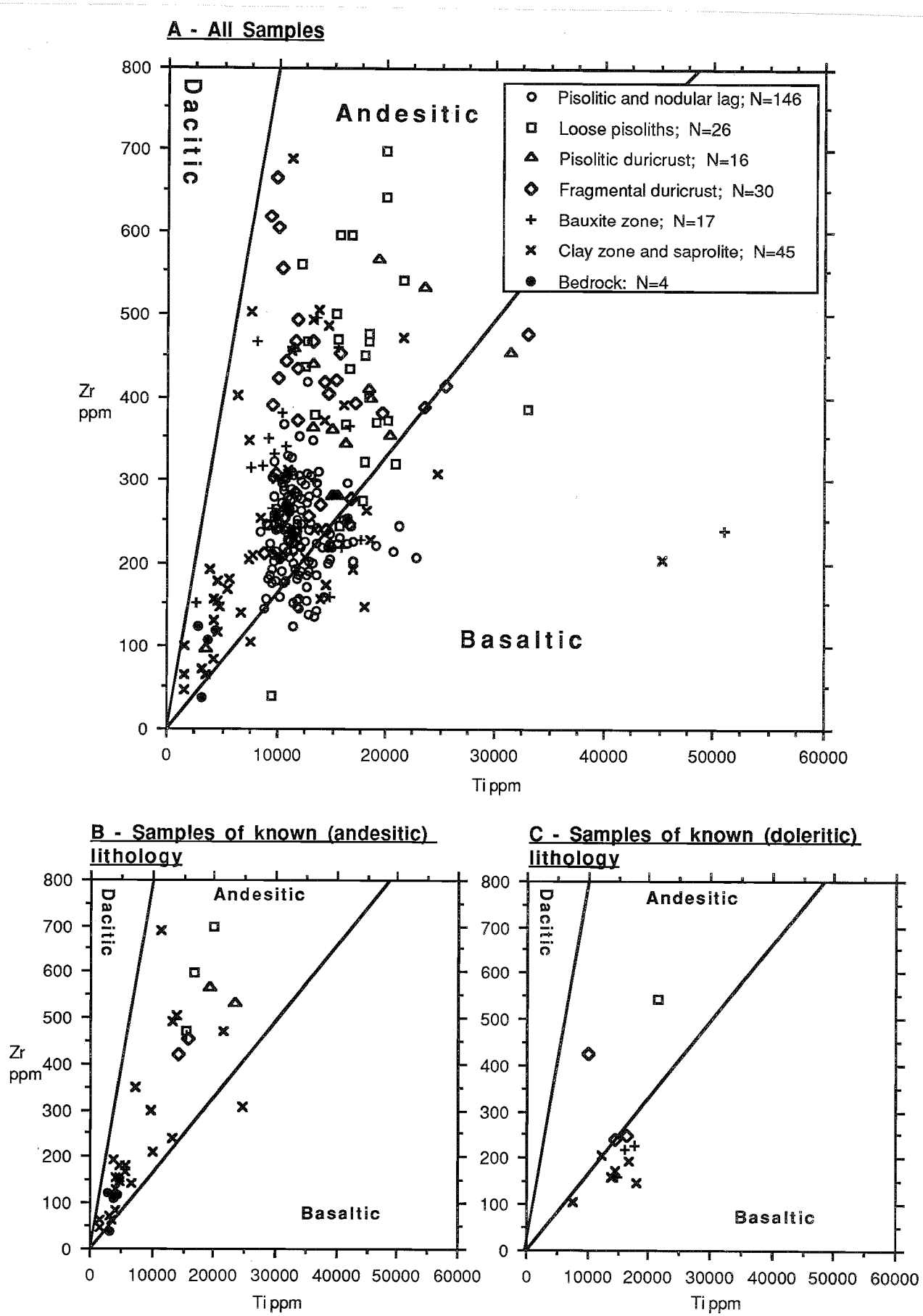

Fig. 44 Ti-Zr plots for weathered materials and bedrocks. Lithological fields from Hallberg (1984)

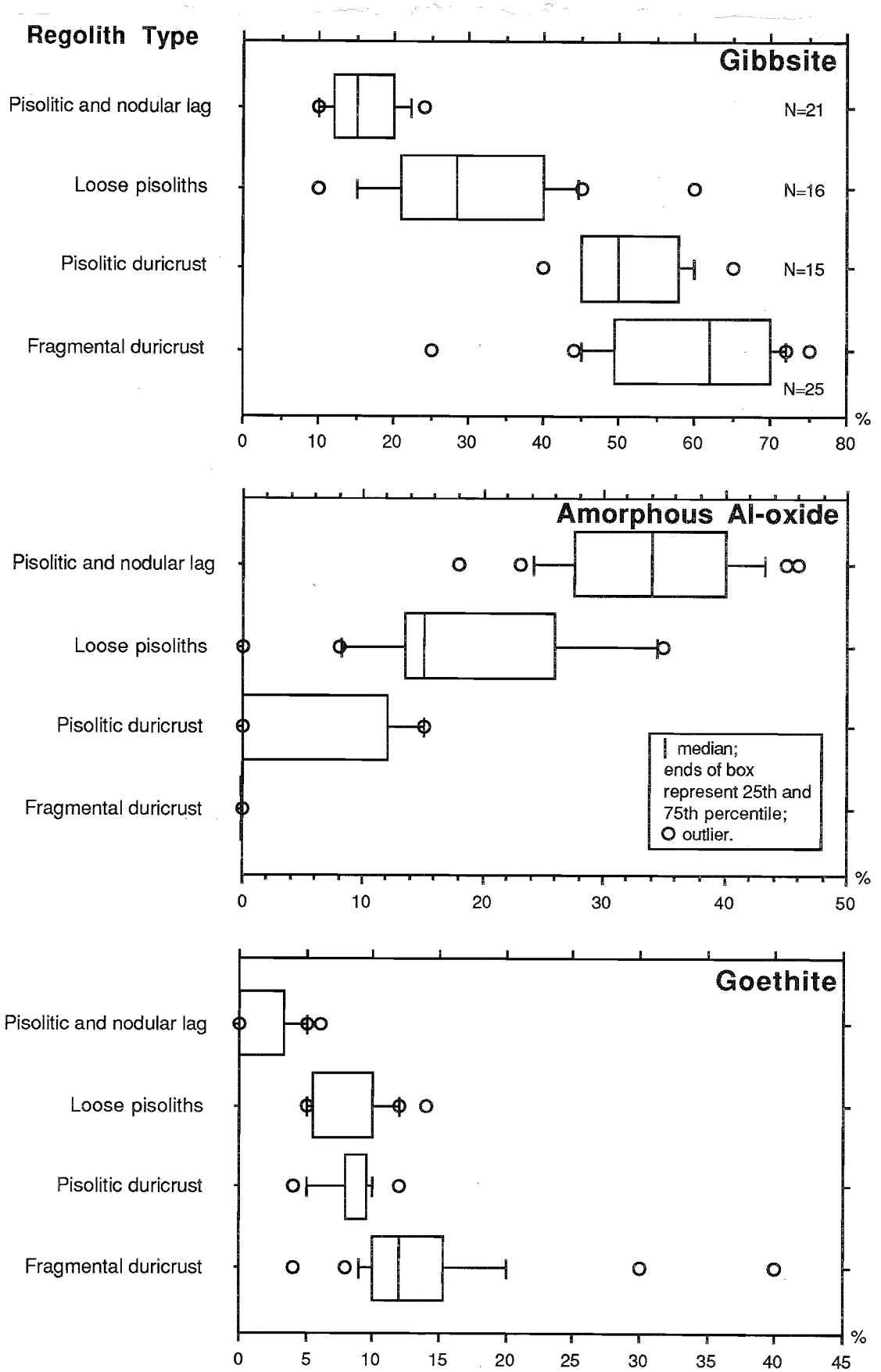

Fig. 45 Box plots showing the distribution of gibbsite, amorphous Al-oxide and goethite in several regolith materials arranged vertically in order of the regolith stratigraphy.

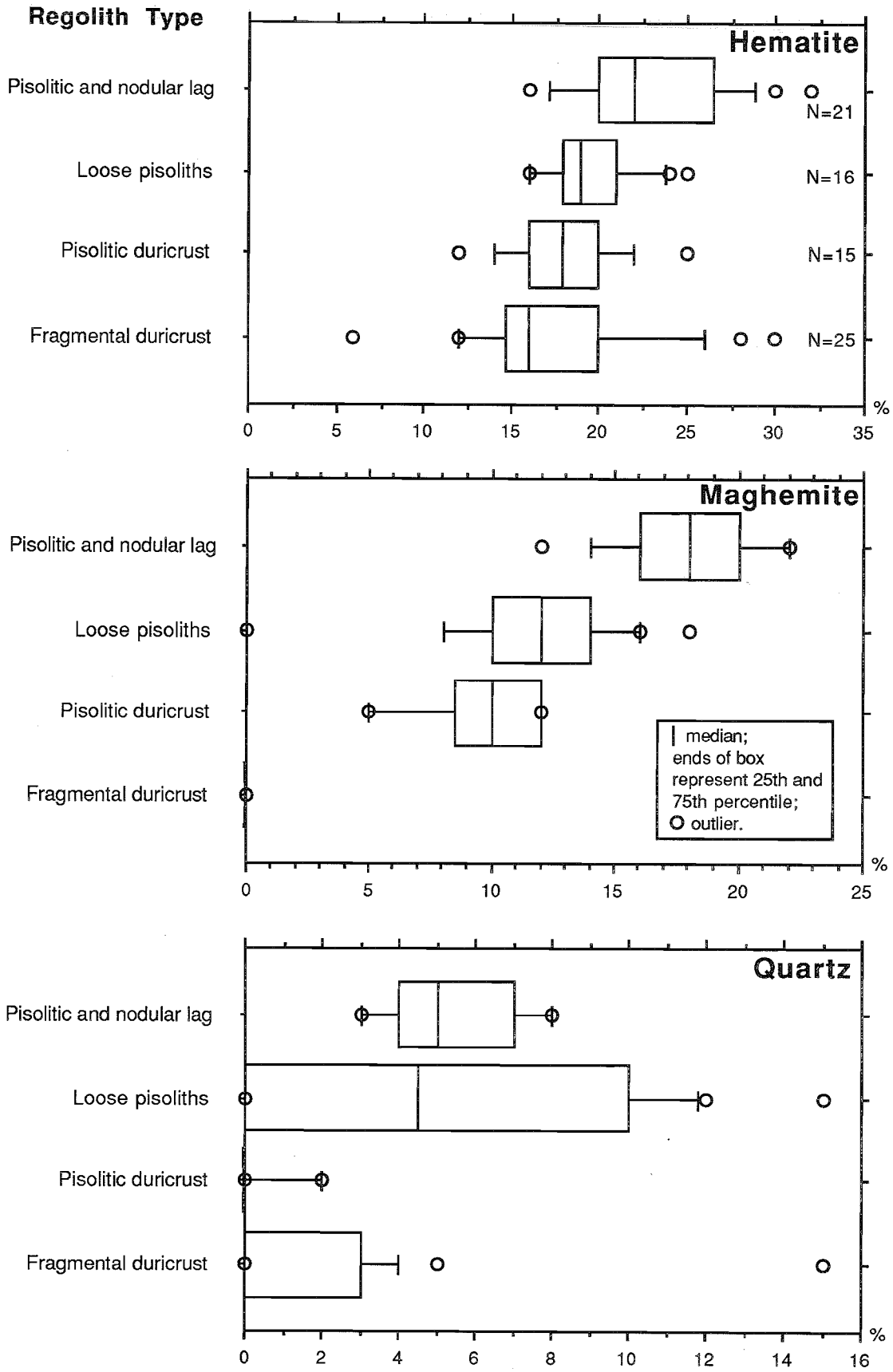

Fig. 46 Box plots showing the distribution of hematite, maghemite and quartz in several regolith materials arranged vertically in order of the regolith stratigraphy.

5.3.4.4 *Geochemistry*

Summary statistics

Summary statistics for the six sample groups are given in Tables 6-11. The summary tables list the number of samples analysed for each group, the 25th, 50th, 75th, 90th, 95th, 98 and 99th percentiles, minimum, maximum, mean values, and the standard deviation. All censored values (less than lower limit of determination) were assigned one-third of the detection limit as the default minimum value for statistical analyses. For measuring the centre of a population, the 50th percentile is more useful than the mean as it is less influenced by extreme levels. The dispersion of the data relative to the mean is measured by the standard deviation. A high standard deviation indicates a spread out distribution while a low standard deviation indicates a distribution close around the mean.

An immediately-obvious feature of the results shown in Tables 6 to 11 is the wide spread of values in all the categories. The lateritic duricrusts and loose pisoliths have large concentrations of Fe_2O_3, Al_2O_3 and lower contents of SiO_2 relative to the underlying saprolite. Among the various types of duricrusts and loose pisoliths, the pisolitic and nodular lag contain the highest concentrations of Fe_2O_3. Iron is less abundant in the fragmental duricrust and bauxite zone than in the pisolitic duricrust. Lateritic duricrust, loose pisoliths, and the bauxite zone are highly depleted in MgO, CaO, Na_2O, and K_2O relative to typical felsic or mafic bedrock contents. Inspection of the Tables using the 25th, 50th and 75th percentile shows that all the six sample groups are anomalous in As, Bi, Cu, Mo, W, Sn, and Au. However, the magnitude of the anomalies particularly in Cu, W, and Au, differ between the sample types. The saprolite shows very high concentrations of Cu (to 125193 ppm), W (to 322 ppm), As (to 564 ppm), Co (127 ppm), Mo (to 113 ppm) and Au (to 12 ppm). However, the range of all these elements in saprolite is large. The bauxite zone is characterized by high concentrations of Au (median 0.60 ppm) relative to the overlying fragmental (median 0.25 ppm) and pisolitic (median 0.07 ppm) duricrusts and loose pisoliths (median 0.08 ppm). The lowest concentration of Au occurs in the pisolitic lag (median 0.02 ppm). Among the various types of duricrust, fragmental duricrust shows highest concentration of Au (median 0.25 ppm).

Histograms

Histograms of the data were plotted for all the analysed elements and are shown in Appendix 8. Each figure comprises six histograms; pisolitic and nodular lag (LG103), loose pisoliths (LT102), pisolitic duricrust (LT202), fragmental duricrust (LT205), bauxite zone (BZ), and clay zone and saprolite (SAP). Histograms for the six sample groups show that there is an overlap in the concentrations for many elements. Some elements show bimodal or polymodal distributions. This occurs with elements that reflect underlying lithologies and mineralizations. Elements that exhibit these characteristics are Fe_2O_3, TiO_2, V, Zr, Cu, Mo, W, Bi, and As. Elements such as Fe, K, V, Ti, and Zr reflect the differences in underlying lithologies (felsic vs. mafic), whereas W, Bi, As, and Cu are associated with mineralization.

Box Plots

Box plots for all the elements are given in Figs. 47 to 56 and display the 10th, 25th, 50th, 75th, and 90th percentiles for each element. Each figure comprises six box plots; pisolitic and nodular lag, loose pisoliths, pisolitic duricrust, fragmental duricrust, bauxite zone, clay zone and saprolite, and bedrock. Box plots summarize the distribution of elements in a lateritic weathering profile on a greenstone parent material.

The box plots for SiO_2, Al_2O_3 and Fe_2O_3 illustrates the evolution of bedrock to lateritic pisoliths in terms of these three major components. These are gradually enriched upwards. Iron and Al_2O_3 are the most abundant components of the lateritic duricrust and pisolitic lag. Aluminium is a residual element and, in comparison with bedrock, is enriched in the lateritic profile. There is an abrupt rise in total Al_2O_3 at the bedrock-clay interface. Above the bauxite zone, the total Al_2O_3 content varies little, with only a slight increase towards the surface.

Iron distribution in the profile varies in a series of steps which marks the contacts between the pisolitic duricrust and the fragmental duricrust, and between the bauxite zone and clay zone. Iron in the lateritic nodules and pisoliths and pisolitic duricrust is always substantially higher than it is in the bedrock; however, it does reflect the nature of the bedrock, with less Fe in the duricrust over felsic andesite than that over dolerite. Silica, CaO, MgO, and K_2O are lost through the profile. The

Table 6 Summary statistics for pisolitic and nodular lag LG103.

Element		Method	lld	#values	25th	50th	75th	90th	95th	98th	99th	Min	Max	Mean	S.D.
SiO2	wt%	icp	0.1	146	3.84	4.58	6.18	8.128	9.25	11.136	13.302	1.2	14.59	5.288	2.214
Al2O3	wt%	icp	0.01	146	40.795	44.97	47.71	50.45	51.496	52.16	52.415	28.53	54.23	44.016	5.267
Fe2O3	wt%	icp	0.01	146	36.58	39.55	42.75	46.668	49.994	50.843	53.091	23.7	55.33	40.078	5.233
MgO	wt%	icp	0.003	146	0.02	0.031	0.042	0.053	0.071	0.082	0.093	0.001	0.125	0.033	0.02
CaO	wt%	icp	0.007	146	0.055	0.064	0.078	0.091	0.101	0.112	0.115	0.038	0.167	0.068	0.018
Na2O	wt%	icp	0.007	146	0.012	0.016	0.019	0.022	0.024	0.027	0.03	0.009	0.036	0.016	0.005
K2O	wt%	icp	0.06	146	0.02	0.06	0.1	0.15	0.194	0.262	0.291	0.02	0.41	0.07	0.066
TiO2	wt%	icp	0.002	146	1.76	1.92	2.15	2.478	2.74	3.173	3.472	1.42	3.79	2.014	0.396
LOI	wt%		0.01	146	5.315	6.2	8.12	10.156	11.255	12.887	14.665	3.65	16.81	6.901	2.359
Mn	ppm	xrf	15	146	69	91	127	182.6	237.8	351.12	432.68	28	626	112.47	79.294
Cr	ppm	icp	20	146	399.5	492	589.5	687	762.8	860	867.02	84	879	502.41	152.55
V	ppm	icp	5	146	622.5	721	860	988.2	1097.5	1216.8	1244.6	84	1430	749.96	190.77
Cu	ppm	aas	2	146	10	15	23	33.6	61.6	68.64	80.86	0.66	120	19.532	16.945
Pb	ppm	xrf	2	146	14	18	22	26.8	30	32	35.24	0.66	80	18.735	8.284
Zn	ppm	aas	2	146	15	18	20	24	25	30.64	38	10	58	18.5	5.523
Ni	ppm	aas	4	146	25	30	34	42	63	80.16	87.4	16	125	32.527	14.828
Co	ppm	aas	4	146	1.33	1.33	4	4	5	6	6	1.33	6	2.395	1.46
As	ppm	xrf	2	146	17	32	79	160	234	330.8	340	8	350	64.288	74.335
Sb	ppm	xrf	2	146	0.66	3	4.5	6	6	7.08	8	0.66	10	3.046	2.069
Bi	ppm	xrf	2	146	0.66	2	5	9.4	15.7	18.56	29.86	0.66	52	4.287	6.304
Mo	ppm	xrf	1	146	13.5	24	29	38	47.4	60.16	64.16	5	125	23.705	14.962
Ag	ppm	aas	0.1	146	0.5	0.6	0.6	0.7	0.7	0.7	0.754	0.3	0.8	0.571	0.09
Sn	ppm	xrf	2	146	9	15	22	26.8	32	36.48	44.16	2	48	16.384	9.213
Ge	ppm	xrf	2	146	0.66	0.66	2	2	3	3.08	4	0.66	5	1.15	0.883
Ga	ppm	xrf	4	146	86	96	105	110	115	120	122.7	58	130	95.055	13.997
W	ppm	xrf	4	146	14	36	56	70	84	101.6	120	1.33	130	38.593	27.309
Ba	ppm	icp	5	146	34	45	58.5	75.4	85.8	120.52	138	23	149	50.096	21.958
Zr	ppm	icp	5	146	206.5	238	266	303	310.7	348.48	361.56	124	419	238.03	49.977
Nb	ppm	xrf	2	146	13	15	16	18.4	19	20	21.08	8	24	14.658	2.803
Se	ppm	xrf	2	146	0.667	0.667	2	4	5	6.08	7	0.667	8	1.594	1.576
Be	ppm	icp	1	146	1	1	1	2	2	2	2	1	2	1.144	0.352
Au	ppm	gf-aas	0.001	146	0.01	0.02	0.05	0.204	0.334	0.654	0.943	0.001	1.58	0.081	0.191

Table 7 Summary statistics for loose pisoliths LT102

Element		Method	lld	#values	25th	50th	75th	90th	95th	98th	99th	Min	Max	Mean	S.D.
SiO2	wt%	icp	0.1	26	1.08	2.57	8.77	12.836	15.016	31.418	40.094	0.64	48.77	6.88	9.686
Al2O3	wt%	icp	0.01	26	36.33	40.6	42.945	45.868	46.688	48.222	49.046	15.43	49.87	39.566	6.46
Fe2O3	wt%	icp	0.01	26	34.155	36.04	38.755	40.798	41.892	43.951	44.976	14.59	46	36.019	5.604
MgO	wt%	icp	0.003	26	0.02	0.04	0.05	0.07	0.126	1.796	2.688	0.01	3.58	0.175	0.695
CaO	wt%	icp	0.007	26	0.03	0.05	0.08	0.208	0.22	4.962	7.531	0.03	10.1	0.456	1.968
Na2O	wt%	icp	0.007	26	0.01	0.02	0.03	0.04	0.047	0.972	1.471	0.003	1.97	0.095	0.383
K2O	wt%	icp	0.06	26	0.02	0.02	0.12	0.182	0.221	0.249	0.26	0.02	0.27	0.079	0.074
TiO2	wt%	icp	0.002	26	2.395	2.77	3.1	3.392	3.54	4.492	4.991	1.57	5.49	2.852	0.749
LOI	wt%		0.01	26	10.7	14.2	16.4	17.68	18.99	21.468	22.534	1.67	23.6	13.712	4.34
Mn	ppm	xrf	15	26	60	85	126	184.8	452.1	1021.8	1271.4	5	1521	165.15	294.42
Cr	ppm	icp	20	26	349	399	450.5	518.8	561.7	596.8	612.4	68	628	402.92	108.08
V	ppm	icp	5	26	578	669	692.5	768.6	788	926.48	998.24	356	1070	655.39	131.25
Cu	ppm	aas	2	26	7	11	18.5	41	67.9	123.4	150.7	2	178	21.885	35.678
Pb	ppm	xrf	2	26	6	14	19.5	20.8	22	22.48	22.74	0.67	23	12.768	7.371
Zn	ppm	aas	2	26	9	12	13.5	36	46	96.52	122.26	7	148	20.231	28.18
Ni	ppm	aas	4	26	6.665	18	23	27.4	40.6	86.8	108.9	1.33	131	20.615	24.869
Co	ppm	aas	4	26	1.33	1.33	1.33	3.198	6.7	33.88	48.44	1.33	63	4.1	12.096
As	ppm	xrf	2	26	20	75	182	280.4	327	421.68	471.34	6	521	120.81	128.51
Sb	ppm	xrf	2	26	0.67	2	3.5	6	8.1	9.48	9.74	0.67	10	2.741	2.694
Bi	ppm	xrf	2	26	2	4	5	7.4	10.1	11.48	11.74	0.67	12	4.088	2.984
Mo	ppm	xrf	1	26	28	36	43	55.8	61.4	62	62	0.33	62	35.743	14.772
Ag	ppm	aas	0.1	26	0.03	0.03	0.03	0.03	0.03	0.03	0.03	0.03	0.03	0.03	0
Sn	ppm	xrf	2	26	10.5	13	23	54.8	56	58.88	60.44	3	62	21.808	18.284
Ge	ppm	xrf	2	26	0.67	0.67	0.67	0.67	2.298	3.96	4.48	0.67	5	0.917	0.951
Ga	ppm	xrf	4	26	74	87	102.5	110	124	137.2	141.1	14	145	87.885	25.475
W	ppm	xrf	4	26	16	24	48	189	195	197.4	198.7	1.33	200	53.551	63.856
Ba	ppm	icp	5	26	16	25	40	47	53.7	58.8	61.4	8	64	28.923	15.352
Zr	ppm	icp	5	26	344.5	435	489.5	596	628.9	670.36	685.18	40	700	428.08	138.68
Nb	ppm	xrf	2	26	19.5	22	24.5	28.4	29.7	30.96	31.48	0.67	32	21.718	6.259
Se	ppm	xrf	2	26	0.67	0.67	3	4.4	5	5.48	5.74	0.67	6	1.821	1.736
Be	ppm	icp	1	26	0.33	0.33	2	2.4	3	3	3	0.33	3	0.987	0.991
Au	ppm	gf-aas	0.001	26	0.02	0.08	0.14	0.314	0.576	0.785	0.852	0.01	0.92	0.152	0.212

Table 8 Summary statistics for pisolitic duricrust LT202.

Element		Method	lld	#values	25th	50th	75th	90th	95th	98th	99th	Min	Max	Mean	S.D.
SiO2	wt%	icp	0.1	16	1.07	1.7	2.78	3.17	5.552	10.621	12.31	0.64	14	2.593	3.159
Al2O3	wt%	icp	0.01	16	39.29	42.3	44.5	45.78	46.556	47.41	47.695	7.38	47.98	39.991	9.491
Fe2O3	wt%	icp	0.01	16	30.46	31.1	35.4	42.648	48.676	61.17	65.335	24.31	69.5	34.766	10.612
MgO	wt%	icp	0.003	16	0.01	0.02	0.02	0.03	0.064	0.146	0.173	0.01	0.2	0.029	0.046
CaO	wt%	icp	0.007	16	0.03	0.04	0.04	0.05	0.072	0.125	0.142	0.03	0.16	0.047	0.031
Na2O	wt%	icp	0.007	16	0.003	0.01	0.02	0.03	0.032	0.037	0.038	0.003	0.04	0.014	0.011
K2O	wt%	icp	0.06	16	0.02	0.02	0.02	0.02	0.054	0.136	0.163	0.02	0.19	0.031	0.043
TiO2	wt%	icp	0.002	16	2.2	2.52	3.07	3.582	4.16	4.784	4.992	0.6	5.2	2.749	0.977
LOI	wt%		0.01	16	17.6	19.3	22.2	23.92	24.5	24.74	24.82	7.6	24.9	19.625	4.248
Mn	ppm	xrf	15	16	42	56	68	348.2	758.8	1293.52	1471.76	5	1650	191	409.407
Cr	ppm	icp	20	16	352	402	453	510.6	571.2	574.08	575.04	243	576	404.625	91.939
V	ppm	icp	5	16	490	584	648	708.6	721.6	747.04	755.52	405	764	579.5	105.806
Cu	ppm	aas	2	16	10	18	33	95.8	113.2	123.28	126.64	3	130	33.938	38.853
Pb	ppm	xrf	2	16	4	7	9	11.6	23.2	45.28	52.64	0.66	60	9.729	13.864
Zn	ppm	aas	2	16	6	9	11	13.8	82.4	236.96	288.48	3	340	29.438	82.887
Ni	ppm	aas	4	16	1.33	14	18	21.6	32.4	52.56	59.28	1.33	66	15.103	15.698
Co	ppm	aas	4	16	1.33	1.33	1.33	2.398	6.4	12.16	14.08	1.33	16	2.414	3.684
As	ppm	xrf	2	16	19	47	125	410	420	444	452	13	460	131.812	159.283
Sb	ppm	xrf	2	16	0.66	2	4	5	5.4	6.36	6.68	0.66	7	2.831	1.999
Bi	ppm	xrf	2	16	2	3	5	8.4	14.2	26.68	30.84	0.66	35	5.749	8.224
Mo	ppm	xrf	1	16	26	36	50	66.4	70.8	72.72	73.36	6	74	40.062	19.716
Ag	ppm	aas	0.1	16	0.03	0.03	0.03	0.03	0.03	0.03	0.03	0.03	0.03	0.108	0.16
Sn	ppm	xrf	2	16	12	17	54	62	73.6	79.84	81.92	2	84	33.25	25.629
Ge	ppm	xrf	2	16	0.66	0.66	0.66	0.66	0.66	0.66	0.66	0.66	0.66	0.66	0
Ga	ppm	xrf	4	16	72	76	100	107	114.6	125.64	129.32	38	133	85.562	23.085
W	ppm	xrf	4	16	22	31	154	188	206	220.4	225.2	16	230	92.688	78.407
Ba	ppm	icp	5	16	11	15	23	26.4	78	200.4	241.2	9	282	33	66.697
Zr	ppm	icp	5	16	279	361	440	488.2	538.4	553.76	558.88	97	564	373.125	111.505
Nb	ppm	xrf	2	16	15	19	22	24.8	26.8	28.72	29.36	3	30	18.625	6.206
Se	ppm	xrf	2	16	0.667	0.667	3	3	3	3	3	0.667	3	1.479	1.109
Be	ppm	icp	1	16	0.333	2	2	2	2.2	2.68	2.84	0.333	3	1.375	0.91
Au	ppm	gf-aas	0.001	16	0.03	0.07	0.13	0.204	0.308	0.399	0.43	0.001	0.46	0.109	0.116

Table 9 Summary statistics for fragmental duricrust LT205.

Element		Method	lld	#values	25th	50th	75th	90th	95th	98th	99th	Min	Max	Mean	S.D.
SiO2	wt%	icp	0.1	30	0.9	1.51	2.995	5.63	10.005	24.42	33.66	0.41	42.9	3.741	7.788
Al2O3	wt%	icp	0.01	30	39.25	43.7	47.05	49.2	49.4	49.892	50.261	19.1	50.63	42.196	7.466
Fe2O3	wt%	icp	0.01	30	21.38	25.32	31.865	41.59	43.045	47.422	50.596	8.87	53.77	27.592	9.422
MgO	wt%	icp	0.003	30	0.01	0.02	0.02	0.03	0.05	0.072	0.081	0.01	0.09	0.022	0.017
CaO	wt%	icp	0.007	30	0.02	0.03	0.04	0.04	0.045	0.078	0.099	0.02	0.12	0.033	0.018
Na2O	wt%	icp	0.007	30	0.003	0.003	0.01	0.03	0.03	0.038	0.044	0.003	0.05	0.01	0.012
K2O	wt%	icp	0.06	30	0.02	0.02	0.055	0.13	0.185	0.274	0.337	0.02	0.4	0.059	0.082
TiO2	wt%	icp	0.002	30	1.7	1.97	2.585	3.24	4.055	4.72	5.095	1.47	5.47	2.352	0.887
LOI	wt%		0.01	30	21.45	25.3	27.35	28	28.75	29.04	29.07	10.5	29.1	23.91	4.828
Mn	ppm	xrf	15	30	22	36	75.5	113	177	522.6	769.801	5	1017	85.467	181.358
Cr	ppm	icp	20	30	287.5	349	396	420	440.5	452.8	457.9	113	463	337	79.741
V	ppm	icp	5	30	372	431	585	791	915.5	1113.6	1191.3	169	1269	510.433	235.242
Cu	ppm	aas	2	30	21	30	43.5	90	188.5	290.6	299.3	8	308	50.833	69.395
Pb	ppm	xrf	2	30	1.33	5	7	14	15.5	41.4	59.7	0.66	78	7.587	13.947
Zn	ppm	aas	2	30	7	9	11.5	14	14.5	18.6	21.3	4	24	9.833	3.983
Ni	ppm	aas	4	30	1.33	12	16	16	20	24	27	1.33	30	10.454	7.856
Co	ppm	aas	4	30	1.33	1.33	1.33	7	7.5	8	8	1.33	8	2.486	2.268
As	ppm	xrf	2	30	15.5	26	97.5	280	319.5	352	361	7	370	83.3	105.402
Sb	ppm	xrf	2	30	0.66	2	3	4	5.5	6.8	7.4	0.66	8	2.175	1.877
Bi	ppm	xrf	2	30	3	4	5.5	7	9	11.6	12.8	0.66	14	4.577	2.923
Mo	ppm	xrf	1	30	24	38	54	58	74	104.8	117.4	3	130	40.667	25.289
Ag	ppm	aas	0.1	30	0.03	0.03	0.03	0.2	0.45	0.5	0.5	0.03	0.5	0.09	0.136
Sn	ppm	xrf	2	30	12	25	46	48	54	56.8	57.4	2	58	28.367	17.934
Ge	ppm	xrf	2	30	0.66	0.66	0.66	0.66	2	2	2	0.66	2	0.794	0.409
Ga	ppm	xrf	4	30	60.5	70	78	80	85	88.4	90.2	42	92	69.4	12.602
W	ppm	xrf	4	30	16.5	57	147.5	175	190	192	193.5	1.33	195	80.889	68.582
Ba	ppm	icp	5	30	12	20	32.5	53	86.5	307.8	456.9	1.66	606	44.466	108.285
Zr	ppm	icp	5	30	281	405	461	556	611.5	637.2	651.6	212	666	402.3	116.128
Nb	ppm	xrf	2	30	12	14	20	24	24.5	26.2	27.1	8	28	16.167	5.18
Se	ppm	xrf	2	30	0.667	0.667	3	5	7	8.4	8.7	0.667	9	2.178	2.314
Be	ppm	icp	1	30	0.333	1	1.5	2	2	2	2	0.333	2	1	0.678
Au	ppm	gf-aas	0.001	30	0.11	0.25	0.555	1.45	2.03	3.394	4.207	0.001	5.02	0.612	0.991

Table 10 Summary statistics for bauxite zone samples bz.

Element		Method	lld	#values	25th	50th	75th	90th	95th	98th	99th	Min	Max	Mean	S.D.
SiO2	wt%	icp	0.1	17	1.433	4.275	7.903	14.717	29.88	63.132	74.216	0.43	85.3	10.026	20.041
Al2O3	wt%	icp	0.01	17	30.93	40.05	47.362	50.938	52.106	52.126	52.133	7.85	52.14	38.637	12.221
Fe2O3	wt%	icp	0.01	17	16.122	20.08	35.82	42.91	45.318	51.127	53.064	2.93	55	25.856	13.633
MgO	wt%	icp	0.003	17	0.01	0.02	0.037	0.135	0.182	0.223	0.236	0.01	0.25	0.049	0.067
CaO	wt%	icp	0.007	17	0.02	0.02	0.03	0.043	0.063	0.109	0.125	0.003	0.14	0.03	0.031
Na2O	wt%	icp	0.007	17	0.01	0.02	0.03	0.04	0.041	0.047	0.048	0.003	0.05	0.022	0.014
K2O	wt%	icp	0.06	17	0.02	0.052	0.165	0.323	0.645	1.002	1.121	0.02	1.24	0.172	0.305
TiO2	wt%	icp	0.002	17	1.467	1.755	2.56	2.801	3.752	6.583	7.526	0.43	8.47	2.299	1.718
LOI	wt%		0.01	17	21.525	22.95	26.55	28.34	29.705	30.062	30.181	2.01	30.3	22.771	6.69
Mn	ppm	xrf	15	17	9.5	23	81.25	108.4	415.599	1417.24	1751.12	2	2085	160.294	497.491
Cr	ppm	icp	20	17	220.25	323	377.25	485.1	494.95	511.78	517.39	75	523	317.176	120.487
V	ppm	icp	5	17	277.75	359.5	771.25	913.5	929	969.8	983.4	51	997	510.647	298.276
Cu	ppm	aas	2	17	36	61	98.75	124.3	126.35	130.94	132.47	17	134	69.235	39.487
Pb	ppm	xrf	2	15	1	3	6.5	13.5	18.5	26.6	29.3	1	32	6.133	8.34
Zn	ppm	aas	2	17	7	9.5	11.75	13.6	18.75	31.5	35.75	5	40	11.412	7.882
Ni	ppm	aas	4	17	3	3	11	18.9	21.75	24.3	25.15	3	26	7.824	7.544
Co	ppm	aas	4	17	1.333	2	2	2	2.6	4.64	5.32	1.333	6	2.039	1.066
As	ppm	xrf	2	17	10.25	34	69.75	169.7	296.35	300.94	302.47	5	304	69.882	92.992
Sb	ppm	xrf	2	12	1	2	4	4	4.8	5.52	5.76	1	6	2.75	1.658
Bi	ppm	xrf	2	13	4	5.5	11.5	21.6	24.35	24.74	24.87	2	25	9.154	7.872
Mo	ppm	xrf	1	17	7.5	14.5	23.75	56	65.6	98.24	109.12	1	120	26.059	29.805
Ag	ppm	aas	0.1	17	0.03	0.167	0.167	0.167	0.167	0.167	0.167	0.03	0.167	0.123	0.064
Sn	ppm	xrf	2	17	6	16.5	31.25	53.8	73.05	76.62	77.81	1	79	23.176	23.458
Ge	ppm	xrf	2	10	1.333	1.333	2	2	3	3.6	3.8	1	4	1.767	0.861
Ga	ppm	xrf	4	17	47.25	57	60.75	69.5	80	80	80	22	80	55.647	13.729
W	ppm	xrf	4	17	7	25	99.5	155	171.4	179.56	182.28	4	185	61.118	63.414
Ba	ppm	icp	5	17	16.5	38.5	56	95.7	164.4	233.76	256.88	2	280	54.529	67.458
Zr	ppm	icp	5	17	231	316.5	361.5	464.1	473.2	487.48	492.24	153	497	317.471	100.837
Nb	ppm	xrf	2	17	10	13	14.75	21.3	23.8	29.92	31.96	4	34	14.294	6.989
Se	ppm	xrf	2	17	1	1	3.75	7.3	8.45	9.98	10.49	1	11	3.059	2.989
Be	ppm	icp	1	17	0.333	0.333	1	2	2.15	2.66	2.83	0.333	3	0.863	0.85
Au	ppm	gf-aas	0.001	17	0.333	0.605	2.062	6.246	6.686	8.134	8.617	0.05	9.1	1.954	2.66

Table 11 Summary statistics for saprolite samples sap.

Element		Method	lld	#values	25th	50th	75th	90th	95th	98th	99th	Min	Max	Mean	S.D.
SiO2	wt%	icp	0.1	45	16.895	36.9	60.48	67.165	69.625	71.38	72.055	1.93	72.73	38.686	21.918
Al2O3	wt%	icp	0.01	45	21.815	29.755	33.528	39.29	46.47	50.591	51.271	8.05	51.95	29.109	9.604
Fe2O3	wt%	icp	0.01	45	5.295	11.29	27.315	38.25	41.115	44.285	47.952	1.36	51.62	17.235	13.818
MgO	wt%	icp	0.003	45	0.03	0.05	0.125	0.805	1.128	1.151	1.155	0.01	1.16	0.209	0.347
CaO	wt%	icp	0.007	45	0.02	0.035	0.04	0.165	0.273	0.55	0.73	0.01	0.91	0.08	0.155
Na2O	wt%	icp	0.007	45	0.032	0.07	0.11	0.26	0.315	0.434	0.452	0.01	0.47	0.106	0.107
K2O	wt%	icp	0.06	45	0.082	0.195	0.707	1.07	1.283	1.717	2.918	0.02	4.12	0.488	0.69
TiO2	wt%	icp	0.002	45	0.77	1.34	2.312	3.01	3.45	4.435	5.987	0.25	7.54	1.74	1.29
LOI	wt%		0.01	45	7.967	12.4	15.475	20.75	24.075	25.43	26.915	5.03	28.4	13.048	5.742
Mn	ppm	xrf	15	45	5	34.5	145.25	278	322.5	524.398	1156.2	5	1788	128.689	274.524
Cr	ppm	icp	20	45	86.25	128	261.75	420	476.25	529.7	631.85	6.66	734	193.851	160.65
V	ppm	icp	5	45	103.75	220	483.5	736	790.5	836.4	838.2	71	840	317.4	249.034
Cu	ppm	aas	2	45	104.5	199	383.25	3735	5615	7066	8533	10	10000	1069.84	2120.48
Pb	ppm	xrf	2	45	0.66	3.5	6	9.5	14	20.2	21.1	0.66	22	4.857	4.913
Zn	ppm	aas	2	45	13	18.5	35.75	101	115.25	118.1	118.55	2	119	35.444	34.772
Ni	ppm	aas	4	45	19	36	49.5	61.5	84.5	116.5	127.75	1.33	139	38.807	27.534
Co	ppm	aas	4	45	1.33	6	8.75	14	14.75	29.8	78.4	1.33	127	8.754	18.648
As	ppm	xrf	2	45	7.25	19	55.5	128.5	186	371.4	467.7	0.66	564	55.088	101.202
Sb	ppm	xrf	2	45	0.66	0.66	1.665	2.5	4.75	6	6	0.66	6	1.328	1.39
Bi	ppm	xrf	2	45	0.66	2	5	15	19.25	23.3	24.65	0.66	26	4.841	6.506
Mo	ppm	xrf	1	45	5	11	21	41.5	55.25	89.6	101.3	0.33	113	18.555	22.358
Ag	ppm	aas	0.1	45	0.03	0.03	0.03	0.03	2	4.05	6.525	0.03	9	0.372	1.458
Sn	ppm	xrf	2	45	4	14.5	24.75	47	55	65.5	67.75	0.66	70	19.407	18.366
Ge	ppm	xrf	2	45	0.66	0.66	2	3.5	4	4.1	4.55	0.66	5	1.693	1.244
Ga	ppm	xrf	4	45	24	35.5	45	58	70.75	82.1	82.55	1.33	83	37.03	18.029
W	ppm	xrf	4	45	6.25	15	27	60	77.75	171.7	246.85	1.33	322	30.429	52.648
Ba	ppm	icp	5	45	23.25	98	218.5	631	690.5	759.9	889.95	1.66	1020	185.496	239.657
Zr	ppm	icp	5	45	148.25	204.5	312.75	480	500.75	524.3	606.65	48	689	246.511	146.733
Nb	ppm	xrf	2	45	6	11	14	19.5	21.75	25.9	34.45	0.66	43	11.177	7.625
Se	ppm	xrf	2	45	0.667	0.667	2	4	4	21.4	50.2	0.667	79	3.4	11.761
Be	ppm	icp	1	45	0.333	0.333	0.333	0.333	0.333	1.1	1.55	0.333	2	0.385	0.265
Au	ppb	gf-aas	0.001	45	0.155	0.505	1.683	4.055	5.142	7.527	9.763	0.01	12	1.519	2.305

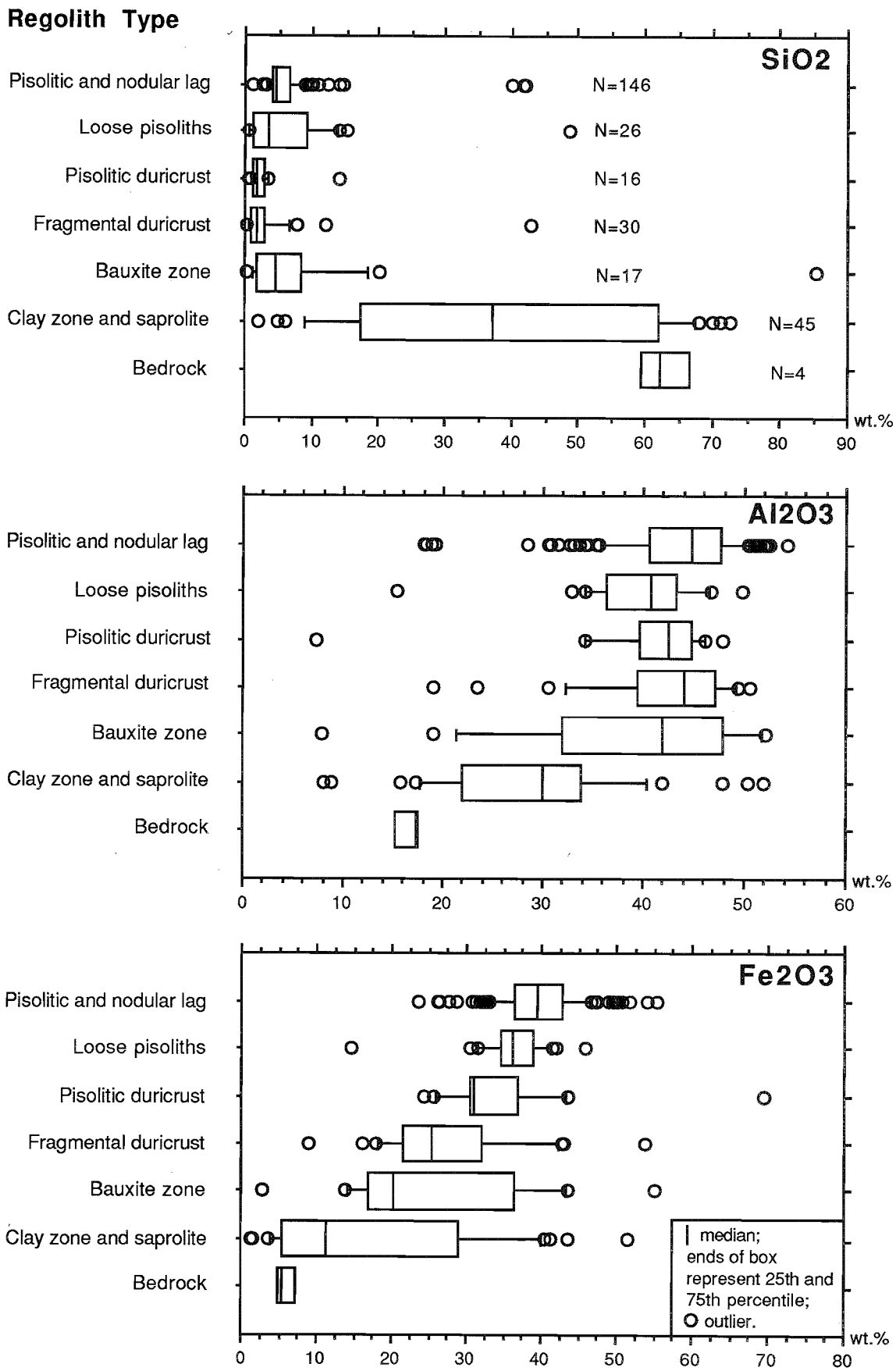

Fig. 47 Box plots showing the distribution of SiO2, Al2O3 and Fe2O3 in several regolith materials and bedrock arranged vertically in order of the regolith stratigraphy.

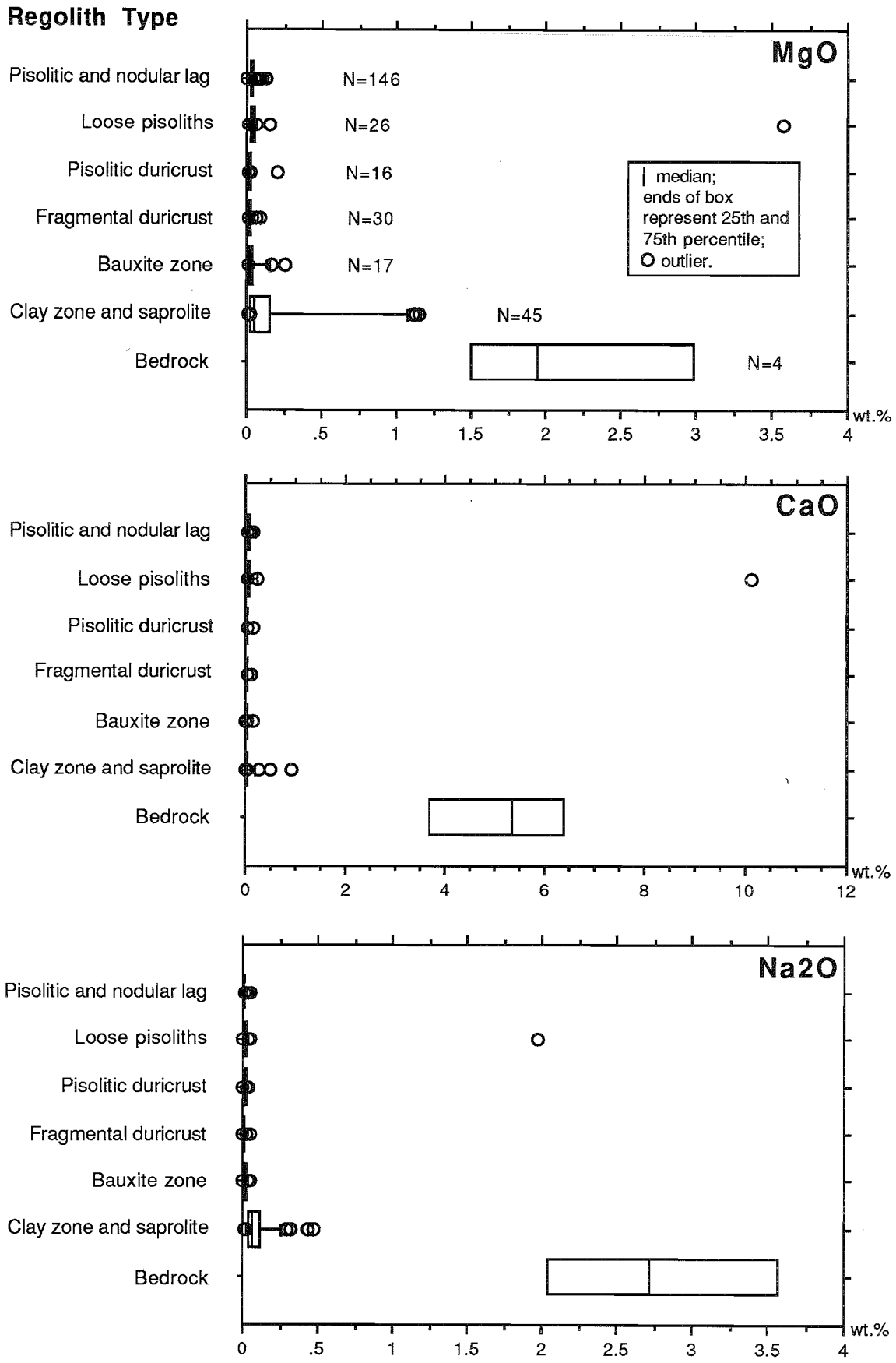

Fig. 48 Box plots showing the distribution of MgO, CaO and Na2O in several regolith materials and bedrock arranged vertically in order of the regolith stratigraphy.

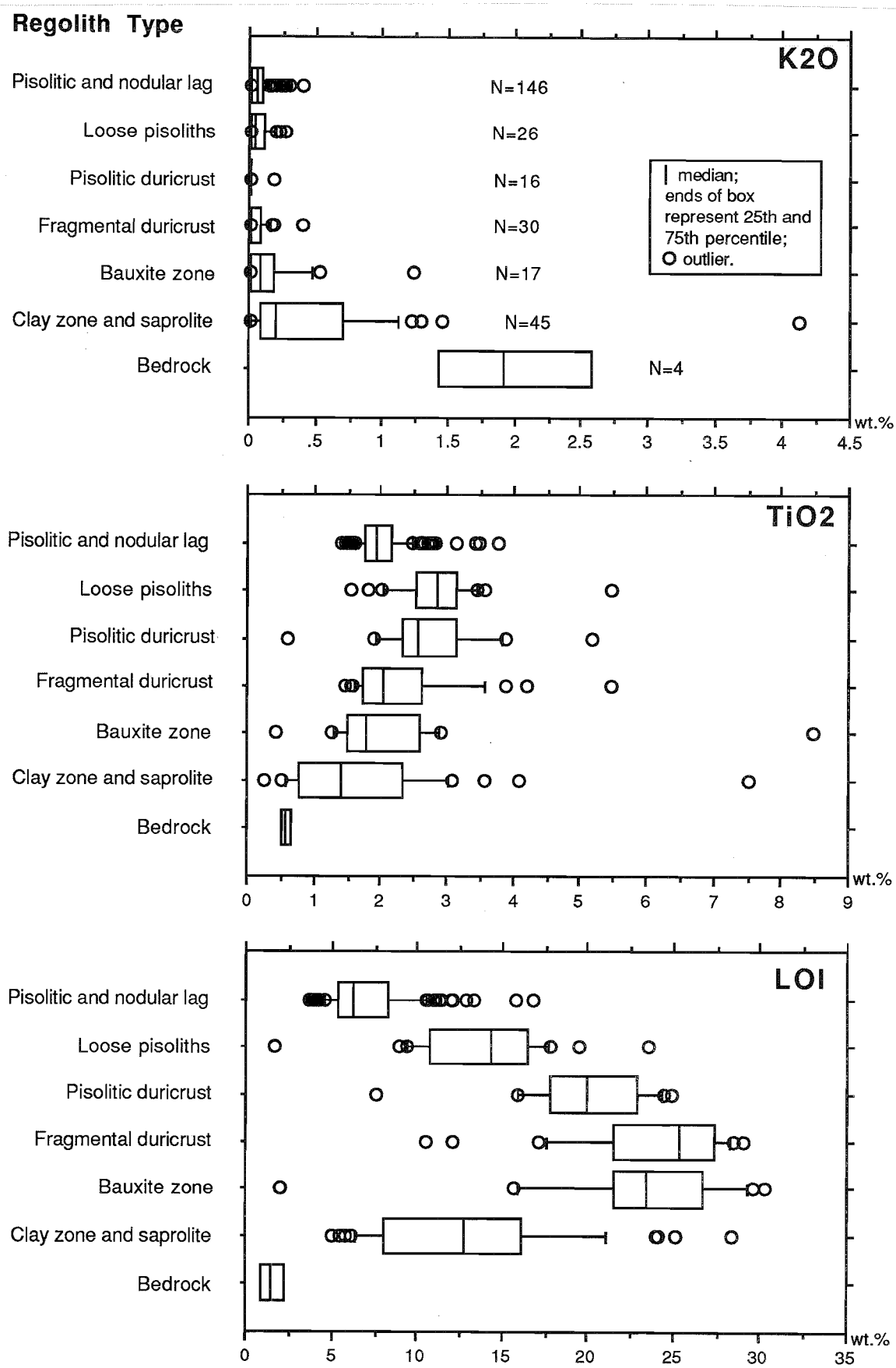

Fig. 49 Box plots showing the distribution of K_2O, TiO_2 and LOI in several regolith materials and bedrock arranged vertically in order of the regolith stratigraphy.

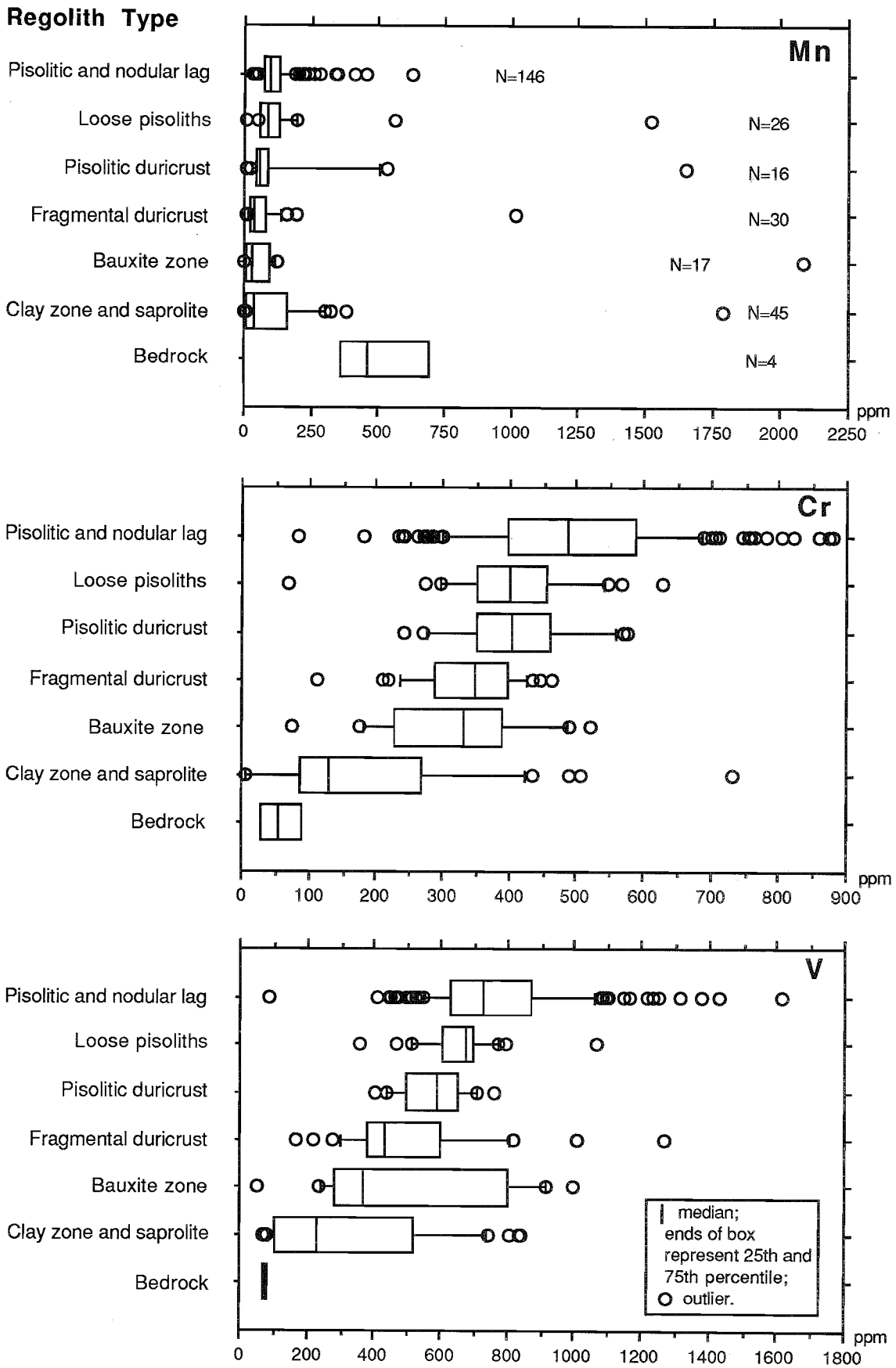

Fig. 50 Box plots showing the distribution of Mn, Cr and V in several regolith materials and bedrock arranged vertically in order of the regolith stratigraphy.

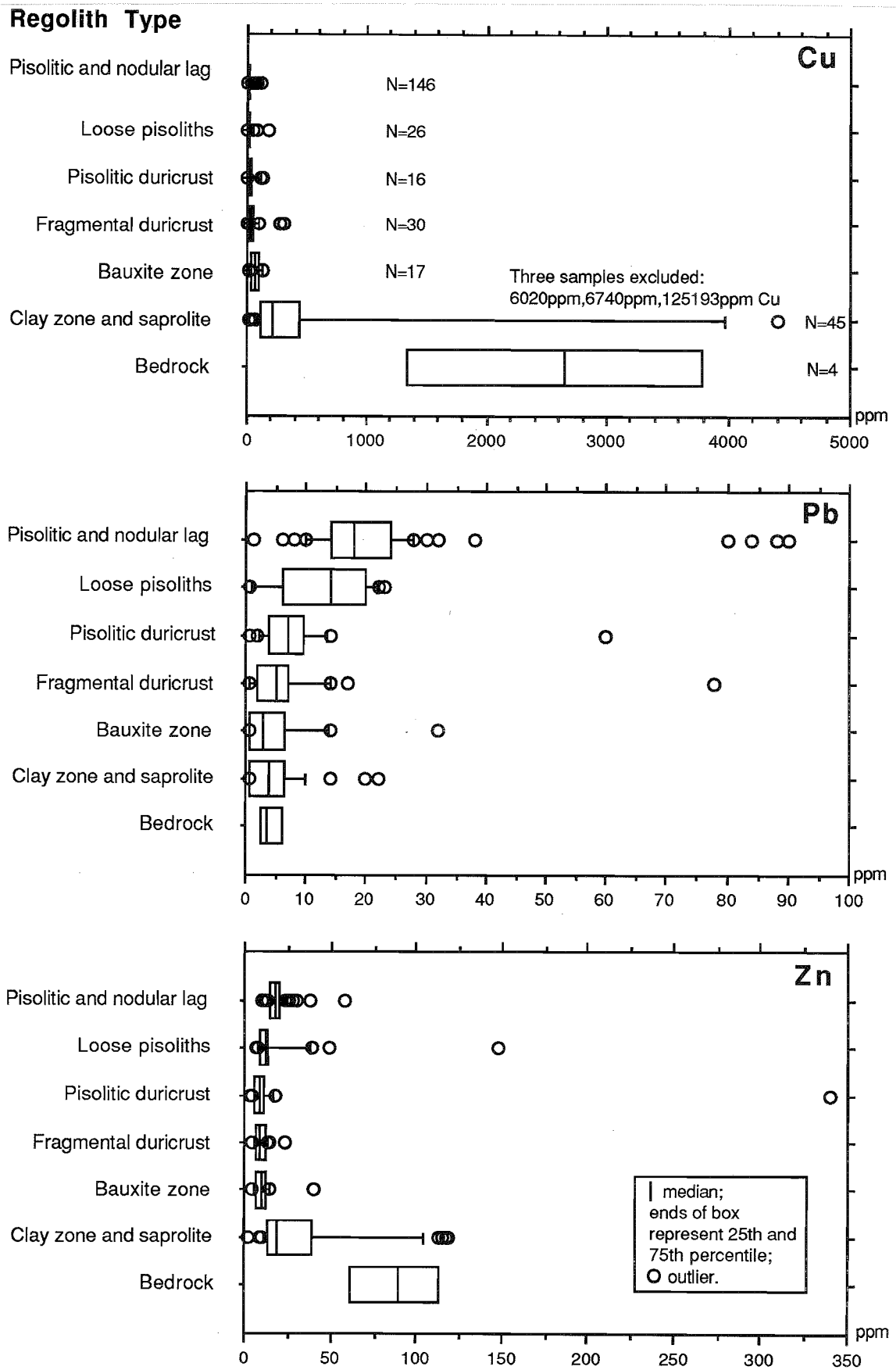

Fig. 51 Box plots showing the distribution of Cu, Pb and Zn in several regolith materials and bedrock arranged vertically in order of the regolith stratigraphy.

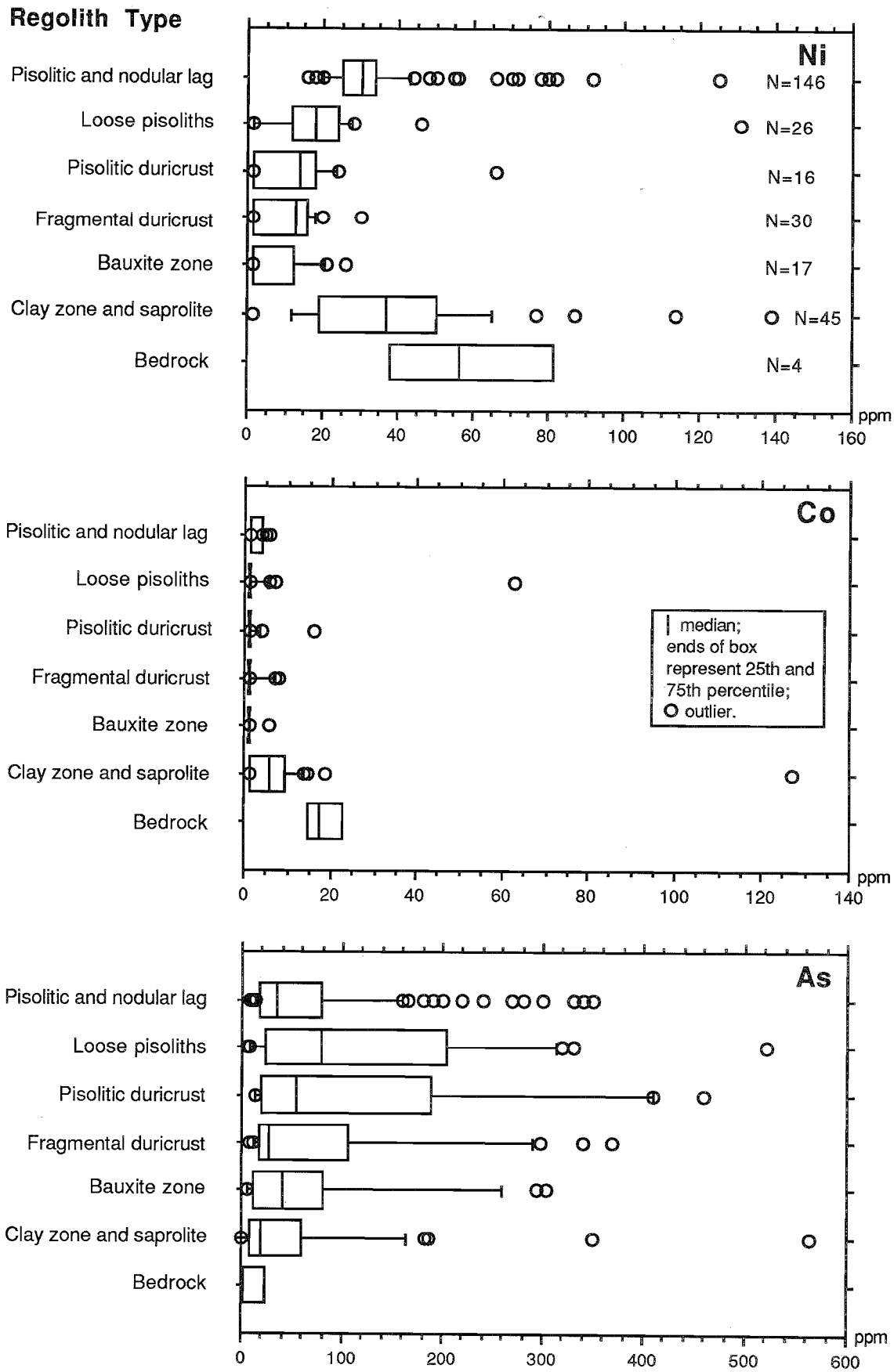

Fig. 52 Box plots showing the distribution of Ni, Co and As in several regolith materials and bedrock arranged vertically in order of the regolith stratigraphy.

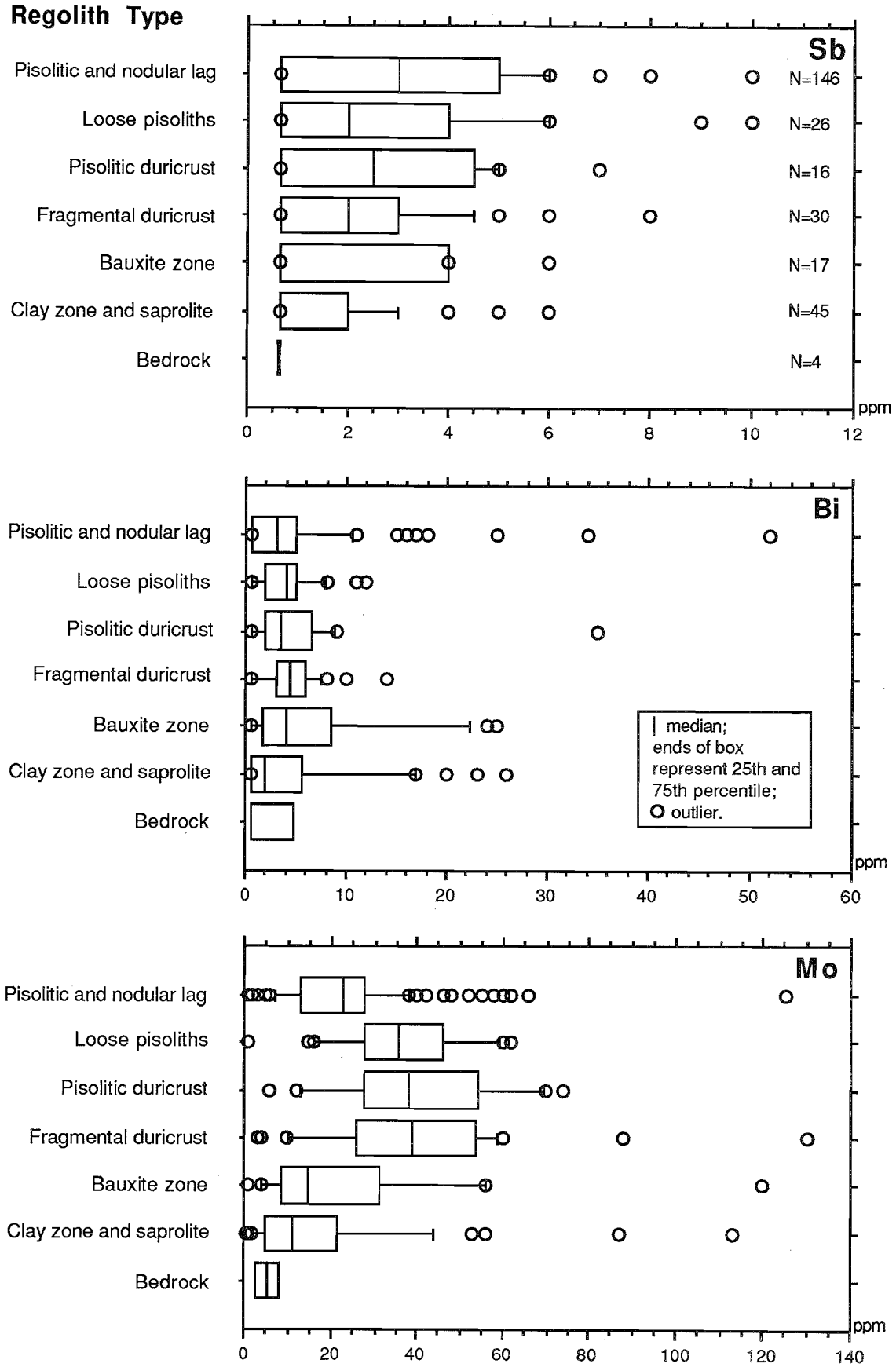

Fig. 53 Box plots showing the distribution of Sb, Bi and Mo in several regolith materials and bedrock arranged vertically in order of the regolith stratigraphy.

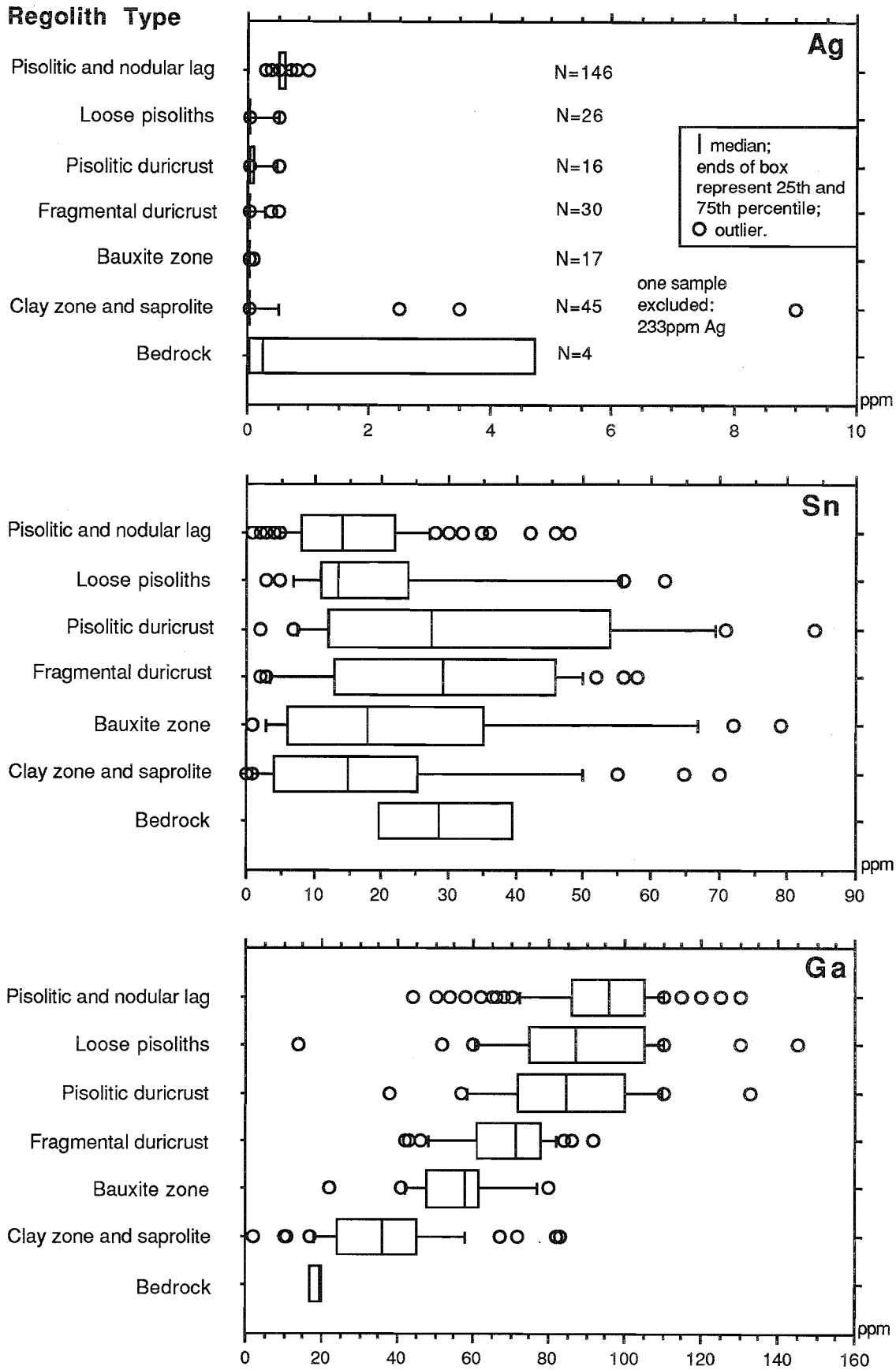

Fig. 54 Box plots showing the distribution of Ag, Sn and Ga in several regolith materials and bedrock arranged vertically in order of the regolith stratigraphy.

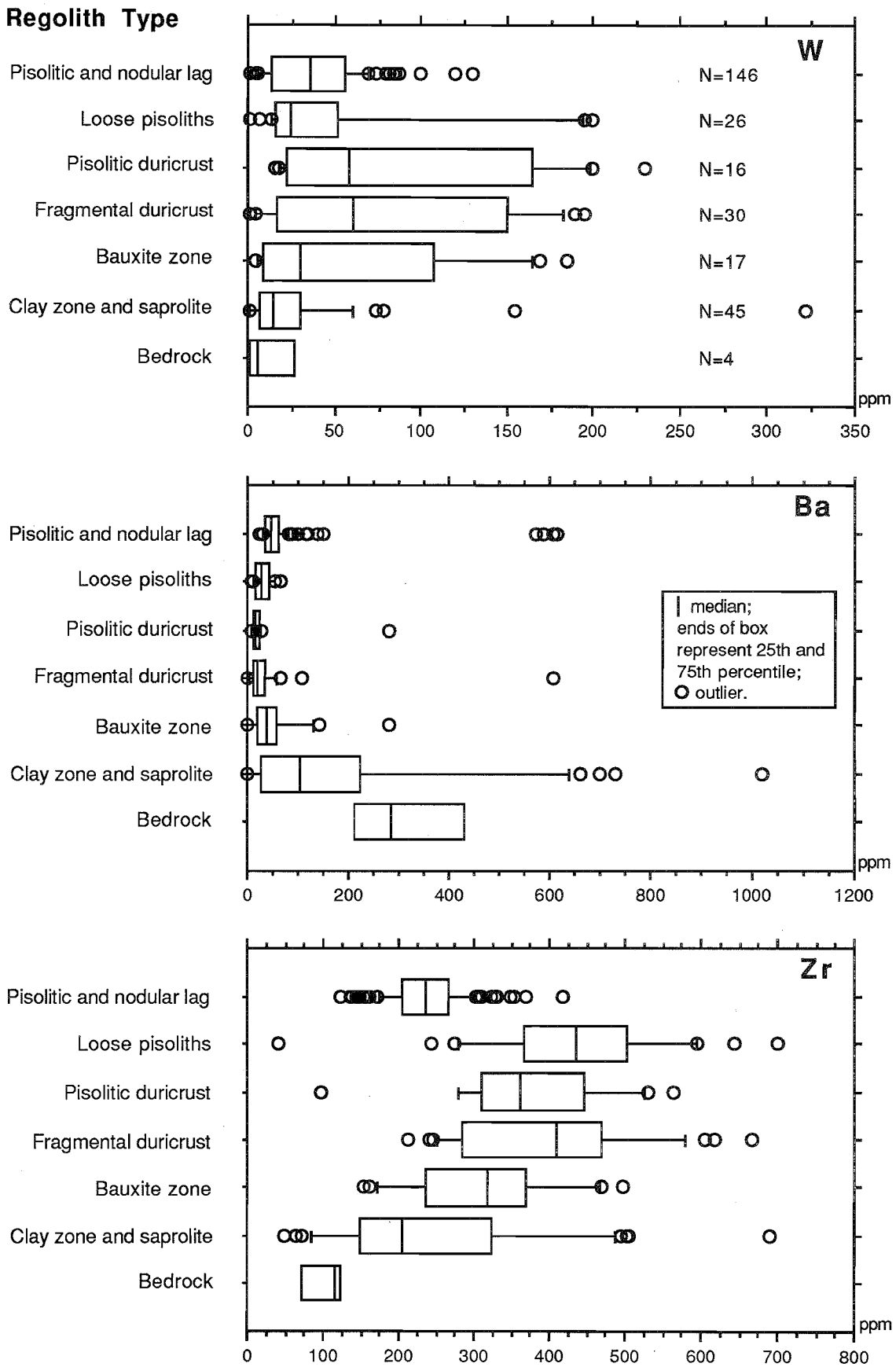

Fig. 55 Box plots showing the distribution of W, Ba and Zr in several regolith materials and bedrock arranged vertically in order of the regolith stratigraphy.

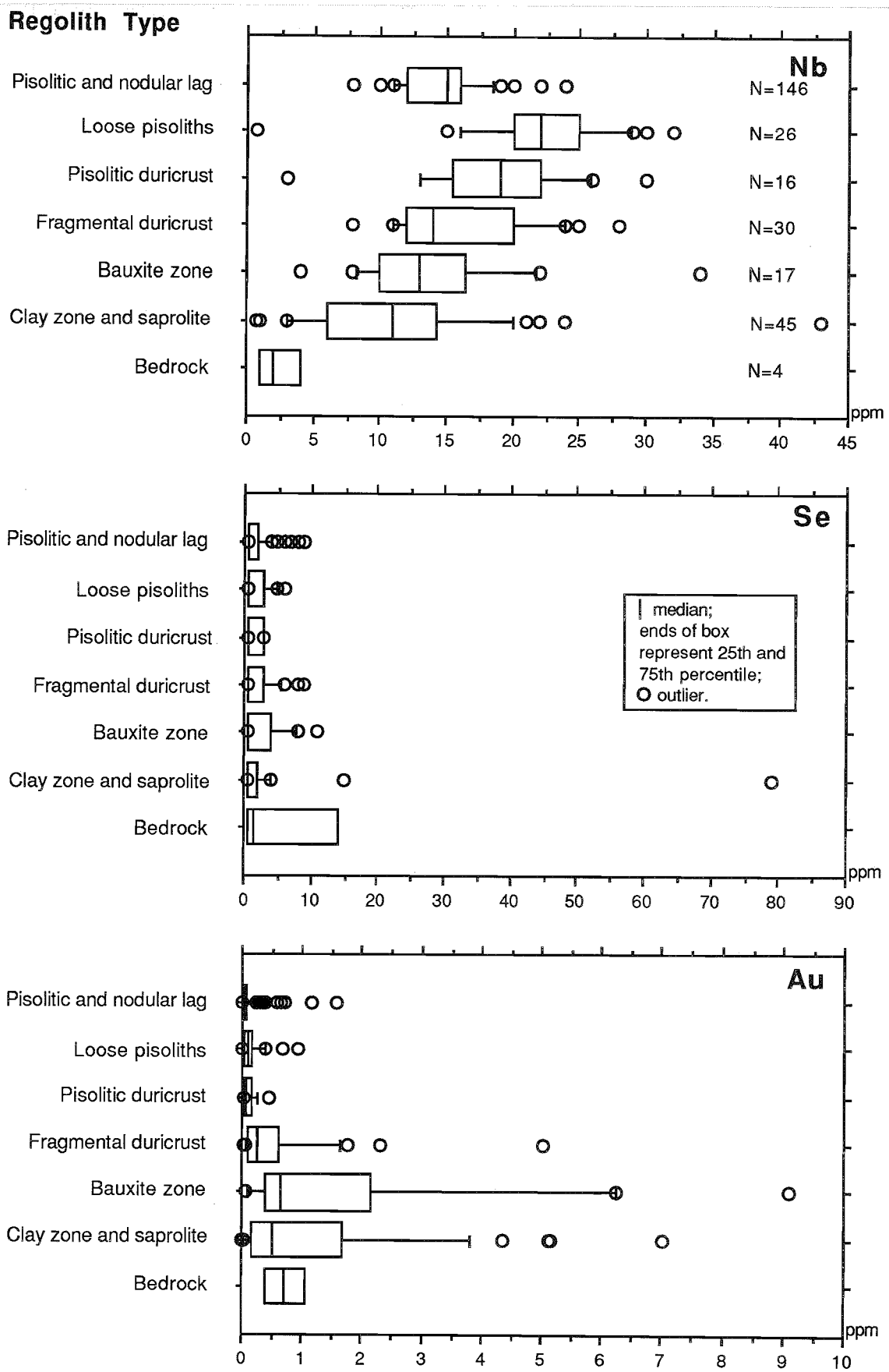

Fig. 56 Box plots showing the distribution of Nb, Se and Au in several regolith materials and bedrock arranged vertically in order of the regolith stratigraphy.

trend in SiO_2 distribution appears to be more complex. It decreases first appreciably and then concentrated towards the surface in pisolitic and nodular lag. There is a sharp break in the SiO_2 concentration between the clay zone and bauxite zone suggesting intensive desilification to form gibbsite.

Progressive LOI gains reflect the formation of gibbsite. It is interesting to note that the LOI drops markedly above the fragmental duricrust. This is consistent with the mineralogical data which suggest that amorphous Al-oxide instead of gibbsite becomes the dominant Al bearing mineral in the surface or near surface horizons.

Other elements include Ti, Cr, V, Ga, Nb, and Zr, all of which have higher concentrations in the lateritic duricrust and loose nodules and pisoliths, and progressively increase from the bedrock to the surface. However, Ti, Nb, and Zr contents in nodular and pisolitic lag are lower than in the underlying loose pisoliths and pisolitic duricrust.

Manganese, Zn, Ni, Cu, Ag, Ba, and to a lesser extent, Co, decrease in abundances upwards throughout the profile, although there is a general near-surface increase in these components in the pisolitic and nodular lag. In contrast, As, Bi, Mo, Sn, and W are concentrated up the profile but decrease appreciably in pisolitic and nodular lag. The mean Ag concentrations are much higher in the pisolitic and nodular lag than in the pisolitic duricrust, bauxite zone and saprolite.

It is interesting to note that the Au concentrations, Fig. 56, are highest in the bauxite zone, being slightly higher than concentrations for the fragmental duricrust, clay zone, and saprolite. Pisolitic and nodular lag contain the lowest concentrations of Au. Analyses of black (magnetic) and red fragments/pisoliths (non-magnetic) separated from bulk specimens show that red pisoliths in general, are higher in Au than are black pisoliths (Table 12). No relationship was observed between

Table 12. Chemical composition of sub-samples

Sample Type	Sample No.	Al_2O_3 %	Fe_2O_3 %	Au ppb
Magnetic pisoliths*	07-0381A	40.2	45.3	82
Non-magnetic pisoliths**	07-0381B	43.6	38.0	737
Magnetic pisoliths	07-0385A	50.6	34.9	38
Non-magnetic pisoliths	07-0385B	39.1	33.8	82
Magnetic pisoliths	07-0372A	50.2	34.1	16
Non-magnetic pisoliths	07-0372B	51.6	15.0	301
Magnetic pisoliths	07-0383A	34.7	44.5	3
Non-magnetic pisoliths	07-0383B	47.1	40.0	22
Magnetic pisoliths	07-0378A	48.9	39.1	79
Non-magnetic pisoliths	07-0378B	44.6	26.7	114
Magnetic Pisoliths	07-0371A	37.3	43.4	95
Non-magnetic pisoliths	07-0371B	41.4	37.8	150
Magnetic pisoliths	07-0379A	42.4	41.4	437
Non-magnetic pisoliths	07-0379B	48.5	36.8	864
Magnetic pisoliths	07-0382A	40.8	44.6	28
Non-magnetic pisoliths	07-0382B	43.4	35.6	50

* Magnetic pisoliths are black

** Non-magnetic pisoliths are generally red

the Au abundances in fragmental duricrust and the overlying pisolitic duricrust (Fig. 57). In contrast, a strong relationship exists between the Au abundances in the bauxite zone and the overlying fragmental duricrust. This suggests a precipitation of Au at the bauxite zone, and subsequent gradual leaching/modification during the formation of pisoliths.

Another possible explanation for a low Au concentration in the loose pisoliths and pisolitic duricrust may be due to the transported nature of the pisoliths and nodules. Field relationships suggest that loose pisoliths in the lower slopes are transported and even those in the mid slopes are semi-residual. This is also shown by the presence of black and red pisoliths in the pisolitic horizon which have different contents of Au and different mineralogies. The composition of bulk samples comprising variable mixtures of black and red pisoliths also may result in the low concentrations of Au.

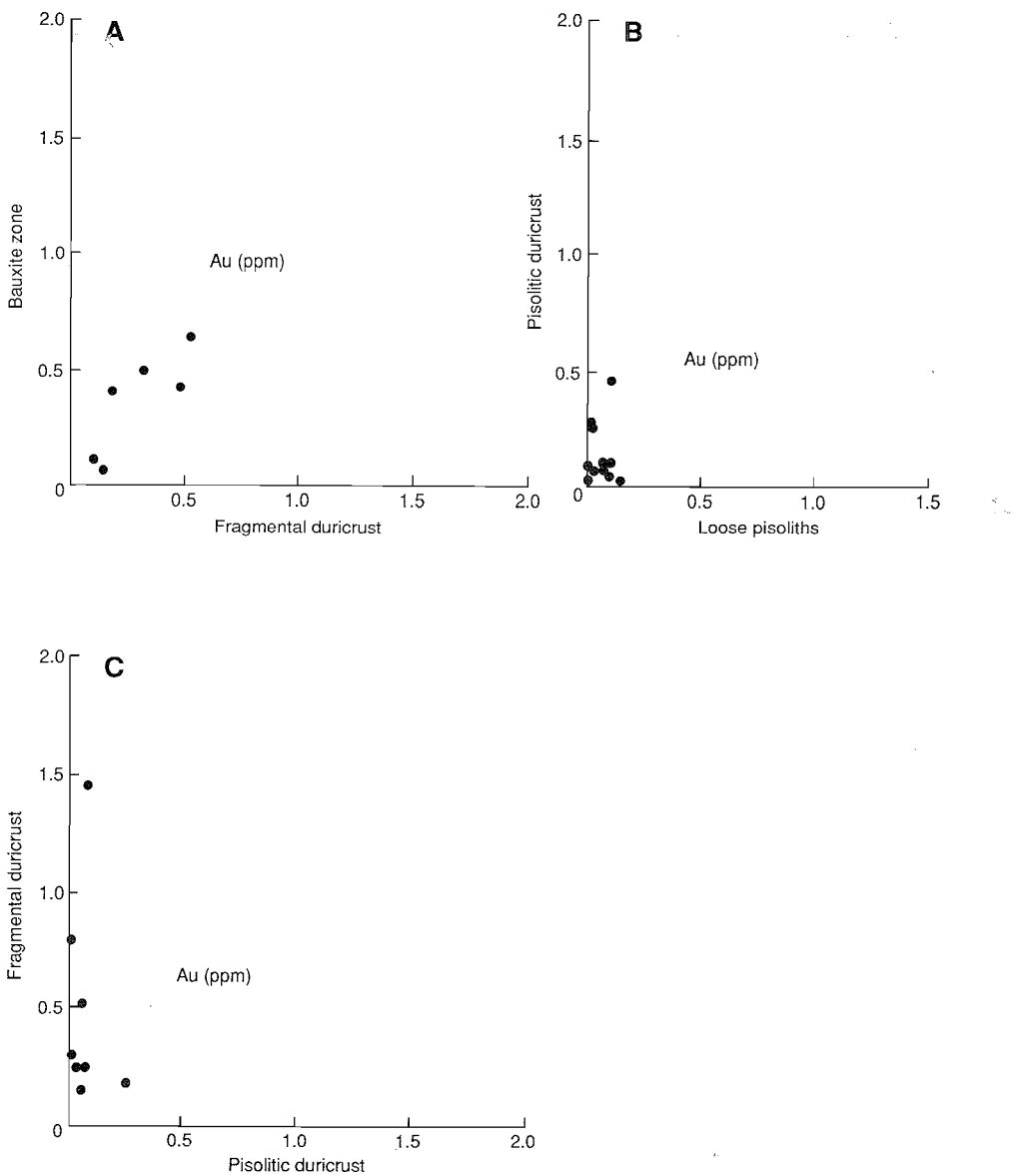

Fig. 57. Relationship between the Au abundances in (A) bauxite zone and fragmental duricrust, (B) pisolitic duricrust and loose pisoliths, and (C) fragmental duricrust and pisolitic duricrust.

5.3.5 Element associations

The Pearson sample correlation coefficients provide one method of assessing element associations. Correlation matrices were calculated for all the elements but only those elements having significant correlation are shown. The validity of correlation coefficients has been assessed for each element pair by an x-y plot. Figures 58 and 59, derived from the correlation matrices of six major units of the weathering profiles, show the effect of lateritization and bauxitization on major and trace element interrelationships. The major conclusion is that the associations between the elements are not consistent throughout the weathered profile, suggesting that differences in the behaviour of the elements are due to changing chemical or mineral environment.

A strong negative correlation exists between SiO_2 and Fe_2O_3 in saprolite and remains stronger throughout the whole profile except in pisolitic and nodular lag. In contrast, Al_2O_3 and Fe_2O_3 show a very strong negative relationship for the upper part of the weathering profile and a weak or no correlation in saprolite. The positive relationship between the Al_2O_3 and LOI is much stronger for saprolite, bauxite zone, fragmental and pisolitic duricrusts than for loose pisoliths and becomes an inverse relationship for pisolitic and nodular lag.

Elements Fe, V, Al and Ga and Ti and Nb, K, and Ba are positively correlated throughout the whole profile. However the strengths of the associations vary between the regolith type. Some associations are not evident in the lateritic residuum and pisolitic and nodular lag, for example, Mg and Zn, Mg and Mn, Cu and Ag which were strongly associated in saprolite, are almost independent in the bauxite zone, lateritic duricrust, and pisolitic and nodular lag. The relationships between Ga and Zr, Ga and Nb, and Ti and V become less stronger towards the upper part of the weathering profile. Manganese and Co are strongly correlated with each other throughout the whole profile except in pisolitic and nodular lag.

Arsenic and Sb, Sn and Bi, and W and Sn are moderately to strongly associated with each other, being more strongly associated in saprolite. Gold is more closely correlated to Bi, Mo, and Sn in saprolite and pisolitic duricrust than in the bauxite zone and fragmental duricrust.

The variations in association between elements reflect mineralogical transformations and leaching of elements. The largest change in relationships occurs between the saprolite and the lateritic residuum, implying that many elements were dissolved/leached and reprecipitated in the lateritic horizons. The dispersion of the elements into lateritic residuum tends to homogenize the trace element contents in these horizons.

5.3.6 *Element-mineral associations*

The work already described above has demonstrated the significance of chalcophile elements and Au in lateritic duricrust and loose nodules and pisoliths from the study area. The anomalously-high concentrations of some of the elements, namely As, Cu, Zn, W, and Au in selected samples were the subject of specific investigations to establish the mode of occurrence of these elements.

Examination of Au-rich material from the different parts of the profile revealed only three small (<5 μ) droplet-like Au grains in the clay and bauxite zones (Fig. 60A). No Au was found in lateritic duricrust nor loose pisoliths, suggesting that it is in a form of invisible Au or that the surfaces examined contained no Au.

Scanning electron microscope studies of polished sections of lateritic nodules and pisoliths show that much of the Sn occurs as irregularly-shaped cassiterite (Fig. 60B). This suggests that most Sn is dispersed mechanically during laterite formation. Some W occurs as scheelite, only two grains of scheelite were identified in samples of the bauxite zone and lateritic duricrust. The most common resistant minerals were zircon, ilmenite, and partially-weathered ilmenite grains (Figs 60B and D). These grains either occurred in the matrix or the cores of pisoliths. Analyses of ilmenite grains showed that large concentrations of Mn (up to 5%) occur in ilmenite grains. Manganese can substitute for Fe in ilmenite.

Some As occurs as arsenopyrite. Two grains of arsenopyrite were recognized in the cores of pisoliths (Fig. 60C). Because of susceptibility to weathering, their presence in loose pisoliths was surprising however, it appears that arsenopyrite grains are protected by the formation of Fe-oxide coatings around them.

Electron-microprobe analyses of secondary minerals were undertaken in an attempt to determine if the Cu, Zn, W, and As were contained in Fe-oxides or gibbsite. Lines of point analyses were completed to investigate the composition of Fe-rich and Al-rich areas. A total of 296 analyses were completed. Elements or oxides determined for the study were SiO_2, Al_2O_3, TiO_2, Al_2O_3, Cu, Zn, As, and W.

Points analysed vary in composition from gibbsite-rich to hematite-maghemite rich (Fig. 61). Generally, the cores of pisoliths and nodules are enriched in Fe_2O_3 relative to the matrix and cutans.

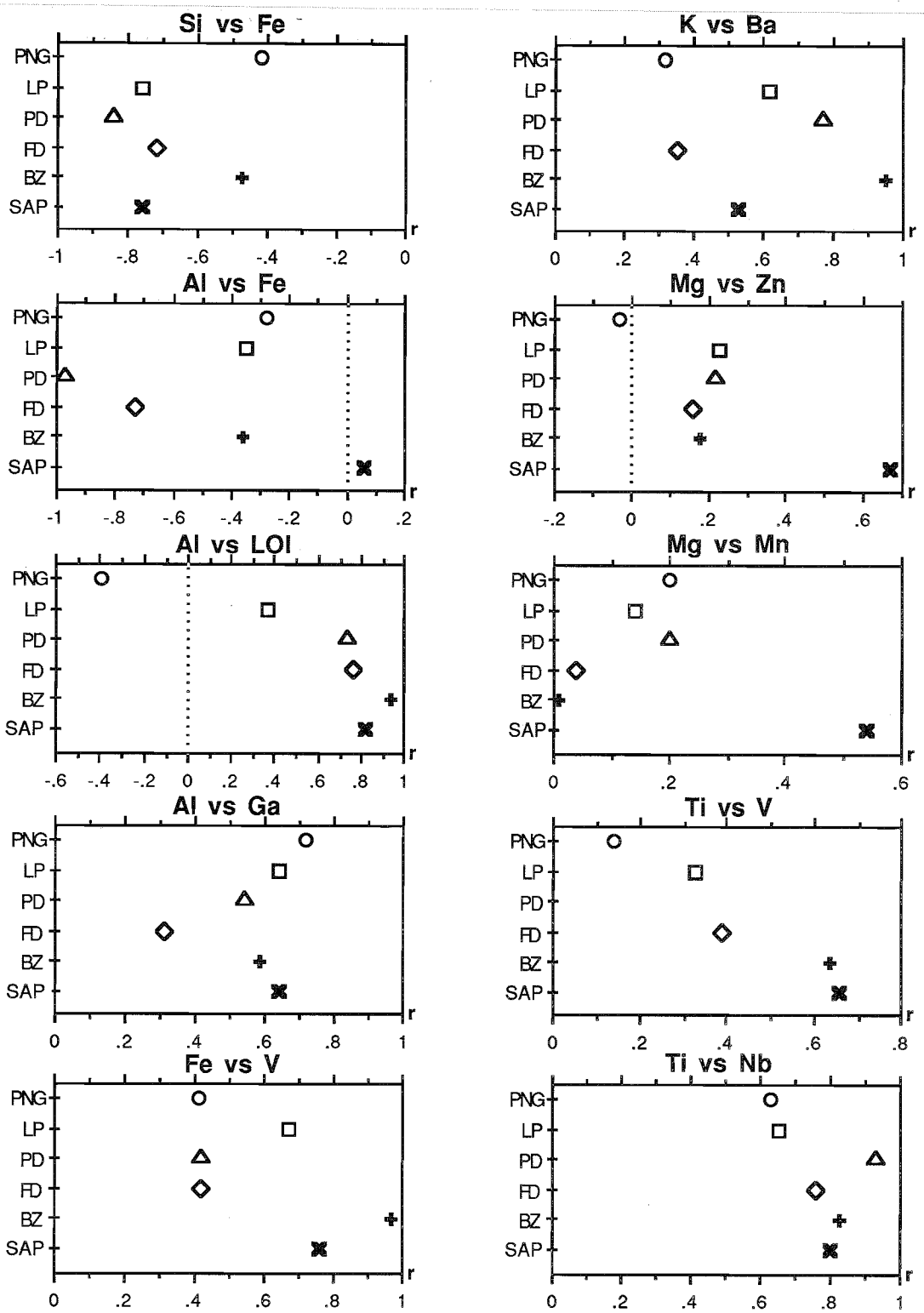

Fig. 58 The correlation coefficient (r) for elements in several regolith materials arranged vertically in order of the regolith stratigraphy.

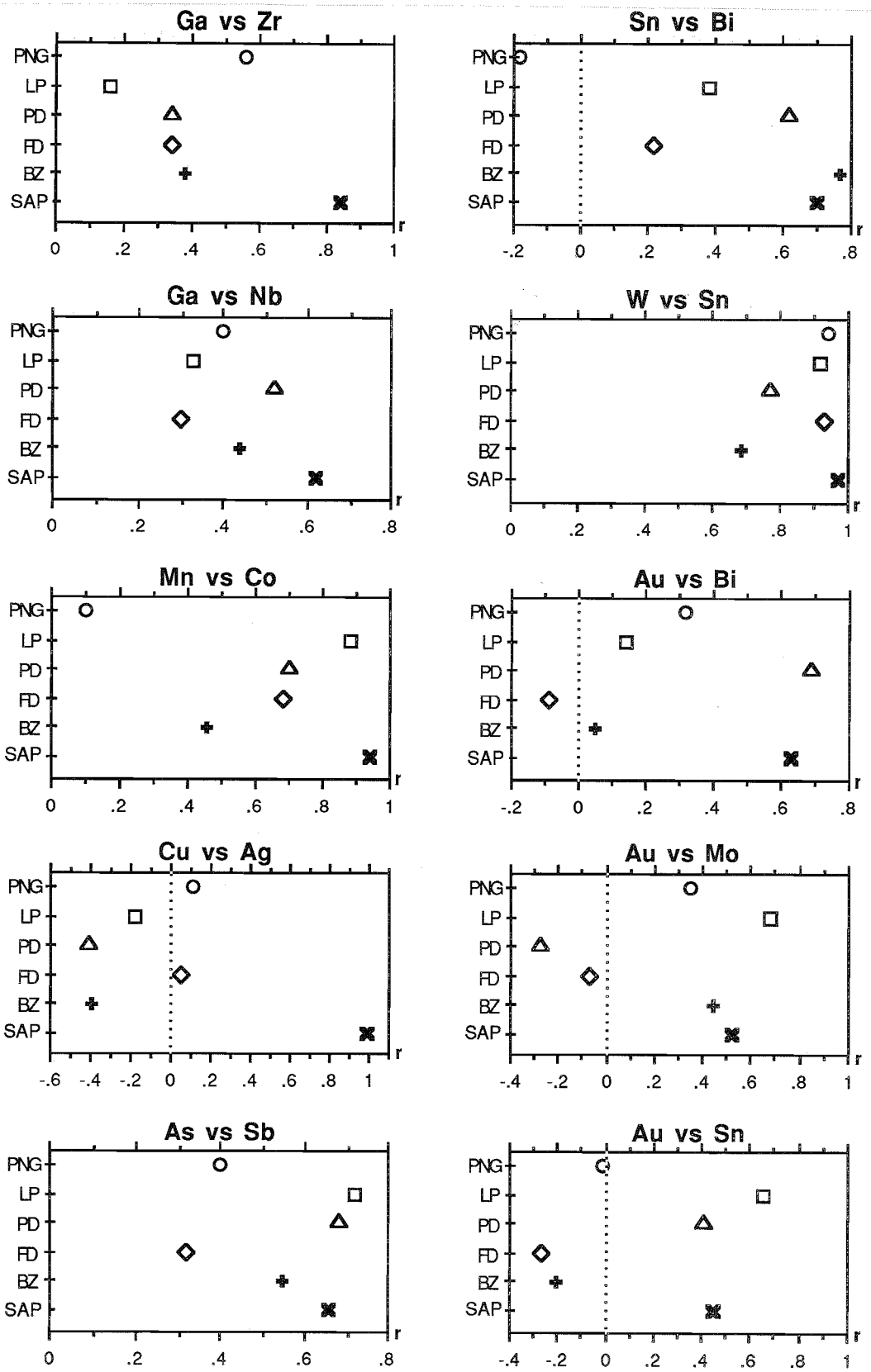

Fig. 59 The values of correlation coefficient (r) for elements in several regolith materials arranged vertically in order of the regolith stratigraphy.

This page has been left blank.

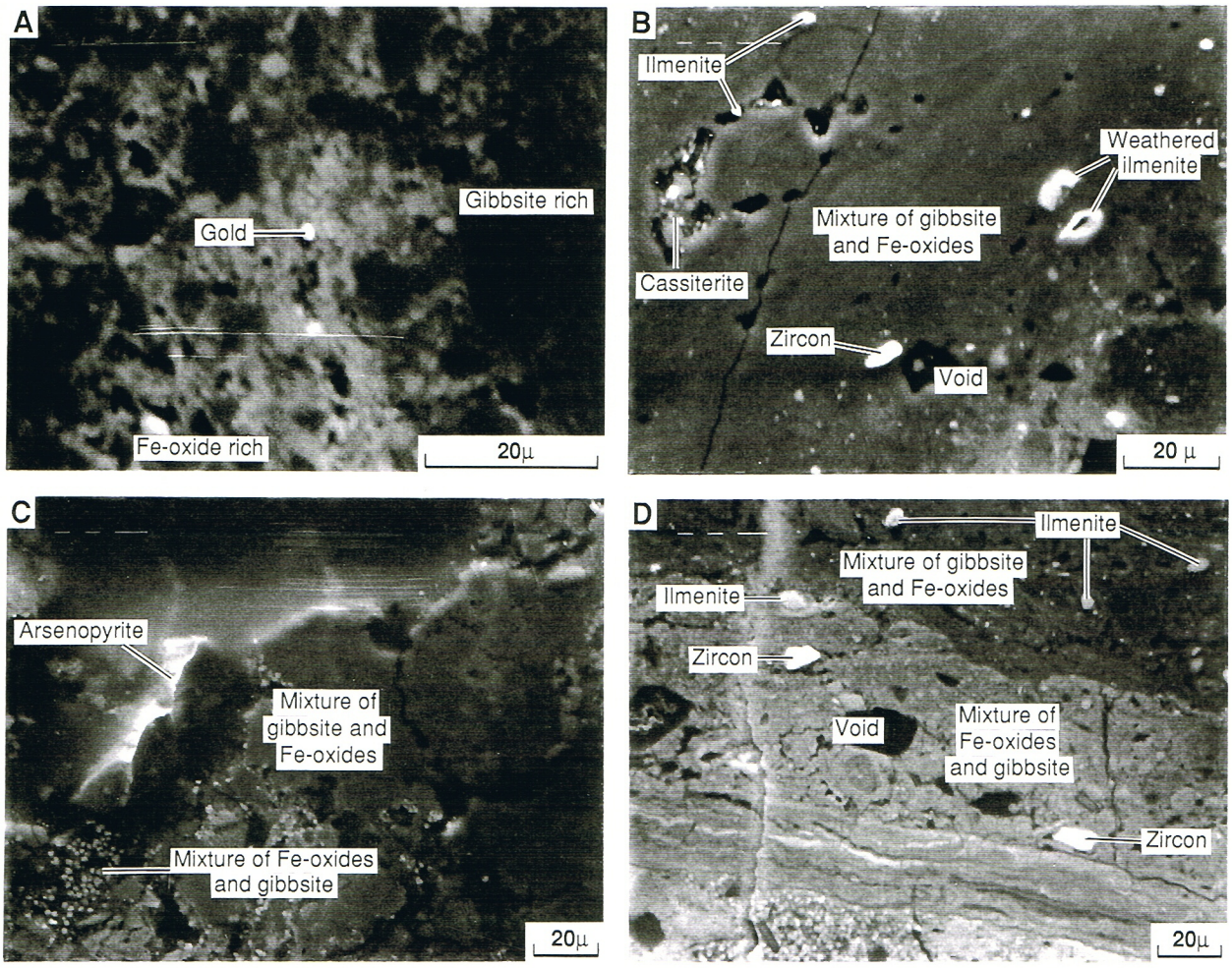

Fig. 60A Scanning electron photomicrograph of part of a bauxite zone showing an Au grain in a goethite-rich matrix. Sample No. 07-0417.WBC21.
Fig. 60B Scanning electron photomicrograph of part of a lateritic pisolith showing cassiterite, ilmenite and zircon grains. Sample No.07-1116.Pit A.
Fig. 60C Scanning electron photomicrograph of part of bauxite zone showing arsenopyrite. Sample No. 07-0346, costean 2.
Fig. 60D Scanning electron photomicrograph of part of a pisolitic duricrust showing ilmenite and zircon grains.Sample No. 07-1079.Pit D.

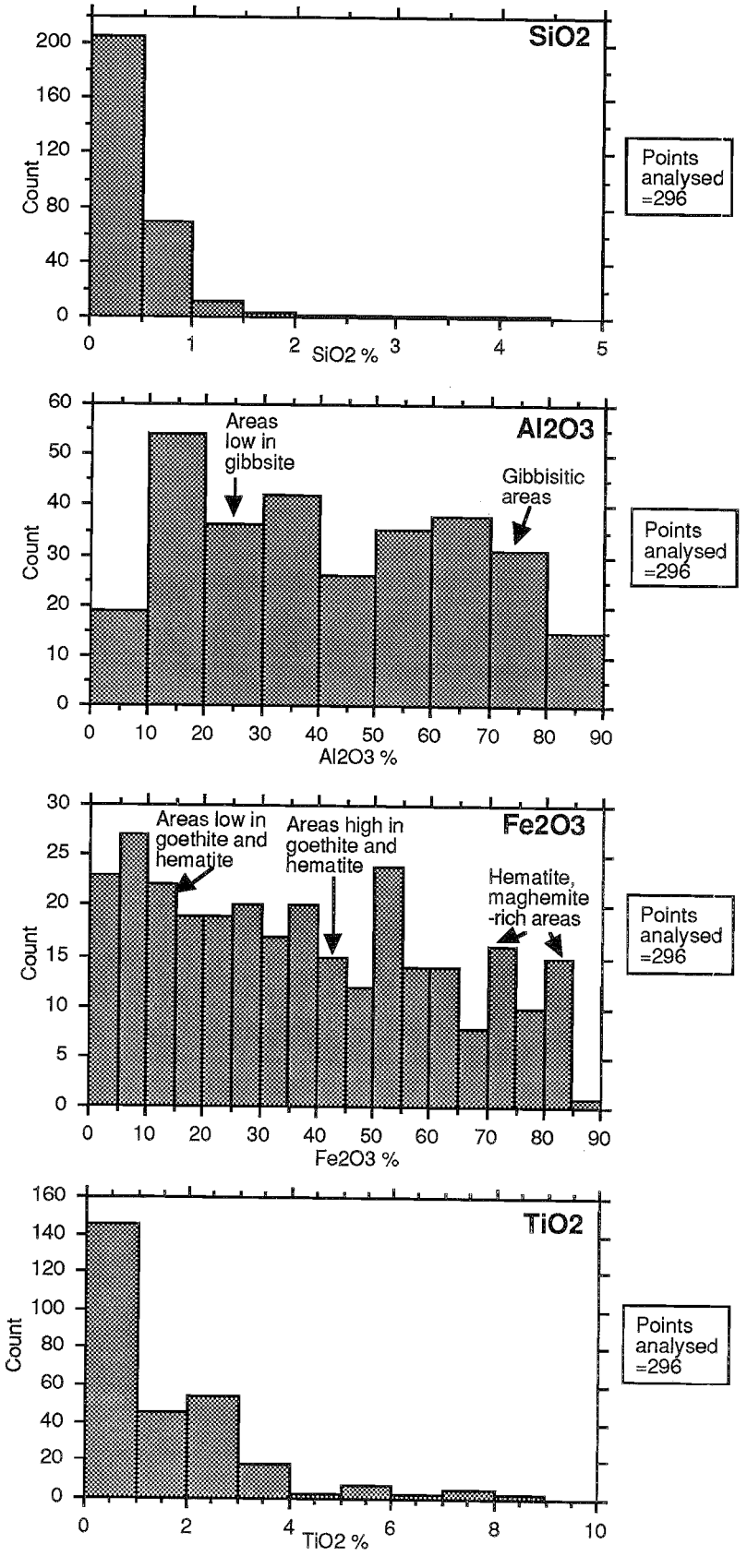

Fig. 61 Frequency distribution of SiO2, Al2O3, Fe2O3 and TiO2 for the electromicroprobe data obtained from analysing lateritic duricrust and loose pisolith samples.

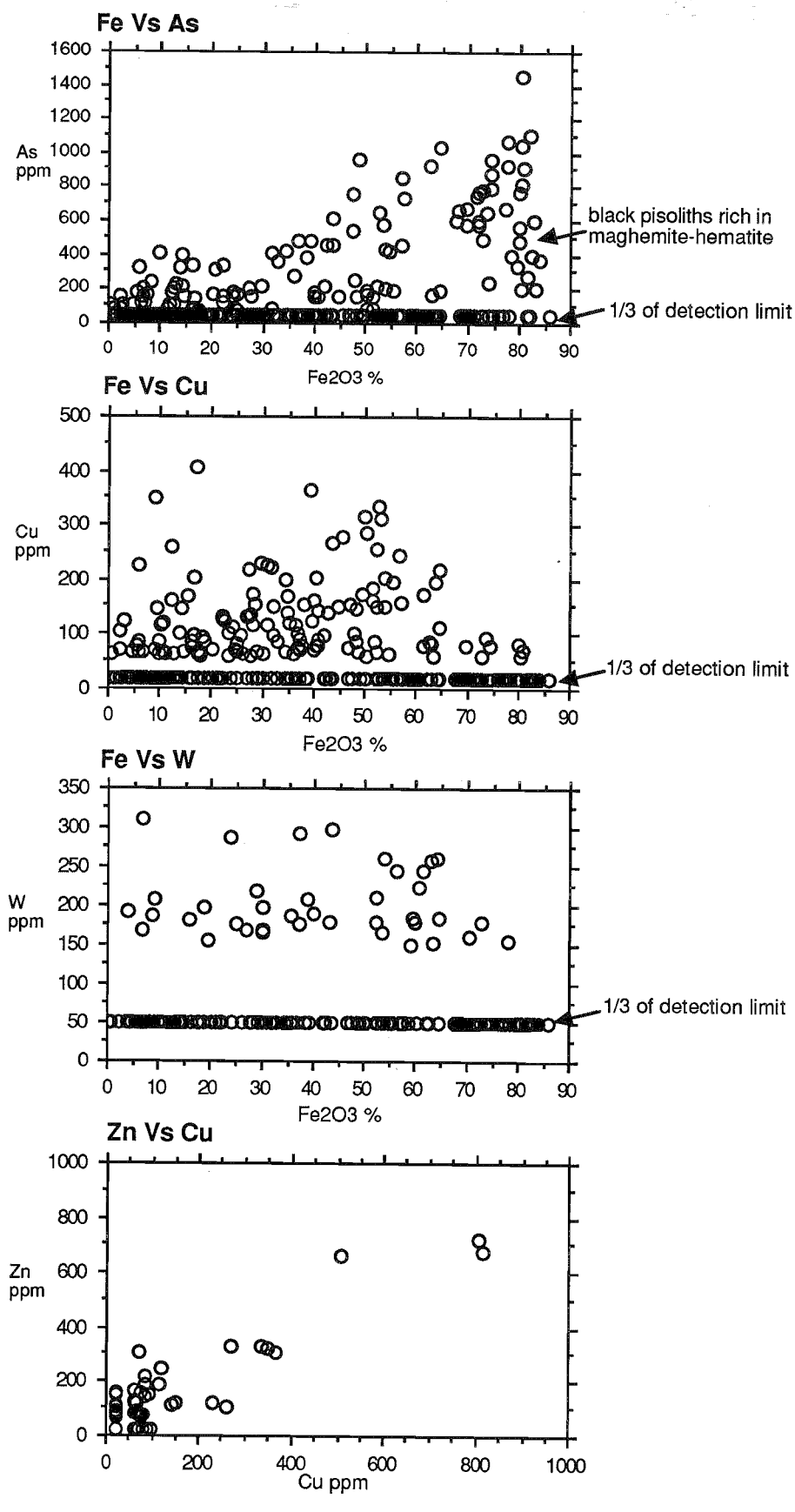

Fig. 62 Correlation diagrams for the electromicroprobe data obtained from analysing lateritic duricrust and loose pisolith samples.

However, the cores of pisoliths may show either the gibbsite-filled dissolution cavities or the zones which are gibbsite-rich. The abundances of SiO_2 are low. The concentrations of TiO_2 are between 0.3% and 4% with some analyses as high as 10%.

Inter-element correlations have been investigated by means of a correlation matrix (Table 13). For 296 points, any correlation over 0.14 is statistically significant at the 99% confidence level. The inter-element correlations may be used to provide a hint as to the mineralogical siting of trace elements.

Iron is moderately correlated with As which suggests that As is associated with Fe-oxides. However, its abundance is primarily determined by the environment in which Fe-oxides are formed (Fig. 62) and possibly the Fe-oxide species. For example, areas very high in Fe, dominated by hematite and maghemite, are relatively low in As, suggesting their formation in low As environments. Another possible reason for the low As in high Fe-rich areas is that the As, which was originally present in goethite, was ejected out during its transformation to hematite and maghemite.

There appears to be no correlation between Fe and Cu and W. The distribution of W is uniform irrespective of the contents of Fe (Fig. 62). Copper correlates well with Zn.

Table 13. Correlation Matrix

	SiO2	Al2O3	TiO2	Fe2O3	Cu	As	Zn	W
SiO2	1.000	-.033	-.071	-.048	.220	-.035	.012	.050
Al2O3	-.033	1.000	-.118	-.882	-.103	-.520	-.016	.093
TiO2	-.071	-.118	1.000	.026	.037	.252	.037	-.004
Fe2O3	-.048	-.882	.026	1.000	-.051	.475	-.043	-.058
Cu	.220	-.103	.037	-.051	1.000	.046	.647	-.113
As	-.035	-.520	.252	.475	.046	1.000	.085	-.326
Zn	.012	-.016	.037	-.043	.647	.085	1.000	-.107
W	.050	.093	-.004	-.058	-.113	-.326	-.107	1.000

n=296, p=0.01, r=0.14

6.0 DISCUSSION AND CONCLUSIONS ON REGOLITH EVOLUTION, GEOCHEMISTRY OF REGOLITH AND EXPLORATION SIGNIFICANCE

In this section, the findings documented in the preceding chapters are integrated and a model presented for the regolith evolution and geochemical dispersion, including mobilization and deposition of Au and the distribution of ore-associated elements within the regolith of Boddington. Implications of these findings in exploration are discussed.

6.1 Regolith evolution

6.1.1 Field relationships

The regolith of Boddington developed over a long period, which is inferred to have taken place sequentially under the three major climatic episodes (Fig. 63):

(i) under a seasonally-warm, humid climate with high watertables, deep weathering of andesite and dolerite resulted in the development of a lateritic profile. Weathering profiles are thicker on andesite than on dolerite;

(ii) under a subsequent arid climate, the profile dried and the watertable declined, resulting in the deposition of Fe-oxides in the profile, with reduced weathering at depth and the formation of a lateritic duricrust at the surface. Vegetation changed with climate, resulting in slope instability. With decreased vegetation and channelling of surface drainage, the regolith, in particular on upper slopes and valley floors, was truncated by erosion.

(iii) development of gibbsite during the recent climate. Several workers (e.g. Tomich, 1964; Loughnan and Sadleir, 1984; Anand *et al.*, 1991) observed that the better class bauxite appeared to correspond with areas of high rainfall (i.e. 1000 mm). They took this to indicate that either recent rainfall was a factor in bauxite development or that the present rainfall distribution patterns were similar to those in existence when the bauxite was formed. Bauxitization requires effective internal drainage to minimize the residence time of silica-laden solutions and assure a high level of leaching intensity, and hence Si removal and bauxite development. The extensive development of bauxite on mid-slopes, as opposed to hill crests or valley floors, illustrates the role of good drainage and large volumes of water moving through depositional sites. Bauxite deposits formed preferentially in areas of moderate relief where drainage was good, but not rapid nor dominated by surface runoff; very steep slopes tend to be areas of 'physical' erosion rather than 'chemical' weathering.

The profile at Boddington contains components of the regolith stratigraphy seen elsewhere in the Yilgarn. However, at Boddington, the bauxite zone is present, whereas, hardpan and calcrete that are extensive in the arid terrains of the Yilgarn, are absent.

Lateritic residuum forms a blanket over some 30% of the landscape; however, the thickness and facies of lateritic residuum vary with topographic position. The undulating characteristic of the original laterite landsurface, together with differential stripping have resulted in an undulating and partly-dissected land surface. The extent to which the profile is retained depends upon post-laterite erosion. Laterite is either more developed or more preserved on midslope than on crest or lower slope. In the valley floors the laterite is absent, possibly because of truncation. Soil materials derived by erosion of the lateritic duricrust on crest- and upslope-positions have been transported as colluvium to lower slopes, a process presently continuing. As a result, the sandy gravels are shallow on crests and upper slopes and increase in thickness downslope. The gravels, consisting mostly of lateritic nodules and pisoliths, have been deposited on the slopes while the fine earth fraction has been transported further downslope to the valley floor by fluvial action. The processes active in transporting these materials result from gravity and water movement, including surface wash.

Lateral variations in duricrust morphologies occur in the Boddington area. Some relate to their location in the landscape while others reflect differences in the nature of the parent rock. The duricrust is more ferruginous than the underlying bauxite zone and may be fragmental, nodular, pisolitic, or vermiform. The midslope positions are dominated by pisolitic duricrust which is typically underlain by fragmental duricrust. By contrast, pisolitic and nodular duricrust and loose pisoliths and nodules are generally absent in crest- and upslope-positions where only fragmental duricrust occurs. The absence of pisolitic duricrust

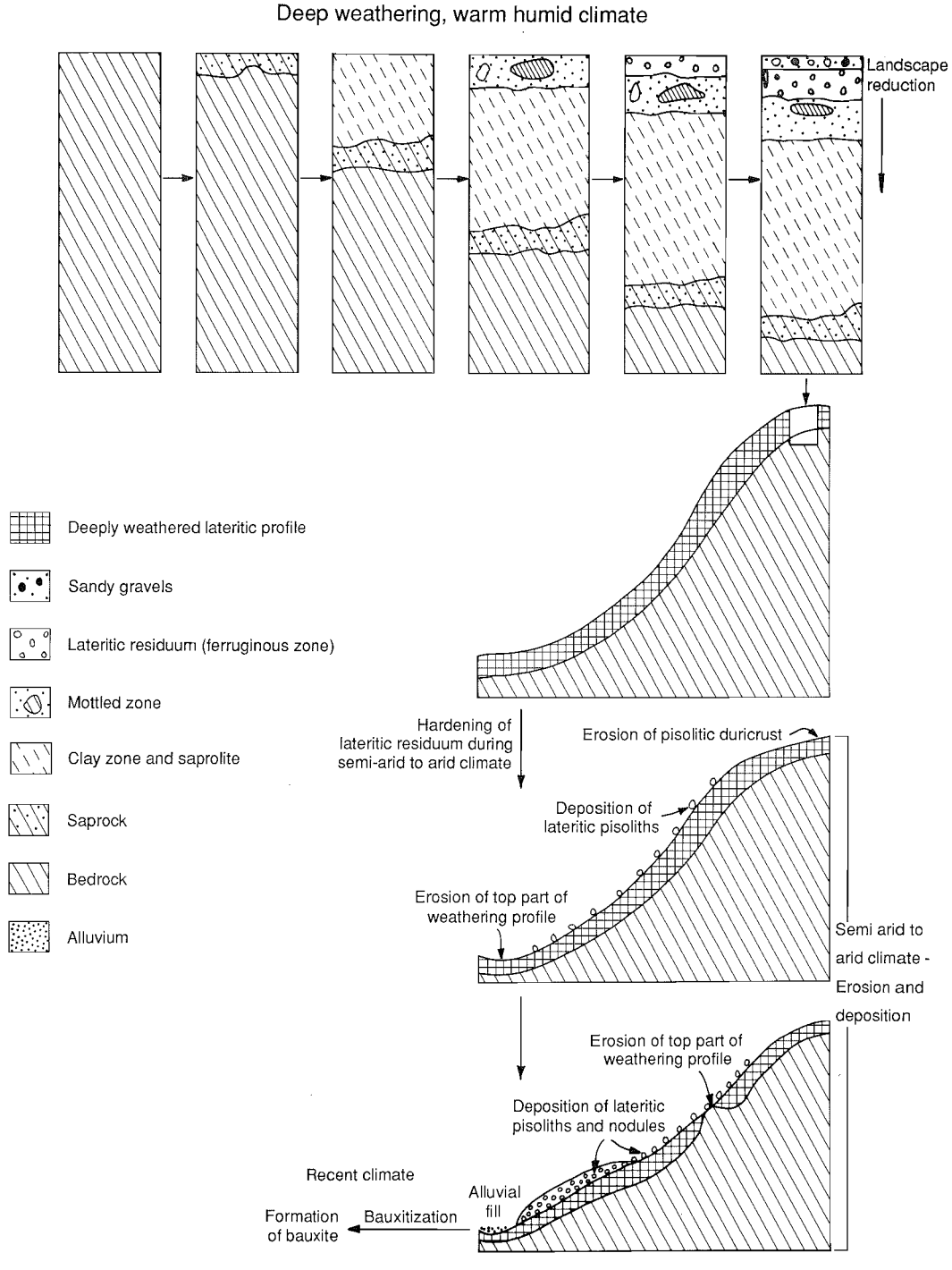

Fig. 63.Generalized regolith model for the Boddington district.

suggests removal by erosion and the detrital components (the gravel as well as the fine fractions) have been deposited on the lower slopes and valley floors. However, the possibility that pisolitic duricrust may never have existed on some crests cannot be excluded.

Fragmental duricrusts are commonly not developed on the lower slopes. Lower slope positions are occupied by packed pisolitic gravels which can sometimes reach a thickness of 5 m. Packed gravels may develop with the destruction of the matrix of lateritic duricrust in the upper slopes, followed by colluviation of the nodules and pisoliths, their subsequent deposition, and later recementation by secondary enrichment with Fe and Al minerals (Pullan, 1967). However, *in situ* breakdown of the duricrust due to the dissolution of the components of the matrix can also result in packed gravels. Indeed, evidence for both mechanisms of formation (i.e. lateral transportation and breakdown of the duricrust) have been observed in Pit A and D.

6.1.2 Development of laterite and nodules and pisoliths

Field relationships and laboratory data suggest that the lateritic duricrust and associated lateritic pisoliths and nodules at Boddington are largely residual, with transported nodules and pisoliths on the lower slopes. Relict textures after andesite are visible through some of the profiles to the level of the fragmental duricrust and correlate with the bedrock relationships which have been established through drilling. Feldspars, in fabrics similar to those of the bedrock, have been pseudomorphed by gibbsite, showing that the fragmental duricrust is essentially residual. Relict textures derived from dolerite are also present as residual ilmenite in the bauxite zone and in the fragmental duricrust. The dolerite results in a redder fragmental duricrust and bauxite zone than in these horizons derived from the felsic andesite.

Comparisons between the respective chemical and mineralogical compositions of bauxitic laterite and their parent rocks (chiefly either felsic andesite or dolerite) reveal a relatively simple relationship. Parent rock mineralogy and chemistry strongly influence the composition of laterite. Lateritization and bauxitization have involved the residual enrichment of Al and Fe (with addition of H_2O) in proportion to the combined effect of Si depletion and the almost total loss of Mg, Ca, Na, and K. Intense leaching occurred in the bauxite and laterite zones, where Fe, precipitated as Fe-oxides, and most of the kaolinite are desilicified to form gibbsite. Iron is generally enriched towards the surface by solution, transport, and precipitation in the form of Fe-oxides and oxyhydroxides as a result of ferrolysis, and then by residual accumulation.

Brimhall *et al.* (1988) suggested that Al and Fe enrichment in the lateritic weathering profile were due partly to the addition of aeolian material transported westwards from the Yilgarn Craton. However, the close relationship between laterite composition and bedrock type suggests that aeolian-derived constituents are generally minor. The upper section (soils, loose pisoliths, and pisolitic duricrust) of the laterite profiles include variable amounts of transported material, but the source of this material is uncertain, and it is difficult to distinguish exotic aeolian constituents from more, locally-derived alluvial or colluvial material.

Figure 64 shows the generalized evolutionary sequence of some common secondary structures in a lateritic profile from Boddington. At the base of the weathering profile, saprolite exhibits a texture inherited from the parent rock, the result of isovolumetric weathering (Millot, 1970). In this material, many weathering products are present that are pseudomorphs after primary minerals (Fig. 64A). Higher in the weathering profile, removal of Si and redistribution of Fe continue, resulting in the formation of the bauxite zone and lateritic residuum (Figs 64B, C, and D). On a centimetric scale, zones of Fe concentration occur with the well-preserved fabric of the andesite and dolerite rock (Fig. 64B). These areas are referred to as fragments. Microscopic examination of the fragments showed microcrystalline aggregates of gibbsite in pseudomorphs

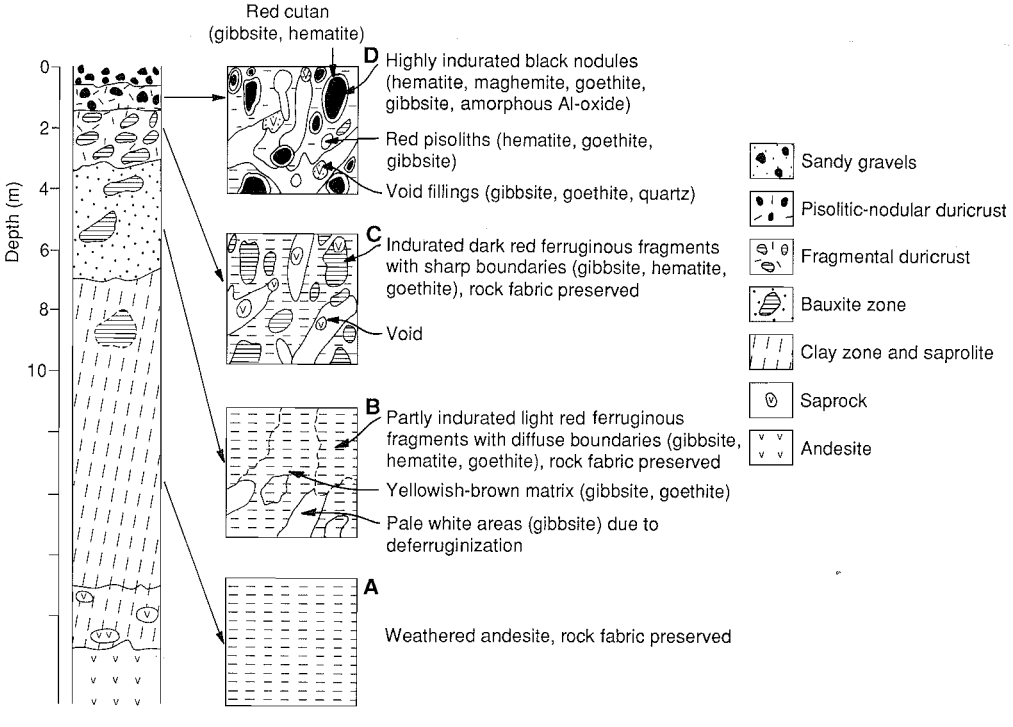

Fig. 64. Generalized evolutionary sequence of secondary structures in a lateritic profile.

after feldspars. The ferruginous fragments in the bauxite zone are red, gibbsite-hematite-rich, more or less diffuse outer rims, partly indurated and bordered by a porous, friable, less Fe-rich matrix. Ferruginization and induration of fragments increase upwards in the fragmental duricrust. Fragments in the fragmental duricrust are dark red, angular to subrounded of various dimensions from a few mm to more than 3 centimetres cemented in a variable amount of fine-grained pale to light red gibbsite-rich matrix (Fig. 64C). In the matrix, a network of deferruginized zones, consisting only of gibbsite and quartz occurs. These pale, white deferruginized zones are more abundant in the pisolitic-nodular (overlying fragmental duricrust), and ferruginous fragments become dark brown to black, highly indurated, and their boundaries with the matrix become distinct. During this process of ferruginization, rock texture in most fragments is destroyed and we refer to these black structures as nodules. Nodules in pisolitic-nodular duricrust are irregular to subrounded, black, hematite-rich, non-porous and have similar sizes and shapes to those of the fragments (Fig. 64D). Black nodules are generally magnetic because of the presence of maghemite. As the sphericity of nodules increases, generally by dissolution of irregular edges, some nodules develop into round structures, pisoliths. In the same duricrust, red dusky porous pisoliths, though less abundant, also appear with black nodules (Fig. 64D). Red pisoliths develop from the deferruginization of the matrix and migration of Fe and thence its concentration in the matrix. The red pisoliths retain the morphology (porosity) and mineralogy of the matrix. Quartz and pseudomorphs after feldspars can also be enveloped in this way. This weathering process results in the formation of a pisolitic-nodular duricrust consisting of black and red nodules and pisoliths. This horizon is highly indurated and often crops out as a very resistant duricrust.

The areas within the duricrust from which Fe is moved exhibit a progressively white or grey colour. These changes are accompanied by a marked increase of microporosity leading subsequently to the formation of the voids. In the upper part of the duricrust, these voids may become numerous and can lead to a cellular or vermiform fabric. A system of voids of various sizes marks the pale zone. The voids left by dissolution of the matrix are generally occupied by secondary accumulations of gibbsite, quartz, and goethite.

Both nodules and pisoliths generally have gibbsite-goethite-rich cutans (~1 mm thick) around them. These cutans have developed by the removal of Fe from the matrix and its accumulation around cores of the nodules. In some cases, pisoliths are strongly banded. Where alternate darker and light cutans are seen under the microscope, the light cutans have high Al and less Fe and are gibbsite-rich.

6.2 Origin of magnetic nodules and pisoliths

Magnetic nodules and pisoliths are more ferruginous than co-existing non-magnetic nodules and pisoliths. Their magnetism is due to the presence of maghemite. In this study, amorphous Al-oxide has also been identified as an important Al-bearing mineral in magnetic pisoliths. Maghemite and corundum formation by surface heating of goethite during bush fires is the most likely process responsible for the magnetic character of surface pisoliths and nodules, as there is no evidence of maghemite below the lateritic residuum (Anand and Gilkes, 1987). Amorphous Al-oxide can also form from heating of gibbsite. The high temperatures in forest fires can adequately explain the observed transformations.

6.3 Degradation of laterite

Near the surface, the duricrust displays numerous voids, cracks, and fissures which develop laterally and vertically that break the duricrust into fragments, nodules, and pisoliths. In upper part of the Pits, the duricrust was crumbly and forming essentially *in situ* a gravelly horizon composed of fragments, nodules, and pisoliths.

The duricrust matrix is breaking down by dissolution of gibbsite and Fe-oxides which allows the separation of nodules and pisoliths producing a highly porous horizon of nodules and pisoliths dispersed in a clayey sand matrix. Colluviation leads to the deposition of these gravels on the mid- and lower-slopes.

6.4 Geochemical dispersion in the regolith

During the oxidation of sulphides (pyrite, chalcopyrite, pyrrhotite) at the base of the profile and the destruction of primary minerals, the following trends in the distribution of the major elements during lateritic weathering are evident:

Major elements

- Silica contents decrease progressively from the base of the profile to the top of the pisolitic duricrust. In overlying loose pisoliths, the SiO_2 contents increase.

- Iron and Ti concentrations increase towards the top of the profile, with a strong enrichment in the pisolitic duricrust and loose pisoliths.

- Aluminium concentrations increase progressively from the saprolite to the bauxite zone and fragmental duricrust, and then decrease slightly in the pisolitic duricrust and loose pisoliths.

Trace elements
Weathering and secondary dispersion have disturbed primary trace element associations and created some new ones. Some trace element associations which occur in saprolite are not present in laterite suggesting differences in the behaviour of the elements due to changing chemical or mineral environments. Thus trace-element correlations from the surface samples are not representative of primary associations. The following trends were recognized:

- The distribution patterns of Mn, Cu, Zn, Ni, and Co have a number of similarities. These elements are dissolved at the early stages of weathering and are leached from the upper horizons of the profile. However, there are some near surface concentrations of Mn, Zn, Ni, and Co suggesting that these elements are accumulated by pedogenetic processes. Similarities between the distributions of Zn, Co, Ni, and Mn deep in the profile imply that these elements are hosted by the same primary minerals, i.e. ferromagnesian minerals, and are released together on weathering. These elements are present mostly in octahedral sites in biotite and amphiboles, where they substitute for Mg and Fe^{2+}. The major losses of these elements from these minerals, indicate that they were lost during weathering, and thus behave similarly to Mg.

- Silver is the most mobile element. It is dissolved at the early stages of weathering and is strongly leached in the pisolitic duricrust and loose pisoliths.

- Elements such as V, Cr, As, Bi, Sn, Ga, W, Zr, Nb, Mo, and Pb are essentially retained or enriched throughout the whole profile. These elements tend to increase progressively from the bedrock to the surface and have higher abundances in the pisolitic duricrust than in the bedrock. They are either associated with Fe-oxides or occur as resistant primary minerals such as zircon, cassiterite, and scheelite.

- A comparison between the laterite profile above andesite and dolerite rocks shows that the behaviour of the elements is similar. Most of the leaching in the dolerite profile has taken place in the lower part of the saprolite.

A geochemical dispersion model for the Boddington area is shown in Fig. 65. The dispersion mostly results from a combination of hydromorphic(H), residual(R), and mechanical(M) processes, both past and present, related to the formation or modification of the lateritic profile. In the kaolinitic saprolite, Cu, Mo, W, Bi, and Sn are mostly residual with some hydromorphic dispersion of Cu and Mo. The dispersion halo widens in the bauxite zone, but reaches its greatest in the pisolitic duricrust and loose pisoliths. The protore mineralization is depicted by a multi-element geochemical halo in the lateritic residuum, both in the duricrust and loose pisoliths. Compared to the bedrock, the concentrations observed in this halo are enriched in As, Mo, Bi, Sn, and W and depleted in Cu and Au. Tungsten, As, Mo, and to some degree Sn show a more widespread and homogeneous distribution than Cu and Bi. Copper, Mo, and As exhibit different dispersion characteristics in the various horizons of the lateritic weathering profile. Molybdenum has a strong affinity for the Fe-oxides and is therefore abundant in the loose pisoliths and pisolitic duricrust; possibly after some hydromorphic migration, an enlarged dispersion halo has resulted. Conversely, Cu is less stable in the Fe-rich environment, and is relatively depleted in the ferruginous horizon (Zeegers *et al.*, 1981). Bismuth is little remobilized and disperses very slightly, whereas Ag is completely leached and can only be detected near the source. In the samples studied, most of the As is associated with goethite and hematite, but some As is there as arsenopyrite; Sn is held in cassiterite, some Cu in goethite, and most of the W is in the Fe oxides and gibbsite while some is held in scheelite. These observations indicate residual and hydromorphic dispersion. However, in the undulating landscape of Boddington, mechanical dispersion has enlarged the halo, particularly on the slopes, although simultaneously causing dilution of element concentrations. There, loose

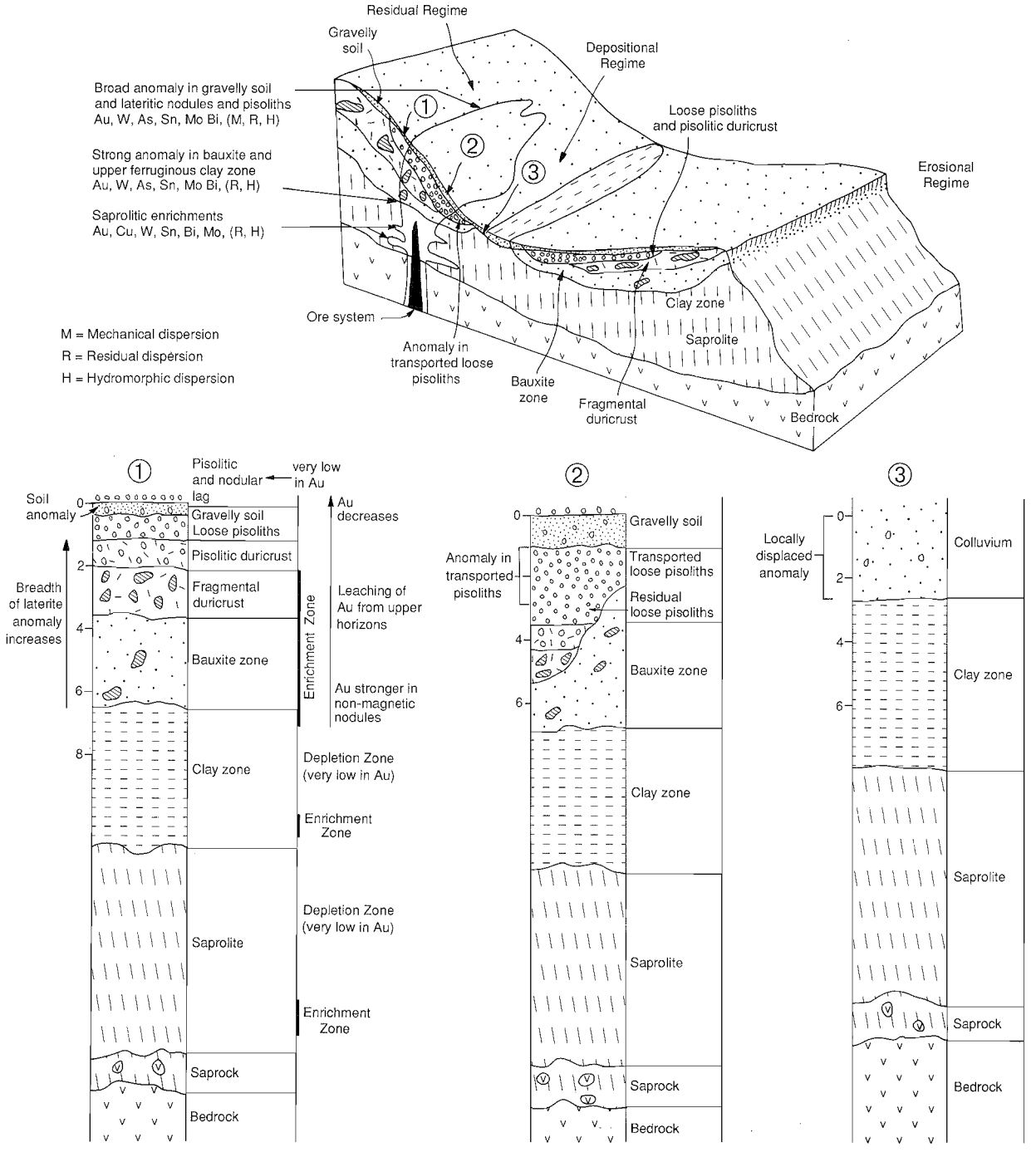

Fig. 65. Geochemical dispersion model for the Boddington gold deposit.

pisoliths and nodules are semi-residual. The formation of pisoliths and nodules involves intense chemical alteration and it is probable that at least part of the Fe accumulated in them has been transported for some distance; some trace elements (As, Mo) may have behaved similarly, resulting in a large dispersion halo.

Gold distribution

There is a wide anomalous zone of Au close to the surface, within the fragmental duricrust and bauxite zone. In this part of the profile, Au was precipitated, in association with Fe-oxides, at a redox front at or near the Tertiary water table. The mobility of Au during deep lateritic weathering in a humid environment is best explained by the ferrolysis model of Mann (1984). This model involves the oxidation of sulphides in the

saprolite zone of the weathering profile, to produce acidic ferrous solutions. These circulate upward in the ground water, oxidise at the redox interface (the water table) and precipitate goethite and hematite to form the laterite. In this acidic oxidizing environment, any Au in the system may be mobilized as either organic, thiosulphate or chloride complexes, and dispersed laterally in the redox front, i.e. in the zone of laterite formation. As a result of ground water flow, Au solutions may travel for some distance and re-enter the reduction field, where they precipitate as elemental particles. This process is a co-precipitation along with Fe as Fe-oxides and oxyhydroxides, a process which traps the micron scale Au in the laterite.

The changes to a drier climate, perhaps with some epirogenic uplift, cause a lowering of the water table. As a result of this, upper horizons of the profile are unsaturated and the pre-existing profile is subjected to decreased leaching with alkalis and alkaline earths being retained in the profile. Evaporation exceeds precipitation so that sodium chloride and other salts, derived largely from rainfall, concentrates both in the unsaturated zone and in the ground water. In the Darling Range, reversal to a humid climate has restored conditions conducive to deep weathering (Bowler, 1982). Accordingly, the lowering of the water table would have been punctuated by still stands or temporary rises. The increased rainfall leaches precipitated salts and recreates redox conditions suitable for ferrolysis, and thus produces an acidic, saline and oxidizing ground water capable of dissolving Au (Mann, 1984). This results in Au depletion in the middle part of the clay zone, and enrichment in the lower horizons. During these humid periods, therefore, Au may be dissolved and mobilized, to be re-precipitated with Fe-oxides by reduction by Fe^{2+} at the water table. Successive humid periods during the general lowering of the water table can account for the presence of two subhorizontal enrichments within the saprolite. However, this view is not shared by Symons et al. (1988) who reported that the disposition of Au within the clay zone reflects a primary Au.

Gold gradually decreases towards the surface, i.e. from the bauxite zone through the lateritic duricrust (fragmental, pisolitic) to the loose pisoliths. Loose pisoliths and the pisolitic duricrust commonly contain Au below 0.1 ppm. In contrast, there is enrichment of Au in the fragmental duricrust and the bauxite zone. Gold depletion in loose pisoliths and nodules suggests its leaching from loose pisoliths and concentration in the fragmental duricrust and bauxite zone. Gold has probably been mobilized as organic complexes.

6.5 Comparison with the Mt. Gibson gold deposit

Table 14 provides a summary comparison of the Boddington lateritic deposit with that at Mt. Gibson, 300 km northeast of Perth, using Anand et al. (1989, 1991) as the main sources. These deposits were probably formed during the same lateritization period, when climatic conditions were similar over most of the Yilgarn Craton. However, differences in the present climate and geomorphology are probably responsible for the differences in the nature of the laterite and the distribution of Au in the profile. Thus the non-bauxitic nature of the laterite at Mt. Gibson compared with the bauxitic laterite at Boddington may be a function of the difference in present rainfall, vegetation, and drainage characteristics (intensity of leaching) at the two deposits. Bauxite formation has been shown to be related to the present day topography and required an adequate, seasonal rainfall to remove Si from the clay zone. The surface lateritic pisoliths and nodules in the Boddington area differ in mineralogy and chemical composition from those at Mt. Gibson and other parts of the Yilgarn Craton. Abundant maghemite and amorphous Al-oxide in surface lateritic pisoliths and nodules at Boddington are explained by the common bush fires due to thick vegetation in Boddington.

The trend in the distribution of Au in the ferruginous part of the profile at Boddington is opposite to that of the Mt. Gibson Au deposit. At Boddington, Au decreases in abundance from the bauxite zone through lateritic duricrust to loose nodules and pisoliths, while Au increases in abundance from the mottled zone to loose nodules and pisoliths at Mt. Gibson. Gold is almost absent in the surficial lateritic pisoliths and nodules at Boddington. The differences in the abundance and position of Au within the ferruginous part of the profile may be a function of the differences in leaching. The current climatic conditions experienced at Mt. Gibson are different from those at Boddington. At Boddington, high rainfall and water rich in organic materials produced from the abundant vegetation may result in the leaching of Au from the loose pisoliths. The leached Au is dissolved by organic acids and reprecipitated at the base of the bauxite zone.

6.6 Implications in exploration

The Boddington Au deposit highlights some of the problems of Au exploration in lateritic terrains. This is exemplified by the leaching of Au from surface lateritic pisoliths and nodules. Modification of the laterite profiles remobilized the Au, leaching to near-surface depletion. The distribution pattern for elements

Table 14. Comparison of the Boddington and Mt. Gibson Gold Deposits

	Boddington	**Mt. Gibson**
Rainfall	810 mm	250 mm
Landform	Undulating lateritic plateau high relief	Gently undulating terrain, low relief
Lateritic deposit	Gold occurs in lateritic residuum	Gold occurs in lateritic residuum
Lateritic residuum	Bauxitic	Non-bauxitic
Carbonates, Silcrete	Calcified/silicified duricrust	Not present
Kaolinite in laterite	Minor	Abundant
Gibbsite in laterite	Abundant	Traces
Maghemite in loose pisoliths	Abundant	Minor
Au in loose pisoliths	Little or no (0.08 ppm*)	Abundant (2.51 ppm)
Au in lateritic duricrust	Minor (0.11 ppm pisolitic duricrust, 0.61 ppm fragmental duricrust)	Abundant (1.83 ppm)
Au in mottled/ bauxite zone	Abundant (1.96 ppm)	Moderate (0.80 ppm mean)
Size of Au	Fine grained < 5μm	Fine grained 15-100 μm
Depletion zone	Occurs in clay zone and saprolite	Occurs in clay zone and saprolite
Primary Au	Occurs in quartz veins	Occurs in quartz veins
Lateritic enrichment	Evident in saprolite	No trend
Dispersion of Au	More than 500 m (Davy and El-Ansary, 1986)	50-100 m
Multi-element dispersion	As, W, Sn, Mo, Bi	Au, Cu, Bi, As, Pb, W

* Mean abundance

associated with Fe-oxides (Mo, As, Bi) and those elements in resistant minerals (W and Sn), however, appear commonly to remain. The Au mineralization is depicted by multi-element geochemical haloes throughout the whole weathered profile including the surficial pisolitic and nodular lag.

Whilst a strong Au anomaly in lateritic residuum will always be important in exploration, it is unwise to expect Au to always dominate the dispersion anomaly in lateritic residuum above a primary deposit. A large strong, consistent multi-element anomaly, with or without Au, seems to be the best and most reliable indicator of a large Au deposit.

For Au exploration in the Boddington area, samples of fragmental duricrust instead of loose pisoliths or pisolitic duricrust, should be collected.

7.0 ACKNOWLEDGEMENTS

We wish to thank the management and staff of Boddington Gold Mines for their co-operation and hospitality without which this study would not have been possible. The collection and storage of surface samples collected over the mine site prior to mining by the company is gratefully acknowledged. We also acknowledge the funding provided through AMIRA by the consortium of 30 sponsoring companies of the CSIRO-AMIRA Laterite Geochemistry Project. Thanks go to Dr Ray Smith who provided critical comments on the manuscript.

Sample preparation was carried out by Ms Angela Janes under the supervision of Mr John Crabb. The XRD analyses were performed by Mr M.K.W. Hart. Polished sections were prepared by Mr A.G. Bowyer. Assistance on SEM and Cameca microprobe was given by Mr Greg Hitchen.
Diagrams were drafted by Angelo Vartesi. Typing was admirably carried out by Jenny Porter and Cheryl Harris.

My sincere thanks go to Dr Sylvia Llorca who carried out certain aspects of this work. Thanks also go to John Wildman and Jenny Wilson who provided help in certain aspects of this work. I should also like to thank Mr John Perdrix who assisted with checking the final document.

8.0 REFERENCES

Anand, R.R. and Gilkes, R.J., 1984. Weathering of hornblende, plagioclase and chlorite in meta-dolerite, Australia. *Geoderma*, **34**:261-80.

Anand, R.R. and Butt, C.R.M., 1988. The terminology and classification of the deeply weathered regolith. Discussion paper, CSIRO Division of Exploration Geoscience, Perth. (Unpublished), 29 pp.

Anand, R.R., Smith, R.E., Innes, J., Churchward, H.M., Perdrix, J.L. and Grunsky, E.C., August 1989. Laterite types and associated ferruginous materials, Yilgarn Block, WA. *Terminology, Classification and Atlas.* CSIRO Division of Exploration Geoscience, Restricted Report 60R (unpaginated).

Anand, R.R., Smith, R.E., Innes, J. and Churchward, H.M., March 1989. Exploration Geochemistry about the Mt. Gibson gold deposits, Western Australia. CSIRO Division of Exploration Geoscience, Restricted Report 20R, 93 pp.

Anand, R.R. and Gilkes, R.J., 1987. The association of maghemite and corundum in Darling Range laterites, Western Australia. *Aust. J. Soil Res.*, **25**:303-11.

Anand, R.R., Gilkes, R.J. and Roach, G.I.D., 1991. Geochemical and mineralogical characteristics of bauxites, Darling Range, Western Australia. *Appl. Geochem.*, **6**:233-48.

Anand, R.R., Churchward, H.M. and Smith, R.E., 1991. Regolith-landform development and siting and bonding of elements in regolith units, Mt. Gibson District, Western Australia. CSIRO Division of Exploration Geoscience, Restricted Report 165R, 95 pp.

Andrew-Jones, 1968. The application of geochemical techniques to mineral exploration. *Color. School Mines, Min. Indus. Bull.*, **11**, No. 6.

Bowler, J.M., 1982. Aridity in the late Tertiary and Quaternary of Australia. In: W.R. Barker and P.J.M. Greenslade (eds.), *Evolution of flora and fauna of arid Australia.* Peacock Publications, Adelaide, S.A., pp. 35-45.

Brimhall, G.H., Lewis, C.J., Ague, J.J., Dietrich, W.E., Hampel, J., Teague, T. and Rix, P., 1988. Metal enrichment in bauxites by deposition of chemically mature aeolian dust. *Nature*, **333**:819-24.

Butt, C.R.M., Gray, D.C., Lintern, M.J., Robertson, I.D.M., Taylor, G.F. and Scott, K.M., 1991. Gold and associated elements in the regolith-dispersion processes and implications for exploration. CSIRO Division of Exploration Geoscience, Restricted Report 167R, 114 pp.

Davy, R., 1979. A study of laterite profiles in relation to bedrock in the Darling Range, near Perth, W.A. *West. Aust. Geol. Surv., Rep. Ser.*, 8, 87 pp.

Davy, R. and El-Ansary, M., 1986. Geochemical patterns in the laterite profile at the Boddington gold deposit, Western Australia. *J. Geochem. Explor.*, **26**:119-44.

El-Ansary, M., 1980. Exploration for commodities other than bauxite in the Worsley Project area. Reynolds Australia Mines Pty. Ltd., unpublished report.

Fitzpatrick, R.W. and Schwertmann, U., 1982. Al substituted goethite – an indicator of pedogenic and other weathering environments in South Africa. *Geoderma*, **27**:335-47.

Hallberg, J.A., 1984. A geochemical aid to igneous rock identification in deeply weathered terrain. *J. Geochem. Explor.*, **20**:1-8.

Loughnan, F.C. and Sadleir, S.B., 1984. Geology of established bauxite producing areas in Australia. In: L. Jacob (ed.), *Bauxite Proc. 1984 Bauxite Symposium, Los Angeles, California.* The Society of Mining Engineers of American Institute of Mining, Metallurgical and Petroleum Engineers, pp. 435-461.

McFarlane, M.J., 1976. *Laterite and landscape.* Academic Press Inc. (London) Ltd., 151 pp.

Mann, A.W., 1984. Mobility of gold and silver in lateritic weathering profiles: Some observations from Western Australia. *Econ. Geol.*, **79**:38-49.

Millot, G., 1970. *Geology of clays.* Chapman and Hall, London, 576 pp.

Monti, R., 1987. The Boddington laterite gold deposit, Western Australia: a product of supergene enrichment processes, in Recent advances on understanding Precambrian gold deposits (Ed. S.E. Ho and D.I. Groves). Geology Department and University Extension, University of W.A. Publication 11, pp. 355-368.

Pullan, R.A., 1967. A morphological classification of lateritic ironstones and ferruginized rocks in Northern Nigeria. *Niger. J. Sci.*, 1:161-74.

Schulze, D.G., 1984. The influence of aluminium on iron oxides. VIII. Unit cell dimensions of Al-substituted goethites and estimation of Al from them. *Clays Clay Miner.*, **32**:36-44.

Smith, R.E., 1987. Patterns in laterite geochemistry, Mt. Gibson, Western Australia. Progress report to Geochemex Australia to Forsayth NL, December, 37 pp.

Symons, P.M., Anderson, G., Beard, T.J., Hamilton, L.M., Reynolds, G.D., Robinson, J.M. and Staley, R.W., 1988. The Boddington gold deposit. *The Second International Conference on Prospecting in Arid Terrain, Perth, Excursion Guidebook*, pp. 77-84.

Symons, P.M., Anderson, G., Beard, T.J., Hamilton, L.M., Reynolds, G.D., Robinson, J.M., Staley, R.W. and Thompson, C.M., 1990. Boddington gold deposit, In: F.E. Hughes (ed.), *Geology of the Mineral Deposits of Australia and Papua New Guinea*, pp. 165-9.

Tomich, S.A., 1964. Bauxite in the Darling Range, Western Australia. *Aust. Inst. Min. and Met. Proceed.* **212**:125-35.

Wilde, S.A. and Low, G.H., 1980. Pinjarra, Western Australia - 1:250,000 geological series, Geol. Surv. West. Aust. Explanatory Notes S1, 50-2.

Wilde, S.A., 1976. The Saddleback Group - a newly discovered Archaean greenstone belt in the southwestern Yilgarn Block. *West. Aust. Geol. Survey, Ann. Rept.* pp. 92-5.

Wilde, S.A. and Pidgeon, R.T., 1986. Geology and geochronology of the Saddleback Greenstone Belt in the Archaean Yilgarn Block, southwestern Australia. *Aust. J. Earth Sci.*, **33**:491-501.

Zeegers, H., Goni, J. and Wilhelm, E., 1981. Geochemistry of lateritic profiles over a disseminated Cu-Mo mineralization in Upper-Volta (West Africa). Preliminary results. In: *Lateritisation processes*, Balkema Publishers, Rotterdeam, pp. 359-68.

9.0 APPENDICES

APPENDICES 1 to 7
LISTINGS

Appendix 1 Boddington pisolitic and nodular lag LG103.

sampno	sample code	easting	northing	SiO2 wt%	Al2O3 wt%	Fe2O3 wt%	MgO wt%	CaO wt%	Na2O wt%	K2O wt%	TiO2 wt%	LOI wt%	TOTAL wt%
02-3901	LG103	9950	8950	5.8	52.09	32.18	0.079	0.078	0.021	0.30	1.77	5.65	98.01
02-3903	LG103	10050	8950	4.3	47.99	39.32	0.016	0.051	0.013	0.02	1.62	6.25	99.56
02-3905	LG103	10150	8950	4.8	45.90	41.45	0.028	0.068	0.016	0.02	2.00	5.32	99.62
02-3907	LG103	10250	8950	8.3	35.43	46.45	0.036	0.075	0.017	0.02	2.00	7.60	99.87
02-3909	LG103	10350	8950	7.8	36.98	44.82	0.036	0.055	0.017	0.02	1.80	7.00	98.52
02-3911	LG103	10450	8950	4.2	41.44	41.03	0.028	0.055	0.012	0.02	2.04	9.76	98.57
02-3914	LG103	10000	9000	5.1	52.06	34.50	0.049	0.057	0.014	0.15	1.75	4.19	97.84
02-3916	LG103	10100	9000	3.8	44.40	42.76	0.030	0.108	0.013	0.02	1.58	4.56	97.24
02-3918	LG103	10200	9000	10.0	35.81	41.23	0.047	0.088	0.017	0.02	1.95	9.83	98.98
02-3920	LG103	10300	9000	9.8	41.00	34.88	0.055	0.072	0.018	0.07	1.64	12.06	99.64
02-3922	LG103	10400	9000	5.5	43.93	36.13	0.028	0.062	0.012	0.07	1.70	9.63	97.02
02-3924	LG103	10500	9000	4.9	46.86	34.64	0.044	0.055	0.013	0.11	1.84	8.63	97.11
02-3925	LG103	9950	9050	5.2	52.15	34.03	0.071	0.073	0.015	0.23	1.87	6.43	100.03
02-3927	LG103	10050	9050	3.8	46.52	39.32	0.026	0.059	0.012	0.06	1.90	5.82	97.53
02-3929	LG103	10150	9050	8.6	35.82	41.92	0.053	0.059	0.018	0.18	1.77	9.34	97.72
02-3931	LG103	10250	9050	14.6	34.26	33.64	0.073	0.077	0.021	0.09	1.55	16.81	101.11
02-3933	LG103	10350	9050	6.2	43.65	36.46	0.047	0.049	0.015	0.10	1.70	10.54	98.76
02-3935	LG103	10450	9050	4.1	54.23	34.03	0.032	0.044	0.011	0.06	1.62	6.69	100.85
02-3938	LG103	10000	9100	4.8	51.30	33.91	0.032	0.065	0.012	0.06	1.87	5.31	97.35
02-3940	LG103	10100	9100	4.3	37.98	47.32	0.034	0.052	0.012	0.07	1.49	9.15	100.40
02-3942	LG103	10200	9100	14.0	30.80	42.89	0.042	0.065	0.017	0.02	2.37	10.14	100.33
02-3944	LG103	10300	9100	6.9	43.65	36.31	0.059	0.055	0.016	0.16	1.79	8.32	97.21
02-3946	LG103	10400	9100	5.4	46.29	35.17	0.032	0.067	0.011	0.10	1.82	8.23	97.09
02-3948	LG103	10500	9100	4.5	48.79	36.03	0.030	0.052	0.011	0.09	1.66	6.20	97.38
02-3949	LG103	9950	9150	4.9	51.58	33.17	0.071	0.064	0.013	0.25	1.62	5.48	97.19
02-3951	LG103	10050	9150	6.7	40.06	43.32	0.030	0.068	0.015	0.06	1.69	7.13	99.09
02-3953	LG103	10150	9150	7.2	28.53	54.19	0.030	0.068	0.015	0.02	2.12	7.09	99.27
02-3955	LG103	10250	9150	3.7	50.45	31.88	0.053	0.070	0.013	0.24	1.54	9.76	97.66
02-3957	LG103	10350	9150	4.7	47.97	34.46	0.051	0.068	0.013	0.16	1.77	7.82	97.04
02-3959	LG103	10450	9150	4.5	49.01	36.60	0.042	0.059	0.012	0.15	1.72	6.11	98.24
02-3962	LG103	10000	9200	4.3	39.21	42.75	0.018	0.051	0.010	0.02	1.75	10.12	98.17
02-3964	LG103	10100	9200	6.1	33.05	48.90	0.028	0.072	0.012	0.02	1.92	7.17	97.25
02-3966	LG103	10200	9200	7.4	36.37	45.18	0.028	0.067	0.012	0.06	1.75	8.56	99.41
02-3968	LG103	10300	9200	3.8	46.29	37.89	0.036	0.052	0.010	0.12	1.61	6.94	96.78
02-3970	LG103	10400	9200	3.8	51.96	33.88	0.053	0.081	0.013	0.17	1.62	6.08	97.69
02-3972	LG103	10500	9200	6.2	49.73	32.17	0.055	0.067	0.013	0.18	1.75	6.57	96.70
02-3973	LG103	9950	9250	5.8	46.39	36.74	0.024	0.060	0.009	0.08	1.84	6.01	96.95

Appendix 1 Boddington pisolitic and nodular lag LG103.

sampno	sample code	easting	northing	SiO2 wt%	Al2O3 wt%	Fe2O3 wt%	MgO wt%	CaO wt%	Na2O wt%	K2O wt%	TiO2 wt%	LOI wt%	TOTAL wt%
02-3975	LG103	10050	9250	5.3	34.35	50.35	0.014	0.039	0.009	0.02	1.70	5.73	97.47
02-3977	LG103	10150	9250	9.2	32.67	43.46	0.038	0.051	0.014	0.07	1.80	10.48	97.77
02-3979	LG103	10250	9250	4.0	44.91	41.32	0.028	0.054	0.010	0.10	1.94	6.12	98.48
02-3981	LG103	10350	9250	3.4	46.18	39.75	0.036	0.078	0.011	0.10	1.87	5.74	97.18
02-3983	LG103	10450	9250	4.6	47.65	38.32	0.034	0.052	0.011	0.12	1.89	4.27	96.96
02-3986	LG103	10000	9300	5.1	38.96	47.25	0.018	0.060	0.010	0.02	1.74	4.24	97.32
02-3988	LG103	10100	9300	8.6	30.50	49.47	0.030	0.062	0.011	0.02	2.02	8.23	98.96
02-3990	LG103	10200	9300	4.3	44.63	40.03	0.040	0.090	0.015	0.10	1.84	7.48	98.54
02-3992	LG103	10300	9300	3.4	45.63	41.53	0.028	0.065	0.010	0.10	1.89	4.91	97.54
02-3994	LG103	10400	9300	3.3	46.73	40.40	0.022	0.042	0.009	0.07	2.02	6.72	99.31
02-3996	LG103	10500	9300	5.7	45.50	39.03	0.036	0.055	0.012	0.10	1.95	5.49	97.83
02-3997	LG103	9950	9350	6.9	43.95	38.46	0.020	0.049	0.010	0.02	1.99	5.47	96.85
02-3999	LG103	10050	9350	5.9	35.81	50.18	0.020	0.049	0.010	0.02	1.94	5.33	99.21
02-4001	LG103	10150	9350	4.8	43.61	42.46	0.032	0.064	0.011	0.07	1.70	6.63	99.35
02-4003	LG103	10250	9350	4.1	46.71	41.53	0.024	0.041	0.014	0.06	2.17	4.14	98.75
02-4005	LG103	10350	9350	4.1	47.99	38.46	0.044	0.055	0.011	0.10	1.92	5.26	97.90
02-4007	LG103	10450	9350	4.2	46.69	40.46	0.034	0.047	0.010	0.08	2.12	5.52	99.15
02-4010	LG103	10000	9400	4.7	39.87	46.32	0.030	0.067	0.010	0.02	1.84	4.31	97.15
02-4012	LG103	10100	9400	4.1	48.30	39.46	0.034	0.059	0.011	0.06	1.79	6.53	100.35
02-4014	LG103	10200	9400	4.1	46.12	41.89	0.036	0.067	0.010	0.06	1.79	5.18	99.21
02-4016	LG103	10300	9400	4.6	48.24	39.60	0.038	0.054	0.010	0.08	1.95	4.56	99.11
02-4018	LG103	10400	9400	5.1	47.63	38.03	0.032	0.047	0.010	0.08	1.87	4.28	97.11
02-4020	LG103	10500	9400	7.3	45.25	35.67	0.040	0.051	0.012	0.09	1.85	6.99	97.30
02-4021	LG103	9950	9450	8.0	44.97	34.17	0.038	0.054	0.012	0.07	2.02	6.85	96.22
02-4023	LG103	10050	9450	4.4	49.68	38.03	0.036	0.104	0.010	0.02	1.64	5.81	99.70
02-4025	LG103	10150	9450	3.6	52.28	31.74	0.024	0.060	0.009	0.02	1.62	8.62	97.99
02-4026	LG103	10250	9450	7.1	49.18	32.90	<0.003	0.057	0.015	0.02	2.15	8.39	99.81
02-4028	LG103	10350	9450	6.4	49.16	36.11	<0.003	0.049	0.013	0.02	2.15	4.79	98.69
02-4030	LG103	10450	9450	6.4	51.17	33.85	<0.003	0.040	0.013	0.02	2.19	5.85	99.49
02-4040	LG103	10250	9550	5.1	46.03	40.42	<0.003	0.045	0.013	0.02	1.80	4.89	98.27
02-4042	LG103	10350	9550	4.8	44.86	42.08	<0.003	0.061	0.015	0.02	1.94	5.95	99.67
02-4044	LG103	10450	9550	9.1	36.47	41.33	0.016	0.056	0.018	0.02	1.72	8.53	97.25
02-4055	LG103	9950	9650	5.5	41.85	46.11	<0.003	0.067	0.015	0.02	2.09	4.95	100.55
02-4058	LG103	10100	9650	4.9	47.88	39.55	<0.003	0.048	0.013	0.02	1.90	4.92	99.19
02-4059	LG103	10250	9650	4.5	40.91	45.07	0.069	0.089	0.018	0.02	1.60	5.41	97.62
02-4061	LG103	10350	9650	7.9	33.71	50.76	0.043	0.067	0.024	0.02	1.42	6.01	99.95
02-4065	LG103	10600	12100	4.1	43.25	42.02	<0.003	0.086	0.016	0.02	1.97	6.03	97.46

Appendix 1 Boddington pisolitic and nodular lag LG103.

sampno	sample code	easting	northing	SiO2 wt%	Al2O3 wt%	Fe2O3 wt%	MgO wt%	CaO wt%	Na2O wt%	K2O wt%	TiO2 wt%	LOI wt%	TOTAL wt%
02-4066	LG103	10700	12100	6.8	42.50	38.14	0.020	0.061	0.018	0.02	1.77	8.71	97.98
02-4067	LG103	10800	12100	4.6	47.62	37.30	0.009	0.059	0.016	0.02	1.63	6.25	97.50
02-4068	LG103	10900	12100	4.0	49.73	36.61	0.009	0.057	0.017	0.02	1.95	5.82	98.16
02-4069	LG103	10600	12200	6.6	35.66	46.62	0.018	0.086	0.018	0.02	1.77	7.64	98.44
02-4070	LG103	10700	12200	6.1	42.04	45.90	0.020	0.075	0.018	0.02	1.72	5.87	101.69
02-4071	LG103	10800	12200	4.0	47.43	38.69	<0.003	0.049	0.017	0.02	1.66	5.49	97.34
02-4072	LG103	10900	12200	4.5	45.93	39.90	<0.003	0.046	0.015	0.02	1.92	5.68	98.00
02-4073	LG103	10700	12300	8.3	36.64	45.36	0.024	0.072	0.022	0.02	1.57	9.82	101.85
02-4074	LG103	10800	12300	4.0	48.56	42.44	0.016	0.053	0.015	0.02	1.82	5.14	102.00
02-4075	LG103	10900	12300	5.0	47.22	37.87	0.018	0.057	0.017	0.02	2.25	6.05	98.51
02-4076	LG103	11000	12300	3.0	38.55	50.06	<0.003	0.051	0.016	0.02	2.12	4.08	97.91
02-4077	LG103	10700	12400	3.9	43.74	42.27	0.018	0.059	0.017	0.02	1.99	7.08	99.09
02-4078	LG103	10800	12400	6.7	45.08	37.51	0.043	0.058	0.023	0.18	1.79	7.45	98.85
02-4079	LG103	10900	12400	7.2	38.89	41.49	0.033	0.102	0.021	0.07	1.56	11.08	100.43
02-4080	LG103	11000	12400	4.0	44.38	43.20	0.013	0.051	0.016	0.02	1.79	4.93	98.34
02-4081	LG103	11100	12400	3.2	37.41	50.76	0.039	0.112	0.020	0.02	1.90	4.00	97.41
02-4082	LG103	9850	12450	7.9	52.53	27.60	0.080	0.070	0.025	0.26	2.19	7.05	97.74
02-4084	LG103	9950	12450	9.3	41.17	33.73	0.043	0.078	0.024	0.06	3.79	10.53	98.70
02-4086	LG103	10050	12450	4.5	42.80	39.70	0.029	0.075	0.018	0.02	3.15	8.07	98.32
02-4088	LG103	10150	12450	3.2	41.82	45.03	0.024	0.075	0.018	0.02	2.77	5.66	98.57
02-4090	LG103	9900	12500	4.1	50.49	32.56	0.050	0.059	0.019	0.12	2.07	10.61	100.04
02-4092	LG103	10000	12500	4.7	48.90	37.35	0.050	0.081	0.019	0.10	2.74	7.18	101.13
02-4094	LG103	10100	12500	3.3	43.87	39.11	0.026	0.048	0.017	0.02	2.72	8.55	97.66
02-4095	LG103	10700	12500	3.9	44.97	39.52	0.035	0.061	0.019	0.07	2.10	8.17	98.82
02-4096	LG103	10800	12500	8.8	44.20	30.87	0.046	0.064	0.022	0.09	2.04	15.82	101.94
02-4097	LG103	10900	12500	7.8	38.72	39.20	0.037	0.057	0.021	0.02	1.99	13.31	101.16
02-4098	LG103	11000	12500	3.2	42.04	46.00	0.024	0.062	0.019	0.02	1.95	6.21	99.54
02-4099	LG103	11100	12500	3.4	40.57	51.80	0.024	0.061	0.018	0.02	2.15	3.65	101.68
02-4100	LG103	9850	12550	11.0	47.77	23.70	0.099	0.113	0.036	0.28	2.25	12.85	98.12
02-4102	LG103	9950	12550	7.6	46.65	33.96	0.082	0.067	0.027	0.20	2.49	8.54	99.61
02-4104	LG103	10050	12550	4.5	44.01	39.70	0.050	0.097	0.021	0.08	3.44	7.79	99.65
02-4106	LG103	10150	12550	3.5	43.65	38.82	0.033	0.062	0.018	0.02	2.47	7.41	95.93
02-4108	LG103	9900	12600	5.4	43.91	39.88	0.048	0.092	0.023	0.09	2.27	6.66	98.40
02-4110	LG103	10000	12600	5.8	48.66	35.35	0.085	0.094	0.023	0.14	2.59	6.89	99.59
02-4112	LG103	10100	12600	4.3	45.59	39.66	0.056	0.081	0.022	0.09	2.82	6.05	98.65
02-4114	LG103	10700	12600	4.2	43.18	43.13	0.029	0.073	0.019	0.02	1.99	5.55	98.21
02-4115	LG103	10800	12600	7.1	41.27	38.86	0.024	0.073	0.021	0.02	1.63	10.18	99.14

Appendix 1 Boddington pisolitic and nodular lag LG103.

sampno	sample code	easting	northing	SiO2 wt%	Al2O3 wt%	Fe2O3 wt%	MgO wt%	CaO wt%	Na2O wt%	K2O wt%	TiO2 wt%	LOI wt%	TOTAL wt%
02-4116	LG103	10900	12600	5.6	39.30	39.38	0.020	0.057	0.020	0.02	1.51	11.43	97.32
02-4117	LG103	11000	12600	3.4	38.17	46.74	<0.003	0.053	0.017	0.02	1.50	7.86	97.73
02-4118	LG103	11100	12600	3.2	38.55	49.84	<0.003	0.064	0.016	0.02	2.22	3.94	97.82
02-4119	LG103	9850	12650	11.0	40.62	31.26	0.125	0.091	0.030	0.41	2.17	11.96	97.65
02-4121	LG103	9950	12650	5.5	44.42	41.72	0.043	0.081	0.022	0.13	2.15	5.37	99.40
02-4123	LG103	10050	12650	3.7	45.46	39.41	0.046	0.078	0.020	0.08	2.47	5.98	97.26
02-4125	LG103	10150	12650	4.6	46.65	36.56	0.035	0.057	0.019	0.10	2.47	7.47	97.96
02-4127	LG103	9900	12700	5.7	41.00	44.24	0.041	0.094	0.020	0.09	2.10	6.75	100.05
02-4129	LG103	10000	12700	4.1	46.03	40.20	0.022	0.085	0.017	0.06	2.15	5.98	98.68
02-4131	LG103	10100	12700	3.4	47.96	39.26	0.038	0.072	0.017	0.09	2.45	5.40	98.65
02-4133	LG103	9850	12750	12.5	36.43	38.16	0.041	0.085	0.025	0.06	2.25	10.98	100.50
02-4135	LG103	9950	12750	4.5	46.76	37.86	0.037	0.086	0.019	0.12	1.90	6.86	98.09
02-4137	LG103	10050	12750	2.8	46.86	40.08	0.024	0.062	0.015	0.08	1.61	4.78	96.29
02-4139	LG103	10150	12750	3.2	50.45	35.92	0.037	0.069	0.017	0.10	1.97	5.02	96.81
02-4141	LG103	9900	12800	7.4	39.72	39.52	0.046	0.092	0.023	0.11	2.44	8.34	97.65
02-4143	LG103	10000	12800	3.9	46.10	39.11	0.039	0.070	0.018	0.12	1.80	6.03	97.21
02-4145	LG103	10100	12800	3.5	47.90	38.67	0.031	0.062	0.018	0.08	1.84	5.99	98.12
02-4147	LG103	9850	12850	4.1	39.66	47.47	0.031	0.095	0.020	0.02	2.80	4.91	99.12
02-4149	LG103	9950	12850	3.6	44.50	39.89	0.046	0.074	0.019	0.10	1.87	6.35	96.44
02-4151	LG103	10050	12850	3.6	46.52	40.46	0.029	0.076	0.017	0.07	1.92	4.79	97.45
02-4153	LG103	10150	12850	4.4	47.39	38.53	0.024	0.059	0.018	0.07	1.92	5.11	97.48
02-4155	LG103	9900	12900	3.0	41.15	46.04	0.031	0.167	0.018	0.02	2.62	4.73	97.71
02-4157	LG103	10000	12900	3.1	47.03	42.60	0.013	0.067	0.016	0.02	2.25	4.66	99.78
02-4159	LG103	10100	12900	3.2	51.00	37.03	0.024	0.089	0.021	0.02	1.97	3.87	97.19
02-4161	LG103	9850	12950	2.7	31.56	55.33	0.044	0.078	0.029	0.02	3.50	3.92	97.13
02-4163	LG103	9950	12950	2.6	45.54	42.75	0.033	0.117	0.021	0.02	2.15	3.95	97.17
02-4166	LG103	10150	12950	3.3	51.20	35.78	0.024	0.060	0.016	0.08	2.29	5.40	98.15
02-4167	LG103	10050	12950	2.9	48.09	40.46	0.015	0.083	0.017	0.02	2.02	4.79	98.38
02-4169	LG103	9900	13000	3.7	41.80	46.04	0.018	0.098	0.021	0.02	2.44	4.73	98.88
02-4171	LG103	10000	13000	1.2	40.68	42.53	<0.003	0.038	0.015	0.02	2.72	11.33	98.51
02-4173	LG103	10100	13000	3.2	51.20	37.16	0.018	0.074	0.019	0.08	2.25	4.84	98.81
02-4175	LG103	9850	13050	4.9	41.38	44.95	0.011	0.069	0.020	0.02	2.34	5.61	99.30
02-4177	LG103	9950	13050	3.9	43.50	42.16	0.015	0.109	0.021	0.02	2.74	4.97	97.36
02-4179	LG103	10050	13050	4.2	48.24	36.31	0.024	0.078	0.017	0.11	2.12	6.29	97.38
02-4181	LG103	10150	13050	3.2	46.22	39.17	0.015	0.084	0.017	0.02	2.65	6.45	97.82

Appendix 1 Boddington pisolitic and nodular lag LG103.

sampno	Mn ppm	Cr ppm	V ppm	Cu ppm	Pb ppm	Zn ppm	Ni ppm	Co ppm	As ppm	Sb ppm	Bi ppm	Mo ppm	Ag ppm	Sn ppm	Ge ppm	Ga ppm	W ppm	Ba ppm	Zr ppm	Nb ppm	Se ppm	Au ppm
02-3901	88	494	444	8.00	26.00	58.00	24.00	1.33	14.00	2.00	4.00	8.00	0.40	36.00	1.33	100.00	100.00	138.00	368	16.00	0.67	0.0100
02-3903	102	879	649	15.00	16.00	22.00	28.00	5.00	18.00	3.00	0.67	18.00	0.30	26.00	1.33	105.00	50.00	39.00	202	15.00	0.67	0.0100
02-3905	137	422	880	22.00	22.00	38.00	26.00	1.33	10.00	2.00	0.67	13.00	0.50	22.00	1.33	80.00	54.00	33.00	187	12.00	0.67	0.0100
02-3907	239	444	1102	64.00	15.00	22.00	34.00	4.00	15.00	2.00	2.00	8.00	0.60	7.00	1.33	66.00	20.00	33.00	157	11.00	6.00	0.0003
02-3909	160	475	939	32.00	14.00	14.00	25.00	4.00	22.00	0.67	0.67	25.00	0.60	16.00	1.33	82.00	54.00	35.00	213	11.00	2.00	0.0400
02-3911	102	387	788	25.00	18.00	17.00	26.00	1.33	28.00	4.00	3.00	28.00	0.50	22.00	1.33	90.00	68.00	40.00	248	17.00	0.67	0.0200
02-3914	95	707	577	11.00	22.00	18.00	28.00	1.33	14.00	0.67	2.00	14.00	0.40	24.00	1.33	100.00	54.00	83.00	286	13.00	0.67	0.0003
02-3916	147	445	848	15.00	28.00	19.00	28.00	1.33	8.00	2.00	4.00	16.00	0.40	16.00	1.33	86.00	45.00	40.00	212	11.00	0.67	0.0100
02-3918	174	277	1079	120.00	20.00	17.00	32.00	4.00	15.00	2.00	0.67	15.00	0.60	9.00	1.33	62.00	20.00	31.00	149	11.00	4.00	0.0200
02-3920	127	321	749	66.00	30.00	15.00	32.00	1.33	16.00	0.67	3.00	25.00	0.60	24.00	1.33	68.00	68.00	45.00	214	13.00	0.67	0.0400
02-3922	91	409	809	30.00	18.00	22.00	26.00	1.33	22.00	3.00	5.00	28.00	0.50	32.00	1.33	76.00	85.00	45.00	205	15.00	0.67	0.0300
02-3924	91	379	665	12.00	25.00	14.00	22.00	1.33	22.00	2.00	5.00	30.00	0.50	32.00	1.33	86.00	85.00	62.00	266	13.00	0.67	0.0300
02-3925	91	590	450	11.00	20.00	18.00	28.00	1.33	17.00	0.67	3.00	10.00	0.40	32.00	1.33	105.00	70.00	119.00	327	16.00	0.67	0.0003
02-3927	91	398	805	12.00	18.00	13.00	28.00	1.33	10.00	0.67	0.67	30.00	0.50	28.00	1.33	88.00	66.00	44.00	199	13.00	0.67	0.0500
02-3929	99	303	987	45.00	20.00	16.00	38.00	1.33	22.00	0.67	3.00	52.00	0.60	14.00	1.33	76.00	18.00	65.00	176	15.00	0.67	0.2800
02-3931	126	263	717	85.00	26.00	13.00	40.00	4.00	12.00	0.67	2.00	30.00	0.60	17.00	1.33	58.00	36.00	56.00	185	10.00	0.67	0.2500
02-3933	77	461	691	25.00	18.00	16.00	20.00	1.33	22.00	3.00	0.67	26.00	0.50	26.00	1.33	75.00	66.00	54.00	247	12.00	0.67	0.1000
02-3935	59	471	618	18.00	22.00	13.00	26.00	1.33	19.00	5.00	3.00	22.00	0.30	30.00	1.33	98.00	80.00	48.00	260	16.00	2.00	0.0300
02-3938	92	403	699	14.00	25.00	12.00	32.00	1.33	14.00	3.00	0.67	32.00	0.30	26.00	1.33	100.00	56.00	49.00	237	14.00	0.67	0.0800
02-3940	65	382	1041	22.00	32.00	15.00	34.00	1.33	14.00	4.00	5.00	30.00	0.60	18.00	1.33	70.00	44.00	44.00	247	12.00	0.67	0.0800
02-3942	217	84	930	42.00	10.00	19.00	32.00	4.00	11.00	5.00	0.67	10.00	0.70	4.00	1.33	58.00	12.00	34.00	161	16.00	0.67	0.1000
02-3944	102	401	654	30.00	10.00	15.00	34.00	4.00	36.00	0.67	2.00	17.00	0.50	20.00	1.33	84.00	58.00	78.00	255	15.00	0.67	0.0500
02-3946	70	489	675	19.00	22.00	13.00	18.00	1.33	28.00	2.00	0.67	22.00	0.50	20.00	1.33	94.00	62.00	62.00	235	14.00	0.67	0.0300
02-3948	62	440	604	17.00	30.00	15.00	28.00	4.00	28.00	4.00	5.00	19.00	0.40	22.00	1.33	98.00	55.00	57.00	251	12.00	0.67	0.2000
02-3949	84	556	409	7.00	24.00	18.00	22.00	4.00	14.00	4.00	5.00	10.00	0.40	32.00	1.33	100.00	68.00	138.00	303	15.00	2.00	0.0100
02-3951	85	356	960	28.00	22.00	18.00	36.00	1.33	16.00	3.00	2.00	125.00	0.60	20.00	1.33	86.00	52.00	41.00	242	13.00	0.67	0.1500
02-3953	175	183	1237	65.00	16.00	25.00	30.00	1.33	14.00	0.67	0.67	10.00	0.70	5.00	1.33	68.00	1.33	28.00	155	13.00	3.00	0.0200
02-3955	118	242	463	24.00	12.00	22.00	34.00	4.00	58.00	5.00	6.00	13.00	0.60	25.00	1.33	80.00	56.00	100.00	245	11.00	0.67	0.7000
02-3957	69	390	585	25.00	6.00	13.00	24.00	1.33	35.00	0.67	5.00	14.00	0.60	26.00	1.33	96.00	70.00	80.00	291	15.00	2.00	0.0200
02-3959	67	443	580	12.00	24.00	16.00	32.00	1.33	30.00	5.00	0.67	15.00	0.40	25.00	1.33	110.00	66.00	80.00	296	15.00	0.67	0.0200
02-3962	76	299	775	32.00	28.00	15.00	28.00	1.33	14.00	0.67	7.00	58.00	0.40	22.00	1.33	80.00	54.00	34.00	254	11.00	0.67	1.5800
02-3964	132	272	1086	56.00	12.00	22.00	38.00	1.33	18.00	4.00	2.00	13.00	0.70	6.00	1.33	76.00	14.00	32.00	154	13.00	0.67	0.0100
02-3966	111	285	882	40.00	22.00	24.00	36.00	1.33	10.00	2.00	0.67	60.00	0.60	22.00	1.33	76.00	45.00	42.00	210	10.00	0.67	0.2100
02-3968	65	353	633	10.00	26.00	12.00	30.00	1.33	46.00	6.00	11.00	16.00	0.70	20.00	1.33	105.00	56.00	64.00	281	11.00	0.67	0.0500
02-3970	55	566	506	12.00	16.00	13.00	35.00	4.00	45.00	6.00	5.00	14.00	0.60	25.00	1.33	100.00	65.00	87.00	323	15.00	0.67	0.0200
02-3972	66	509	514	9.00	24.00	17.00	32.00	1.33	32.00	2.00	5.00	17.00	0.70	26.00	1.33	100.00	70.00	80.00	304	17.00	0.67	0.3200
02-3973	84	488	524	6.00	30.00	19.00	30.00	1.33	17.00	4.00	0.67	28.00	0.60	28.00	1.33	110.00	60.00	49.00	261	20.00	2.00	0.0300

Appendix 1 Boddington pisolitic and nodular lag LG103.

sampno	Mn ppm	Cr ppm	V ppm	Cu ppm	Pb ppm	Zn ppm	Ni ppm	Co ppm	As ppm	Sb ppm	Bi ppm	Mo ppm	Ag ppm	Sn ppm	Ge ppm	Ga ppm	W ppm	Ba ppm	Zr ppm	Nb ppm	Se ppm	Au ppm
02-3975	106	282	963	32.00	16.00	22.00	50.00	1.33	18.00	4.00	5.00	30.00	0.70	13.00	1.33	84.00	16.00	27.00	160	14.00	0.67	0.0400
02-3977	143	181	798	26.00	14.00	18.00	26.00	1.33	17.00	2.00	0.67	25.00	0.70	19.00	1.33	68.00	38.00	43.00	229	16.00	0.67	0.1000
02-3979	88	275	725	6.00	20.00	19.00	30.00	1.33	20.00	2.00	0.67	22.00	0.60	18.00	1.33	98.00	60.00	45.00	238	14.00	0.67	0.0400
02-3981	61	506	681	8.00	14.00	17.00	28.00	1.33	36.00	4.00	3.00	20.00	0.60	24.00	1.33	105.00	64.00	61.00	310	14.00	2.00	0.1000
02-3983	71	564	630	2.00	24.00	18.00	30.00	1.33	35.00	0.67	4.00	19.00	0.60	22.00	1.33	110.00	64.00	60.00	290	14.00	0.67	0.0100
02-3986	121	235	871	26.00	24.00	24.00	70.00	1.33	10.00	0.67	6.00	28.00	0.60	11.00	1.33	84.00	22.00	33.00	190	13.00	0.67	0.0200
02-3988	174	239	1010	40.00	20.00	19.00	40.00	1.33	10.00	3.00	0.67	17.00	0.70	14.00	1.33	70.00	18.00	31.00	190	16.00	5.00	0.0100
02-3990	96	319	707	9.00	28.00	22.00	34.00	1.33	13.00	0.67	0.67	38.00	0.60	24.00	1.33	105.00	54.00	60.00	264	14.00	0.67	0.0400
02-3992	89	336	715	2.00	22.00	25.00	34.00	1.33	22.00	2.00	4.00	24.00	0.60	20.00	1.33	105.00	52.00	47.00	241	14.00	5.00	0.0100
02-3994	71	483	735	10.00	20.00	15.00	82.00	1.33	28.00	0.67	0.67	22.00	0.60	20.00	1.33	105.00	58.00	40.00	263	13.00	0.67	0.0100
02-3996	91	454	655	11.00	22.00	19.00	36.00	1.33	32.00	0.67	5.00	22.00	0.60	20.00	1.33	100.00	60.00	50.00	279	20.00	3.00	0.0200
02-3997	141	298	686	11.00	30.00	18.00	92.00	4.00	12.00	2.00	0.67	19.00	0.50	13.00	1.33	85.00	30.00	34.00	221	14.00	5.00	0.0100
02-3999	143	298	810	16.00	12.00	20.00	30.00	1.33	10.00	0.67	0.67	17.00	0.70	11.00	1.33	90.00	12.00	26.00	194	16.00	0.67	0.0003
02-4001	95	412	732	11.00	14.00	18.00	32.00	1.33	16.00	0.67	5.00	22.00	0.50	35.00	1.33	90.00	84.00	47.00	260	13.00	0.67	0.0500
02-4003	82	351	720	13.00	22.00	22.00	34.00	1.33	13.00	0.67	3.00	32.00	0.60	22.00	1.33	105.00	62.00	45.00	247	16.00	3.00	0.0700
02-4005	99	339	659	3.00	18.00	20.00	34.00	1.33	16.00	0.67	3.00	24.00	0.60	24.00	1.33	115.00	54.00	50.00	266	13.00	8.00	0.0500
02-4007	81	471	692	11.00	10.00	19.00	66.00	1.33	22.00	0.67	5.00	25.00	0.50	24.00	1.33	110.00	84.00	49.00	272	16.00	0.67	0.0200
02-4010	122	361	759	20.00	18.00	24.00	40.00	4.00	17.00	2.00	0.67	14.00	0.50	13.00	1.33	90.00	16.00	37.00	206	16.00	0.67	0.0500
02-4012	75	437	619	14.00	16.00	22.00	78.00	1.33	17.00	0.67	0.67	24.00	0.60	46.00	1.33	88.00	130.00	51.00	268	15.00	0.67	0.0200
02-4014	83	475	675	8.00	18.00	20.00	80.00	1.33	17.00	4.00	0.67	26.00	0.50	30.00	1.33	96.00	82.00	48.00	270	17.00	0.67	0.0800
02-4016	88	456	633	16.00	18.00	30.00	42.00	1.33	12.00	0.67	2.00	30.00	0.60	20.00	1.33	105.00	52.00	50.00	237	14.00	0.67	0.0200
02-4018	88	566	611	9.00	25.00	19.00	28.00	1.33	20.00	0.67	3.00	28.00	0.50	20.00	1.33	110.00	54.00	45.00	238	16.00	0.67	0.0500
02-4020	84	492	549	18.00	26.00	15.00	56.00	1.33	24.00	3.00	0.67	28.00	0.50	22.00	1.33	115.00	54.00	57.00	226	15.00	0.67	0.0200
02-4021	139	329	546	9.00	32.00	18.00	38.00	1.33	15.00	0.67	4.00	15.00	0.50	19.00	1.33	92.00	38.00	48.00	218	19.00	2.00	0.0100
02-4023	81	540	575	5.00	24.00	19.00	30.00	4.00	12.00	0.67	0.67	24.00	0.50	42.00	1.33	96.00	120.00	50.00	241	16.00	0.67	0.0100
02-4025	64	509	468	17.00	14.00	20.00	28.00	1.33	22.00	0.67	2.00	26.00	0.50	48.00	1.33	92.00	120.00	46.00	246	12.00	0.67	0.0600
02-4026	77	592	606	8.00	38.00	18.00	30.00	5.00	15.00	4.00	4.00	34.00	0.70	28.00	1.33	105.00	74.00	42.00	281	18.00	0.67	0.0003
02-4028	69	662	634	9.00	22.00	16.00	30.00	4.00	18.00	3.00	5.00	40.00	0.70	26.00	1.33	110.00	64.00	35.00	279	13.00	0.67	0.0200
02-4030	49	685	620	26.00	30.00	22.00	55.00	6.00	18.00	2.00	0.67	30.00	0.60	24.00	1.33	115.00	54.00	31.00	200	17.00	0.67	0.0100
02-4040	45	860	654	7.00	80.00	18.00	34.00	1.33	12.00	0.67	10.00	38.00	0.70	32.00	1.33	110.00	70.00	33.00	279	10.00	2.00	0.0200
02-4042	51	690	763	13.00	18.00	18.00	72.00	4.00	26.00	0.67	0.67	28.00	0.60	18.00	1.33	92.00	36.00	36.00	194	11.00	0.67	0.0200
02-4044	66	757	995	36.00	24.00	22.00	44.00	6.00	52.00	5.00	0.67	32.00	0.70	17.00	1.33	88.00	36.00	44.00	207	11.00	3.00	0.0300
02-4055	177	485	889	19.00	25.00	24.00	42.00	4.00	26.00	0.67	0.67	14.00	0.70	17.00	1.33	80.00	34.00	37.00	227	15.00	0.67	0.0100
02-4058	51	685	645	12.00	30.00	17.00	32.00	1.33	15.00	0.67	2.00	28.00	0.60	22.00	1.33	105.00	62.00	33.00	234	13.00	0.67	0.0200
02-4059	51	621	691	14.00	12.00	22.00	35.00	4.00	20.00	3.00	5.00	28.00	0.60	26.00	1.33	95.00	70.00	42.00	254	13.00	0.67	0.0100
02-4061	44	873	954	19.00	16.00	25.00	30.00	4.00	50.00	5.00	0.67	28.00	0.80	26.00	1.33	105.00	48.00	60.00	238	8.00	0.67	0.0100
02-4065	140	654	811	10.00	15.00	22.00	42.00	4.00	22.00	0.67	0.67	10.00	0.60	12.00	1.33	88.00	22.00	34.00	182	12.00	0.67	0.0003

Appendix 1 Boddington pisolitic and nodular lag LG103.

sampno	Mn ppm	Cr ppm	V ppm	Cu ppm	Pb ppm	Zn ppm	Ni ppm	Co ppm	As ppm	Sb ppm	Bi ppm	Mo ppm	Ag ppm	Sn ppm	Ge ppm	Ga ppm	W ppm	Ba ppm	Zr ppm	Nb ppm	Se ppm	Au ppm
02-4066	104	526	658	19.00	18.00	25.00	40.00	5.00	26.00	5.00	3.00	11.00	0.60	9.00	1.33	80.00	25.00	48.00	219	12.00	3.00	0.0003
02-4067	40	559	612	4.00	28.00	18.00	125.00	4.00	28.00	2.00	0.67	12.00	0.60	11.00	1.33	96.00	36.00	29.00	262	12.00	0.67	0.0700
02-4068	53	566	593	8.00	18.00	20.00	32.00	4.00	32.00	8.00	0.67	16.00	0.60	13.00	1.33	94.00	52.00	32.00	230	11.00	0.67	0.0100
02-4069	120	662	906	24.00	18.00	28.00	42.00	4.00	32.00	0.67	0.67	8.00	0.60	6.00	4.00	88.00	14.00	33.00	239	12.00	4.00	0.0003
02-4070	62	604	724	7.00	14.00	17.00	30.00	4.00	40.00	6.00	0.67	10.00	0.60	8.00	1.33	105.00	24.00	41.00	273	14.00	0.67	0.0003
02-4071	42	571	572	5.00	20.00	17.00	32.00	4.00	46.00	3.00	2.00	11.00	0.60	14.00	1.33	110.00	52.00	35.00	243	12.00	0.67	0.0400
02-4072	54	639	597	0.67	24.00	16.00	30.00	4.00	68.00	0.67	3.00	15.00	0.70	14.00	1.33	110.00	38.00	33.00	305	17.00	0.67	0.0003
02-4073	41	645	743	7.00	14.00	19.00	32.00	4.00	52.00	3.00	0.67	8.00	0.50	13.00	1.33	94.00	44.00	34.00	303	13.00	0.67	0.0003
02-4074	28	702	625	9.00	15.00	18.00	32.00	4.00	96.00	4.00	4.00	9.00	0.60	14.00	1.33	105.00	42.00	42.00	330	15.00	4.00	0.0003
02-4075	61	821	84	13.00	15.00	16.00	26.00	4.00	88.00	0.67	2.00	8.00	0.60	20.00	1.33	96.00	58.00	38.00	242	16.00	0.67	0.0100
02-4076	98	760	955	5.00	18.00	18.00	32.00	4.00	20.00	4.00	4.00	11.00	0.70	17.00	1.33	105.00	42.00	25.00	171	13.00	0.67	0.0003
02-4077	48	670	654	9.00	8.00	13.00	32.00	1.33	100.00	0.67	0.67	7.00	0.60	19.00	1.33	115.00	46.00	29.00	354	15.00	2.00	0.0100
02-4078	40	510	539	8.00	20.00	18.00	32.00	5.00	340.00	0.67	2.00	5.00	0.60	9.00	1.33	115.00	40.00	75.00	302	15.00	2.00	0.0400
02-4079	75	531	725	25.00	20.00	18.00	42.00	4.00	64.00	3.00	3.00	7.00	0.70	19.00	1.33	90.00	55.00	50.00	223	12.00	2.00	0.0100
02-4080	81	684	700	15.00	14.00	25.00	30.00	5.00	42.00	6.00	0.67	8.00	0.60	24.00	1.33	88.00	44.00	31.00	179	10.00	0.67	0.0100
02-4081	76	764	896	15.00	10.00	22.00	34.00	1.33	24.00	4.00	2.00	6.00	0.70	16.00	1.33	86.00	30.00	27.00	124	11.00	0.67	0.0100
02-4082	85	565	475	12.00	22.00	17.00	30.00	5.00	62.00	4.00	6.00	28.00	0.60	17.00	1.33	115.00	34.00	114.00	348	16.00	0.67	0.0500
02-4084	626	782	613	20.00	18.00	28.00	35.00	6.00	50.00	0.67	8.00	32.00	0.50	12.00	1.33	78.00	12.00	61.00	207	20.00	7.00	1.1500
02-4086	410	550	764	11.00	22.00	38.00	44.00	6.00	58.00	3.00	4.00	28.00	0.70	11.00	1.33	96.00	18.00	47.00	222	16.00	3.00	0.0800
02-4088	340	556	831	6.00	28.00	24.00	35.00	4.00	60.00	4.00	7.00	25.00	0.60	8.00	1.33	100.00	16.00	41.00	244	17.00	4.00	0.0200
02-4090	111	535	613	16.00	12.00	15.00	22.00	1.33	75.00	6.00	5.00	62.00	0.50	14.00	1.33	94.00	22.00	67.00	294	12.00	0.67	0.3400
02-4092	278	604	708	12.00	10.00	14.00	25.00	1.33	56.00	3.00	2.00	34.00	0.60	14.00	1.33	100.00	8.00	68.00	255	14.00	2.00	0.0500
02-4094	259	556	748	14.00	24.00	16.00	22.00	1.33	46.00	0.67	0.67	28.00	0.50	9.00	1.33	86.00	10.00	40.00	224	19.00	0.67	0.0200
02-4095	61	545	677	10.00	8.00	14.00	20.00	1.33	130.00	2.00	3.00	8.00	0.60	16.00	1.33	105.00	46.00	49.00	419	17.00	3.00	0.0600
02-4096	61	430	499	9.00	12.00	10.00	25.00	1.33	82.00	0.67	0.67	6.00	0.50	11.00	1.33	84.00	16.00	49.00	299	15.00	0.67	0.1300
02-4097	109	683	801	68.00	10.00	15.00	34.00	4.00	40.00	2.00	0.67	6.00	0.50	25.00	1.33	65.00	88.00	38.00	147	12.00	0.67	0.0500
02-4098	80	860	903	24.00	22.00	16.00	30.00	4.00	32.00	3.00	4.00	6.00	0.60	15.00	1.33	92.00	54.00	30.00	155	13.00	0.67	0.0003
02-4099	91	748	954	16.00	1.33	20.00	25.00	1.33	20.00	4.00	2.00	6.00	0.60	16.00	1.33	94.00	34.00	25.00	138	10.00	0.67	0.0200
02-4100	134	657	412	25.00	12.00	13.00	25.00	1.33	110.00	7.00	34.00	36.00	0.60	13.00	1.33	100.00	20.00	101.00	284	19.00	0.67	0.4000
02-4102	137	454	675	19.00	8.00	16.00	20.00	1.33	65.00	5.00	11.00	42.00	0.60	10.00	1.33	98.00	16.00	80.00	218	17.00	2.00	0.2100
02-4104	452	557	781	11.00	18.00	17.00	20.00	1.33	80.00	5.00	8.00	28.00	0.60	9.00	1.33	105.00	8.00	52.00	214	19.00	3.00	0.5900
02-4106	235	459	729	7.00	10.00	14.00	18.00	1.33	75.00	5.00	0.67	24.00	0.50	12.00	1.33	100.00	12.00	44.00	223	16.00	3.00	0.0100
02-4108	158	372	686	14.00	16.00	16.00	20.00	1.33	88.00	0.67	9.00	22.00	0.60	6.00	1.33	100.00	10.00	56.00	186	15.00	0.67	0.0200
02-4110	203	603	659	14.00	8.00	12.00	20.00	1.33	85.00	6.00	17.00	34.00	0.50	12.00	1.33	95.00	15.00	76.00	223	18.00	0.67	0.2900
02-4112	346	713	700	4.00	24.00	19.00	18.00	1.33	68.00	5.00	9.00	25.00	0.60	12.00	1.33	110.00	18.00	59.00	227	19.00	0.67	0.0400
02-4114	61	535	744	64.00	15.00	14.00	22.00	1.33	54.00	2.00	2.00	6.00	0.50	8.00	1.33	100.00	20.00	42.00	306	16.00	0.67	0.0200
02-4115	56	556	575	15.00	15.00	12.00	26.00	1.33	75.00	6.00	0.67	6.00	0.60	11.00	1.33	90.00	20.00	43.00	266	13.00	0.67	0.0200

Appendix 1 Boddington pisolitic and nodular lag LG103.

sampno	Mn ppm	Cr ppm	V ppm	Cu ppm	Pb ppm	Zn ppm	Ni ppm	Co ppm	As ppm	Sb ppm	Bi ppm	Mo ppm	Ag ppm	Sn ppm	Ge ppm	Ga ppm	W ppm	Ba ppm	Zr ppm	Nb ppm	Se ppm	Au ppm
02-4116	127	486	595	40.00	10.00	11.00	30.00	1.33	58.00	2.00	8.00	5.00	0.50	20.00	1.33	78.00	46.00	40.00	181	13.00	0.67	0.0100
02-4117	77	572	843	24.00	22.00	18.00	34.00	1.33	42.00	7.00	10.00	6.00	0.50	22.00	1.33	85.00	46.00	32.00	157	10.00	2.00	0.0400
02-4118	134	589	946	12.00	15.00	20.00	28.00	4.00	15.00	2.00	0.67	7.00	0.50	13.00	1.33	100.00	16.00	29.00	136	10.00	0.67	0.0100
02-4119	102	325	514	32.00	6.00	15.00	22.00	1.33	280.00	7.00	52.00	66.00	0.60	8.00	1.33	92.00	24.00	149.00	306	18.00	4.00	0.6500
02-4121	105	463	793	13.00	22.00	15.00	20.00	1.33	160.00	2.00	16.00	30.00	0.50	5.00	1.33	100.00	8.00	58.00	190	13.00	3.00	0.1000
02-4123	214	672	721	10.00	25.00	15.00	18.00	1.33	105.00	4.00	17.00	24.00	0.50	14.00	1.33	96.00	10.00	58.00	204	15.00	0.67	0.0200
02-4125	223	805	636	9.00	18.00	17.00	20.00	1.33	80.00	5.00	6.00	28.00	0.60	9.00	1.33	100.00	15.00	62.00	221	19.00	6.00	0.0600
02-4127	129	359	771	22.00	12.00	20.00	25.00	1.33	120.00	4.00	16.00	32.00	0.50	7.00	1.33	92.00	12.00	52.00	187	15.00	3.00	0.1200
02-4129	59	561	858	12.00	8.00	18.00	26.00	1.33	180.00	6.00	4.00	30.00	0.60	5.00	1.33	110.00	5.00	39.00	203	16.00	0.67	0.0300
02-4131	191	645	703	10.00	20.00	14.00	20.00	1.33	180.00	10.00	11.00	25.00	0.60	5.00	1.33	110.00	26.00	59.00	236	17.00	0.67	0.0400
02-4133	160	565	811	76.00	18.00	20.00	48.00	4.00	58.00	3.00	0.67	18.00	0.50	8.00	1.33	58.00	6.00	45.00	144	12.00	0.67	0.0200
02-4135	79	539	732	15.00	8.00	13.00	22.00	1.33	330.00	4.00	11.00	46.00	0.50	10.00	1.33	90.00	10.00	72.00	217	14.00	0.67	0.0400
02-4137	95	419	618	8.00	15.00	18.00	20.00	1.33	190.00	6.00	15.00	30.00	0.50	5.00	1.33	105.00	15.00	48.00	209	11.00	0.67	0.0400
02-4139	120	452	610	12.00	12.00	17.00	18.00	1.33	240.00	6.00	18.00	35.00	0.50	9.00	1.33	98.00	14.00	62.00	247	16.00	0.67	0.0300
02-4141	119	540	836	30.00	25.00	15.00	28.00	4.00	155.00	5.00	7.00	38.00	0.60	8.00	1.33	78.00	6.00	58.00	200	15.00	0.67	0.0300
02-4143	63	658	698	18.00	20.00	12.00	28.00	1.33	350.00	7.00	9.00	55.00	0.60	4.00	1.33	105.00	14.00	69.00	242	15.00	0.67	0.0300
02-4145	72	562	815	18.00	18.00	18.00	22.00	1.33	300.00	4.00	5.00	46.00	0.60	5.00	1.33	98.00	4.00	60.00	229	13.00	4.00	0.0300
02-4147	121	390	1167	20.00	12.00	19.00	25.00	1.33	46.00	5.00	2.00	10.00	0.60	2.00	1.33	82.00	1.33	32.00	203	24.00	2.00	0.0100
02-4149	86	510	869	12.00	14.00	17.00	20.00	1.33	220.00	4.00	25.00	32.00	0.70	7.00	4.00	92.00	22.00	64.00	239	14.00	2.00	0.1000
02-4151	84	463	920	14.00	14.00	18.00	30.00	4.00	160.00	6.00	0.67	28.00	0.60	5.00	1.33	94.00	10.00	45.00	225	16.00	0.67	0.0300
02-4153	79	447	827	19.00	18.00	22.00	26.00	4.00	125.00	3.00	4.00	26.00	0.60	4.00	1.33	100.00	5.00	44.00	213	17.00	5.00	0.0100
02-4155	110	407	1251	16.00	16.00	22.00	32.00	4.00	90.00	5.00	0.67	18.00	0.60	8.00	1.33	100.00	1.33	33.00	230	19.00	0.67	0.0100
02-4157	76	432	1099	15.00	12.00	18.00	22.00	1.33	94.00	3.00	0.67	28.00	0.60	3.00	1.33	105.00	4.00	27.00	223	18.00	0.67	0.0100
02-4159	76	529	885	24.00	15.00	22.00	28.00	4.00	78.00	4.00	0.67	28.00	0.60	4.00	1.33	110.00	1.33	39.00	251	15.00	4.00	0.3500
02-4161	142	402	1430	18.00	15.00	26.00	32.00	4.00	78.00	8.00	0.67	12.00	0.80	3.00	5.00	88.00	8.00	23.00	245	22.00	7.00	0.0003
02-4163	77	450	1094	14.00	18.00	22.00	38.00	1.33	72.00	4.00	0.67	24.00	0.60	7.00	1.33	110.00	14.00	31.00	240	15.00	0.67	0.2200
02-4166	97	620	750	20.00	24.00	15.00	16.00	4.00	200.00	4.00	4.00	22.00	0.50	8.00	1.33	130.00	14.00	58.00	311	18.00	0.67	0.0200
02-4167	68	507	874	24.00	12.00	15.00	24.00	1.33	90.00	2.00	0.67	19.00	0.50	3.00	1.33	100.00	1.33	40.00	278	18.00	5.00	0.0200
02-4169	98	392	1148	18.00	10.00	16.00	24.00	1.33	80.00	2.00	3.00	40.00	0.60	8.00	1.33	105.00	5.00	33.00	218	15.00	0.67	0.0200
02-4171	36	530	990	15.00	1.33	13.00	18.00	1.33	135.00	0.67	0.67	48.00	0.50	9.00	1.33	120.00	6.00	25.00	297	20.00	3.00	0.1400
02-4173	132	570	733	18.00	16.00	15.00	22.00	1.33	270.00	6.00	0.67	22.00	0.50	5.00	1.33	125.00	14.00	65.00	297	18.00	3.00	0.0200
02-4175	102	371	913	15.00	20.00	15.00	22.00	1.33	165.00	5.00	0.67	19.00	0.60	5.00	1.33	115.00	10.00	38.00	220	19.00	0.67	0.0100
02-4177	85	486	1215	17.00	16.00	18.00	26.00	1.33	125.00	3.00	0.67	26.00	0.60	6.00	1.33	95.00	4.00	31.00	251	20.00	4.00	0.0100
02-4179	64	614	797	16.00	20.00	13.00	20.00	1.33	340.00	5.00	9.00	25.00	0.50	10.00	1.33	110.00	16.00	69.00	308	18.00	2.00	0.0300
02-4181	215	448	862	19.00	20.00	17.00	26.00	4.00	120.00	5.00	2.00	17.00	0.60	4.00	1.33	120.00	10.00	45.00	252	16.00	4.00	0.0200

Appendix 2 Boddington Loose Pisoliths LT102

sampno	sample code	easting	northing	SiO2 wt%	Al2O3 wt%	Fe2O3 wt%	MgO wt%	CaO wt%	Na2O wt%	K2O wt%	TiO2 wt%	LOI wt%	TOTAL wt%
07-0358	LT102	10000	12150	8.3	39.10	38.90	0.050	0.080	0.030	0.20	3.57	9.78	100.05
07-0363	LT102	10240	12460	0.6	41.37	39.75	0.010	0.030	0.003	0.02	3.34	14.20	99.33
07-0371	LT102	10220	13000	14.1	36.27	34.61	0.060	0.200	0.040	0.17	3.30	11.70	100.47
07-0374	LT102	10215	13000	1.9	41.94	31.89	0.040	0.030	0.010	0.27	1.82	23.60	101.53
07-0377	LT102	10300	12925	0.6	43.26	38.18	0.010	0.030	0.010	0.02	3.05	14.60	99.78
07-0379	LT102	10300	12925	0.9	43.64	37.18	0.020	0.030	0.030	0.02	2.75	14.90	99.41
07-0380	LT102	12490	12640	9.2	38.54	40.33	0.040	0.220	0.030	0.12	2.03	9.03	99.54
07-0381	LT102	12490	12640	6.0	42.69	36.18	0.030	0.050	0.003	0.06	2.09	12.80	99.89
07-0382	LT102	12490	12640	2.6	40.05	38.61	0.010	0.030	0.010	0.02	2.24	16.20	99.72
07-0384	LT102	10200	9580	10.5	38.91	35.61	0.150	0.070	0.010	0.11	2.60	10.90	98.84
07-0390	LT102	10100	9040	4.1	37.40	37.04	0.050	0.060	0.030	0.02	3.05	17.80	99.49
07-0395	LT102	10130	9040	12.0	34.76	39.32	0.040	0.070	0.030	0.11	2.55	10.80	99.66
07-0400	LT102	10180	9020	15.4	34.19	36.04	0.050	0.220	0.040	0.13	3.00	11.90	100.97
07-0401	LT102	10180	9020	48.8	15.43	14.59	3.580	10.100	1.970	0.23	1.57	1.67	97.91
07-0402	LT102	9949	11649	10.9	45.34	31.46	0.070	0.090	0.050	0.12	3.32	9.71	101.06
07-0412	LT102	10098	12780	5.8	46.66	35.18	0.040	0.060	0.040	0.07	2.77	9.43	100.03
07-0414	LT102	10098	12780	1.5	49.87	36.04	0.020	0.040	0.030	0.02	2.57	10.60	100.67
07-1087	LT102	10170	9640	1.0	36.39	42.06	0.020	0.050	0.003	0.02	2.10	17.60	99.24
07-1095	LT102	10310	9400	2.6	46.70	30.52	0.020	0.040	0.003	0.02	2.62	17.30	99.74
07-1096	LT102	10310	9400	2.6	43.20	33.70	0.010	0.040	0.010	0.02	2.95	17.10	99.56
07-1109	LT102	10020	13050	7.3	41.10	32.70	0.070	0.080	0.020	0.12	3.15	15.40	99.92
07-1111	LT102	10070	12975	1.1	41.50	34.89	0.040	0.050	0.010	0.02	5.49	16.50	99.61
07-1115	LT102	10060	12950	0.7	41.90	38.41	0.020	0.030	0.020	0.02	3.05	15.40	99.57
07-1119	LT102	10330	12900	1.7	32.80	46.00	0.020	0.040	0.020	0.02	3.00	16.30	99.90
07-1124	LT102	10070	12975	7.9	40.60	35.80	0.070	0.090	0.020	0.08	3.47	11.80	99.81
07-1162	LT102	9825	12937	0.8	35.10	41.50	0.010	0.030	0.003	0.02	2.69	19.50	99.65

Appendix 2 **Boddington Loose Pisoliths LT102**

sampno	Mn ppm	Cr ppm	V ppm	Cu ppm	Pb ppm	Zn ppm	Ni ppm	Co ppm	As ppm	Sb ppm	Bi ppm	Mo ppm	Ag ppm	Sn ppm	Ge ppm	Ga ppm	W ppm	Ba ppm	Zr ppm	Nb ppm	Se ppm	Au ppm
07-0358	137	424	669	11.00	23.00	14.00	12.00	6.00	82.00	2.00	4.00	30.00	0.03	16.00	1.33	93.00	19.00	64.00	542	29.00	0.67	0.0600
07-0363	85	392	696	6.00	5.00	8.00	1.33	7.00	55.00	0.67	0.67	28.00	0.50	17.00	1.33	87.00	24.00	14.00	372	25.00	3.00	0.1000
07-0371	124	347	677	9.00	16.00	13.00	14.00	1.33	254.00	3.00	4.00	28.00	0.03	12.00	1.33	75.00	17.00	53.00	643	28.00	0.67	0.0400
07-0374	5	476	638	20.00	7.00	10.00	1.33	1.33	521.00	6.00	6.00	38.00	0.03	24.00	1.33	73.00	33.00	10.00	309	15.00	3.00	0.1200
07-0377	61	351	665	7.00	0.67	10.00	1.33	1.33	92.00	0.67	3.00	53.00	0.50	11.00	1.33	130.00	19.00	18.00	401	22.00	0.67	0.1600
07-0379	59	399	689	7.00	0.67	10.00	1.33	1.33	99.00	3.00	4.00	51.00	0.50	7.00	1.33	110.00	14.00	19.00	435	22.00	0.67	0.1100
07-0380	128	398	531	11.00	20.00	12.00	46.00	1.33	86.00	0.67	0.67	16.00	0.03	11.00	1.33	92.00	36.00	43.00	560	20.00	0.67	0.0100
07-0381	78	404	553	17.00	22.00	12.00	28.00	1.33	75.00	0.67	2.00	28.00	0.03	10.00	1.33	80.00	25.00	24.00	438	23.00	0.67	0.0200
07-0382	54	411	609	73.00	13.00	13.00	1.33	1.33	69.00	2.00	5.00	15.00	0.50	13.00	1.33	83.00	35.00	16.00	379	20.00	3.00	0.0100
07-0384	71	353	644	9.00	20.00	12.00	25.00	1.33	31.00	0.67	3.00	28.00	0.03	22.00	1.33	73.00	62.00	39.00	596	32.00	0.67	0.0100
07-0390	70	310	794	31.00	19.00	7.00	12.00	1.33	23.00	0.67	0.67	36.00	0.03	36.00	1.33	63.00	94.00	8.00	468	23.00	0.67	0.1000
07-0395	114	296	774	25.00	22.00	8.00	18.00	1.33	6.00	0.67	2.00	30.00	0.03	17.00	5.00	60.00	30.00	33.00	502	24.00	0.67	0.2600
07-0400	145	273	748	56.00	20.00	10.00	27.00	1.33	7.00	0.67	4.00	19.00	0.03	18.00	1.33	52.00	44.00	43.00	452	22.00	0.67	0.0100
07-0401	1521	68	356	178.00	0.67	148.00	131.00	63.00	6.00	0.67	0.67	1.00	0.03	3.00	1.33	14.00	1.33	54.00	40	0.67	0.67	0.0200
07-0402	113	408	513	9.00	19.00	49.00	16.00	1.33	35.00	0.67	12.00	33.00	0.03	52.00	1.33	83.00	52.00	41.00	700	28.00	0.67	0.0600
07-0412	85	354	678	14.00	20.00	39.00	17.00	1.33	206.00	2.00	7.00	46.00	0.50	9.00	1.33	83.00	13.00	36.00	596	20.00	0.67	0.1100
07-0414	84	391	699	2.00	18.00	32.00	1.33	1.33	204.00	2.00	11.00	38.00	0.03	7.00	1.33	87.00	7.00	25.00	470	16.00	0.67	0.0200
07 1087	59	628	630	11.00	14.00	8.00	20.00	1.33	17.00	2.00	4.00	62.00	0.03	56.00	1.33	105.00	200.00	10.00	468	16.00	4.00	0.6600
07 1095	55	457	469	12.00	8.00	10.00	22.00	1.33	16.00	0.67	4.00	40.00	0.03	54.00	1.33	110.00	195.00	11.00	244	22.00	0.67	0.0800
07 1096	64	496	515	11.00	5.00	9.00	18.00	1.33	15.00	2.00	8.00	46.00	0.03	56.00	1.33	105.00	185.00	16.00	275	20.00	0.67	0.3800
07 1109	112	444	688	5.00	14.00	13.00	18.00	1.33	320.00	10.00	5.00	40.00	0.03	14.00	1.33	94.00	22.00	42.00	369	24.00	3.00	0.0800
07 1111	561	500	683	2.00	6.00	34.00	18.00	1.33	250.00	4.00	2.00	36.00	0.03	12.00	1.33	110.00	24.00	28.00	385	30.00	4.00	0.0400
07 1115	176	568	765	12.00	6.00	9.00	24.00	1.33	150.00	6.00	5.00	60.00	0.03	12.00	1.33	145.00	16.00	30.00	477	20.00	5.00	0.2700
07 1119	86	344	1070	20.00	14.00	9.00	20.00	1.33	330.00	9.00	0.67	30.00	0.03	5.00	1.33	86.00	14.00	22.00	322	16.00	5.00	0.0900
07 1124	198	437	684	3.00	13.00	12.00	24.00	1.33	160.00	6.00	2.00	36.00	0.03	11.00	1.33	92.00	16.00	37.00	320	28.00	6.00	0.2000
07 1162	49	547	603	8.00	6.00	15.00	18.00	1.33	32.00	5.00	6.00	62.00	0.03	62.00	1.33	100.00	195.00	16.00	367	19.00	0.67	0.9200

Appendix 3 Boddington Pisolitic Duricrust LT202

sampno	sample code	easting	northing	SiO2 wt%	Al2O3 wt%	Fe2O3 wt%	MgO wt%	CaO wt%	Na2O wt%	K2O wt%	TiO2 wt%	LOI wt%	TOTAL wt%
07-0378	LT202	10300	12925	0.6	41.75	38.32	0.010	0.030	0.010	0.02	3.05	15.90	99.71
07-0383	LT202	12490	12640	2.8	34.95	43.47	0.010	0.040	0.010	0.02	2.20	16.60	100.06
07-0385	LT202	10200	9580	1.9	42.69	30.46	0.010	0.030	0.002	0.02	2.20	23.60	100.92
07-0389	LT202	10100	9040	3.0	39.29	32.17	0.010	0.040	0.030	0.02	2.70	21.70	98.93
07-0403	LT202	9949	11649	1.7	47.98	24.31	0.010	0.030	0.010	0.02	3.19	23.50	100.73
07-0415	LT202	10098	12780	1.7	45.15	30.89	0.020	0.030	0.030	0.02	3.90	18.20	99.93
07-1079	LT202	10170	9640	1.2	40.10	35.40	0.030	0.050	0.020	0.02	2.50	20.60	99.90
07-1086	LT202	10170	9640	1.1	34.20	42.10	0.020	0.040	0.010	0.02	1.90	20.60	99.94
07-1091	LT202	10310	9400	2.4	44.50	31.10	0.020	0.050	0.002	0.02	2.52	19.30	99.87
07-1094	LT202	10310	9400	2.9	44.40	31.88	0.020	0.050	0.020	0.02	2.50	18.10	99.89
07-1099	LT202	10260	9470	1.6	45.50	25.75	0.020	0.040	0.002	0.02	2.59	24.40	99.90
07-1108	LT202	10020	13050	1.4	42.30	28.30	0.020	0.040	0.010	0.02	3.07	24.90	100.02
07-1110	LT202	10070	12975	0.8	43.66	30.59	0.030	0.040	0.010	0.02	5.20	19.20	99.50
07-1116	LT202	10260	12970	1.0	46.20	31.10	0.020	0.040	0.010	0.02	3.37	17.60	99.30
07-1118	LT202	10330	12900	3.4	39.80	30.92	0.020	0.040	0.002	0.02	2.49	22.20	98.90
07-1120	LT202	10260	12940	14.0	7.38	69.50	0.200	0.160	0.040	0.19	0.60	7.60	99.67

sampno	Mn ppm	Cr ppm	V ppm	Cu ppm	Pb ppm	Zn ppm	Ni ppm	Co ppm	As ppm	Sb ppm	Bi ppm	Mo ppm	Ag ppm	Sn ppm	Ge ppm	Ga ppm	W ppm	Ba ppm	Zr ppm	Nb ppm	Se ppm	Au ppm
07-0378	58	365	711	7	4	10	1.3	1.3	95	2	4	59	0.5	12	1.3	133	23	17	410	22	0.6	0.030
07-0383	42	352	490	109	14	11	1.3	1.3	62	0.6	0.6	12	0.03	13	1.3	71	21	11	440	19	0.6	0.270
07-0385	9	352	564	33	4	9	1.3	1.3	19	0.6	8	30	0.03	38	1.3	74	154	11	362	16	0.6	0.020
07-0389	25	272	764	87	10	8	11	1.3	13	0.6	8	46	0.03	71	1.3	57	151	11	344	17	0.6	0.100
07-0403	30	408	440	19	7	11	1.3	1.3	47	0.6	35	35	0.03	84	1.3	72	85	13	564	24	2	0.460
07-0415	99	334	626	16	7	18	1.3	1.3	123	4	9	41	0.5	17	1.3	93	31	25	532	26	0.6	0.050
07-1079	56	570	590	14	4	9	18	1.3	26	4	4	50	0.03	54	1.3	100	175	20	359	15	0.6	0.020
07-1086	49	576	623	24	9	8	18	1.3	19	0.6	5	70	0.2	56	1.3	100	180	23	459	13	3	0.130
07-1091	54	442	450	20	8	5	18	1.3	13	3	3	36	0.03	50	1.3	110	200	19	279	19	0.6	0.070
07-1094	56	471	498	13	9	6	20	1.3	20	2	2	40	0.03	54	1.3	100	230	9	279	18	0.6	0.150
07-1099	43	359	405	18	2	6	14	1.3	17	2	4	74	0.03	38	1.3	76	125	10	279	19	0.6	0.090
07-1108	62	407	648	10	0.6	3	14	1.3	410	7	3	64	0.03	13	1.3	74	30	15	397	22	3	0.080
07-1110	536	468	584	3	10	11	14	1.3	250	5	0.6	30	0.1	12	1.3	105	18	27	454	30	0.6	0.070
07-1116	223	402	516	6	3	6	18	1.3	125	5	3	26	0.03	11	1.3	94	22	9	354	22	3	0.040
07-1118	68	243	656	34	4	10	24	4	410	3	2	22	0.03	7	1.3	72	22	26	361	13	3	0.160
07-1120	1650	453	707	130	60	340	66	16	460	5	0.6	6	0.1	2	1.3	38	16	282	97	3	3	na

Appendix 4 Boddington Fragmental Duricrust LT205.

sampno	sample code	easting	northing	SiO2 wt%	Al2O3 wt%	Fe2O3 wt%	MgO wt%	CaO wt%	Na2O wt%	K2O wt%	TiO2 wt%	LOI wt%	TOTAL wt%
07-0344	LT205	10000	12150	1.1	42.69	27.03	0.010	0.020	0.010	0.02	2.74	26.40	99.97
07-0345	LT205	10000	12150	0.9	35.51	37.18	0.010	0.020	0.010	0.02	2.40	23.90	99.89
07-0356	LT205	10000	12150	3.0	23.42	53.77	0.030	0.040	0.030	0.19	1.68	18.30	100.46
07-0359	LT205	10240	12460	3.0	39.10	43.19	0.030	0.040	0.030	0.13	2.42	12.10	100.03
07-0360	LT205	10240	12460	0.6	48.17	21.31	0.010	0.050	0.010	0.02	2.77	27.40	100.36
07-0361	LT205	10240	12460	0.4	42.50	36.32	0.010	0.030	0.010	0.02	3.24	17.20	99.74
07-0362	LT205	10240	12460	0.6	34.19	42.90	0.010	0.120	0.010	0.02	4.22	18.00	100.09
07-0372	LT205	10220	13000	2.8	45.15	29.31	0.020	0.030	0.010	0.02	2.55	21.40	101.25
07-0386	LT205	10200	9580	1.5	48.74	20.59	0.010	0.020	0.003	0.02	1.87	27.00	99.73
07-0394	LT205	10130	9040	2.6	46.66	21.45	0.020	0.030	0.030	0.18	1.92	26.00	98.86
07-0416	LT205	10098	12780	3.2	50.63	16.16	0.060	0.020	0.010	0.40	2.62	27.10	100.21
07-0433	LT205	9799	10900	7.9	38.91	32.03	0.020	0.030	0.030	0.02	2.37	18.70	100.00
07-1080	LT205	10170	9640	1.8	39.40	34.06	0.020	0.040	0.010	0.02	1.94	22.70	100.00
07-1081	LT205	10170	9640	1.8	41.10	29.90	0.020	0.040	0.010	0.02	1.79	25.30	100.04
07-1082	LT205	10170	9640	0.9	44.20	25.32	0.010	0.020	0.010	0.02	1.65	27.60	99.73
07-1083	LT205	10170	9640	0.7	49.40	18.61	0.010	0.030	0.003	0.02	1.67	29.00	99.39
07-1084	LT205	10170	9640	1.3	49.40	17.91	0.030	0.030	0.003	0.09	1.97	29.10	99.82
07-1085	LT205	10170	9640	0.9	46.20	22.10	0.010	0.030	0.003	0.02	1.72	28.50	99.50
07-1088	LT205	10170	9640	1.3	40.30	31.70	0.020	0.040	0.003	0.02	1.55	24.90	99.82
07-1089	LT205	10310	9400	42.9	19.10	25.76	0.090	0.040	0.050	0.13	1.47	10.50	100.04
07-1092	LT205	10310	9400	3.1	44.71	24.90	0.010	0.030	0.003	0.02	2.15	24.80	99.65
07-1093	LT205	10310	9400	3.7	43.70	25.90	0.020	0.030	0.003	0.02	2.30	24.20	99.87
07-1100	LT205	10260	9470	2.6	43.30	25.41	0.020	0.030	0.003	0.02	1.97	26.60	99.90
07-1101	LT205	10260	9470	5.6	41.60	25.00	0.040	0.020	0.003	0.11	1.95	25.50	99.84
07-1102	LT205	10260	9470	1.3	47.10	22.50	0.030	0.020	0.003	0.09	1.59	27.30	99.94
07-1106	LT205	10020	13050	1.5	47.20	20.58	0.020	0.030	0.003	0.02	2.85	27.80	99.98
07-1107	LT205	10020	13050	0.9	46.69	21.69	0.020	0.020	0.003	0.02	2.19	27.90	99.37
07-1112	LT205	10070	12975	0.4	30.60	41.59	0.020	0.030	0.003	0.02	5.47	21.50	99.61
07-1117	LT205	10260	12970	1.8	47.00	24.71	0.020	0.040	0.003	0.02	3.89	22.60	100.00
07-1121	LT205	10220	9620	12.1	49.20	8.87	0.010	0.030	0.003	0.02	1.64	28.00	99.84

Appendix 4 Boddington Fragmental Duricrust LT205.

sampno	Mn	Cr	V	Cu	Pb	Zn	Ni	Co	As	Sb	Bi	Mo	Ag	Sn	Ge	Ga	W	Ba	Zr	Nb	Se	Au
	ppm	ppm	ppm	ppm	ppm	ppm	ppm	ppm	ppm	ppm	ppm	ppm	ppm	ppm	ppm	ppm	ppm	ppm	ppm	ppm	ppm	ppm
07-0344	93	211	599	41.00	2.00	12.00	1.33	6.00	76.00	0.67	0.67	11.00	0.03	3.00	1.33	46.00	1.33	1.67	247	11.00	3.00	0.4300
07-0345	95	220	821	98.00	3.00	11.00	1.33	1.33	29.00	2.00	0.67	4.00	0.03	4.00	1.33	42.00	1.33	1.67	241	14.00	9.00	1.7500
07-0356	19	113	169	279.00	6.00	11.00	1.33	1.33	26.00	3.00	3.00	10.00	0.03	2.00	1.33	43.00	6.00	64.00	424	13.00	5.00	5.0200
07-0359	94	446	781	12.00	14.00	13.00	15.00	7.00	106.00	0.67	4.00	40.00	0.03	11.00	1.33	79.00	17.00	42.00	405	20.00	0.67	0.1000
07-0360	16	265	433	35.00	0.67	14.00	1.33	8.00	112.00	2.00	4.00	54.00	0.03	18.00	1.33	61.00	48.00	33.00	278	21.00	0.67	0.5800
07-0361	67	343	635	8.00	4.00	11.00	1.33	8.00	61.00	0.67	3.00	30.00	0.03	16.00	1.33	92.00	31.00	13.00	382	24.00	0.67	0.0800
07-0362	113	419	1010	11.00	6.00	9.00	1.33	7.00	141.00	0.67	3.00	47.00	0.03	19.00	1.33	78.00	22.00	12.00	414	25.00	2.00	0.0200
07-0372	26	355	571	9.00	7.00	10.00	1.33	1.33	299.00	0.67	0.67	44.00	0.03	13.00	1.33	73.00	8.00	26.00	421	28.00	0.67	0.1100
07-0386	5	289	389	34.00	2.00	11.00	1.33	1.33	19.00	0.67	5.00	45.00	0.03	23.00	1.33	74.00	106.00	12.00	278	16.00	0.67	0.8000
07-0394	23	252	431	90.00	5.00	9.00	1.33	1.33	18.00	0.67	5.00	18.00	0.03	33.00	1.33	50.00	65.00	34.00	284	19.00	0.67	0.1800
07-0416	11	286	361	58.00	0.67	12.00	1.33	1.33	89.00	4.00	14.00	34.00	0.03	25.00	1.33	68.00	41.00	109.00	454	20.00	0.67	0.2500
07-0433	34	251	699	308.00	14.00	8.00	1.33	1.33	78.00	0.67	8.00	88.00	0.50	35.00	1.33	78.00	57.00	19.00	420	17.00	3.00	1.0100
07 1080	75	463	535	22.00	4.00	5.00	16.00	1.33	20.00	4.00	7.00	58.00	0.40	46.00	1.33	76.00	190.00	20.00	468	12.00	0.67	0.0800
07 1081	55	392	488	26.00	7.00	15.00	20.00	1.33	24.00	3.00	5.00	56.00	0.03	46.00	1.33	80.00	175.00	21.00	444	13.00	2.00	0.1100
07 1082	32	327	447	40.00	0.67	9.00	16.00	1.33	17.00	2.00	6.00	54.00	0.03	46.00	1.33	76.00	155.00	5.00	666	11.00	3.00	0.3100
07 1083	20	304	322	30.00	5.00	8.00	14.00	1.33	12.00	0.67	0.67	34.00	0.03	56.00	1.33	70.00	160.00	26.00	605	13.00	0.67	0.4100
07 1084	42	297	279	24.00	7.00	7.00	14.00	1.33	13.00	3.00	7.00	28.00	0.03	52.00	1.33	78.00	120.00	45.00	436	14.00	0.67	0.5000
07 1085	20	357	331	56.00	8.00	6.00	14.00	1.33	11.00	0.67	4.00	54.00	0.03	58.00	1.33	86.00	160.00	10.00	556	11.00	0.67	0.0800
07 1088	30	349	417	40.00	8.00	9.00	16.00	1.33	12.00	2.00	6.00	34.00	0.03	46.00	1.33	68.00	145.00	16.00	618	11.00	5.00	0.2300
07 1089	161	399	1269	34.00	78.00	14.00	30.00	4.00	68.00	5.00	10.00	3.00	0.10	2.00	1.33	56.00	4.00	606.00	212	8.00	8.00	na
07 1092	36	379	383	26.00	5.00	4.00	16.00	1.33	13.00	2.00	3.00	38.00	0.03	48.00	1.33	84.00	190.00	5.00	256	16.00	0.67	0.1400
07 1093	35	400	438	20.00	5.00	7.00	12.00	1.33	14.00	3.00	5.00	44.00	0.03	48.00	1.33	78.00	195.00	1.67	270	17.00	0.67	0.1700
07 1100	28	384	424	34.00	8.00	13.00	16.00	1.33	20.00	6.00	7.00	130.00	0.03	38.00	1.33	68.00	120.00	24.00	494	13.00	0.67	1.4500
07 1101	42	420	403	26.00	2.00	6.00	16.00	1.33	26.00	0.67	5.00	60.00	0.03	38.00	1.33	70.00	86.00	32.00	371	13.00	0.67	0.5100
07 1102	21	316	343	48.00	6.00	8.00	10.00	1.33	18.00	0.67	4.00	58.00	0.03	42.00	1.33	70.00	150.00	53.00	390	11.00	2.00	2.3100
07 1106	54	393	426	28.00	0.67	5.00	10.00	1.33	340.00	8.00	2.00	32.00	0.20	15.00	1.33	76.00	18.00	13.00	392	20.00	2.00	0.1100
07 1107	37	404	430	12.00	0.67	6.00	12.00	1.33	370.00	4.00	4.00	42.00	0.20	11.00	1.33	56.00	16.00	20.00	468	14.00	6.00	0.2600
07 1112	1017	435	791	46.00	17.00	24.00	20.00	1.33	280.00	3.00	0.67	26.00	0.50	7.00	1.33	70.00	8.00	32.00	478	24.00	0.67	0.5300
07 1117	193	351	467	8.00	0.67	7.00	16.00	1.33	180.00	0.67	5.00	22.00	0.10	16.00	1.33	76.00	26.00	20.00	388	24.00	4.00	0.1700
07 1121	76	290	221	22.00	0.67	11.00	16.00	4.00	7.00	0.67	5.00	22.00	0.03	34.00	1.33	60.00	105.00	17.00	309	12.00	0.67	0.6700

Appendix 5 Boddington Bauxite Zone bz.

sampno	sam. type	easting	northing	SiO2 wt%	Al2O3 wt%	Fe2O3 wt%	MgO wt%	CaO wt%	Na2O wt%	K2O wt%	TiO2 wt%	LOI wt%	TOTAL wt%
07-0346	bz	10000	12150	1.1	30.41	43.61	0.010	0.020	0.010	0.02	2.47	22.40	100.00
07-0347	bz	10000	12150	4.7	32.49	37.75	0.010	0.020	0.040	0.02	2.65	22.30	99.97
07-0348	bz	10000	12150	1.9	30.41	42.61	0.010	0.003	0.050	0.02	2.92	22.20	100.12
07-0373	bz	10215	13000	1.1	50.44	20.31	0.020	0.020	0.010	0.12	1.78	27.80	101.57
07-0376	bz	10215	13000	0.4	52.14	15.73	0.010	0.020	0.010	0.02	1.35	29.60	99.29
07-0387	bz	10200	9580	4.5	47.41	17.30	0.010	0.020	0.003	0.08	1.45	27.00	97.76
07-0388	bz	10100	9040	2.6	38.16	35.61	0.010	0.030	0.030	0.02	1.73	21.60	99.74
07-0393	bz	10130	9040	4.1	41.94	27.88	0.020	0.030	0.030	0.23	1.62	23.50	99.31
07-0399	bz	10180	9040	12.4	33.06	35.89	0.030	0.140	0.030	0.02	2.75	16.60	100.91
07-0404	bz	9949	11649	8.1	47.22	15.01	0.040	0.020	0.030	0.10	2.25	26.10	98.87
07-0417	bz	10098	12780	4.5	49.30	17.30	0.030	0.020	0.010	0.18	2.59	26.60	100.52
07-1090	bz	10310	9400	9.2	43.00	19.85	0.030	0.040	0.020	0.02	2.24	25.50	99.92
07-1103	bz	10260	9470	7.3	45.80	18.38	0.170	0.040	0.040	0.19	1.59	26.40	99.92
07-1104	bz	10260	9470	20.1	36.00	20.52	0.120	0.020	0.020	0.54	1.27	21.50	100.09
07-1105	bz	10260	9470	85.3	7.85	2.93	0.250	0.003	0.030	1.24	0.43	2.01	100.03
07-1113	bz	10070	12975	1.3	19.10	55.00	0.050	0.050	0.010	0.02	8.47	15.70	99.66
07-1123	bz	10250	9500	1.9	52.10	13.87	0.020	0.020	0.003	0.08	1.52	30.30	99.79

sampno	Mn ppm	Cr ppm	V ppm	Cu ppm	Pb ppm	Zn ppm	Ni ppm	Co ppm	As ppm	Sb ppm	Bi ppm	Mo ppm	Ag ppm	Sn ppm	Ge ppm	Ga ppm	W ppm	Ba ppm	Zr ppm	Nb ppm	Se ppm	Au ppm
07-0346	94	177	912	98.00	3.00	10.00	1.33	1.33	51.0	4.00	0.67	1.0	0.03	1.0	1.33	47.0	6.00	1.67	161	11.00	4.00	0.4200
07-0347	103	198	760	99.00	3.00	13.00	1.33	1.33	63.0	2.00	0.67	9.0	0.03	6.0	1.33	48.0	5.00	1.67	218	13.00	7.00	0.5300
07-0348	92	217	917	124.00	6.00	11.00	1.33	1.33	116.0	4.00	0.67	7.0	0.03	3.0	1.33	52.0	6.00	1.67	228	10.00	8.00	0.8100
07-0373	9	331	484	21.00	3.00	12.00	1.33	1.33	304.0	4.00	4.00	19.0	0.03	19.0	1.33	65.0	30.00	39.00	341	15.00	3.00	2.3100
07-0376	2	357	288	26.00	0.67	15.00	1.33	1.33	295.0	4.00	2.00	14.0	0.03	7.0	1.33	41.0	10.00	23.00	469	9.00	0.67	1.2400
07-0387	5	230	350	36.00	0.67	11.00	1.33	1.33	11.0	0.67	4.00	20.0	0.03	36.0	1.33	63.0	129.00	57.00	317	14.00	0.67	0.2300
07-0388	11	276	775	115.00	14.00	6.00	1.33	1.33	12.0	0.67	16.00	56.0	0.03	79.0	1.33	46.0	169.00	15.00	382	14.00	0.67	0.3100
07-0393	13	315	550	125.00	8.00	9.00	1.33	1.33	40.0	0.67	0.67	17.0	0.03	35.0	1.33	61.0	149.00	43.00	331	10.00	0.67	0.4000
07-0399	121	243	872	134.00	13.00	9.00	21.00	1.33	10.0	0.67	4.00	25.0	0.03	10.0	1.33	50.0	16.00	21.00	365	21.00	0.67	0.0800
07-0404	15	340	283	36.00	0.67	13.00	1.33	1.33	40.0	0.67	25.00	14.0	0.03	72.0	1.33	59.0	43.00	30.00	497	21.00	0.67	0.5600
07-0417	5	490	369	66.00	0.67	11.00	1.33	1.33	109.0	0.67	13.00	15.0	0.03	18.0	1.33	80.0	17.00	75.00	462	22.00	4.00	9.1000
07 1090	36	350	276	74.00	4.00	6.00	26.00	1.33	5.0	0.67	24.00	11.0	0.03	46.0	1.33	80.0	185.00	39.00	299	13.00	0.67	0.0500
07 1103	49	523	261	64.00	0.67	7.00	8.00	1.33	28.0	2.00	6.00	56.0	0.03	20.0	1.33	58.0	98.00	53.00	267	14.00	0.67	2.1100
07 1104	39	483	301	58.00	0.67	9.00	14.00	1.33	20.0	0.67	7.00	50.0	0.03	15.0	1.33	56.0	100.00	144.00	316	8.00	3.00	6.2400
07 1105	18	75	51	17.00	0.67	5.00	4.00	1.33	5.0	0.67	3.00	5.0	0.10	6.0	1.33	22.0	20.00	280.00	153	4.00	3.00	1.9200
07 1113	2085	403	997	38.00	32.00	40.00	18.00	6.00	72.0	6.00	6.00	4.0	0.03	3.0	4.00	60.0	4.00	64.00	240	34.00	11.00	0.6500
07 1123	28	384	235	46.00	0.67	7.00	12.00	1.33	7.0	3.00	5.00	120.0	0.03	18.0	1.33	58.0	52.00	38.00	351	10.00	0.67	6.2600

Appendix 6 Boddington saprolite sap.

sampno	samtype	easting	northing	SiO2	Al2O3	Fe2O3	MgO	CaO	Na2O	K2O	TiO2	LOI	TOTAL
				wt%	wt%	wt%	wt%	wt%	wt%	wt%	wt%	wt%	wt%
07-0349	cz	10000	12150	25.2	27.20	32.03	0.030	0.010	0.010	0.02	2.40	13.50	100.42
07-0350	cz	10000	12150	6.2	30.22	40.47	0.010	0.020	0.030	0.02	3.00	20.70	100.55
07-0351	Fe-sap	10000	12150	26.5	31.55	22.88	0.030	0.030	0.320	0.02	2.07	16.50	99.90
07-0352	Fe-sap	10000	12150	2.1	38.16	32.89	0.030	0.040	0.070	0.02	2.32	24.00	99.65
07-0353	lsap	10000	12150	44.3	28.71	15.30	0.050	0.040	0.110	0.02	1.27	12.80	102.56
07-0354	lsap	10000	12150	16.7	29.47	33.60	0.040	0.040	0.470	0.02	2.80	17.20	100.31
07-0355	lsap	10000	12150	50.5	30.04	9.62	0.060	0.020	0.200	0.24	1.22	12.10	103.98
07-0364	cz	10180	12460	1.9	51.95	17.16	0.020	0.020	0.010	0.17	2.37	28.40	102.03
07-0365	cz	10180	12460	40.2	34.19	11.17	0.060	0.020	0.070	0.33	1.83	13.60	101.48
07-0366	cz	10180	12460	14.6	50.44	8.81	0.080	0.010	0.030	0.65	1.40	25.10	101.07
07-0367	usap	10180	12460	15.4	18.10	51.62	0.020	0.040	0.030	0.11	0.27	14.40	99.99
07-0368	usap	10180	12460	47.7	33.62	5.25	0.030	0.030	0.090	0.13	0.77	13.30	100.92
07-0369	usap	10180	12460	34.0	41.94	3.85	0.110	0.030	0.050	0.82	1.28	17.40	99.49
07-0370	lsap	10180	12460	41.9	35.32	3.55	0.020	0.040	0.030	0.02	7.54	13.10	101.52
07-0375	cz	10215	13000	15.8	40.42	20.45	0.070	0.020	0.050	0.46	2.67	20.80	100.77
07-0391	cz	10100	9040	4.9	32.49	41.33	0.010	0.030	0.030	0.02	1.27	19.70	99.78
07-0392	cz	10130	9040	27.4	31.74	22.16	0.300	0.040	0.120	4.12	1.88	11.80	99.54
07-0396	cz	10180	9040	9.0	32.87	33.60	0.050	0.080	0.050	0.02	3.02	20.70	99.35
07-0397	lsap	10180	9040	23.3	23.61	36.46	0.030	0.050	0.110	0.02	3.09	13.20	99.87
07-0398	cz	10180	9040	11.1	35.70	40.04	0.050	0.280	0.040	0.11	2.44	9.74	99.52
07-0405	cz	9949	11649	34.9	33.25	19.30	0.110	0.020	0.080	0.70	2.19	13.20	103.72
07-0406	cz	9949	11649	37.2	31.74	15.16	0.110	0.030	0.110	0.67	2.29	12.70	100.03
07-0407	cz	9949	11649	34.9	31.17	18.73	0.030	0.020	0.110	0.10	1.22	13.50	99.75
07-0408	usap	9949	11649	17.5	47.98	8.18	0.020	0.010	0.080	0.08	1.67	24.10	99.66
07-0409	lsap	9949	11649	51.8	29.09	6.18	0.050	0.020	0.110	0.14	0.92	11.40	99.67
07-0410	lsap	9949	11649	62.0	22.10	4.70	0.530	0.130	0.120	0.59	0.77	8.14	99.11
07-0418	cz	10098	12780	12.4	26.63	43.47	0.050	0.030	0.040	0.27	1.87	15.80	100.57
07-0419	usap	10098	12780	37.4	36.84	11.41	0.060	0.020	0.110	0.40	1.65	14.50	102.42
07-0420	usap	10098	12780	51.3	32.68	7.46	0.050	0.020	0.120	0.19	1.10	12.10	105.06
07-0421	lsap	10098	12780	55.8	25.69	7.05	1.080	0.200	0.300	1.23	0.93	9.44	101.75
07-0423	cz	9550	11098	29.3	28.15	28.46	0.070	0.050	0.050	0.20	3.57	11.70	101.55
07-0424	cz	9550	11098	36.6	19.08	30.89	0.050	0.040	0.070	0.12	4.09	8.98	99.90
07-0425	cz	9550	11098	66.1	19.65	5.19	0.050	0.030	0.080	0.10	2.22	7.56	100.98
07-0426	cz	9550	11098	65.2	8.05	23.88	0.040	0.040	0.030	0.12	0.25	5.78	103.43
07-0427	usap	9550	11098	71.2	21.72	1.62	0.200	0.040	0.040	0.90	0.65	7.02	103.42
07-0428	usap	9550	11098	62.5	8.76	1.36	0.130	0.040	0.030	0.71	0.25	6.14	79.88
07-0429	lsap	9550	11098	70.2	17.30	3.85	0.200	0.030	0.070	0.72	0.58	6.45	99.36
07-0430	lsap	9550	11098	67.6	17.74	4.25	1.130	0.910	0.430	1.02	0.70	5.52	99.29
07-0431	sr	9550	11098	72.7	15.70	6.43	1.160	0.510	0.260	1.45	0.52	5.03	103.79
07-0434	cz	9799	10900	68.0	23.23	1.37	0.090	0.040	0.030	0.59	0.78	7.88	102.03
07-0435	lsap	9799	10900	65.5	22.29	5.09	0.470	0.040	0.040	0.81	0.77	7.91	102.87
07-0436	lsap	9799	10900	62.2	20.97	6.58	1.120	0.130	0.090	1.30	0.70	7.46	100.59
07-0438	lsap	9799	10900	66.7	21.16	5.43	1.150	0.250	0.260	1.12	0.70	6.89	103.70
07-1114	cz	10040	13040	35.5	38.10	17.50	0.300	0.040	0.240	1.01	1.95	9.90	104.54
07-1122	cz	10160	9550	47.4	33.10	9.80	0.040	0.020	0.030	0.09	1.07	8.50	100.05

Appendix 6 Boddington saprolite sap.

sampno	Mn ppm	Cr ppm	V ppm	Cu ppm	Pb ppm	Zn ppm	Ni ppm	Co ppm	As ppm	Sb ppm	Bi ppm	Mo ppm	Ag ppm	Sn ppm	Ge ppm	Ga ppm	W ppm	Ba ppm	Zr ppm	Nb ppm	Se ppm	Au ppm
07-0349	134	129	737	263	1.6	22.0	27.0	6.0	32.0	2.0	1.6	4.0	0.03	1.6	1.3	36.0	4.0	1.6	174.0	7.0	4.0	0.060
07-0350	127	127	806	112	3.0	13.0	1.3	6.0	13.0	1.6	1.6	<1	0.03	4.0	1.3	44.0	1.3	1.6	149.0	6.0	2.0	0.060
07-0351	22	267	379	144	1.6	15.0	48.0	9.0	58.0	2.0	1.6	4.0	0.03	4.0	1.3	45.0	6.0	8.0	208.0	14.0	4.0	0.040
07-0352	123	119	688	104	3.0	12.0	1.3	1.3	10.0	2.0	1.6	1.0	0.03	1.6	1.3	35.0	1.3	1.6	158.0	6.0	2.0	0.020
07-0353	54	89	301	122	1.6	15.0	40.0	1.3	8.0	2.0	1.6	2.0	0.03	1.6	4.0	22.0	1.3	11.0	106.0	6.0	4.0	0.150
07-0354	87	159	669	194	6.0	18.0	24.0	1.3	14.0	3.0	1.6	2.0	0.03	3.0	1.3	36.0	1.3	12.0	193.0	11.0	2.0	0.060
07-0355	7	227	163	222	3.0	14.0	48.0	6.0	24.0	1.6	1.6	10.0	0.03	3.0	1.3	30.0	21.0	92.0	205.0	12.0	2.0	0.200
07-0364	9	423	382	34	1.6	14.0	1.3	8.0	163.0	1.6	3.0	11.0	0.03	16.0	1.3	72.0	23.0	58.0	372.0	22.0	3.0	0.920
07-0365	13	87	202	115	1.6	21.0	47.0	11.0	87.0	2.0	5.0	13.0	0.03	9.0	4.0	57.0	9.0	139.0	314.0	19.0	1.6	0.840
07-0366	5	274	232	89	1.6	15.0	38.0	8.0	32.0	2.0	1.6	19.0	0.03	42.0	1.3	38.0	21.0	143.0	254.0	12.0	1.6	0.980
07-0367	91	97	103	186	6.0	32.0	33.0	6.0	41.0	1.6	1.6	26.0	0.03	1.6	1.3	11.0	9.0	19.0	101.0	0.7	1.6	0.250
07-0368	7	81	97	96	1.6	12.0	28.0	1.3	1.6	1.6	1.6	53.0	0.03	4.0	1.3	24.0	1.3	34.0	117.0	6.0	1.6	2.460
07-0369	3	86	156	63	6.0	30.0	37.0	8.0	18.0	1.6	1.6	11.0	0.03	18.0	1.3	38.0	9.0	700.0	209.0	14.0	1.6	0.170
07-0370	384	118	542	10	9.0	69.0	19.0	14.0	1.6	1.6	1.6	3.0	0.03	4.0	1.3	45.0	1.3	1020.0	204.0	43.0	1.6	0.030
07-0375	5	235	297	79	1.6	16.0	18.0	6.0	564.0	6.0	3.0	28.0	0.03	7.0	1.3	82.0	27.0	220.0	391.0	20.0	1.6	3.370
07-0391	4	507	597	314	5.0	2.0	12.0	1.3	6.0	1.6	5.0	113.0	0.03	55.0	1.3	46.0	322.0	17.0	503.0	11.0	1.6	2.460
07-0392	32	417	392	155	4.0	12.0	35.0	1.3	187.0	1.6	1.6	24.0	0.03	21.0	1.3	56.0	155.0	662.0	457.0	11.0	1.6	5.120
07-0396	208	225	836	210	1.6	10.0	1.3	1.3	12.0	1.6	1.6	1.0	0.03	1.6	1.3	41.0	7.0	1.6	263.0	13.0	1.6	0.130
07-0397	149	227	840	309	7.0	9.0	15.0	1.3	1.6	1.6	1.6	5.0	0.03	3.0	1.3	36.0	1.3	1.6	228.0	12.0	3.0	0.100
07-0398	179	323	735	20	22.0	10.0	22.0	1.3	11.0	1.6	1.6	18.0	0.03	24.0	1.3	67.0	46.0	35.0	488.0	21.0	1.6	0.010
07-0405	10	490	324	76	1.6	25.0	48.0	8.0	70.0	1.6	26.0	13.0	0.03	55.0	4.0	53.0	79.0	152.0	494.0	15.0	1.6	3.060
07-0406	9	385	253	106	1.6	30.0	58.0	7.0	63.0	1.6	17.0	11.0	0.03	70.0	4.0	58.0	59.0	154.0	506.0	24.0	1.6	1.700
07-0407	2	435	285	84	2.0	53.0	39.0	1.3	61.0	1.6	17.0	15.0	0.03	41.0	1.3	34.0	20.0	31.0	348.0	12.0	1.6	1.270
07-0408	4	325	208	107	1.6	35.0	40.0	1.3	28.0	1.6	7.0	21.0	0.03	38.0	1.3	42.0	24.0	27.0	210.0	17.0	1.6	0.170
07-0409	15	97	121	191	14.0	113.0	65.0	1.3	13.0	1.6	5.0	9.0	0.03	20.0	1.3	24.0	6.0	56.0	170.0	10.0	1.6	0.300
07-0410	227	62	86	566	5.0	98.0	31.0	10.0	1.6	1.6	3.0	2.0	0.03	11.0	1.3	23.0	12.0	104.0	179.0	7.0	1.6	0.010
07-0418	3	734	744	83	6.0	13.0	19.0	1.3	183.0	5.0	13.0	19.0	0.03	18.0	1.3	83.0	14.0	148.0	689.0	12.0	4.0	7.030
07-0419	17	246	193	204	4.0	26.0	77.0	7.0	48.0	1.6	10.0	39.0	0.03	12.0	1.3	38.0	15.0	231.0	301.0	12.0	1.6	3.750
07-0420	9	140	149	288	3.0	13.0	57.0	1.3	31.0	1.6	2.0	21.0	0.03	3.0	1.3	31.0	5.0	116.0	142.0	11.0	1.6	4.360
07-0421	1788	182	126	674	2.0	54.0	139.0	127.0	62.0	1.6	9.0	56.0	0.03	12.0	1.3	24.0	11.0	638.0	181.0	8.0	1.6	1.530
07-0423	306	232	562	316	14.0	24.0	87.0	19.0	43.0	1.6	5.0	33.0	0.50	23.0	1.3	51.0	15.0	67.0	472.0	16.0	1.6	0.220
07-0424	301	156	514	587	20.0	19.0	58.0	14.0	33.0	2.0	2.0	44.0	0.03	14.0	1.3	30.0	17.0	48.0	309.0	18.0	1.6	0.540
07-0425	82	100	266	372	7.0	22.0	53.0	7.0	20.0	1.6	5.0	26.0	0.03	27.0	5.0	26.0	19.0	54.0	241.0	17.0	1.6	2.990
07-0426	15	7	71	3310	9.0	116.0	114.0	15.0	94.0	1.6	23.0	87.0	0.03	65.0	1.3	10.0	27.0	46.0	48.0	4.0	15.0	12.000
07-0427	23	87	89	311	8.0	17.0	12.0	1.3	9.0	1.6	1.6	8.0	0.03	18.0	1.3	22.0	15.0	439.0	192.0	5.0	1.6	0.490
07-0428	50	7	106	125193	5.0	11.0	14.0	8.0	4.0	1.6	20.0	4.0	233.00	50.0	1.3	2.0	55.0	624.0	65.0	0.6	79.0	5.150
07-0429	37	59	123	4400	5.0	49.0	29.0	1.3	7.0	1.6	2.0	12.0	2.50	13.0	1.3	18.0	18.0	198.0	65.0	6.0	1.6	0.870
07-0430	328	74	94	6020	7.0	118.0	44.0	11.0	1.6	1.6	1.6	5.0	0.03	25.0	1.3	22.0	61.0	241.0	157.0	4.0	1.6	0.330
07-0431	234	7	72	3500	1.6	119.0	50.0	12.0	7.0	1.6	1.6	7.0	9.00	26.0	1.3	17.0	8.0	232.0	73.0	<2	3.0	0.240
07-0434	13	7	75	387	2.0	17.0	15.0	1.3	9.0	1.6	7.0	12.0	0.03	15.0	1.3	29.0	38.0	195.0	148.0	8.0	1.6	1.280
07-0435	107	7	90	3970	2.0	36.0	27.0	8.0	11.0	1.6	3.0	9.0	0.03	21.0	1.3	24.0	9.0	214.0	156.0	3.0	4.0	0.490
07-0436	255	116	83	6740	4.0	104.0	52.0	11.0	44.0	1.6	10.0	10.0	0.03	17.0	1.3	26.0	14.0	225.0	132.0	3.0	1.6	1.630
07-0438	235	65	85	2630	3.0	96.0	38.0	14.0	5.0	1.6	1.6	7.0	3.50	10.0	1.3	23.0	44.0	176.0	84.0	5.0	1.6	0.520
07 1114	86	389	258	150	4.0	14.0	50.0	4.0	350.0	6.0	2.0	9.0	0.03	5.0	1.3	38.0	42.0	731.0	235.0	7.0	2.0	0.250
07 1122	20	99	152	230	10.0	12.0	34.0	1.3	1.6	4.0	1.6	9.0	0.03	44.0	1.3	58.0	74.0	22.0	402.0	11.0	1.6	0.740

Appendix 7 Boddington Bedrock br.

sampno	samtype	easting	northing	SiO2 wt%	Al2O3 wt%	Fe2O3 wt%	MgO wt%	CaO wt%	Na2O wt%	K2O wt%	TiO2 wt%	LOI wt%	TOTAL wt%
07-0411	br	9949	11649	57.8	13.37	8.48	3.680	6.480	2.260	1.43	0.48	1.92	95.85
07-0422	br	10098	12780	61.2	17.47	4.86	2.300	6.280	3.940	1.42	0.72	0.87	99.04
07-0432	br	9550	11098	69.7	16.98	4.93	1.380	3.020	1.810	2.75	0.53	2.52	103.65
07-0437	br	9799	10900	63.7	17.51	6.08	1.610	4.380	3.180	2.42	0.62	0.95	100.49

sampno	Mn ppm	Cr ppm	V ppm	Cu ppm	Pb ppm	Zn ppm	Ni ppm	Co ppm	As ppm	Sb ppm	Bi ppm	Mo ppm	Ag ppm	Sn ppm	Ge ppm	Ga ppm	W ppm	Ba ppm	Zr ppm	Nb ppm	Se ppm	Au ppm
07-0411	865.0	53.0	73.0	2730.0	3.0	109.0	72.0	28.0	2.0	0.7	9.0	2.0	0.03	33.0	0.7	15.0	43.0	138.0	124.0	5.0	0.7	1.190
07-0422	516.0	126.0	91.0	92.0	4.0	52.0	91.0	18.0	44.0	0.7	0.7	8.0	0.03	46.0	0.7	20.0	10.0	284.0	120.0	3.0	0.7	0.930
07-0432	305.0	0.7	72.0	4850.0	8.0	71.0	35.0	13.0	2.0	0.7	0.7	8.0	9.00	15.0	0.7	20.0	1.3	577.0	37.0	0.7	26.0	0.290
07-0437	413.0	55.0	66.0	2570.0	2.0	118.0	41.0	17.0	0.7	0.7	0.7	3.0	0.50	24.0	0.7	19.0	1.3	283.0	109.0	0.7	2.0	0.450

APPENDIX 8
HISTOGRAMS

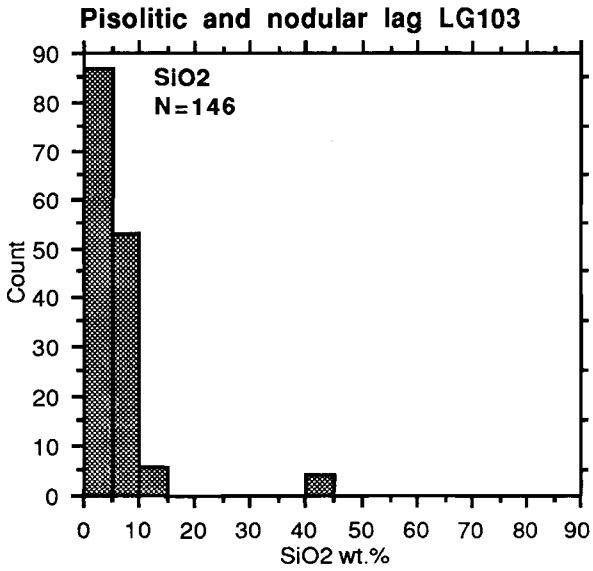
Pisolitic and nodular lag LG103
SiO2
N=146
Count
SiO2 wt.%

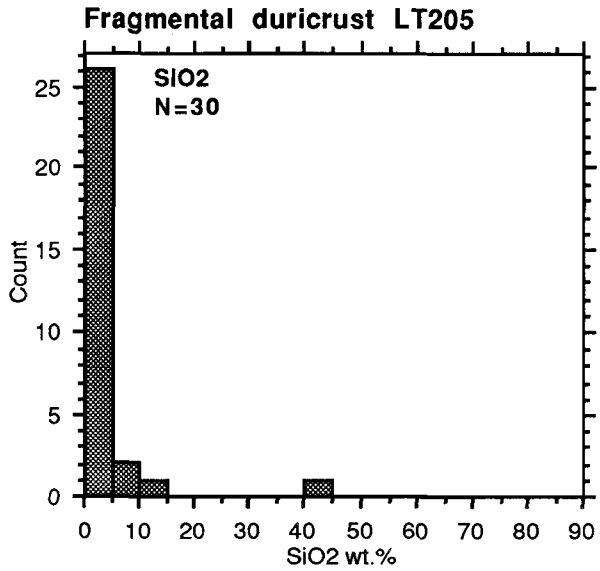
Fragmental duricrust LT205
SiO2
N=30
Count
SiO2 wt.%

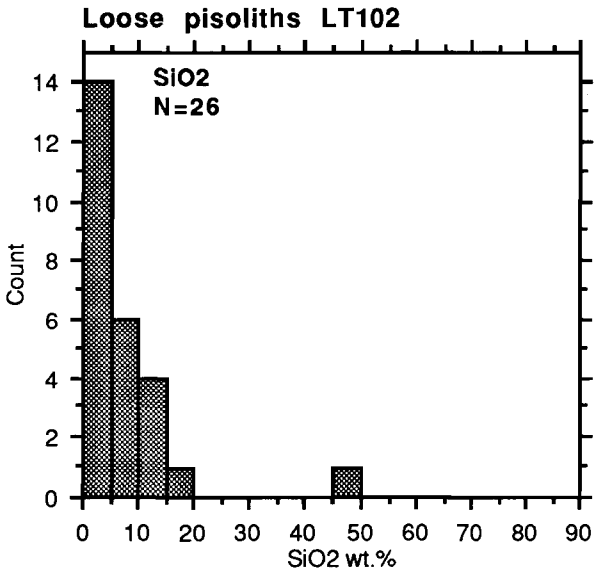
Loose pisoliths LT102
SiO2
N=26
Count
SiO2 wt.%

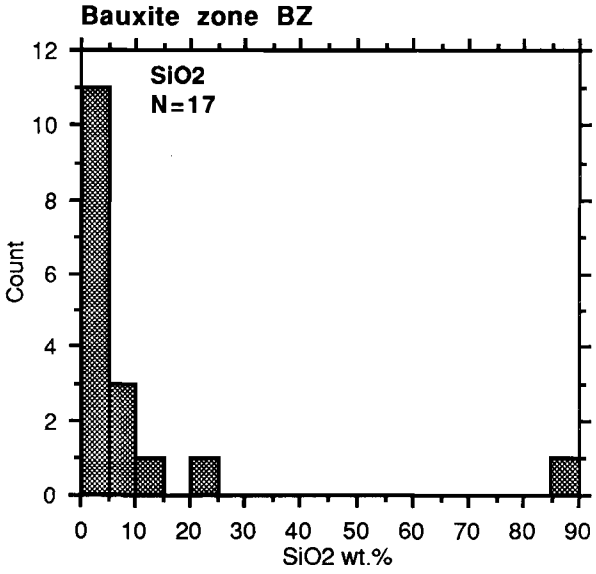
Bauxite zone BZ
SiO2
N=17
Count
SiO2 wt.%

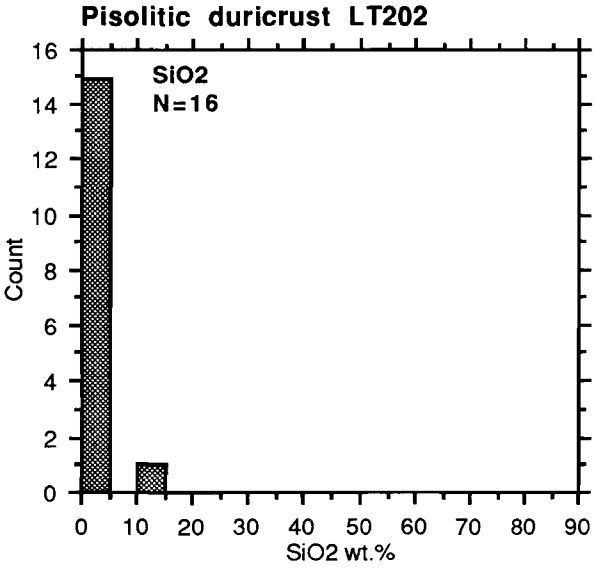
Pisolitic duricrust LT202
SiO2
N=16
Count
SiO2 wt.%

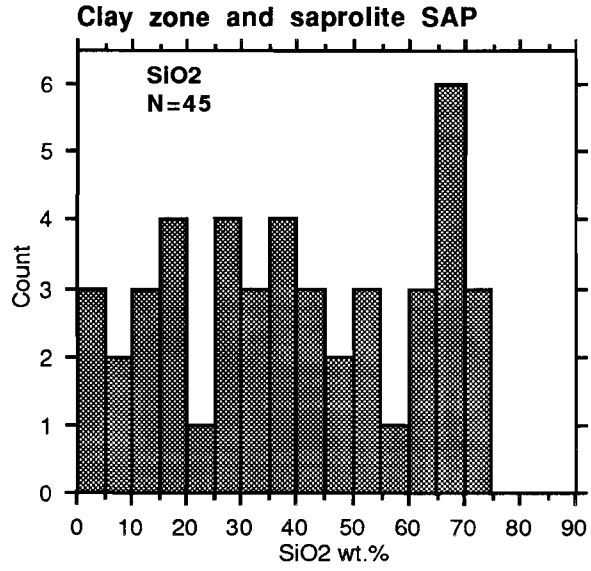
Clay zone and saprolite SAP
SiO2
N=45
Count
SiO2 wt.%

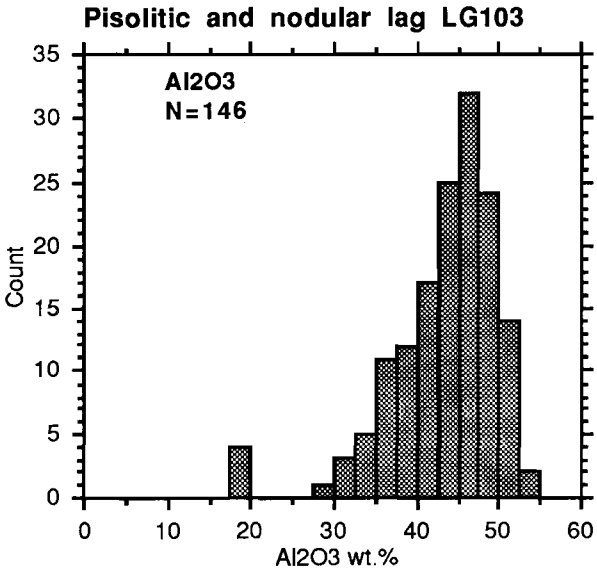
Pisolitic and nodular lag LG103
Al2O3
N=146
Count
Al2O3 wt.%

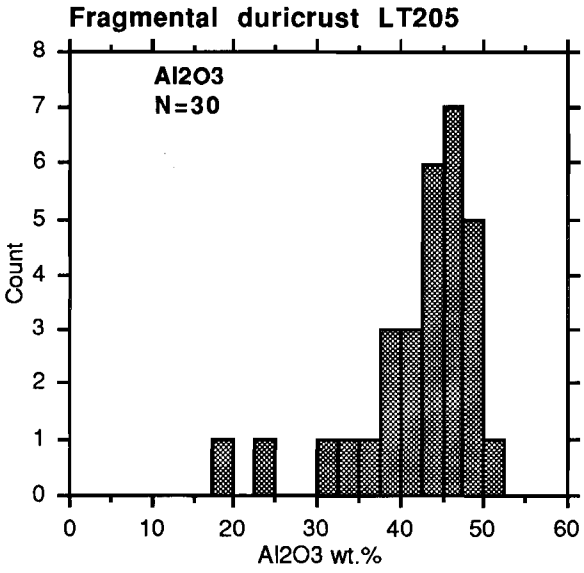
Fragmental duricrust LT205
Al2O3
N=30
Count
Al2O3 wt.%

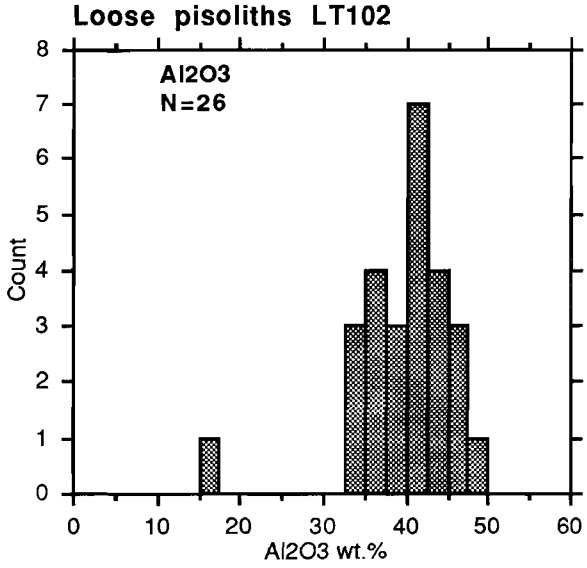
Loose pisoliths LT102
Al2O3
N=26
Count
Al2O3 wt.%

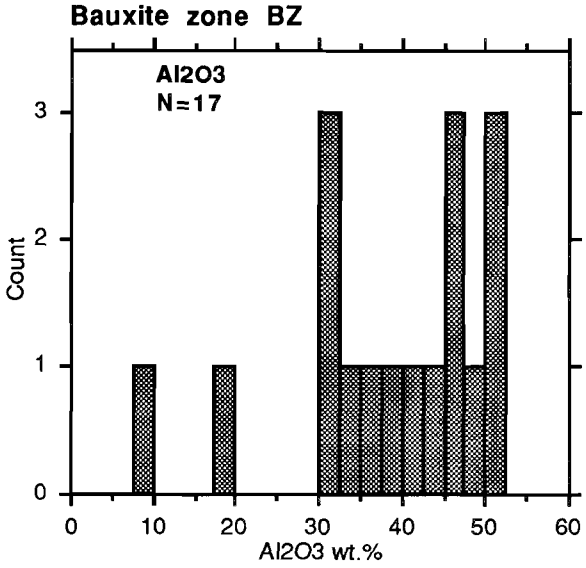
Bauxite zone BZ
Al2O3
N=17
Count
Al2O3 wt.%

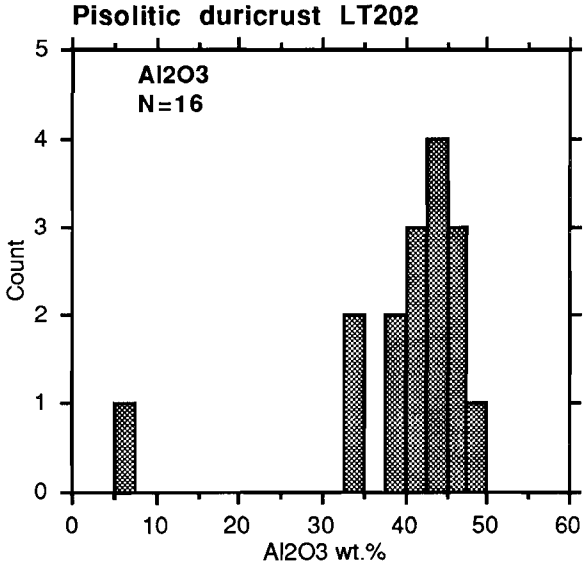
Pisolitic duricrust LT202
Al2O3
N=16
Count
Al2O3 wt.%

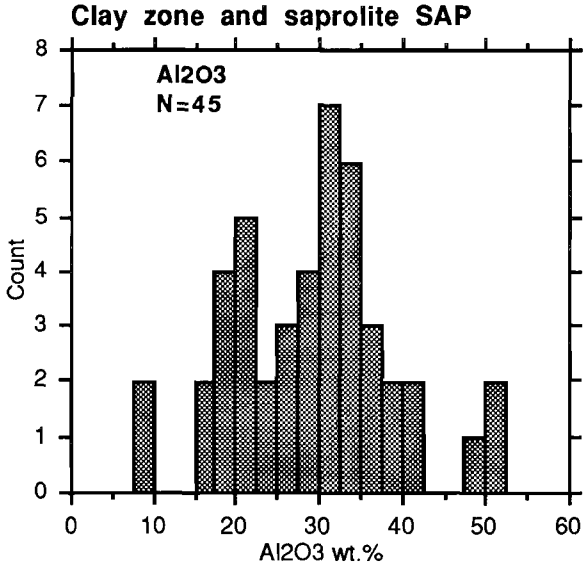
Clay zone and saprolite SAP
Al2O3
N=45
Count
Al2O3 wt.%

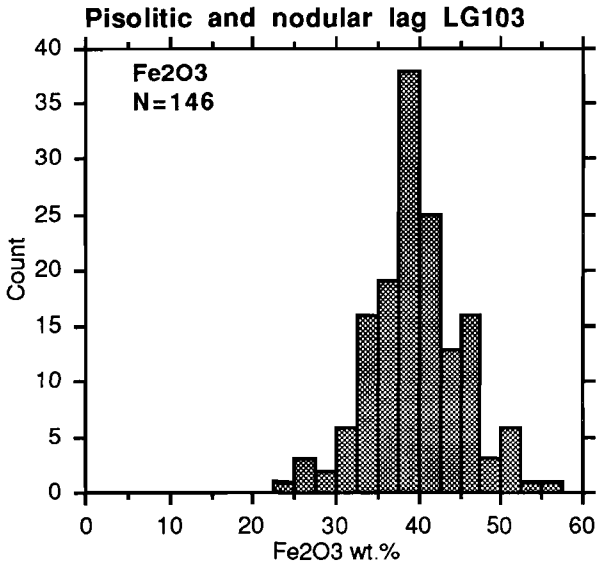
Pisolitic and nodular lag LG103
Fe2O3
N=146
Count
Fe2O3 wt.%

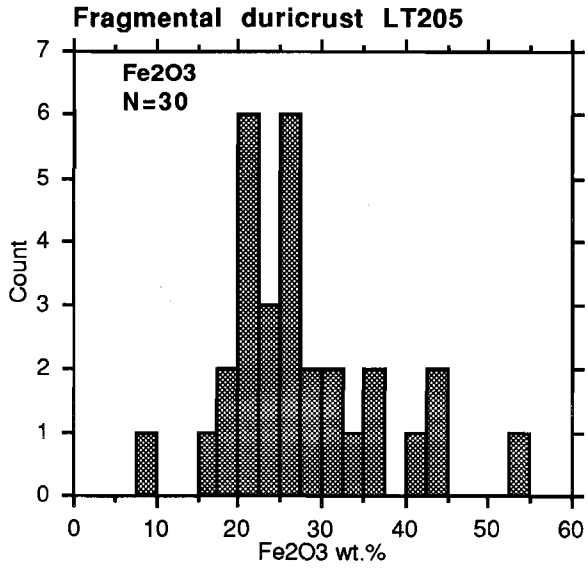
Fragmental duricrust LT205
Fe2O3
N=30
Count
Fe2O3 wt.%

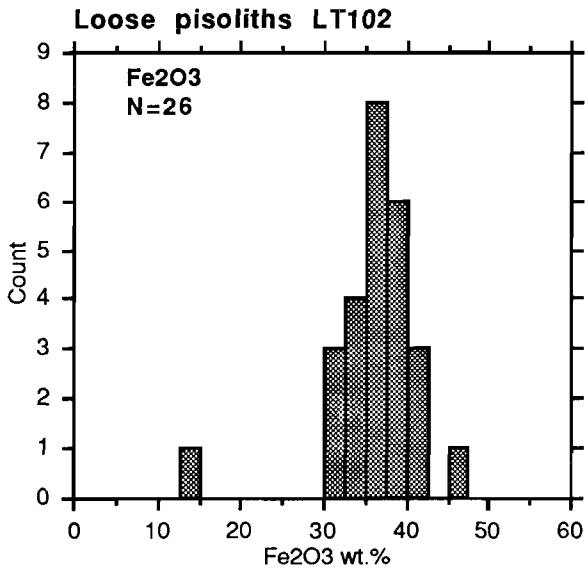
Loose pisoliths LT102
Fe2O3
N=26
Count
Fe2O3 wt.%

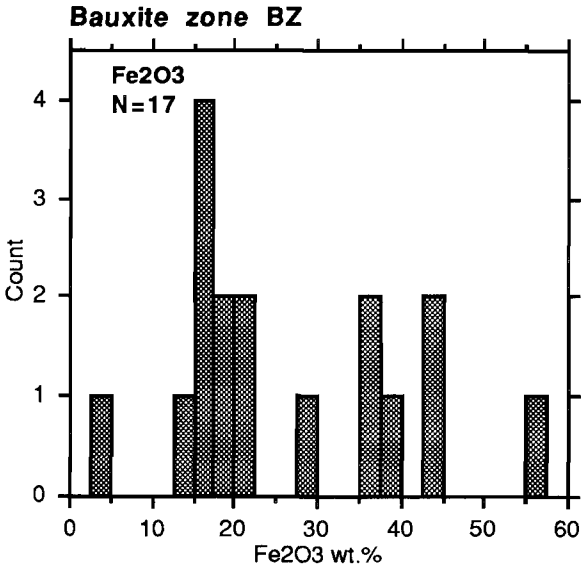
Bauxite zone BZ
Fe2O3
N=17
Count
Fe2O3 wt.%

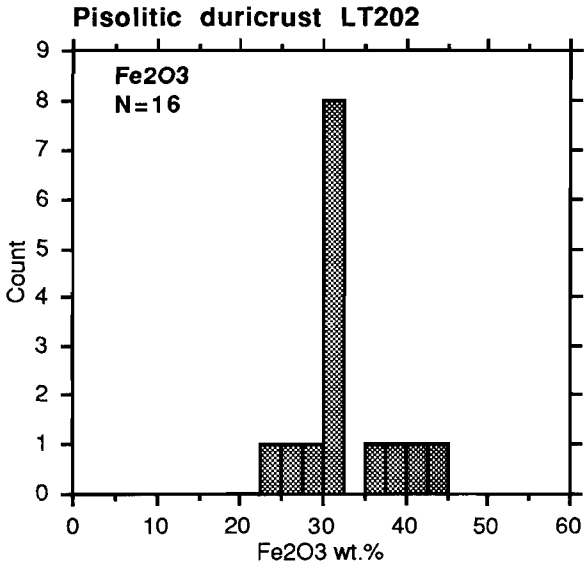
Pisolitic duricrust LT202
Fe2O3
N=16
Count
Fe2O3 wt.%

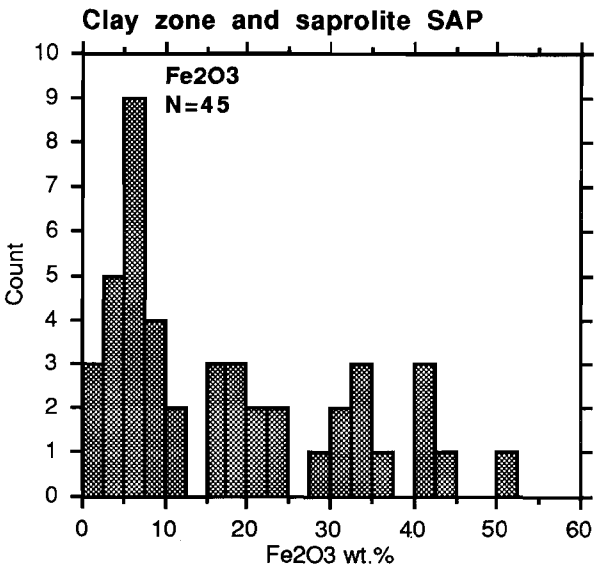
Clay zone and saprolite SAP
Fe2O3
N=45
Count
Fe2O3 wt.%

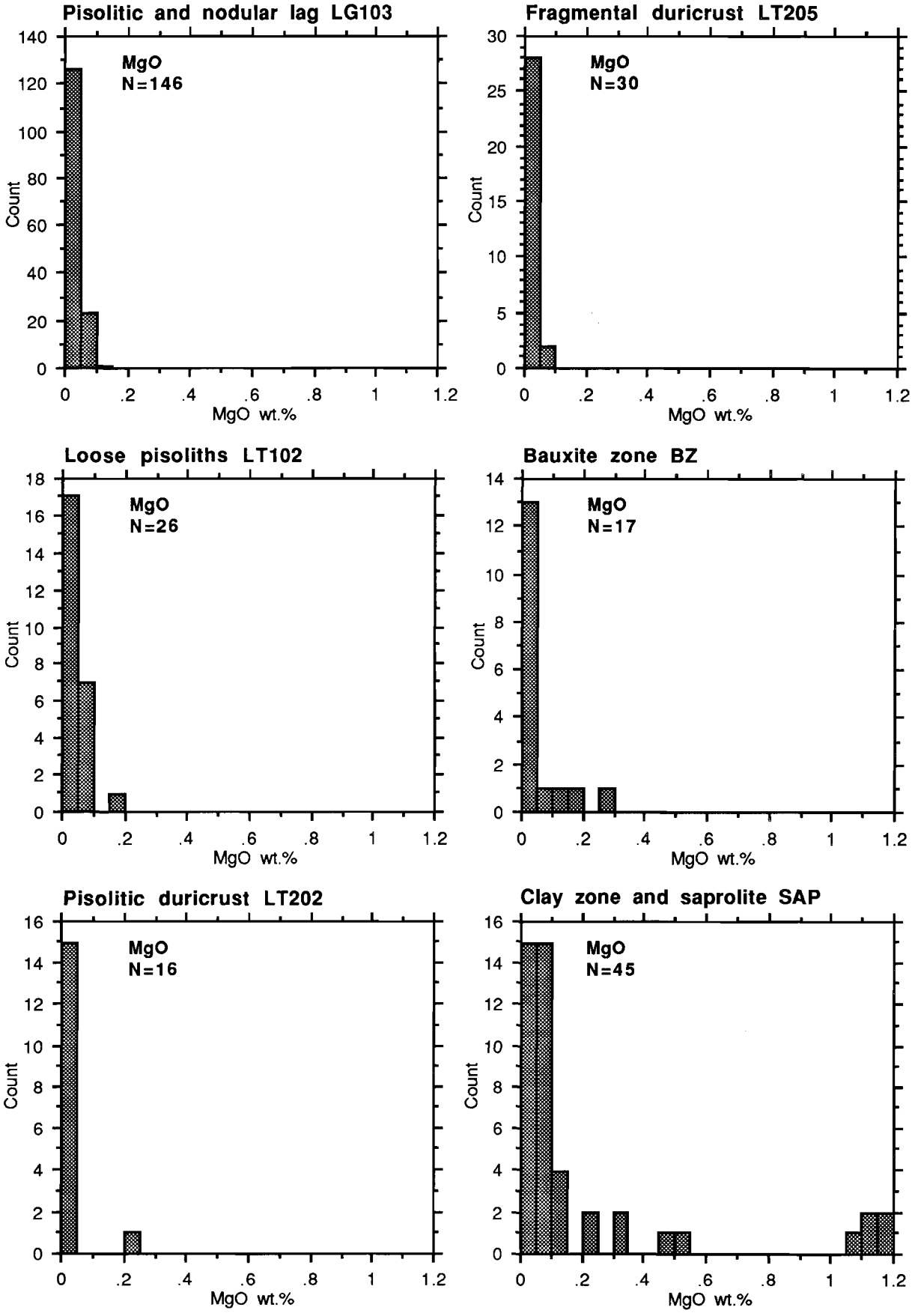
Pisolitic and nodular lag LG103
MgO
N=146
Count
MgO wt.%
Fragmental duricrust LT205
MgO
N=30
Count
MgO wt.%
Loose pisoliths LT102
MgO
N=26
Count
MgO wt.%
Bauxite zone BZ
MgO
N=17
Count
MgO wt.%
Pisolitic duricrust LT202
MgO
N=16
Count
MgO wt.%
Clay zone and saprolite SAP
MgO
N=45
Count
MgO wt.%

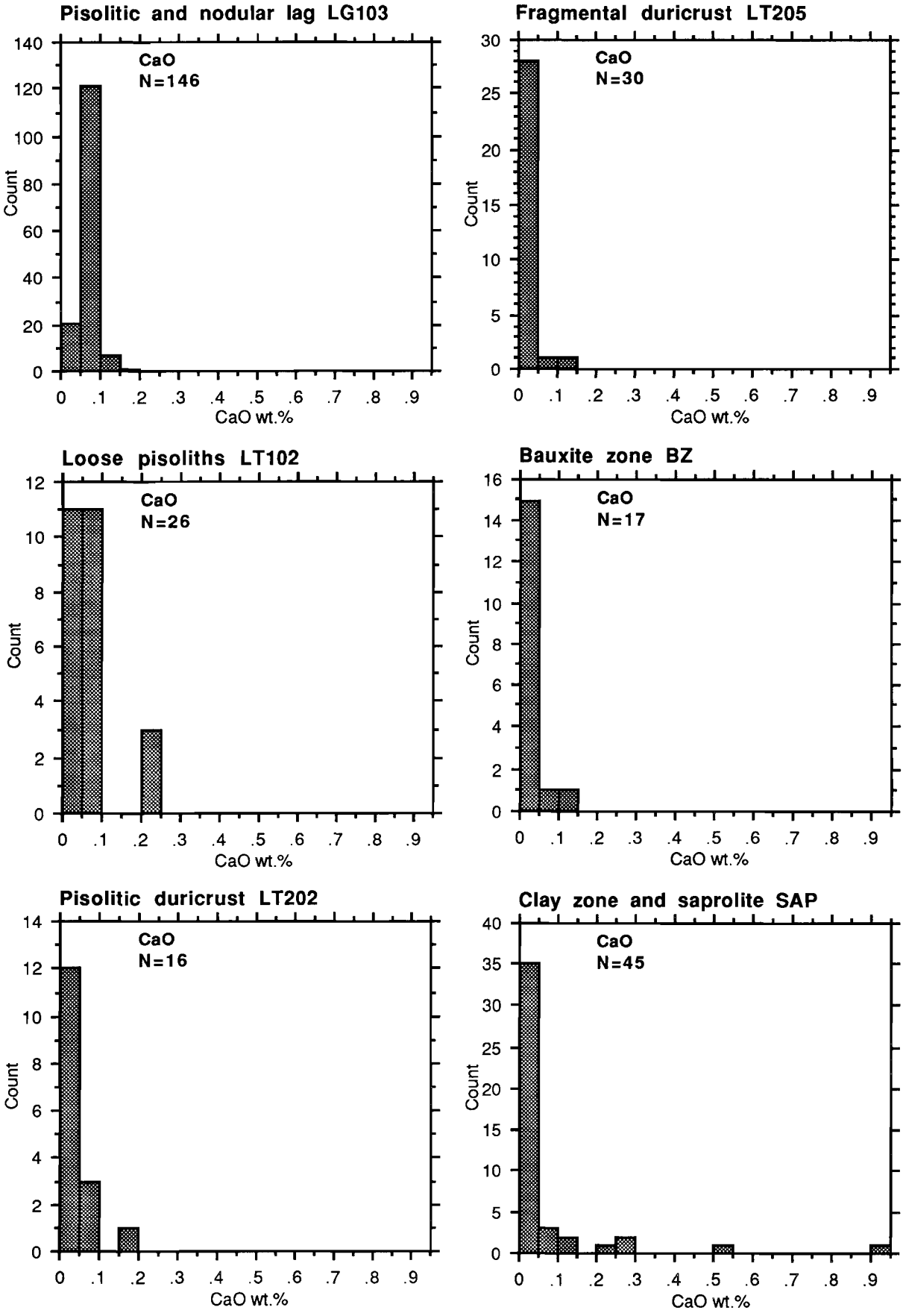
Pisolitic and nodular lag LG103
CaO
N=146
Count
CaO wt.%
Fragmental duricrust LT205
CaO
N=30
Count
CaO wt.%
Loose pisoliths LT102
CaO
N=26
Count
CaO wt.%
Bauxite zone BZ
CaO
N=17
Count
CaO wt.%
Pisolitic duricrust LT202
CaO
N=16
Count
CaO wt.%
Clay zone and saprolite SAP
CaO
N=45
Count
CaO wt.%

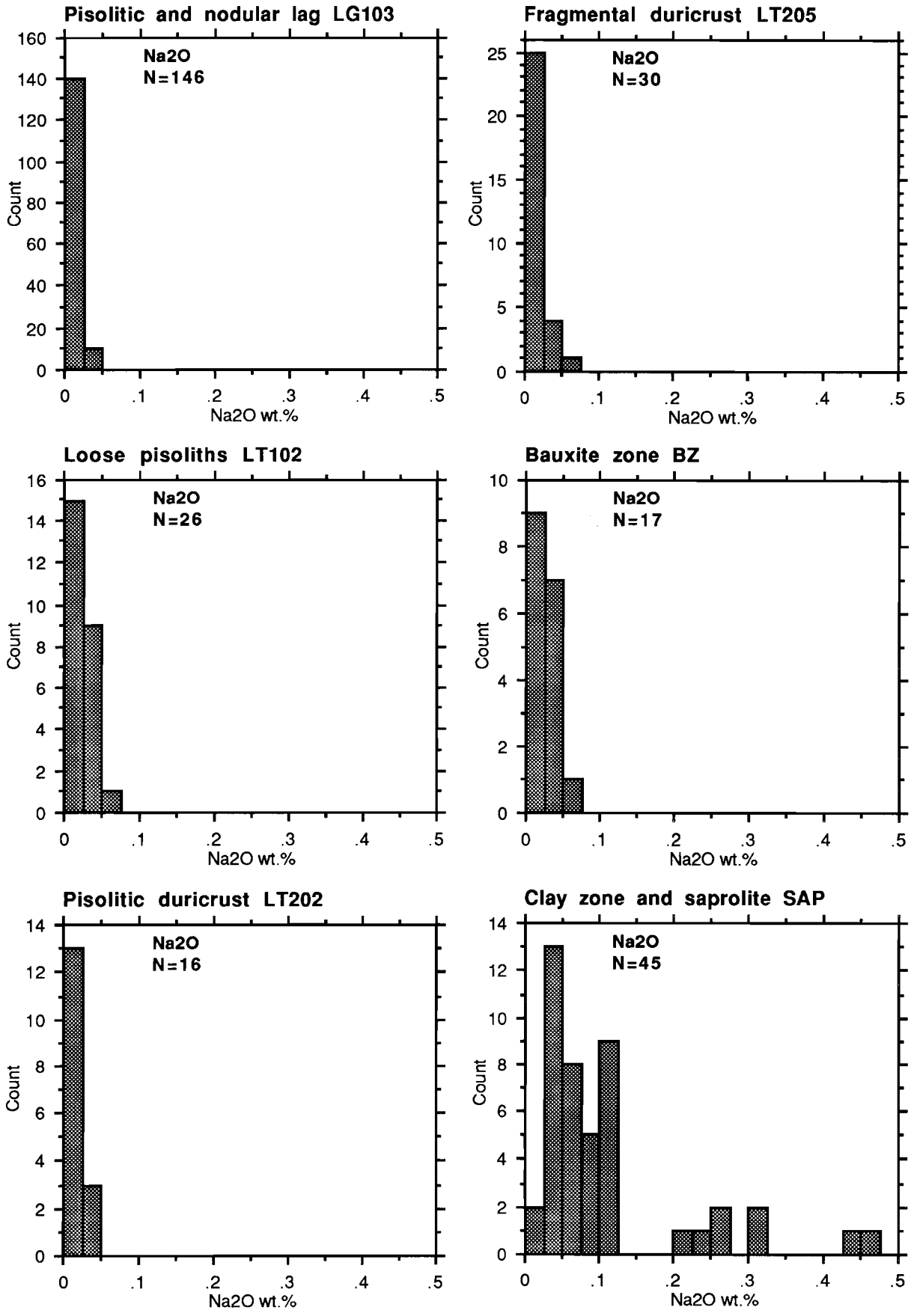
Pisolitic and nodular lag LG103
Na2O
N=146
Count
Na2O wt.%
Fragmental duricrust LT205
Na2O
N=30
Count
Na2O wt.%
Loose pisoliths LT102
Na2O
N=26
Count
Na2O wt.%
Bauxite zone BZ
Na2O
N=17
Count
Na2O wt.%
Pisolitic duricrust LT202
Na2O
N=16
Count
Na2O wt.%
Clay zone and saprolite SAP
Na2O
N=45
Count
Na2O wt.%

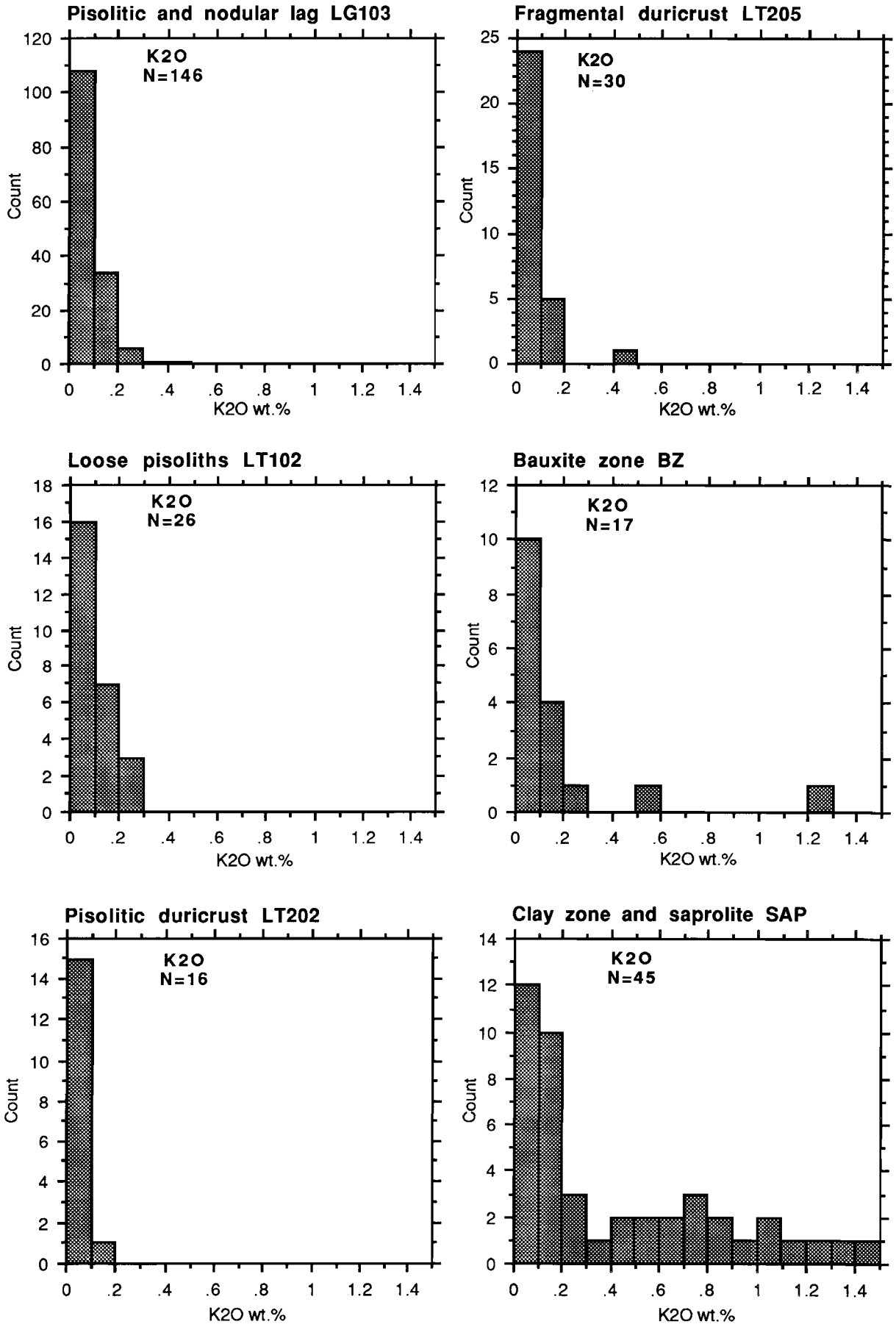
Pisolitic and nodular lag LG103
K2O
N=146
Count
K2O wt.%
Fragmental duricrust LT205
K2O
N=30
Count
K2O wt.%
Loose pisoliths LT102
K2O
N=26
Count
K2O wt.%
Bauxite zone BZ
K2O
N=17
Count
K2O wt.%
Pisolitic duricrust LT202
K2O
N=16
Count
K2O wt.%
Clay zone and saprolite SAP
K2O
N=45
Count
K2O wt.%

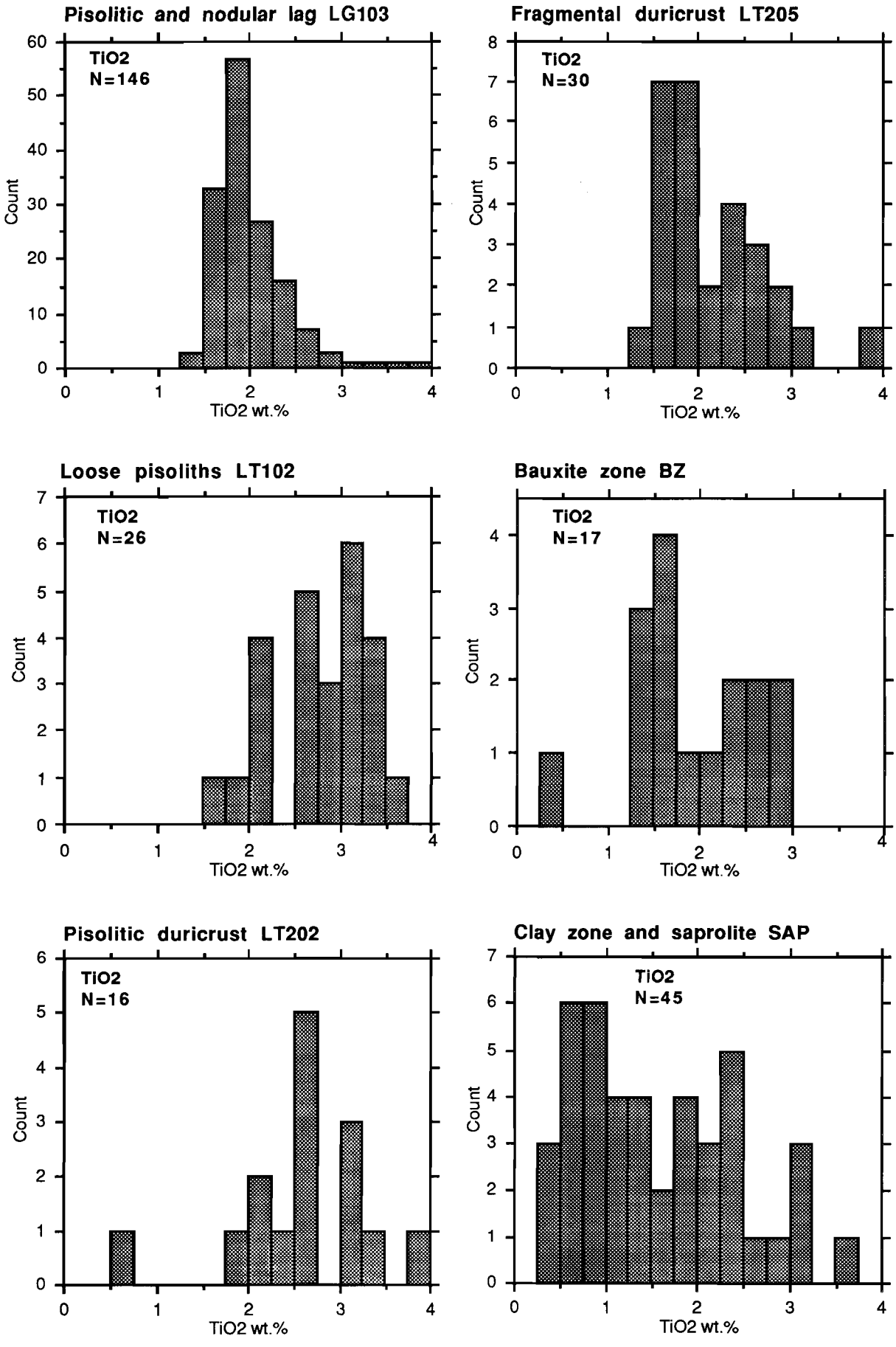
Pisolitic and nodular lag LG103
TiO2
N=146
Count
TiO2 wt.%
Fragmental duricrust LT205
TiO2
N=30
Count
TiO2 wt.%
Loose pisoliths LT102
TiO2
N=26
Count
TiO2 wt.%
Bauxite zone BZ
TiO2
N=17
Count
TiO2 wt.%
Pisolitic duricrust LT202
TiO2
N=16
Count
TiO2 wt.%
Clay zone and saprolite SAP
TiO2
N=45
Count
TiO2 wt.%

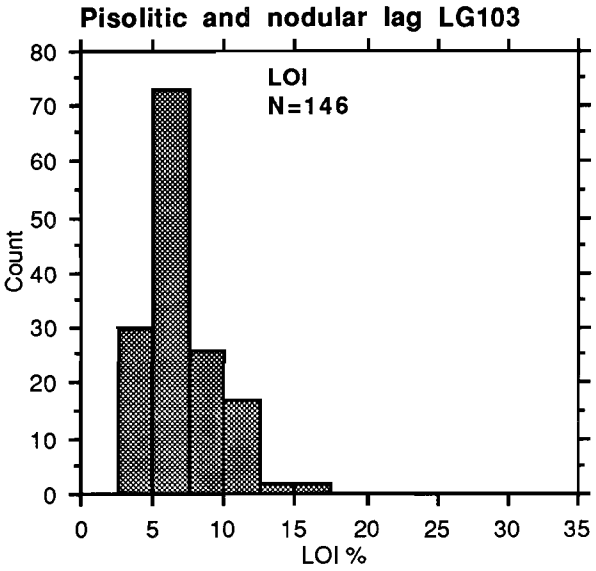
Pisolitic and nodular lag LG103
LOI
N=146
Count
LOI %

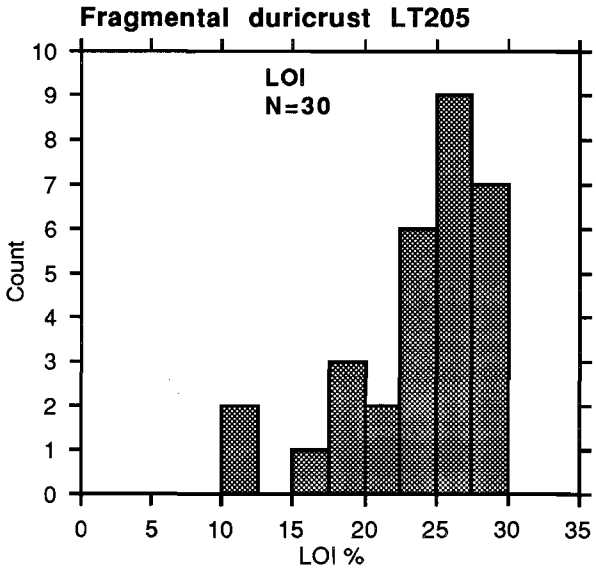
Fragmental duricrust LT205
LOI
N=30
Count
LOI %

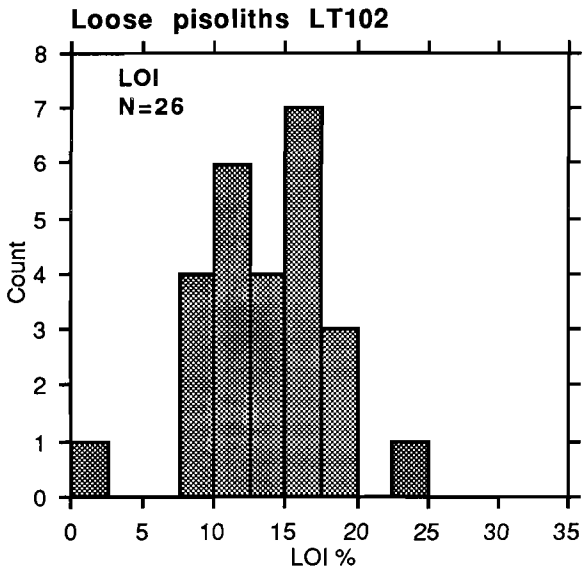
Loose pisoliths LT102
LOI
N=26
Count
LOI %

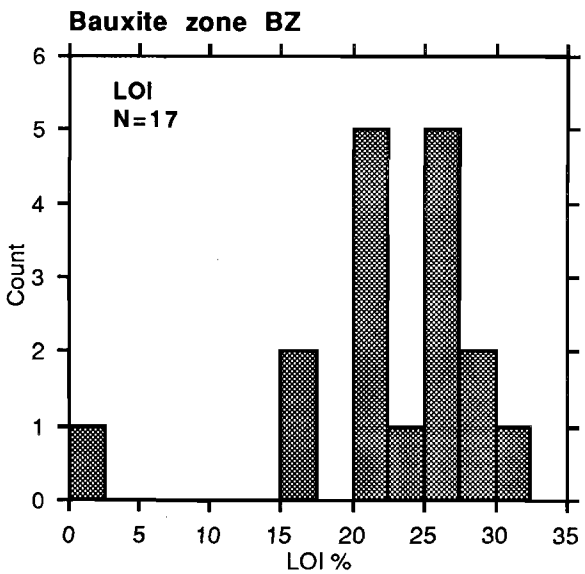
Bauxite zone BZ
LOI
N=17
Count
LOI %

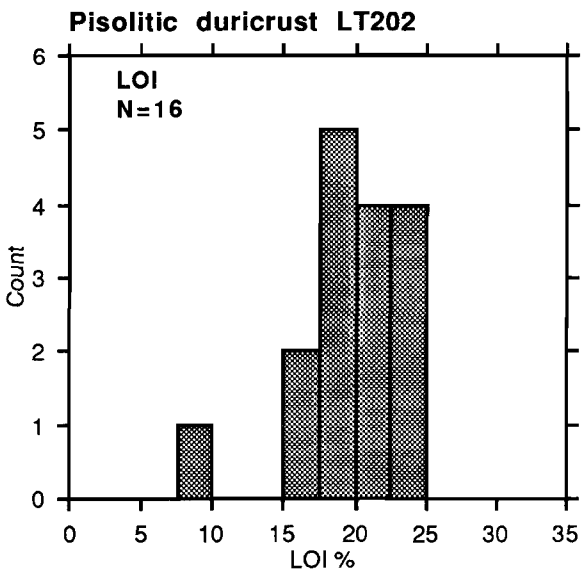
Pisolitic duricrust LT202
LOI
N=16
Count
LOI %

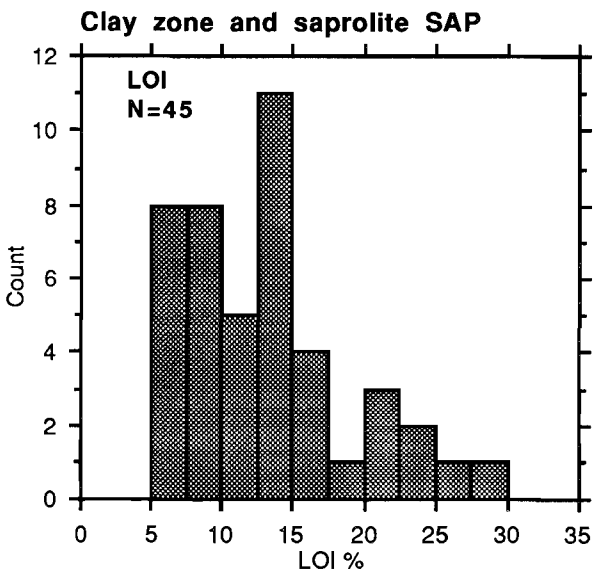
Clay zone and saprolite SAP
LOI
N=45
Count
LOI %

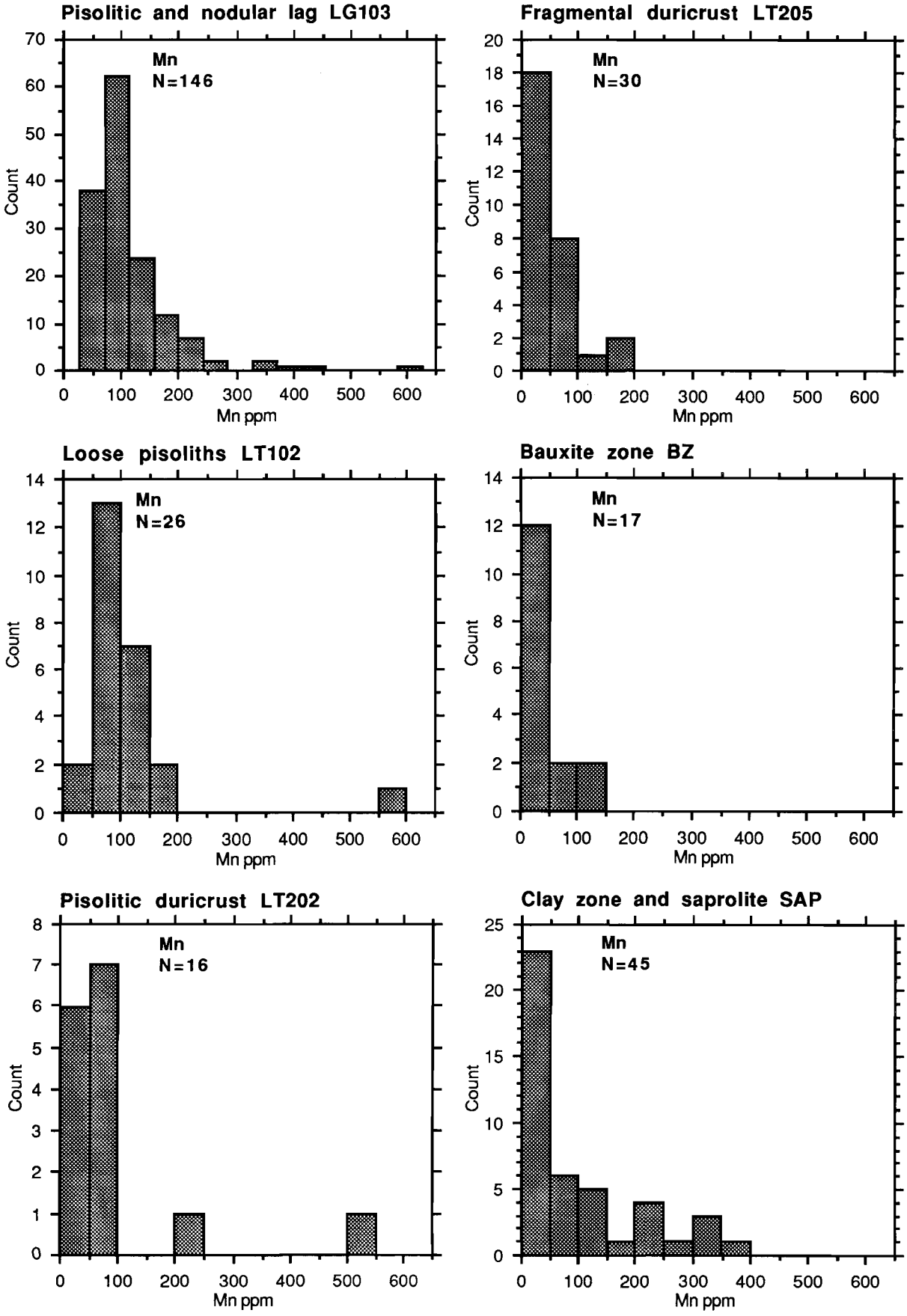
Pisolitic and nodular lag LG103
Mn
N=146
Count
Mn ppm
Fragmental duricrust LT205
Mn
N=30
Count
Mn ppm
Loose pisoliths LT102
Mn
N=26
Count
Mn ppm
Bauxite zone BZ
Mn
N=17
Count
Mn ppm
Pisolitic duricrust LT202
Mn
N=16
Count
Mn ppm
Clay zone and saprolite SAP
Mn
N=45
Count
Mn ppm

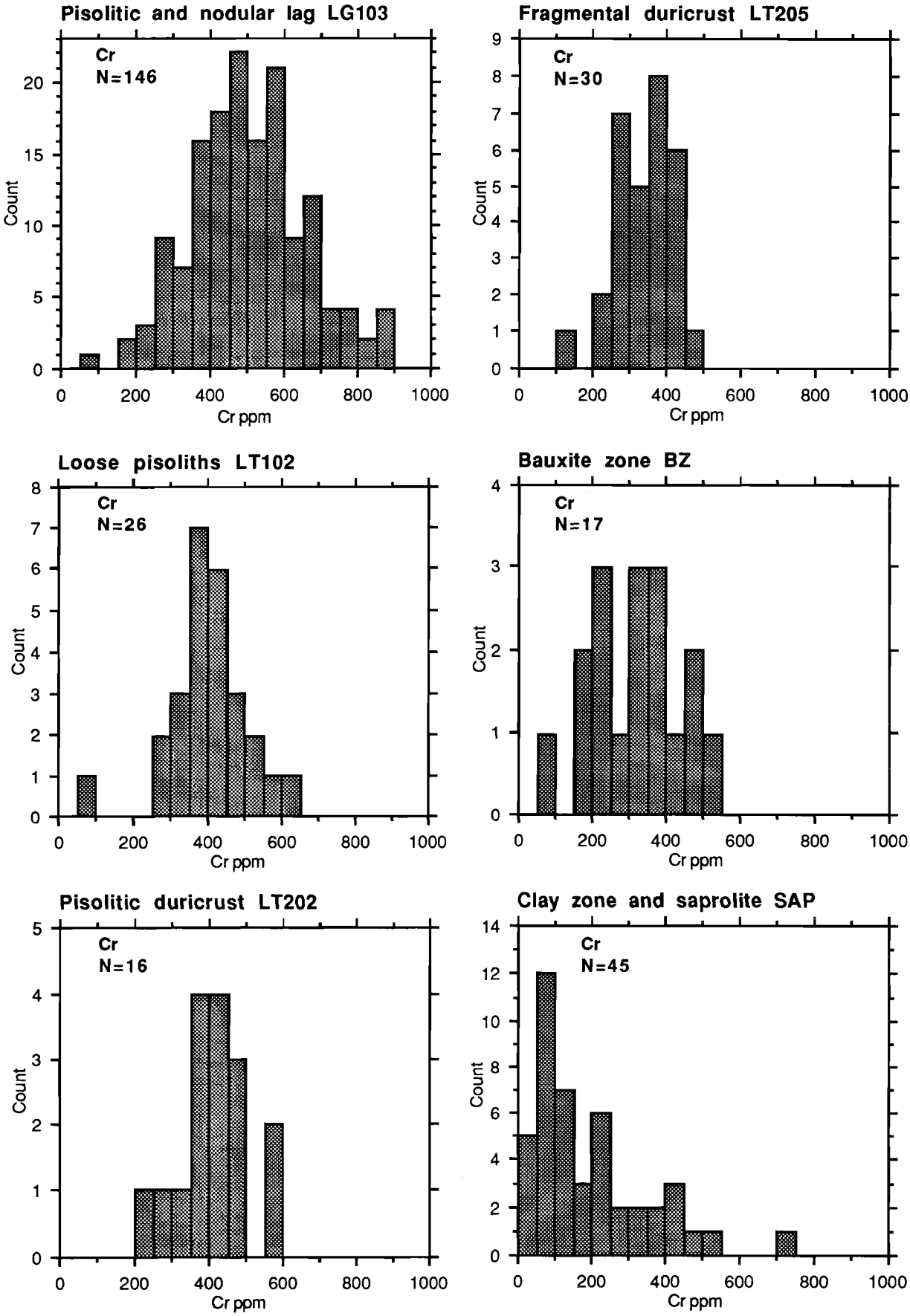
Pisolitic and nodular lag LG103
Cr
N=146
Count
Cr ppm
Fragmental duricrust LT205
Cr
N=30
Count
Cr ppm
Loose pisoliths LT102
Cr
N=26
Count
Cr ppm
Bauxite zone BZ
Cr
N=17
Count
Cr ppm
Pisolitic duricrust LT202
Cr
N=16
Count
Cr ppm
Clay zone and saprolite SAP
Cr
N=45
Count
Cr ppm

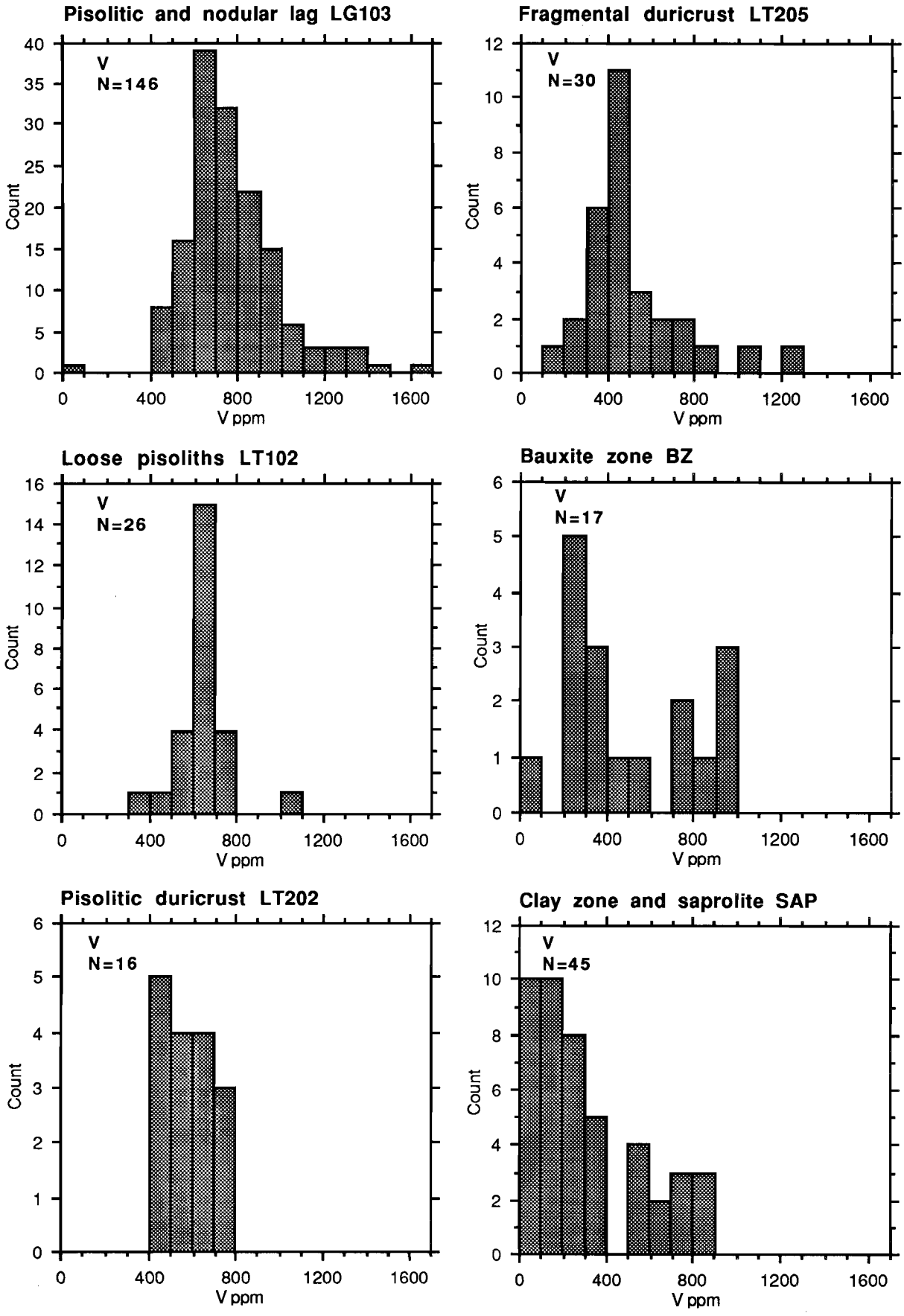
Pisolitic and nodular lag LG103
V
N=146
Count
V ppm
Fragmental duricrust LT205
V
N=30
Count
V ppm
Loose pisoliths LT102
V
N=26
Count
V ppm
Bauxite zone BZ
V
N=17
Count
V ppm
Pisolitic duricrust LT202
V
N=16
Count
V ppm
Clay zone and saprolite SAP
V
N=45
Count
V ppm

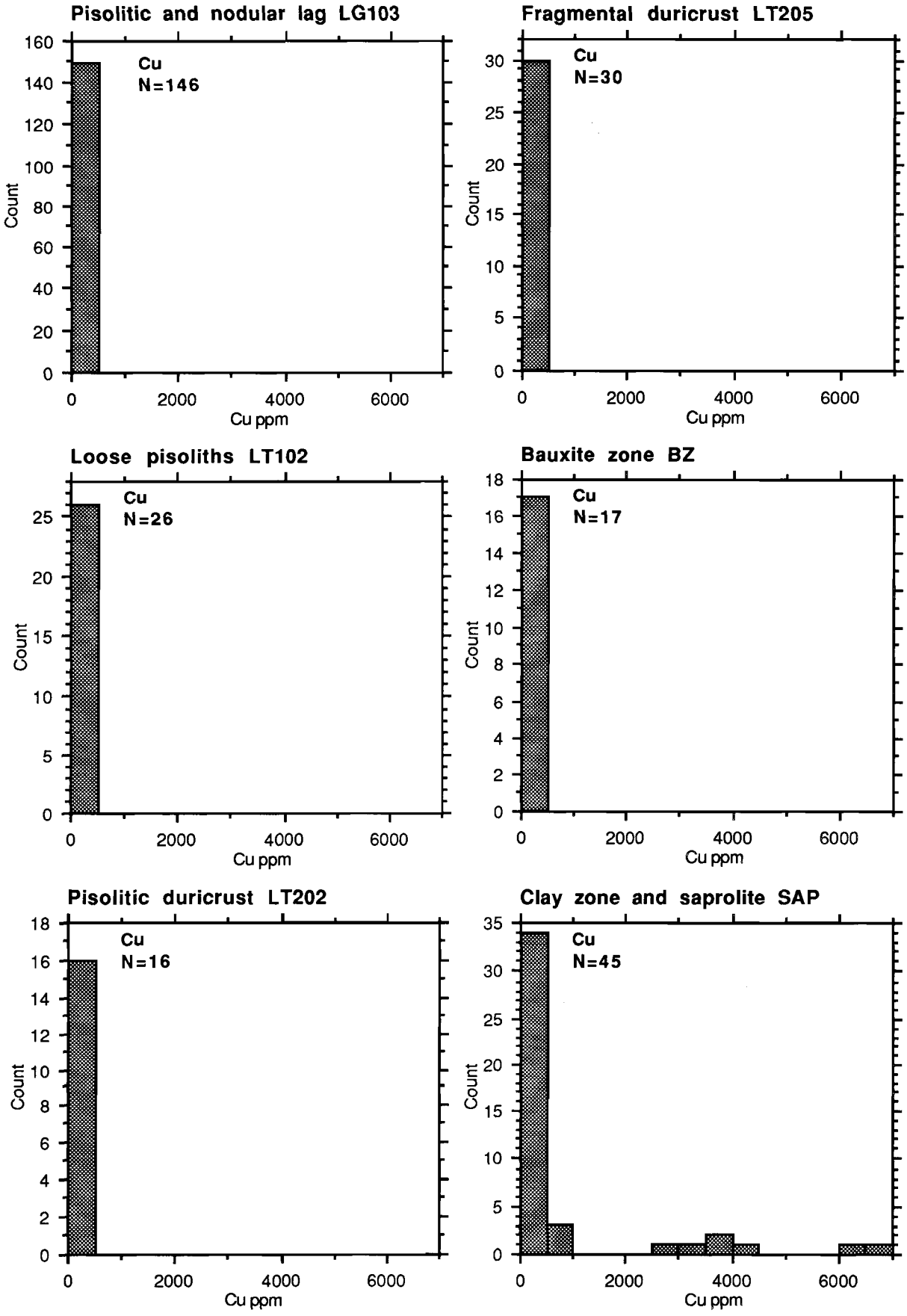
Pisolitic and nodular lag LG103
Cu
N=146
Count
Cu ppm
Fragmental duricrust LT205
Cu
N=30
Count
Cu ppm
Loose pisoliths LT102
Cu
N=26
Count
Cu ppm
Bauxite zone BZ
Cu
N=17
Count
Cu ppm
Pisolitic duricrust LT202
Cu
N=16
Count
Cu ppm
Clay zone and saprolite SAP
Cu
N=45
Count
Cu ppm

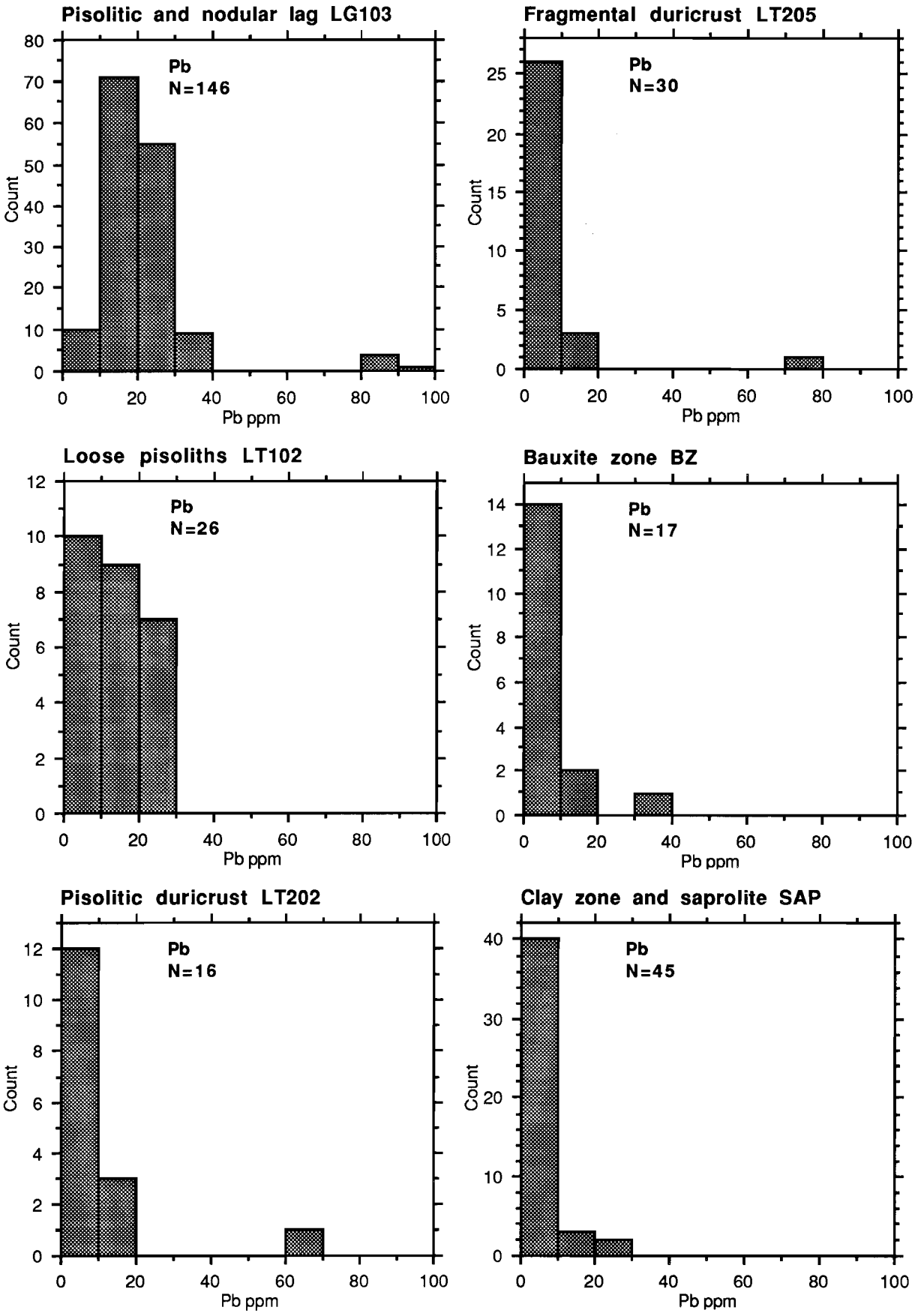
Pisolitic and nodular lag LG103
Pb
N=146
Count
Pb ppm
Fragmental duricrust LT205
Pb
N=30
Count
Pb ppm
Loose pisoliths LT102
Pb
N=26
Count
Pb ppm
Bauxite zone BZ
Pb
N=17
Count
Pb ppm
Pisolitic duricrust LT202
Pb
N=16
Count
Pb ppm
Clay zone and saprolite SAP
Pb
N=45
Count
Pb ppm

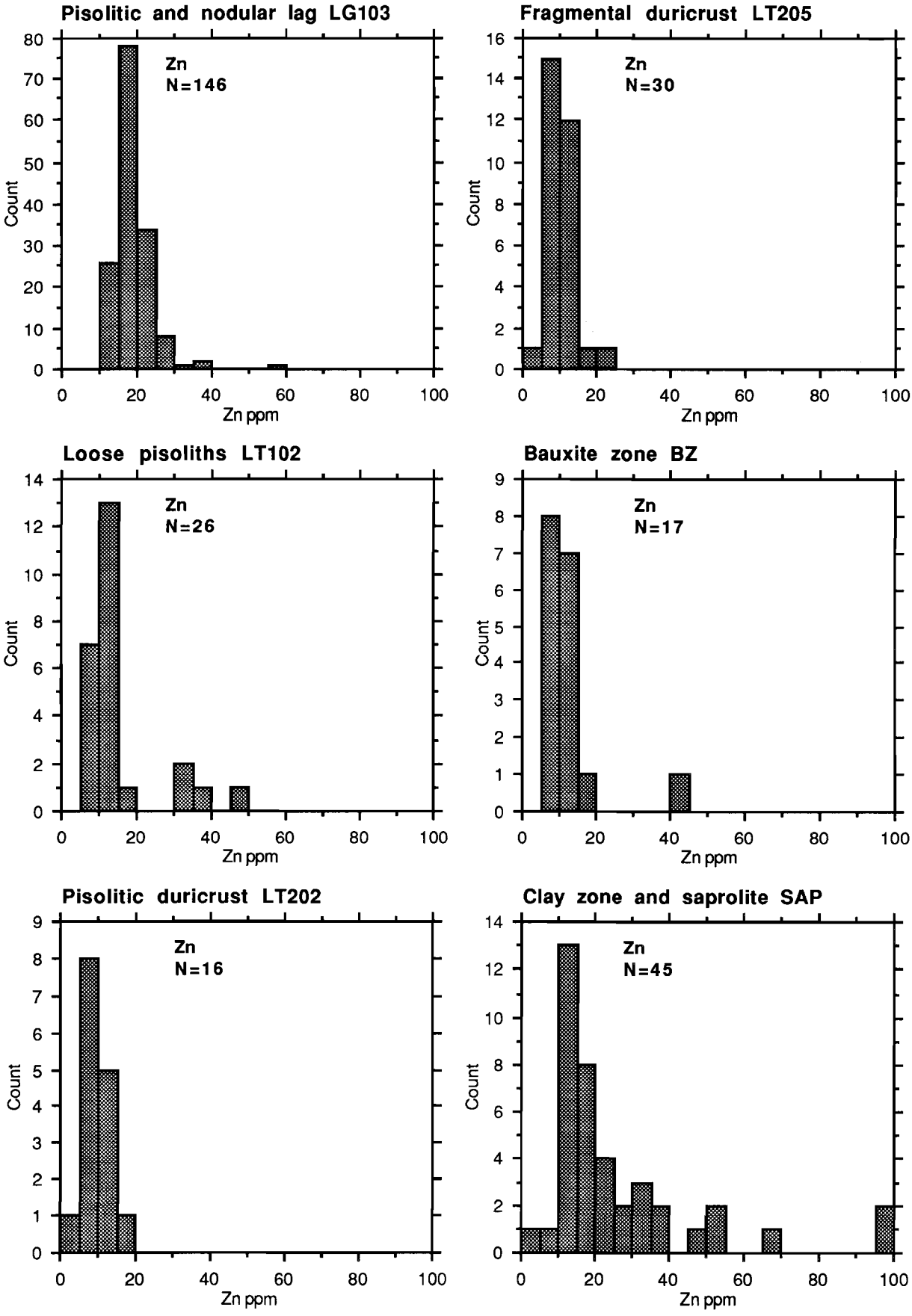
Pisolitic and nodular lag LG103
Zn
N=146
Count
Zn ppm
Fragmental duricrust LT205
Zn
N=30
Count
Zn ppm
Loose pisoliths LT102
Zn
N=26
Count
Zn ppm
Bauxite zone BZ
Zn
N=17
Count
Zn ppm
Pisolitic duricrust LT202
Zn
N=16
Count
Zn ppm
Clay zone and saprolite SAP
Zn
N=45
Count
Zn ppm

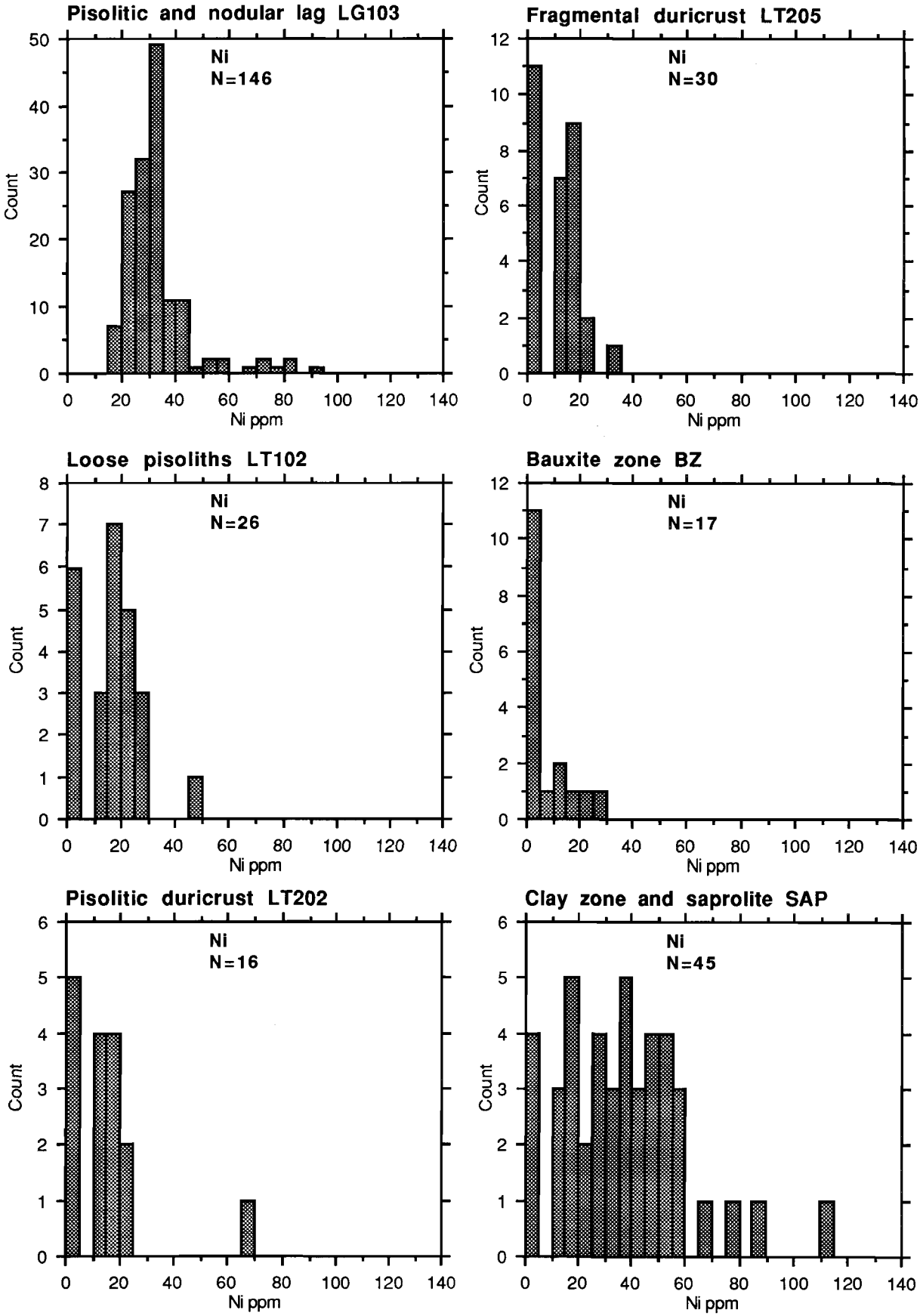
Pisolitic and nodular lag LG103
Ni
N=146
Count
Ni ppm
Fragmental duricrust LT205
Ni
N=30
Count
Ni ppm
Loose pisoliths LT102
Ni
N=26
Count
Ni ppm
Bauxite zone BZ
Ni
N=17
Count
Ni ppm
Pisolitic duricrust LT202
Ni
N=16
Count
Ni ppm
Clay zone and saprolite SAP
Ni
N=45
Count
Ni ppm

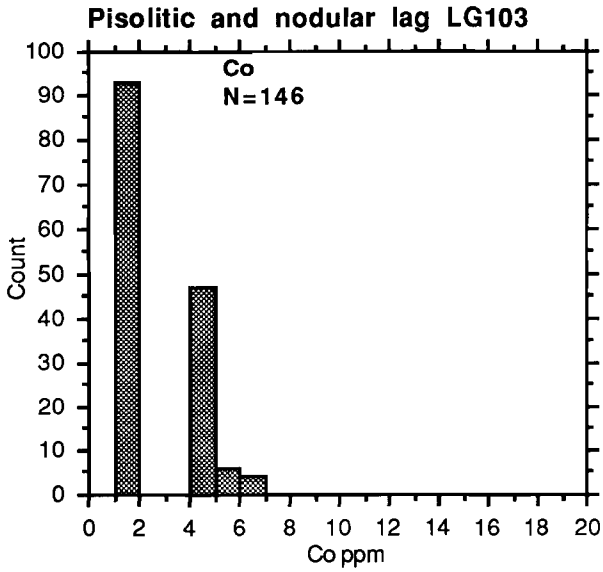
Pisolitic and nodular lag LG103
Co
N=146
Count
Co ppm

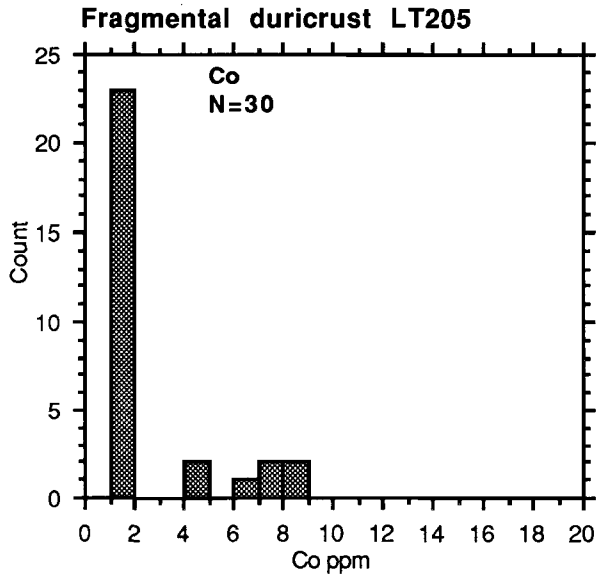
Fragmental duricrust LT205
Co
N=30
Count
Co ppm

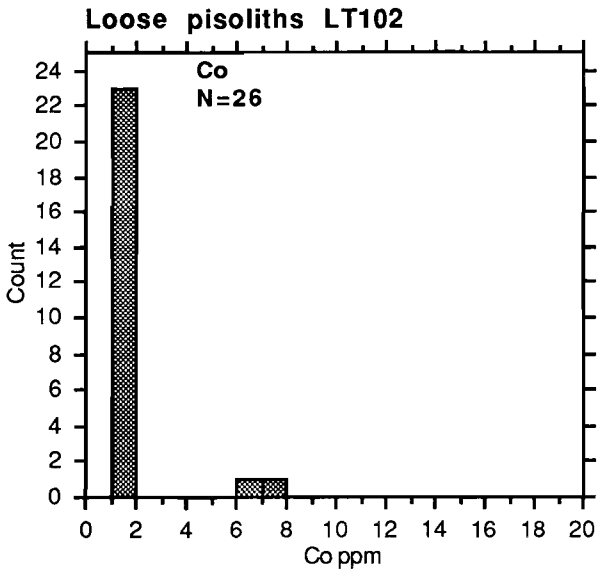
Loose pisoliths LT102
Co
N=26
Count
Co ppm

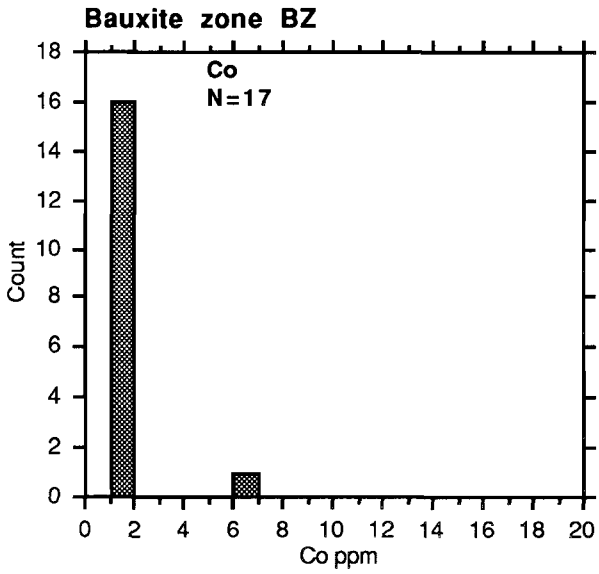
Bauxite zone BZ
Co
N=17
Count
Co ppm

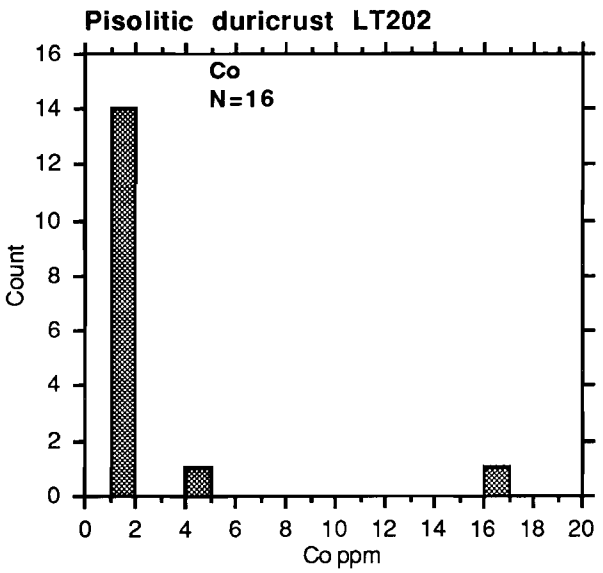
Pisolitic duricrust LT202
Co
N=16
Count
Co ppm

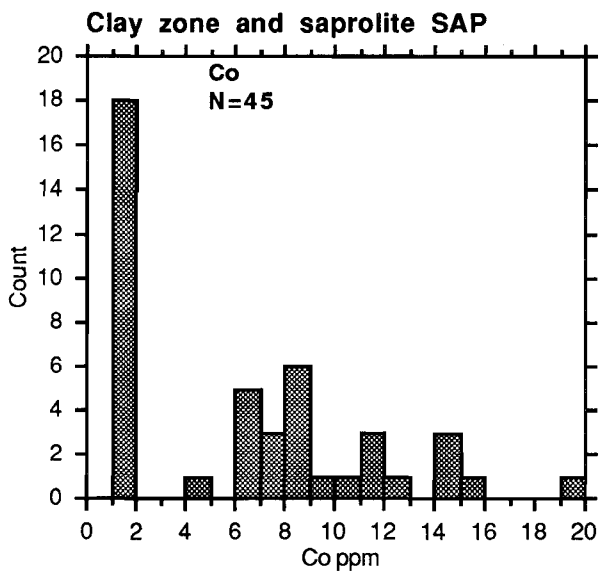
Clay zone and saprolite SAP
Co
N=45
Count
Co ppm

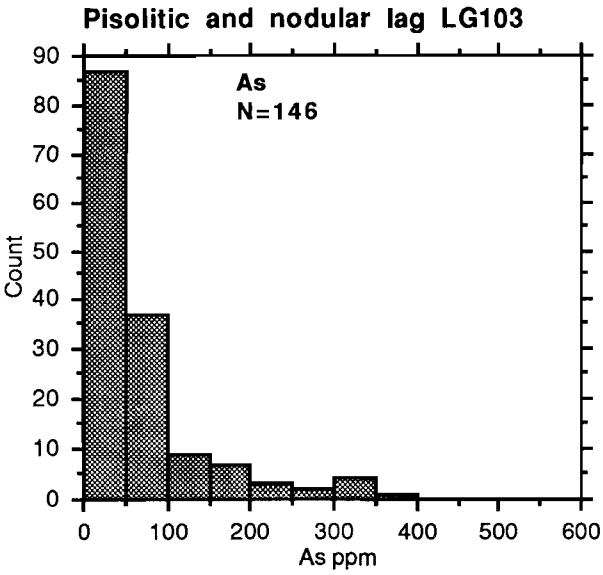
Pisolitic and nodular lag LG103
As
N=146
Count
As ppm

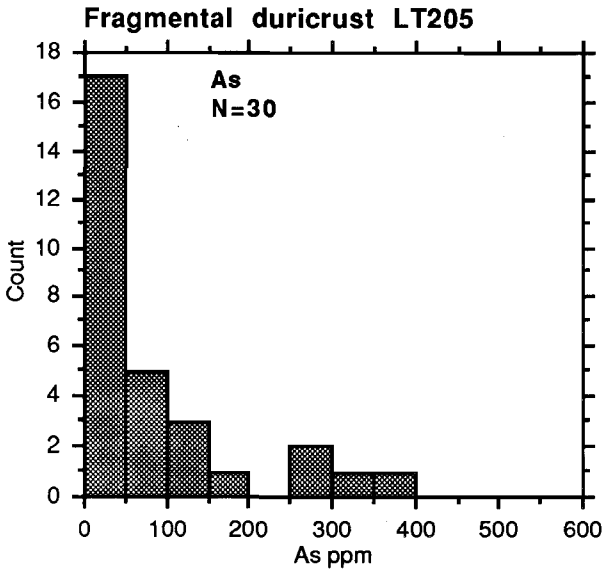
Fragmental duricrust LT205
As
N=30
Count
As ppm

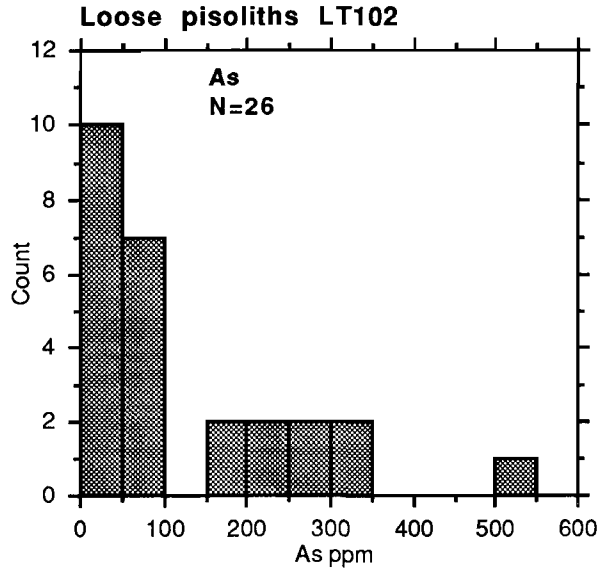
Loose pisoliths LT102
As
N=26
Count
As ppm

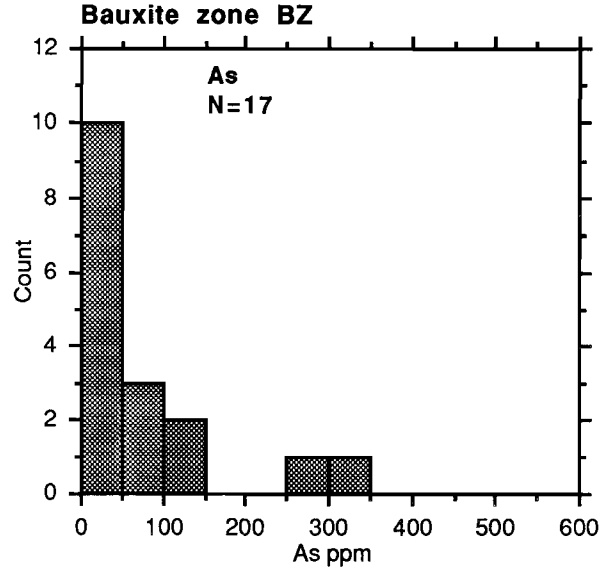
Bauxite zone BZ
As
N=17
Count
As ppm

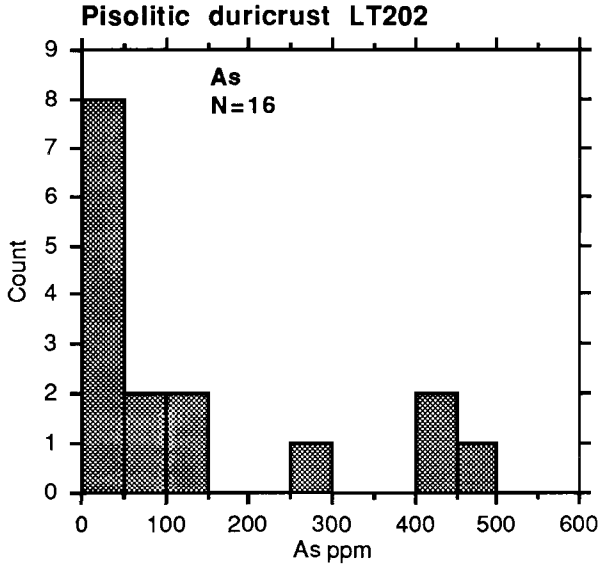
Pisolitic duricrust LT202
As
N=16
Count
As ppm

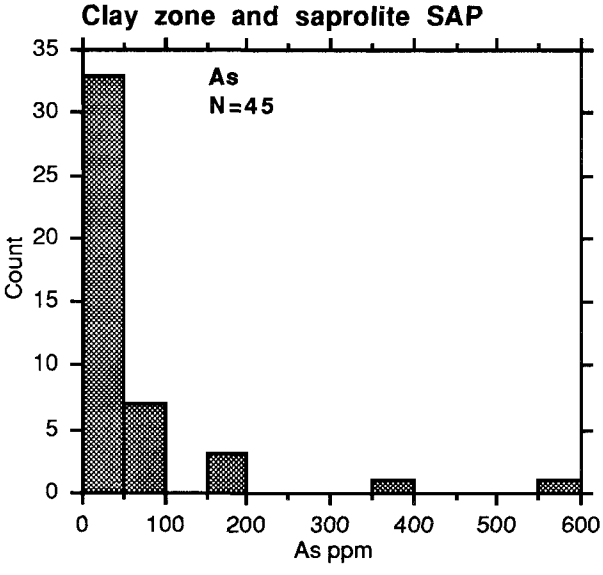
Clay zone and saprolite SAP
As
N=45
Count
As ppm

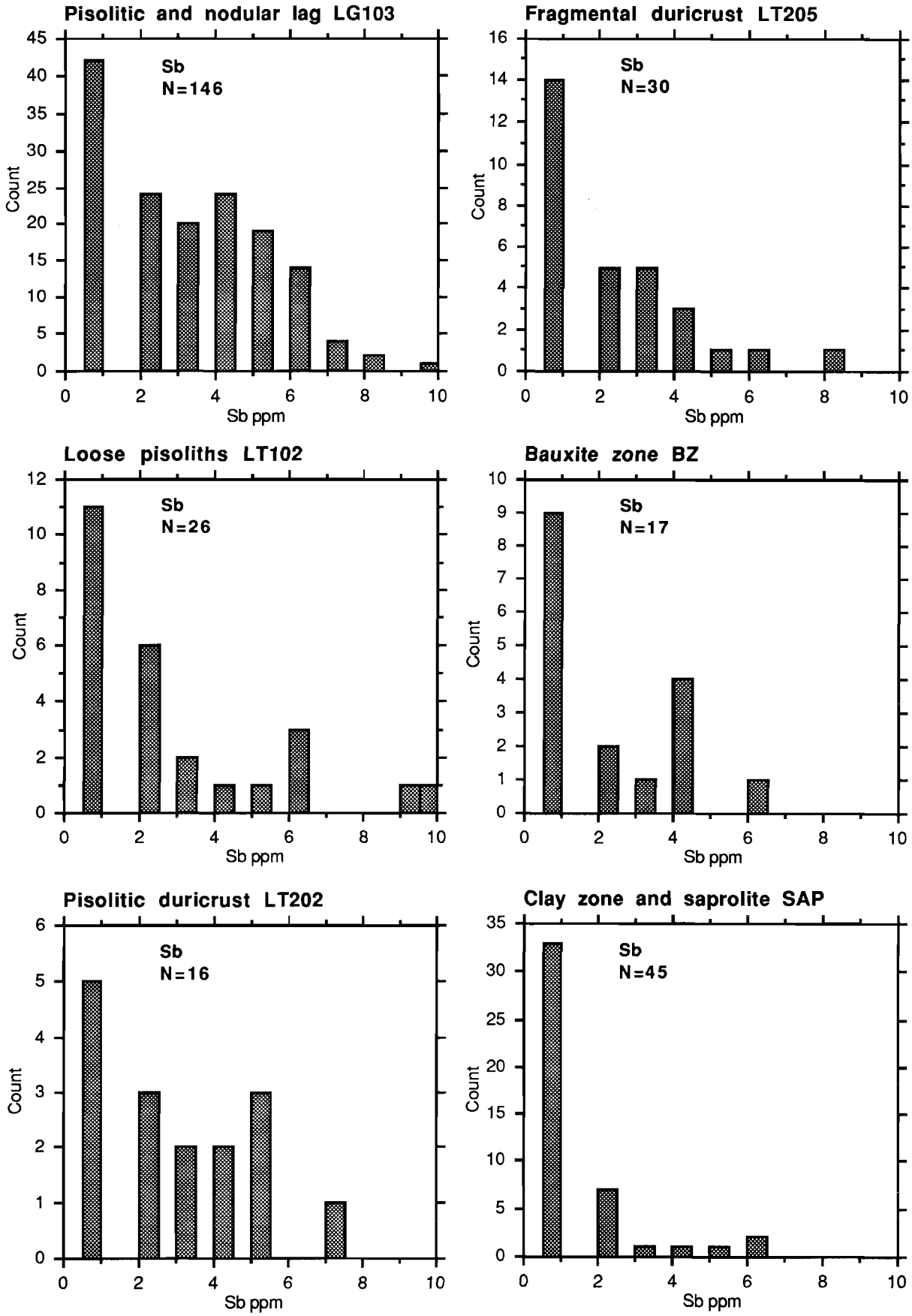
Pisolitic and nodular lag LG103
Sb
N=146
Count
Sb ppm
Fragmental duricrust LT205
Sb
N=30
Count
Sb ppm
Loose pisoliths LT102
Sb
N=26
Count
Sb ppm
Bauxite zone BZ
Sb
N=17
Count
Sb ppm
Pisolitic duricrust LT202
Sb
N=16
Count
Sb ppm
Clay zone and saprolite SAP
Sb
N=45
Count
Sb ppm

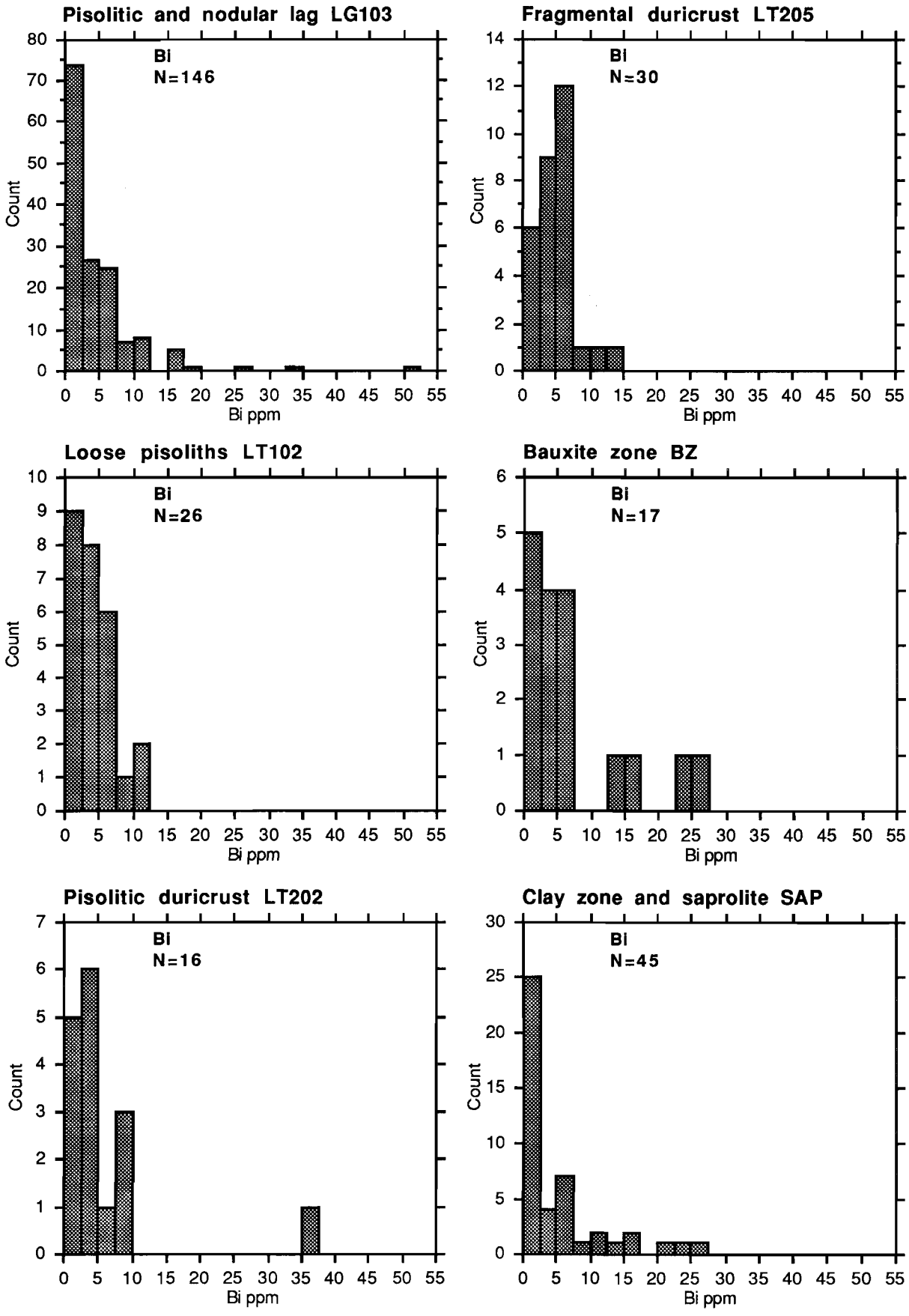
Pisolitic and nodular lag LG103
Bi
N=146
Count
Bi ppm
Fragmental duricrust LT205
Bi
N=30
Count
Bi ppm
Loose pisoliths LT102
Bi
N=26
Count
Bi ppm
Bauxite zone BZ
Bi
N=17
Count
Bi ppm
Pisolitic duricrust LT202
Bi
N=16
Count
Bi ppm
Clay zone and saprolite SAP
Bi
N=45
Count
Bi ppm

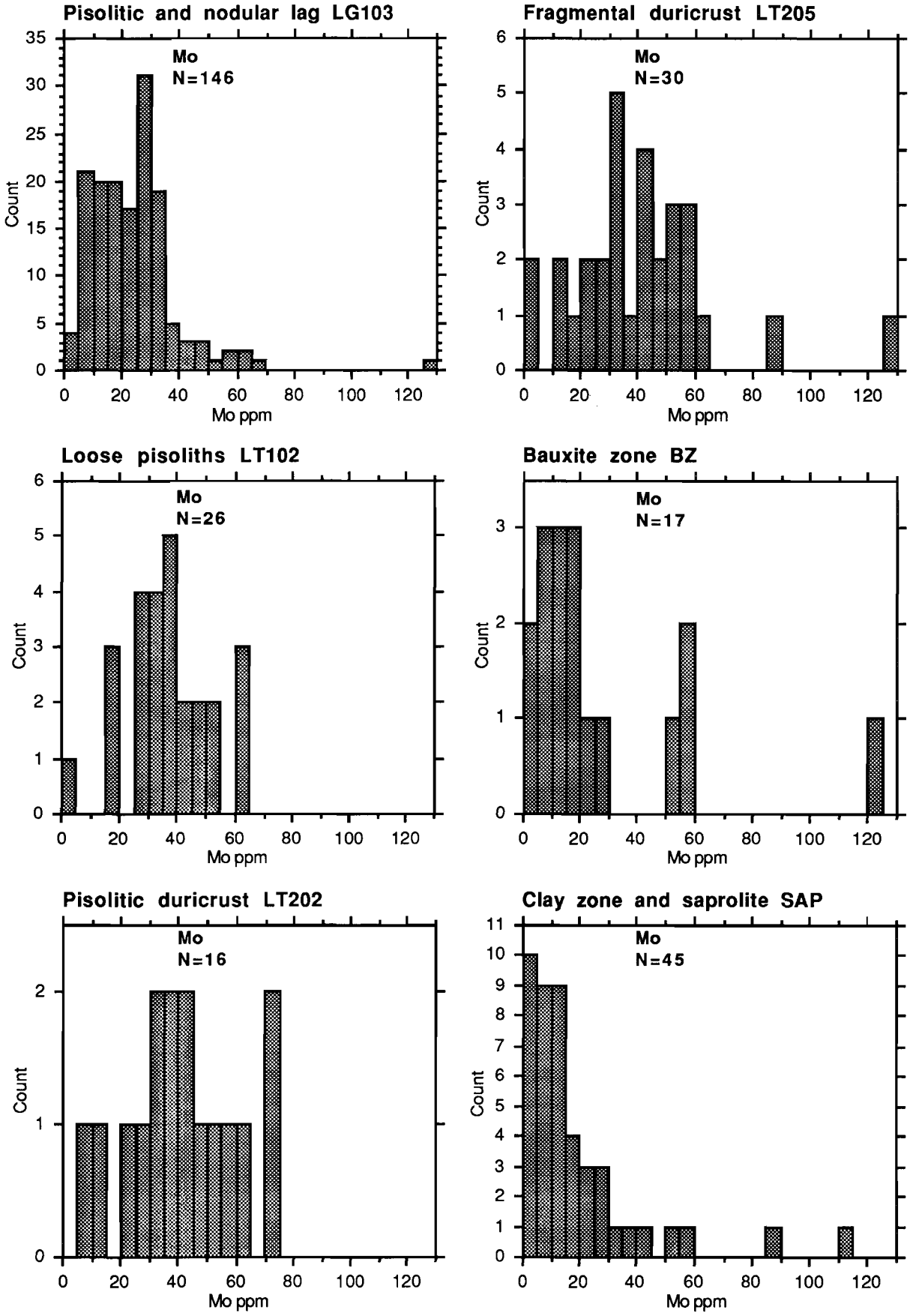
Pisolitic and nodular lag LG103
Mo
N=146
Count
Mo ppm
Fragmental duricrust LT205
Mo
N=30
Count
Mo ppm
Loose pisoliths LT102
Mo
N=26
Count
Mo ppm
Bauxite zone BZ
Mo
N=17
Count
Mo ppm
Pisolitic duricrust LT202
Mo
N=16
Count
Mo ppm
Clay zone and saprolite SAP
Mo
N=45
Count
Mo ppm

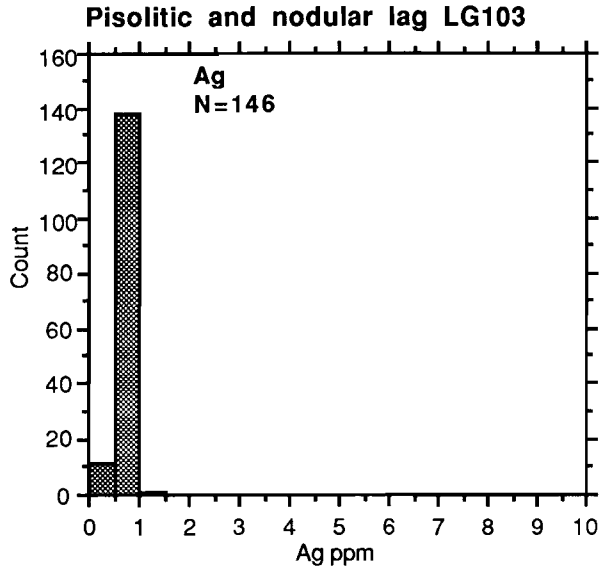
Pisolitic and nodular lag LG103
Ag
N=146
Count
Ag ppm

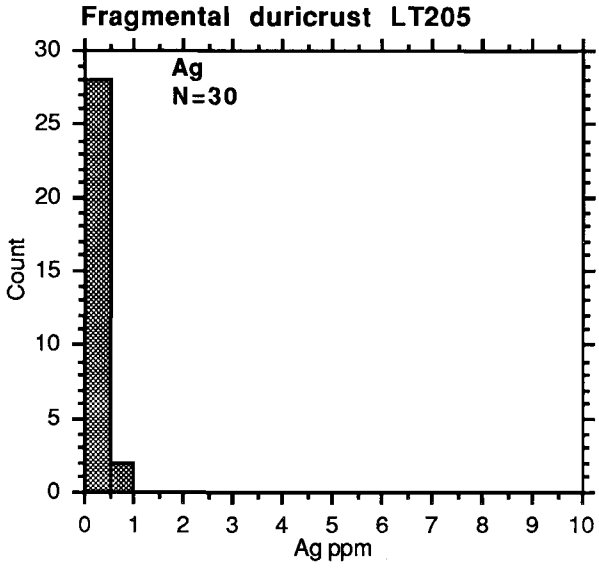
Fragmental duricrust LT205
Ag
N=30
Count
Ag ppm

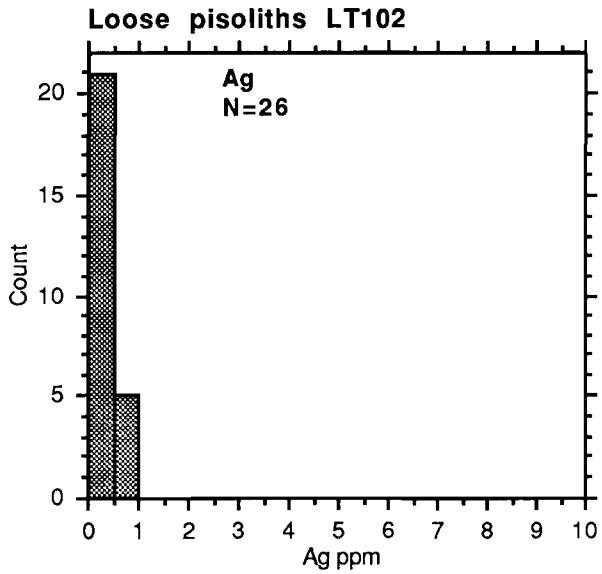
Loose pisoliths LT102
Ag
N=26
Count
Ag ppm

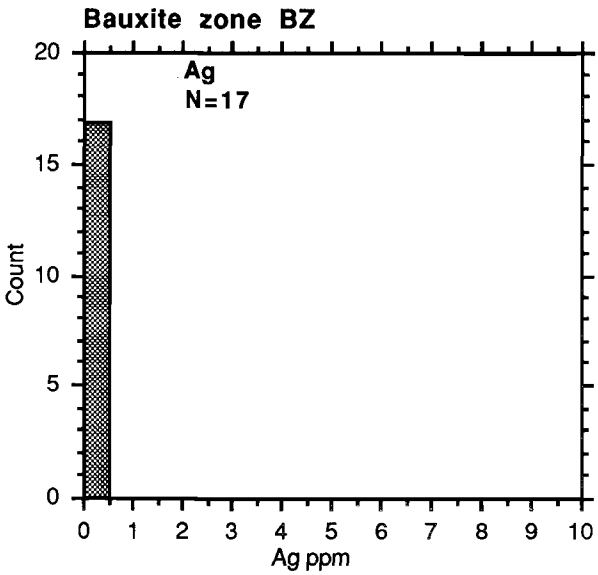
Bauxite zone BZ
Ag
N=17
Count
Ag ppm

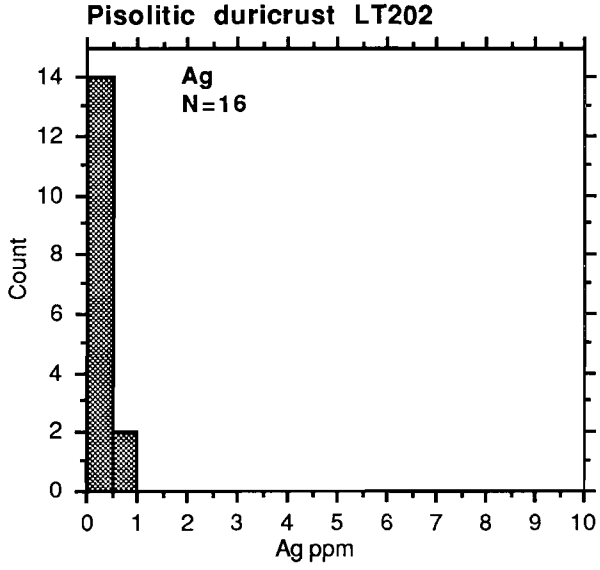
Pisolitic duricrust LT202
Ag
N=16
Count
Ag ppm

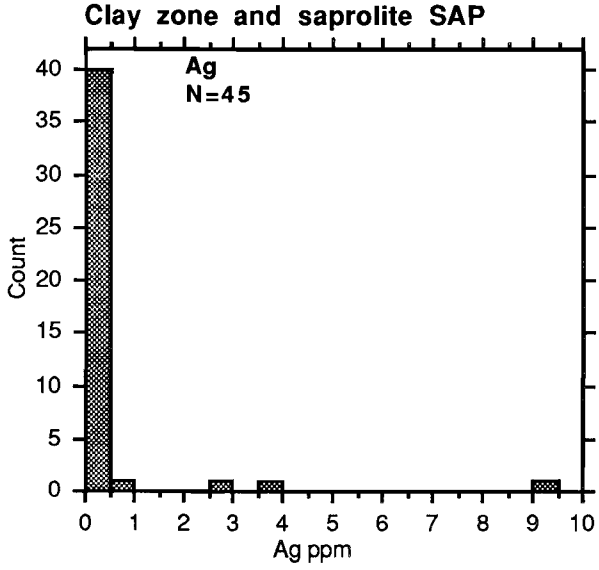
Clay zone and saprolite SAP
Ag
N=45
Count
Ag ppm

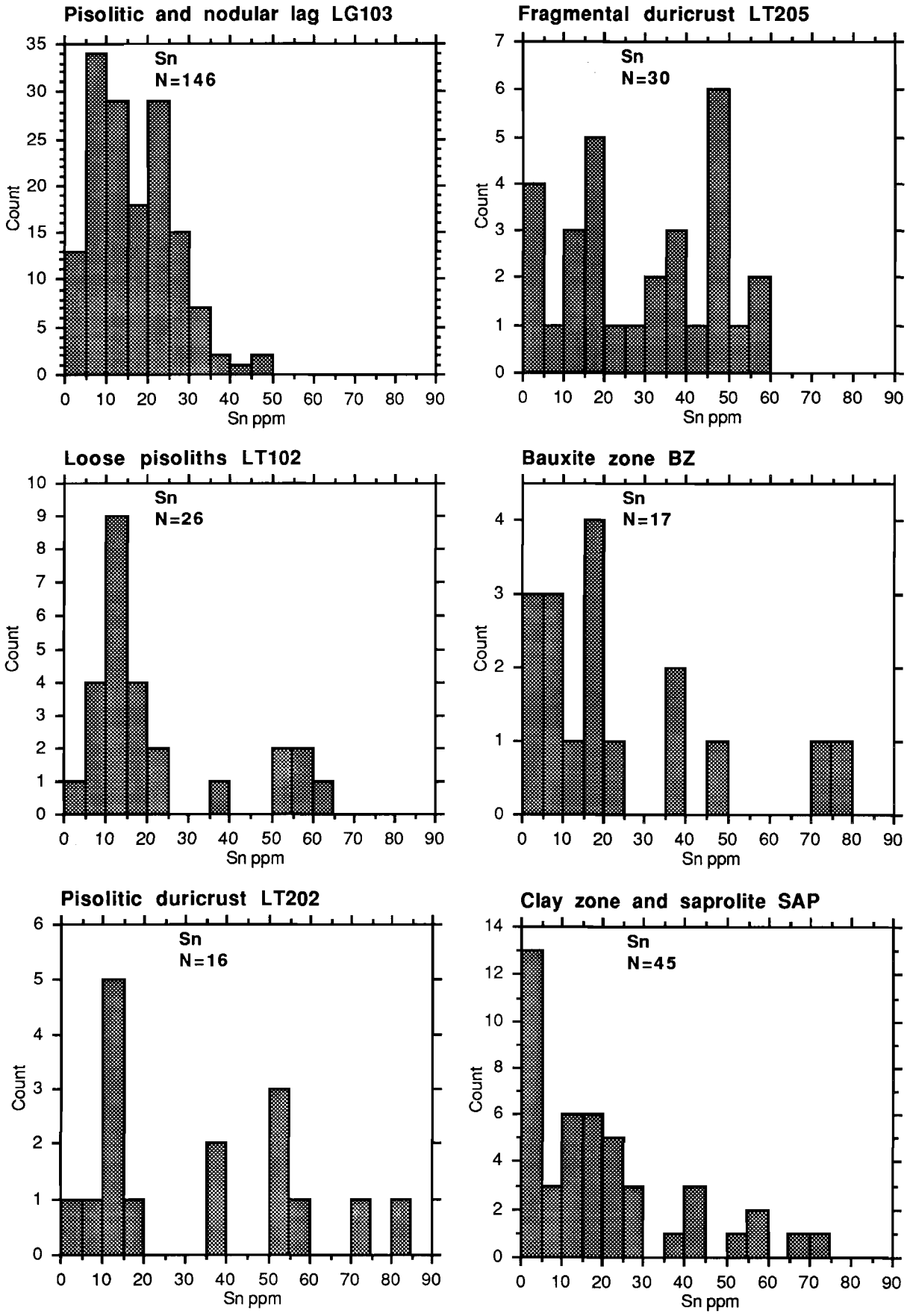
Pisolitic and nodular lag LG103
Sn
N=146
Count
Sn ppm
Fragmental duricrust LT205
Sn
N=30
Count
Sn ppm
Loose pisoliths LT102
Sn
N=26
Count
Sn ppm
Bauxite zone BZ
Sn
N=17
Count
Sn ppm
Pisolitic duricrust LT202
Sn
N=16
Count
Sn ppm
Clay zone and saprolite SAP
Sn
N=45
Count
Sn ppm

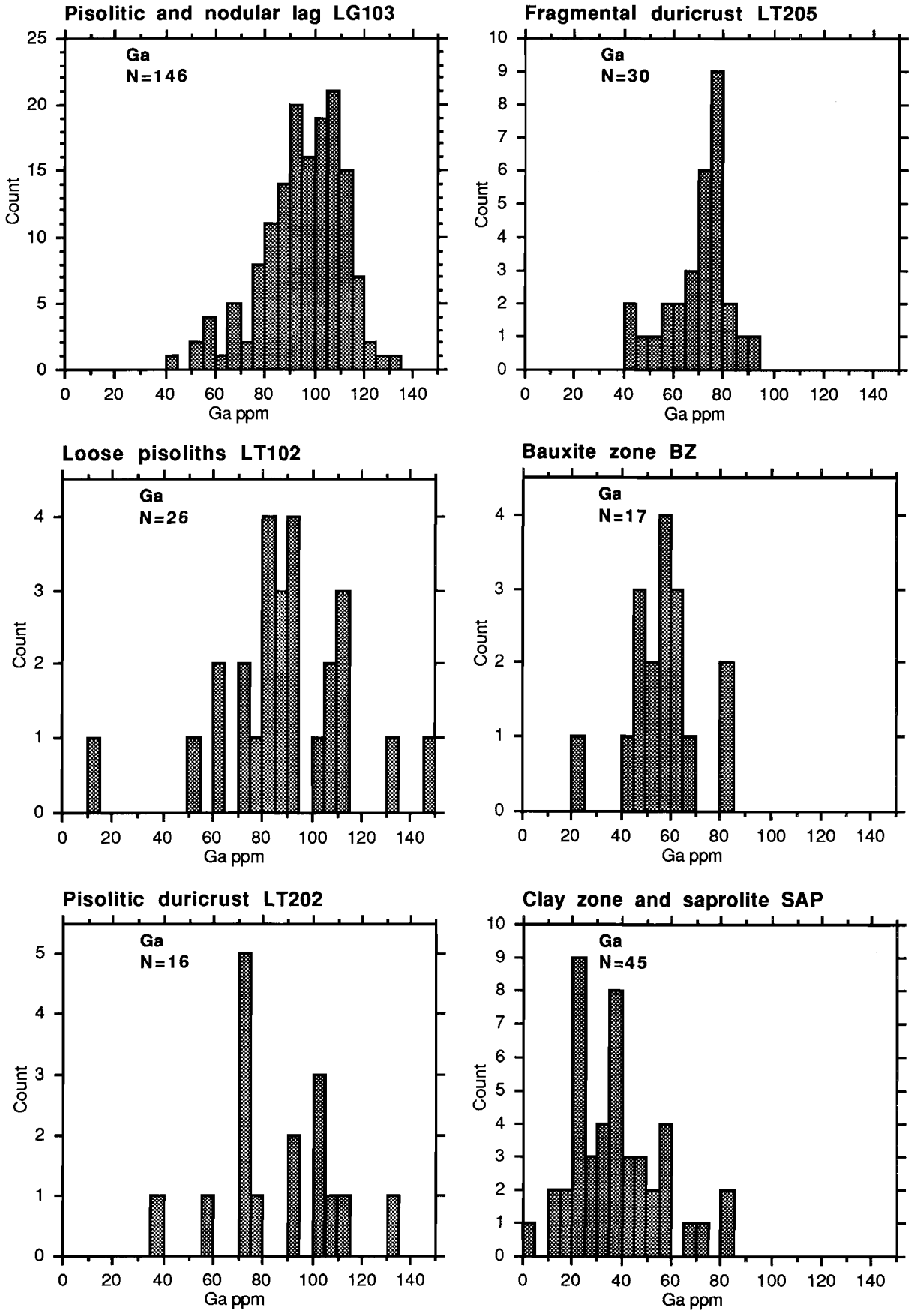
Pisolitic and nodular lag LG103
Ga
N=146
Count
Ga ppm
Fragmental duricrust LT205
Ga
N=30
Count
Ga ppm
Loose pisoliths LT102
Ga
N=26
Count
Ga ppm
Bauxite zone BZ
Ga
N=17
Count
Ga ppm
Pisolitic duricrust LT202
Ga
N=16
Count
Ga ppm
Clay zone and saprolite SAP
Ga
N=45
Count
Ga ppm

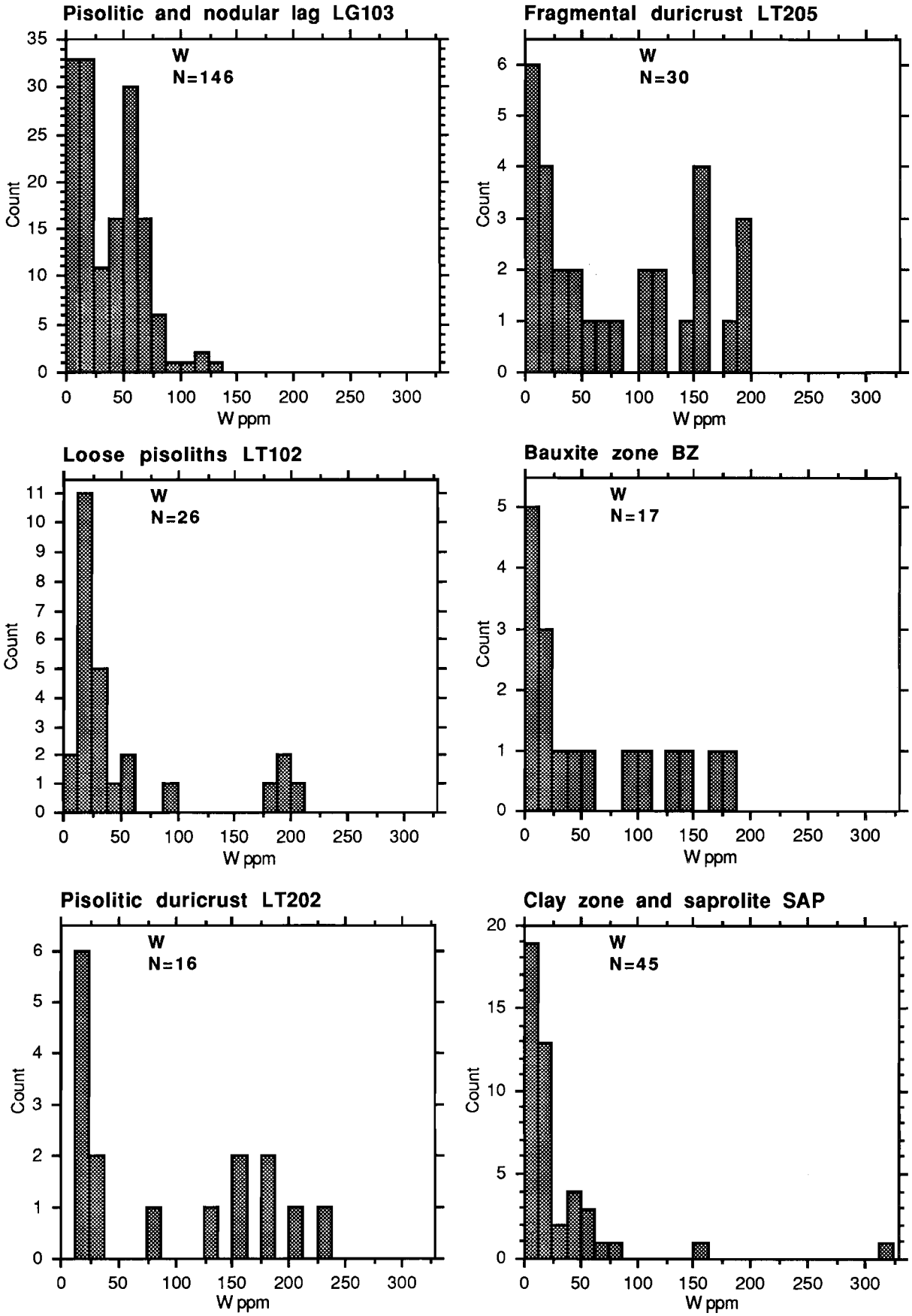
Pisolitic and nodular lag LG103
W
N=146
Count
W ppm
Fragmental duricrust LT205
W
N=30
Count
W ppm
Loose pisoliths LT102
W
N=26
Count
W ppm
Bauxite zone BZ
W
N=17
Count
W ppm
Pisolitic duricrust LT202
W
N=16
Count
W ppm
Clay zone and saprolite SAP
W
N=45
Count
W ppm

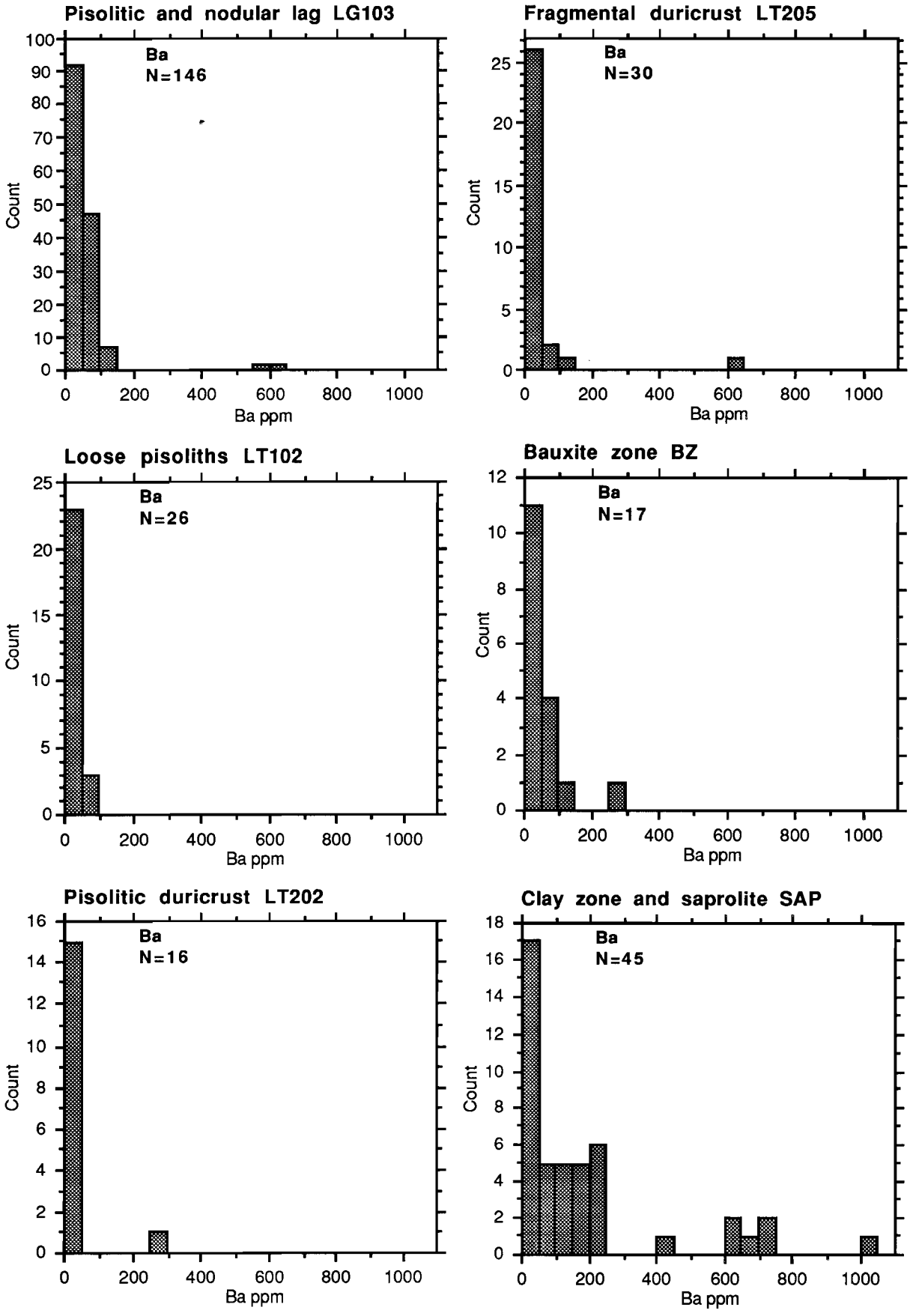
Pisolitic and nodular lag LG103
Ba
N=146
Count
Ba ppm
Fragmental duricrust LT205
Ba
N=30
Count
Ba ppm
Loose pisoliths LT102
Ba
N=26
Count
Ba ppm
Bauxite zone BZ
Ba
N=17
Count
Ba ppm
Pisolitic duricrust LT202
Ba
N=16
Count
Ba ppm
Clay zone and saprolite SAP
Ba
N=45
Count
Ba ppm

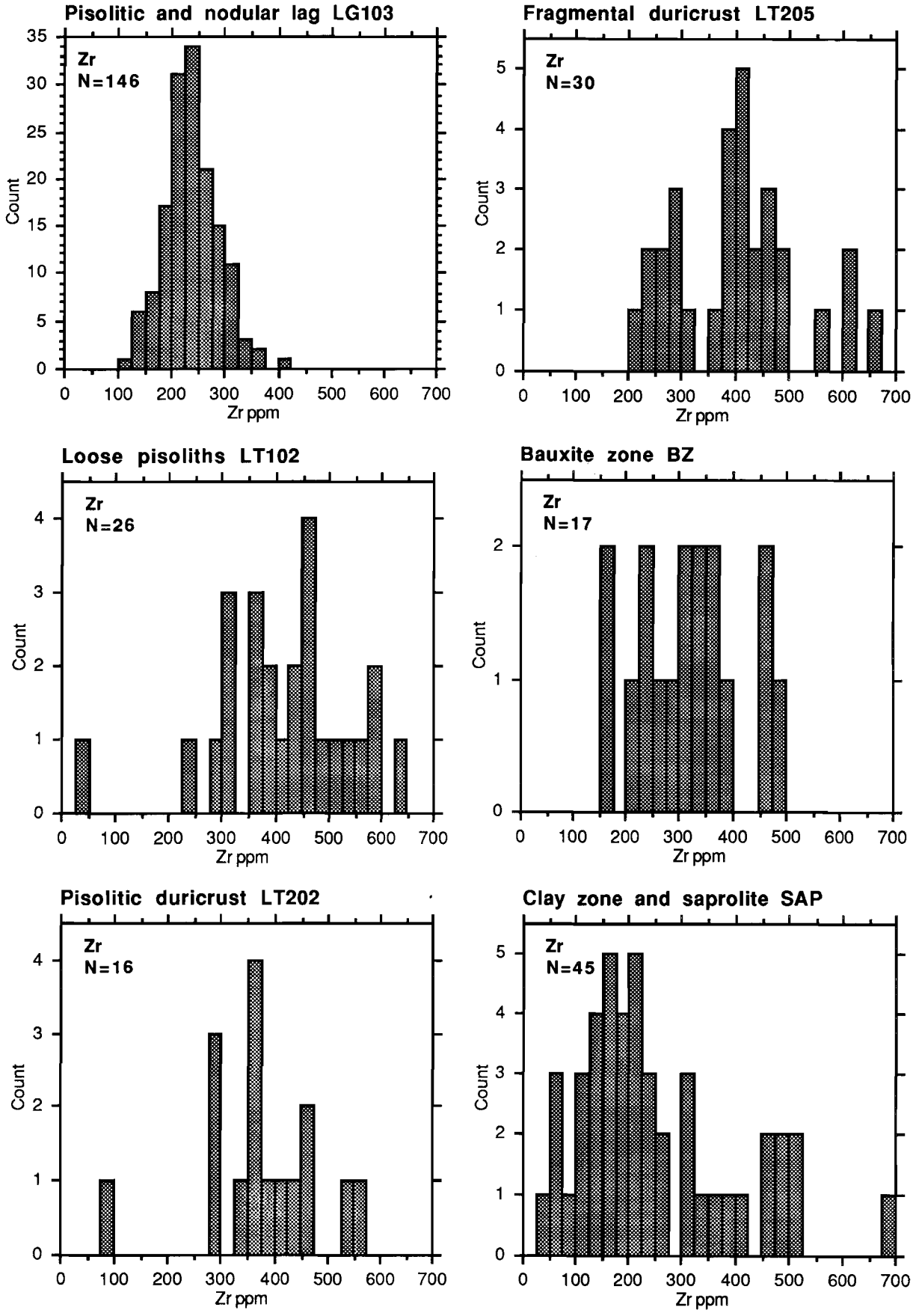
Pisolitic and nodular lag LG103
Zr
N=146
Count
Zr ppm
Fragmental duricrust LT205
Zr
N=30
Count
Zr ppm
Loose pisoliths LT102
Zr
N=26
Count
Zr ppm
Bauxite zone BZ
Zr
N=17
Count
Zr ppm
Pisolitic duricrust LT202
Zr
N=16
Count
Zr ppm
Clay zone and saprolite SAP
Zr
N=45
Count
Zr ppm

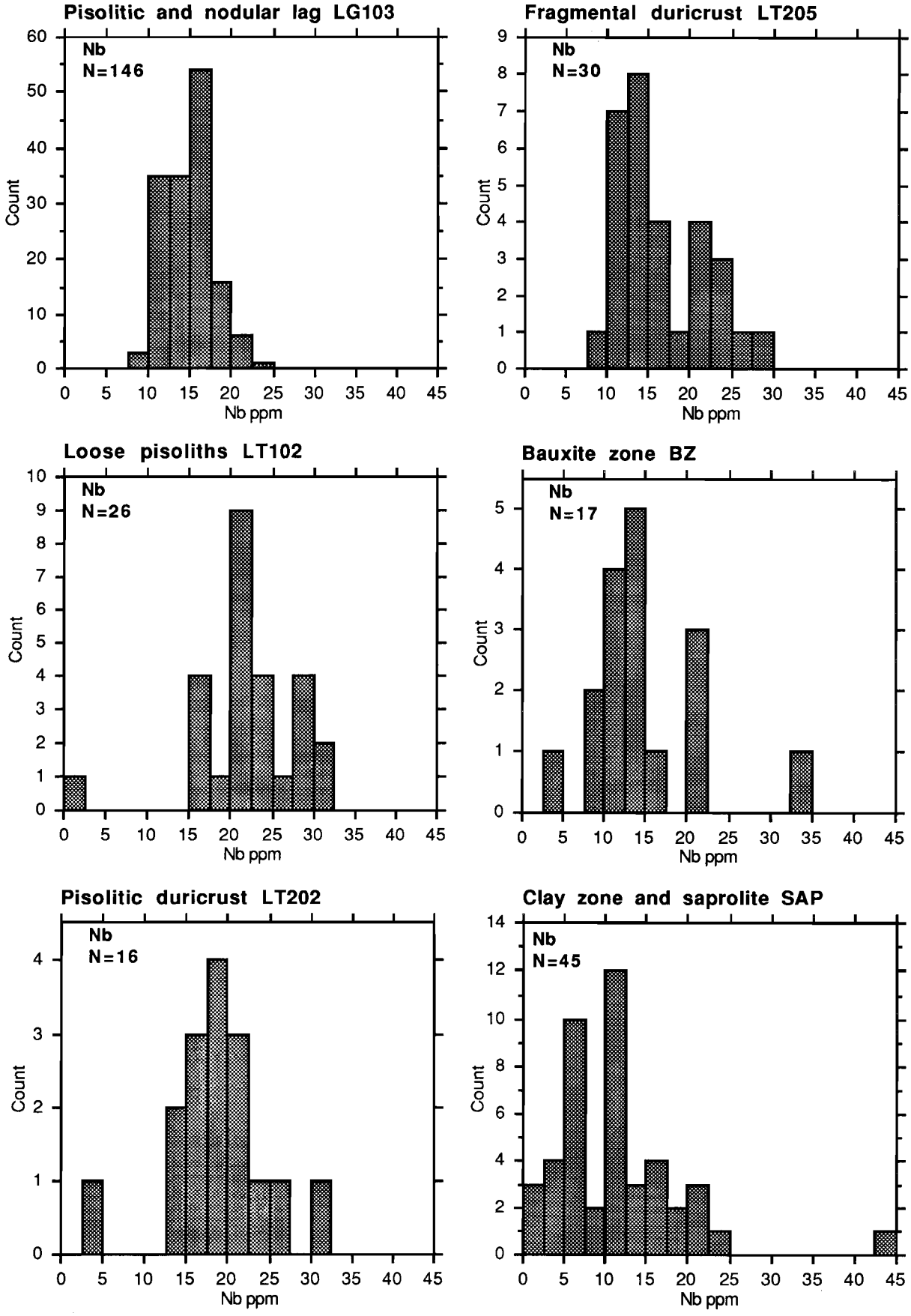
Pisolitic and nodular lag LG103
Nb
N=146
Count
Nb ppm
Fragmental duricrust LT205
Nb
N=30
Count
Nb ppm
Loose pisoliths LT102
Nb
N=26
Count
Nb ppm
Bauxite zone BZ
Nb
N=17
Count
Nb ppm
Pisolitic duricrust LT202
Nb
N=16
Count
Nb ppm
Clay zone and saprolite SAP
Nb
N=45
Count
Nb ppm

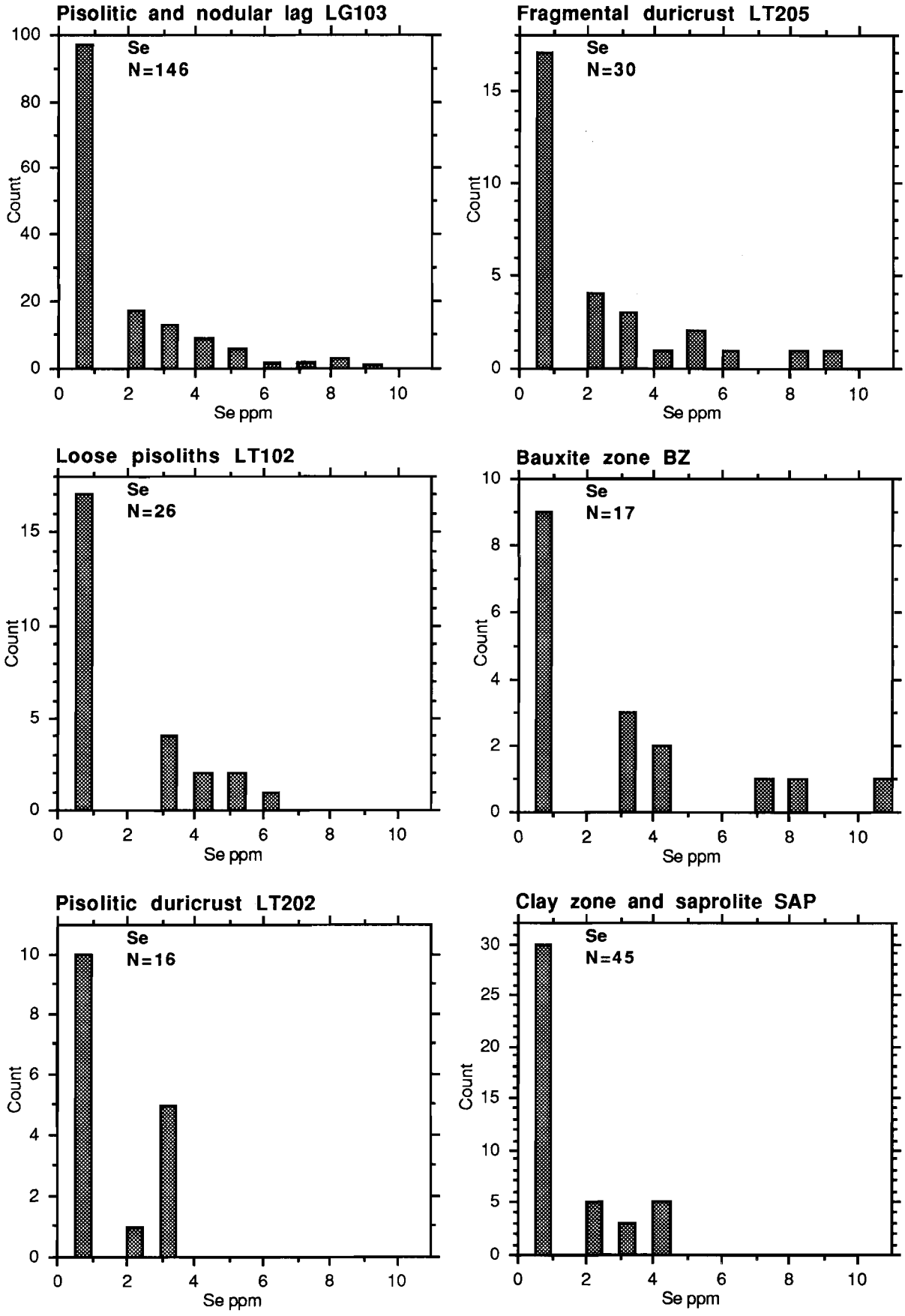
Pisolitic and nodular lag LG103
Se
N=146
Count
Se ppm
Fragmental duricrust LT205
Se
N=30
Count
Se ppm
Loose pisoliths LT102
Se
N=26
Count
Se ppm
Bauxite zone BZ
Se
N=17
Count
Se ppm
Pisolitic duricrust LT202
Se
N=16
Count
Se ppm
Clay zone and saprolite SAP
Se
N=45
Count
Se ppm

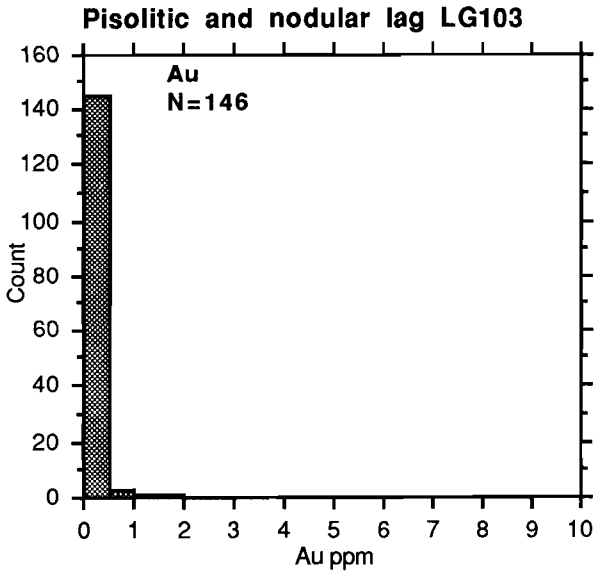
Pisolitic and nodular lag LG103
Au
N=146
Count
Au ppm

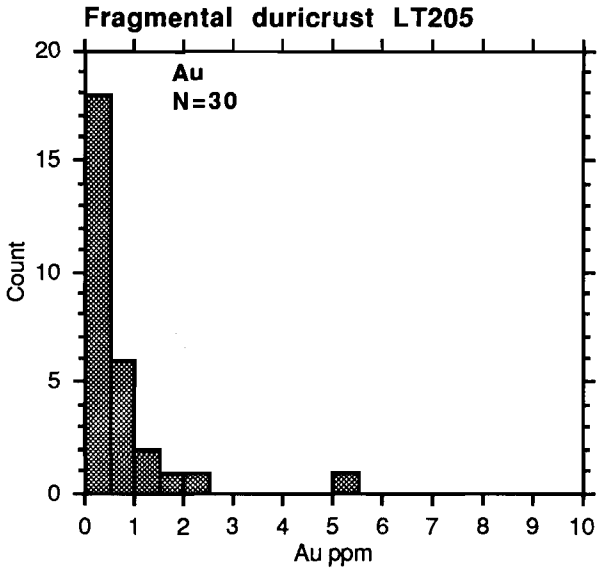
Fragmental duricrust LT205
Au
N=30
Count
Au ppm

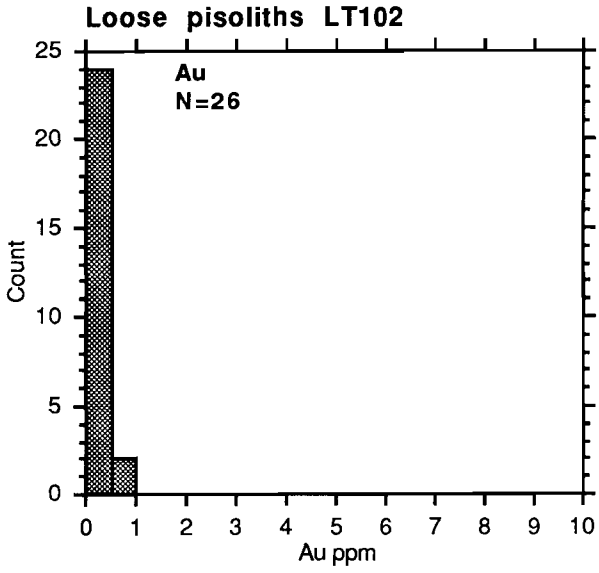
Loose pisoliths LT102
Au
N=26
Count
Au ppm

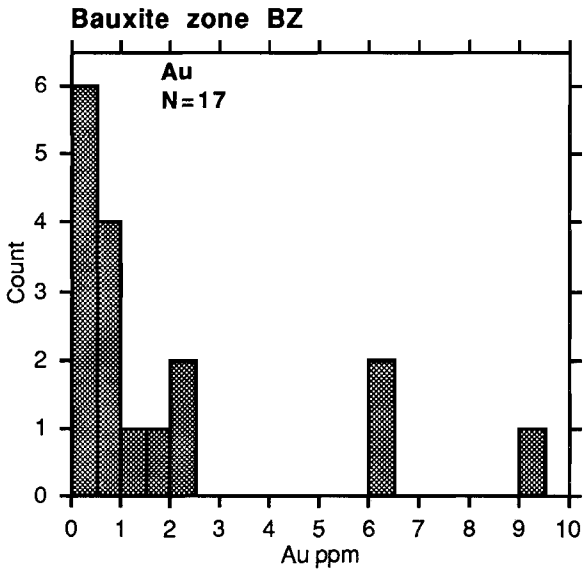
Bauxite zone BZ
Au
N=17
Count
Au ppm

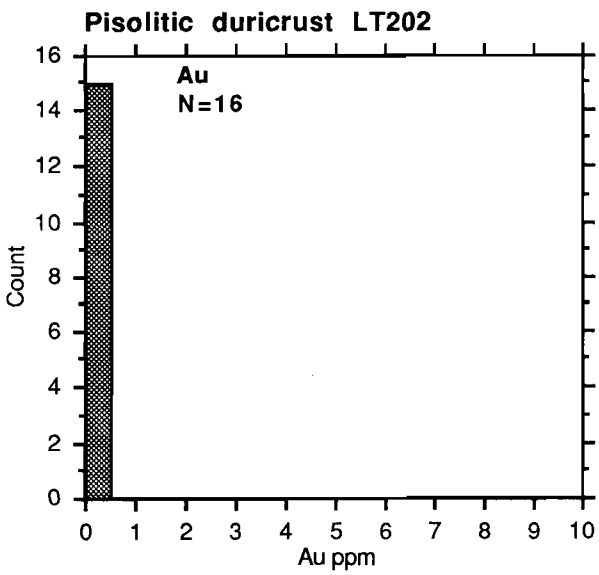
Pisolitic duricrust LT202
Au
N=16
Count
Au ppm

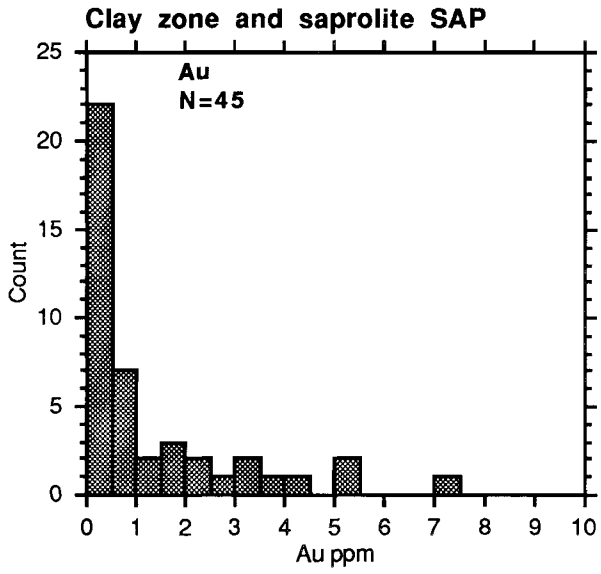
Clay zone and saprolite SAP
Au
N=45
Count
Au ppm